An *in ovo* investigation of the cellular effects of the heavy metals cadmium and chromium alone and in combination

By

Chantelle Venter

Submitted in partial fulfilment of the requirements for the degree of

MASTER OF SCIENCES

(MSc)

In the faculty of Health Sciences

Department of Anatomy

University of Pretoria

South Africa

Supervisor: **Dr HM Oberholzer**

Co-supervisor: **Ms H Taute**

Department of Anatomy

Faculty of Health Sciences

2014

An *in ovo* investigation of the cellular effects of the heavy metals cadmium and chromium alone and in combination

By

CHANTELLE VENTER

Supervisor: Dr HM Oberholzer

Co-supervisor: Ms H Taute

Department: Anatomy

Degree: MSc (Anatomy with specialization in Human Cell Biology)

Abstract

Many heavy metals are essential for biological functions; however some of these metals, especially at high concentrations, can have serious adverse effects on humans. The main sources of heavy metal exposure are through agriculture, transport, mining and related operations. South Africa has a thriving mining industry and is known for its rich mineral resources, but due to the incorrect method of disposal of the waste from these mines, substances, including heavy metals, get into the water and air supply, affecting the people living in close proximity to these mines. Exposure is through inhalation of contaminated air and consumption of contaminated food and water. The most vulnerable to heavy metals are the developing fetus, because of the high rate of cell division and differentiation.

In the current study, two heavy metals cadmium (Cd) and chromium (Cr) were chosen based on the possibility of being exposed to them in South Africa. Thus, the aim of this study was to investigate the possible cellular effects of the heavy metals Cd and Cr alone and in combination, at different concentrations, on brain, liver and kidney tissue by using a chick embryo model.

This model was successfully implemented over a 14 day period after which the embryos were terminated and the brains, livers and kidneys removed and processed for light- and transmission electron microscopy (with energy dispersive spectroscopy and electron energy-loss spectroscopy). In addition, the effect of Cd and Cr alone and in combination on DNA structure and micronuclei formation was evaluated. The levels of the major antioxidant component, glutathione was determined in the brains of the chick embryos.

At low concentration of Cd and Cr alone and in combination, a hormesis effect was observed in the survival rates and weights of the chick embryos, while at x1000 physiological dose (PD) Cr and Cd alone and in combination the effects were toxic. The majority of viable embryos did not have any macro-anatomy abnormalities.

Morphological evaluation of the brain, liver and kidney samples revealed that Cd caused severe alterations at its highest concentration with minor alterations at the lower concentrations. Cr and the metal combination groups on the other hand, only caused minimal alterations throughout the concentration ranges evaluated. The presence of Cd and Cr alone and in combination in the liver tissue was confirmed with the electron energy-loss spectroscopy analysis that detected these metals in the nuclei, mitochondria and Golgi complexes of the hepatocytes. This might contribute to the ultrastructural changes observed in this organ. The genotoxicity testing on the red blood cells revealed no substantial differences, as only a few micronuclei were present.

Although heavy metals cause DNA damage through an indirect mechanism of oxidative damage, the presence of Cd and Cr in the nucleus and mitochondria indicates that these metals may have a direct effect on DNA structure. With DNA agarose gel electrophoresis it was found that Cd and Cr alone and in combination caused DNA fragmentation. In the brain, GSH levels were normal; however changes may be the result of Cd and Cr causing the depletion of other antioxidant elements such as glutathione reductase, glutathione peroxidase, superoxide dismutase and catalase.

In conclusion, this study indicates that Cd and Cr alone and in combination are toxic to the chick embryo. Cd is more toxic than Cr, and both metals accumulate in the nuclei and mitochondria where they induce damage either through oxidative and/or other mechanisms associated directly with DNA damage.

Declaration

I, Chantelle Venter declare that this thesis entitled:

"An *in ovo* investigation of the cellular effects of the heavy metals cadmium and chromium alone and in combination"

which I herewith submit to the University of Pretoria for the Degree Master of Science in Anatomy with specialization in Human Cell Biology and Histology, is my own original work and has never been submitted for any academic award to any other tertiary institution for any degree.

_____ _____

Date **C Venter**

Department of Anatomy, Faculty of Health Sciences,
University of Pretoria
Pretoria
South Africa

Ethical clearance

UNIVERSITEIT VAN PRETORIA
UNIVERSITY OF PRETORIA
YUNIBESITHI YA PRETORIA

Animal Ethics Committee

PROJECT TITLE	**An *in ovo* investigation of the cellular effects of the heavy metals Cadnium and Chromium alone and in combination: Teratogenic effects of the heavy metals cadmium and chromium on chick embryo's**
PROJECT NUMBER	**H006-13**
RESEARCHER/PRINCIPAL INVESTIGATOR	**Ms C Venter**

STUDENT NUMBER (where applicable)	**U29227454**
DISSERTATION/THESIS SUBMITTED FOR	**MSc**

ANIMAL SPECIES	**Embryonated eggs**	
NUMBER OF ANIMALS	**270**	
Approval period to use animals for research/testing purposes		**May - November 2013**
SUPERVISOR	**Dr HM Oberholzer**	

KINDLY NOTE:

Should there be a change in the species or number of animal/s required, or the experimental procedure/s - please submit an amendment form to the UP Animal Ethics Committee for approval before commencing with the experiment

APPROVED	Date **29 April 2013**
CHAIRMAN: UP Animal Ethics Committee	Signature

Acknowledgments

"In whom are hidden all the treasures of wisdom and knowledge."

Colossians 2:3

Firstly I want to thank God for His wisdom, knowledge and guidance He provided me throughout my MSc study.

Dr Nanette Oberholzer, thank you for your guidance, motivation and most important patience throughout my MSc study and always being available for advice. You are the best supervisor that an MSc student can ask for.

I would like to express my appreciation to the following people who also made a valuable contribution to my study:

- Ms Helena Taute for her support and guidance as my co-supervisor.
- Professor Megan Bester, for her studious advice and guidance with the laboratory part of my study.
- Ms June Serem and Ms Ciska van der Schoor for their assistance with the laboratory work and the endless questions I had about the results.
- Mr Chris van der Merwe at the Unit for Microscopy and Microanalysis for his knowledge and insight in the world of microscopy and for his patience in teaching me a part of it. Thank you for your advice and for always being available to provide it.
- The rest of the personnel at the Unit for Microscopy and Microanalysis for their assistance and input in my study.
- Prof Alice Warley from the King's Collage London's Centre for Ultrastructural Imaging (CUI) and Clair Collins from Oxford Instruments for their assistance with my EDS results.
- Dr Franscious Cummings from the University of Western Cape for his assistance with the EELS analysis.

- Dr Liebie Louw and Ms Jaqui Sommerville for their assistance with the statistical analysis.

- Lastly, my parents and brother for their motivation, love and support throughout my MSc study. I would have never been able to achieve this if it were not for your end-less support and guidance.

Articles published

C Venter, CF van der Merwe, HM Oberholzer, MJ Bester and H Taute. Feasibility of high pressure freezing with freeze substitution after long-term storage in chemical fixatives. Microscopy Research and Technique 2013; 76: 942–946.

Table of contents

C Venter, CF van der Merwe, HM Oberholzer, MJ Bester and H Taute. Feasibility of high pressure freezing with freeze substitution after long-term storage in chemical fixatives. Microscopy Research and Technique 2013; 76: 942–946

List of figures, tables and diagrams

List of abbreviations, symbols and chemical formulae

aa	Amino acid
AEC	Animal Ethics Committee
AEM	Analytical electron microscopes
AH	Atypical heterophil
Alb	Albumin
ANOVA	Analysis of variance
ATP	Adenosine triphosphate
ATP + P_i	Adenosine triphosphate and phosphate ion
BBB	Blood brain barrier
BMPs	Bone morphogenetic proteins
CAM	Chorioallantoic membrane
Ca^{2+}	Calcium ion
Cd	Cadmium
$CdCl_2$	Cadmium chloride
CNS	Central nervous system
Cr	Chromium
DCT	Distal convolutes tubules
ddH_2O	Double distilled water
dsb	Double-stranded breaks
DTNB	5'5-dithiobis (2-nitrobenzoic acid)
EDS	Energy dispersive spectroscopy
EDTA	Ethylenediaminetetraacetic acid
EELS	Electron energy-loss spectroscopy
ESI	Electron spectral imaging
EtBr	Ethidium bromide
FA	Formaldehyde
FBF2	Fibroblast growth factor 2
FS	Freeze substitution
GA	Gluteraldehyde
GS•	Glutathione-derived thiol radical
GSH	Glutathione
GSSG	GSH disulfide
H&E	Haematoxylin and Eosin
HBSS	Hank's balanced salt solution
HH stages	Hamilton and Hamburger stages

H_2O_2	Hydrogen peroxide
HPF	High pressure freezing
HSP	Heat shock proteins
I-κB	Inhibitor of NF-κB
JNK	Jun N-terminal kinases
$K_2Cr_2O_7$	Potassium dichromate
MAPKs	Mitogen-activated protein kinases
MT	Metallothionein
$NADP^+$	Nicotinamide adenine dinucleotide phosphate (oxidized form)
NADPH	Nicotinamide adenine dinucleotide phosphate
NADPH + H^+	Nicotinamide adenine dinucleotide phosphate and hydrogen ion
NF-κB	Nuclear factor kappa B
•OH	Hydroxyl radicals
O_2•	Superoxide radical
PCT	Proximal convoluted tubule
PBS	Phosphate buffer saline
PD	Physiological dose
pH	Measure of the acidity and basicity
PO_4	Phosphate
rER	Rough endoplasmic reticulum
RBC(s)	Red blood cell(s)
ROS	Reactive oxygen species
ssb	Single-stranded breaks
SOD	Superoxide dismutase
TAE	Tris, acetic acid and EDTA
TBA	*tert*-Butyl alcohol
TEM	Transmission electron microscopy/e
TIFF	Tagged image format
UV	Ultra-violet
mm^3	Cubic millimetre
ºC	Degree Celsius
eV	Electron volts
g	Gram
g/cm^3	Gram per cubic centimetre
g/µℓ	Grams per microliter
KeV	Kiloelectron volts
kg	Kilogram

µg/mℓ	Microgram per millilitre
µg	Microgram
µℓ	Microlitre
µm	Micrometer
mℓ	Millilitre
M	Molar
nm	Nanometer
%	Percent
x	Times

Chapter 1

General introduction

There is no clear definition of what a heavy metal is, but density is mostly used as the defining factor, thus a heavy metal has a density of more than 5g/cm^3 (Järup, 2003). Many heavy metals are essential for human biological functions as the metals may be structural elements, stabilizers of biological structures, components of control mechanisms like nerves and muscles, and components of redox systems (Nordberg, *et al*., 2007a). However, some of these metals, especially at high concentrations, can have toxic, carcinogenic and/or teratogenic effects in humans. The main anthropogenic sources of human exposure to heavy metals are through agriculture, transport, mining and related operations. These are also the main sources of increased environmental heavy metal levels (Al-Attar, 2011). These increased levels of heavy metals have a direct effect on irrigated crops and through this an indirect effect on people in the affected area. Heavy metals can be absorbed through the skin, orally or through inhalation (Awofolu, *et al.,* 2005). The degree of heavy metal toxicity depends on dose, duration, route of administration and other physiological factors, especially nutrition (Al-Attar, 2011; Chowdhury, 2009).

The South African mining sector is estimated to be the fifth largest in the world, with the largest reserve of manganese and platinum group metals found in South Africa. South Africa also has one of the largest reserves of gold, diamonds, chromium ore and vanadium (Kearney, 2012). When these heavy metals are not correctly disposed of, it can be a large source of heavy metal pollution. In 2001, Binning and Bard investigated chromium, lead, zinc, titanium, manganese, strontium, copper and tin concentrations in the Swartkops River in the Eastern Cape and found that there is a high concentration of these heavy metals in the river (Binning and Baird, 2001). These findings were compared to results obtained twenty years ago and the levels of heavy metals were found to have increased remarkably (Binning and Baird, 2001). Another study examined the gold mining industry in the Witwatersrand region in South Africa and it was found that the ground water contained elevated levels of heavy metals (Naicker, *et al*., 2003). In South Africa heavy metal exposure is mostly through the ingestion of contaminated water; be it by drinking the water, preparing food in it or irrigating crops with it (Awofolu, *et al.,* 2005). Communities using this water and/or living in these regions are most at risk, especially children and pregnant women with the developing fetus being the most vulnerable.

In this study only two heavy metals were chosen, cadmium (Cd) and chromium (Cr). These two metals were selected based on the likelihood of being exposed to them in South Africa.

Cd was chosen based on the high levels that were found in certain rivers and dams in the Eastern Cape Province, that can not only affect the aquatic ecosystem but also the people using this water in the rural communities (Fatoki and Awofolu, 2003). Cr(VI) was chosen based on the high levels of Cr(VI) found in wastewater, due to mining in the Brits area in the North West Province of South Africa, as well as the high levels of Cr(VI) in the air in the eMalahleni (Witbank) and Mpumalanga region (Molokwane, *et al*., 2008; Tempelhoff, 2013). These two heavy metals are thus very relevant to South Africa specifically but also worldwide.

The fetus is particularly vulnerable to the effects of heavy metals such as Cd and Cr, because of the high rate of cell division and differentiation. Low levels of exposure may have little effect on the mother, but may have an adverse effect on the growth and development of the fetus (Taylor, *et al.,* 2014). In addition, exposure is often not limited to a single heavy metal but is a mixture of different types such as a combination of Cd and Cr, as was used in this study. The toxicity of substances can be investigated in terms of their absorption, distribution, metabolism and excretion in order to define its toxic properties. This was applied in the current study. The liver and kidney are associated with the metabolism and excretion of various compounds and are often the primary target sites of toxicity (Coetzee, *et al.,* 2009).

Concern has been expressed regarding the effect of these heavy metals on cognitive development i.e. the effects on the cellular function of the neurons in the brain and their morphology. Cellular and biochemical targets specific to Cd and Cr toxicity is genomic and mitochondrial DNA. This can result in strand breaks that may deplete the intracellular antioxidant elements such as glutathione and antioxidant enzymes such as superoxide dismutase, glutathione peroxidase and catalase (Kalpana, *et al.,* 2008; Matésa, *et al.,* 1999).

Therefore, the aim of this study was to investigate the cellular effects of the heavy metals Cd and Cr alone and in combination on the brain, liver and kidney by implementing the chick embryo model.

Chapter 2

Literature review

2.1. Introduction

Heavy metal contamination has become a major problem worldwide, with heavy metal exposure mainly occurring through agriculture, transport, mining and related operations (Al-Attar, 2011). In South Africa's thriving mining sector, heavy metal contamination occurs due to negligent heavy metal contamination of the water and air in certain provinces and it is in these provinces that people living in the rural communities are most at risk for heavy metal poisoning.

Heavy metals have been used for thousands of years for numerous different applications. For example lead was used by the Romans to sweeten old wine and thus some Romans could have consumed almost a gram of lead per day. Mercury on the other hand was used by the Romans as a cream for teething pain in infants and later was used as a remedy for syphilis (Järup, 2003). In the art industry, cadmium pigments were used by the French painter Claude Monet in the 1800's. Although the harmful health effects of heavy metals have been known for many years, heavy metal exposure is still a major problem around the world. Fortunately, at the end of the 20th century the amount of heavy metal pollution decreased as the developing countries started to decrease their heavy metal emission (Järup, 2003).

In this thesis the *in ovo* model was used to test the effects of the heavy metals cadmium (Cd) and chromium (Cr) alone and in combination. The heavy metals were chosen based on the likelihood of being exposed to them in South Africa. The effects of Cd and Cr will be discussed according to several different parameters including the normal histology and ultrastructure of the brain, liver and kidneys, analysing heavy metal accumulation in the tissues and glutathione depletion and DNA damage in the brain tissue. The brain was chosen to evaluate the possibility of cellular damage due to the fact that the brain has a defence mechanism known as the blood brain barrier (BBB). In embryos the BBB is not fully developed and unwanted particles can easily infiltrate the brain (Nordberg, *et al*., 2007b). Depending on the duration of exposure, acute (short term) or chronic (long term), the effects seen in the developing brain may differ. With chronic exposure, some neurological disorders and carcinogenic effects can be observed. In both acute and chronic exposure, cellular and functional changes can be observed such as DNA damage, activation of the mitogen-activated protein kinases (MAPKs) and nuclear transcription factor B (NF-κB) pathway,

memory deficits, alteration of social contact and altered synaptic functions (Leal, *et al*., 2012; Shi, 2010; Waisberg, *et al*., 2003). The liver and kidneys were chosen based on the fact that they are the body's detoxification and filtering organs respectively and thus are ideal to indicate any cellular damage that may occur due to heavy metal toxicity (Coetzee, *et al.,* 2009).

Therefore, this chapter includes the sources, physiology, excretion and teratogenic effects of Cd and Cr. Also, a section on normal chick and human embryo development are included in this chapter. This chapter ends off with the specific aims and objectives of this study.

2.2. Cadmium

2.2.1. Source of cadmium

Cadmium (Cd) is a transition metal that is found in group IIb of the periodic table of elements (Cullinane, *et al*., 2009). Cd is so widespread throughout nature that it is present in measurable amounts in almost everything we eat, drink and breathe (Thompson and Bannigan, 2008). Cd levels in the environment are increased by human activities that include the combustion of fossil fuels, leechate from landfills sites, run-off from agricultural land and mining residues, especially from zinc and lead mines (Thompson and Bannigan, 2008). The electroplating of steel, production of Nickel-Cd batteries, pigments, stabilizers and alloys also produces Cd as a by-product (Thompson and Bannigan, 2008). Non-occupational exposure to Cd mostly occurs through cigarette smoking. Cigarette smoking is the most significant source of chronic Cd exposure with about 0.2-1.0µg of Cd assimilated with each cigarette smoked (Cullinane, *et al*., 2009).

2.2.2. Physiology of cadmium

Human exposure to Cd mostly occurs through ingestion of contaminated food or water and inhalation of cigarette smoke (Thévenod, 2009). After absorption through either the lungs or gastrointestinal tract, the Cd is transported to the blood where it will be stored mainly in the liver and kidneys. Small amounts are usually also found in the central nervous system (Nordberg, *et al*., 2007b). Cd toxicity affects many cellular processes that include: cell cycle progression, proliferation, differentiation, DNA replication and repair, and apoptotic pathways (Bertin and Averbeck, 2006). The following paragraphs explain the absorption and the influences of Cd on the liver, kidneys and brain.

Liver

After Cd enters the body it is transported to the liver by binding to albumin and other large proteins in the blood plasma (Nordberg, *et al*., 2007b). As the Cd-albumin complex enters the liver, it is separated and the Cd can cause toxicity (Fig. 2.1). The presence of Cd in the liver induces metallothionein (MT) production by hepatocytes and this causes a gradual increase in the proportion of Cd bound to MT in the liver (Nordberg, *et al*., 2007b). The binding of Cd to MT buffers hepatocytes from the toxic effect of Cd. When a hepatocyte contains a considerable amount of the Cd-MT complex, it will be released into the bloodstream and transported to the kidneys (Nordberg, *et al*., 2007b; Prozialeck, *et al*., 2006).

Kidneys

The small molecular size of the Cd-MT complex allows it to effectively filter through the glomerular membrane of the kidneys where it is absorbed by epithelial cells of the proximal tubule (Fig. 2.1) (Nordberg, *et al*., 2007b). If Cd is not bound to MT, it can also bind to lower affinity materials like albumin, amino acids or sulfhydryl compounds like cysteine or glutathione (GSH). Cd-MT complexes will accumulate in the lysosomes of the proximal tubule, where after the MT will be catabolized and the Cd is released into the cytoplasm of the cell, where it can alter certain processes (as described in the following paragraph) and induce oxidative stress (Fig. 2.1) (Prozialeck, *et al*., 2006).

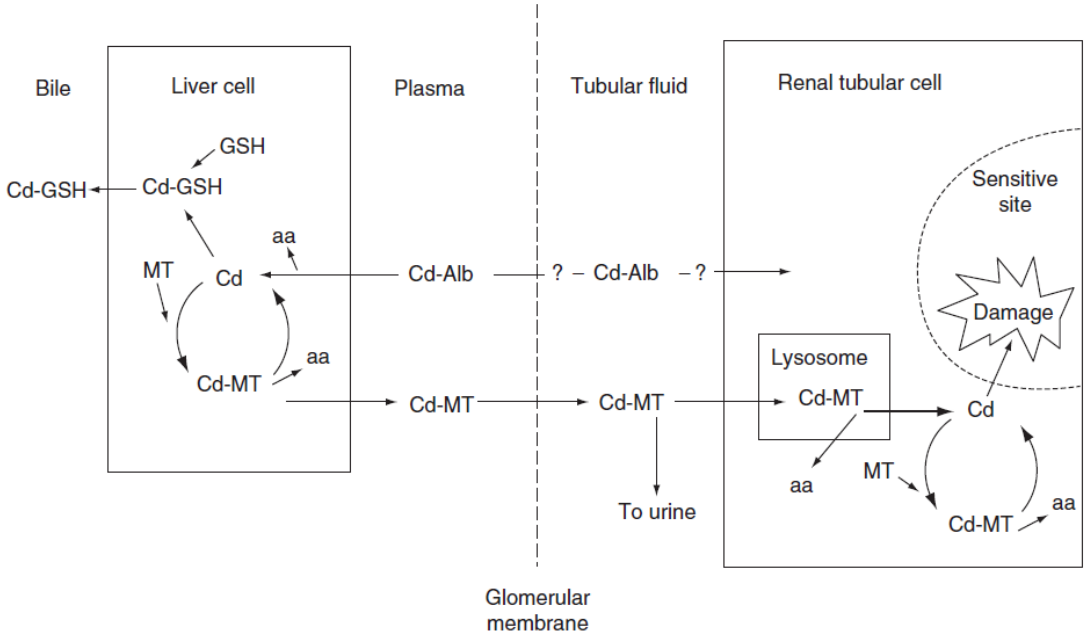

Figure 2.1: Basic flow diagram of Cd as it is transported through the body. aa: amino acids and Alb: albumin (Nordberg, *et al*., 2007b).

Cd toxicity induces oxidative stress by means of indirect processes. These processes are comprised of the decrease in cellular antioxidants and the production of reactive oxygen species (ROS) by the mitochondria. Cd toxicity also increases hydrogen peroxide (H_2O_2), superoxide anion (O_2•) and hydroxyl radical (•OH) production and thus increases oxidative stress in the cell (Fig. 2.2) (Bertin and Averbeck, 2006). The oxidative stress caused by Cd toxicity has many effects on the cells, for example damage to proteins and thus an increase in production of heat shock proteins (HSPs). The HSPs are chaperone proteins that are activated by hyperthermia and several environmental stresses that include Cd toxicity. Cd toxicity causes overexpression of certain HSPs, which helps with the repair of mis-folded proteins or eliminate aggregated proteins by the ubiquitin-proteasome system (Fig. 2.2) (Bertin and Averbeck, 2006).

Cd-induced oxidative stress also causes DNA damage. DNA is important for normal cellular functions that include replication, gene expression and protein synthesis. When DNA is damaged, it can induce cell cycle arrest, mutagenesis, genome instability, cancer and undergo apoptosis (Bertin and Averbeck, 2006). Another effect of Cd-induced oxidative stress is the peroxidation of lipids (Fig. 2.2). Lipid peroxidation may cause cross-linking and polymerization of membrane components and therefore cause cell membrane modification in their lipid composition and will thus affect the cellular functions and mitochondrial membranes (Bertin and Averbeck, 2006).

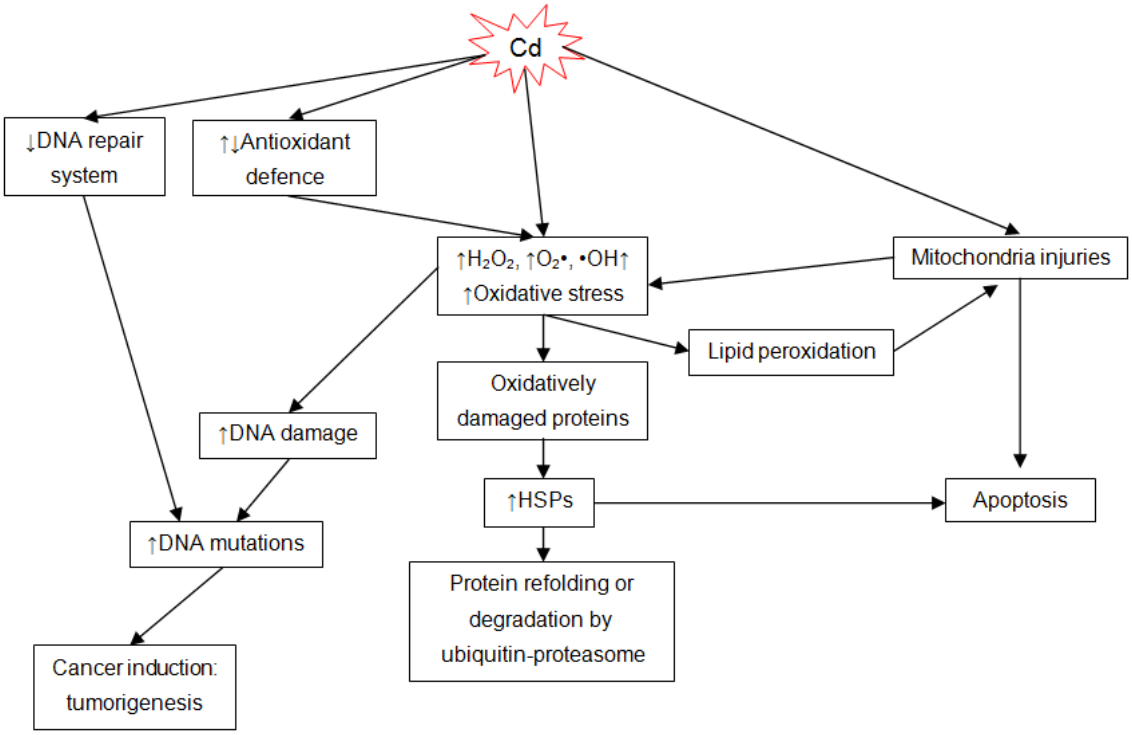

Figure 2.2: The biological pathway of Cd toxicity in cells (modified from Bertin and Averbeck, 2006).

Brain

Cd neurotoxicity occurs mostly in the early stages of embryonic development, as the embryo's BBB is not yet fully developed. The BBB is the protective mechanism of the brain. At later stages of development and in adults the BBB offers considerable protection against the effects of Cd (Nordberg, *et al*., 2007b). Unfortunately small amounts of Cd can still enter the adult brain, due to the selective permeability of the BBB (Méndez-Armenta and Ríos, 2007). Elevated ROS levels, due to Cd toxicity, can also contribute to BBB permeability. An increase in ROS is associated with neurodegenerative disorders, such as Alzheimer's and Parkinson's disease (Chen, *et al*., 2008).

Although Cd can directly affect the brain cells, it is only secondary to the interference of Cd on the calcium ion (Ca^{2+}) concentration and MT in the brain (Méndez-Armenta and Ríos, 2007; Nordberg, *et al*., 2007b). Many neuronal functions can be affected by changes in the homeostasis of cytosolic Ca^{2+} concentration (Méndez-Armenta and Ríos, 2007). When the neurons are excited, there is an increase in intracellular Ca^{2+} and this helps with the neuronal response. The intracellular Ca^{2+} increase is mediated by voltage-dependent channels and it is released from the Ca^{2+} stores (Méndez-Armenta and Ríos, 2007). Cd inhibits all known pathways of cellular Ca^{2+} influx, competes with Ca^{2+} at the voltage-dependent Ca^{2+} channels and is an effective blocker of the Ca^{2+}-dependent neurotransmitter release (Méndez-Armenta and Ríos, 2007). It has also been reported that Cd can increase the intracellular levels of Ca^{2+} and this continued increase may be the main reason for apoptosis (Méndez-Armenta and Ríos, 2007).

Excretion

Cd is excreted in small portions when absorbed over long-term low-level exposure. Cd is excreted daily in the urine and faeces at only approximately 0.01%-0.02% of the total body burden of Cd (Nordberg, *et al*., 2007b). However, as you age, there is an increase in renal damage and thus the rate of Cd excreted in the urine increases dramatically. Total faeces Cd excretion is not age-related and the amount excreted is close to the amount ingested and about 50 times more than excreted in the urine (Nordberg, *et al*., 2007b). This is because a large portion of the ingested Cd remains unabsorbed.

2.3. Chromium

2.3.1. Sources of chromium

Chromium (Cr) is used in many industrial processes including electroplating, steel manufacturing, leather tanning and wood preservation (Kakkar and Jaffery, 2005; Patlolla, *et al*., 2009) and it is these processes that are the main cause of Cr contamination (Kakkar and Jaffery, 2005). Cr is also found in cigarettes, between 0.24-14.6mg/kg of Cr gets inhaled when smoking (Langård and Costa, 2007).

2.3.2. Physiology of chromium

Cr is a naturally occurring heavy metal that may exist in a variety of oxidation states that range from Cr(II) to Cr(VI) (Patlolla, *et al*., 2009; Yoon, *et al*., 2008), where only the trivalent Cr(III) and hexavalent Cr(VI) forms are important in human health (Dayan and Paine, 2001; Langård and Costa, 2007). Cr(III) is an essential nutrient that plays an important role in regulating the levels of glucose in the blood (Quinteros, *et al*., 2007; Valko, *et al*., 2006). Cr(VI) on the other hand, is highly toxic and a strong oxidizing agent (Quinteros, *et al*., 2007) that can cause lung toxicity, bronchial asthma, nephro- and hepatotoxicity and may also affect the brain (Quinteros, *et al*., 2007). Cr(VI) easily enters the cells via non-specific anion channels and once inside the cells it is reduced to the more stable Cr(III), following the formation of reactive intermediate species of Cr, Cr(IV) and Cr(V) and ROS (Raghunathan, *et al*., 2009).

The way by which the different radicals are generated by the reduction of Cr(VI) is through a series of different reactions. First GSH rapidly forms a complex with Cr(VI), this is followed by a slow reduction of Cr(VI) to yield Cr(V) (Valko, *et al*., 2006). With the formation of Cr(V), GSH forms a glutathione-derived thiol radical (GS•) that can cause cellular damage (Fig. 2.3–reaction 1). In previous studies it was found that there are a number of other substances that can reduce Cr(VI). These substances include ascorbate, cystein, lipoic acid, nicotinamide adenine dinucleotide phosphate (NADPH), fructose, ribose and others (Valko, *et al*., 2006). The authors suggested that it is probably NADPH flavo enzymes that reduces Cr(VI) (Fig. 2.3-reaction 2) (Valko, *et al*., 2006).

Once GS• radicals are formed (Fig 2.3-reaction 1) it can further react with other thiol radicals in oxygenated tissue to produce a superoxide radical (O_2•) (Fig. 2.3-reaction 4 and 5)

(Leonard, *et al.,* 2004; Valko, *et al*., 2006). The superoxide radical can reduce Cr(VI) to Cr (V), or produce H_2O_2 which will undergo the Fenton reaction to produce hydroxyl radicals that cause DNA damage (Fig. 2.3-reaction 6 and 7).

When Cr(V) is exposed to H_2O_2 hydroxyl radicals (•OH) may form through the Fenton reaction (Fig 2.3-reaction 3). Hydroxyl radicals can cause DNA damage and activate the p53 pathway (Leonard, *et al.,* 2004). Alternatively Cr(V) can be reduced to Cr(IV) by cellular reductants like ascorbate and GSH (Fig. 2.3-reaction 8). H_2O_2 exposed to Cr (IV) will undergo the Fenton reaction to produce the hydroxyl radical that causes DNA damage (Fig. 2.3-reaction 9) (Valko, *et al*., 2006).

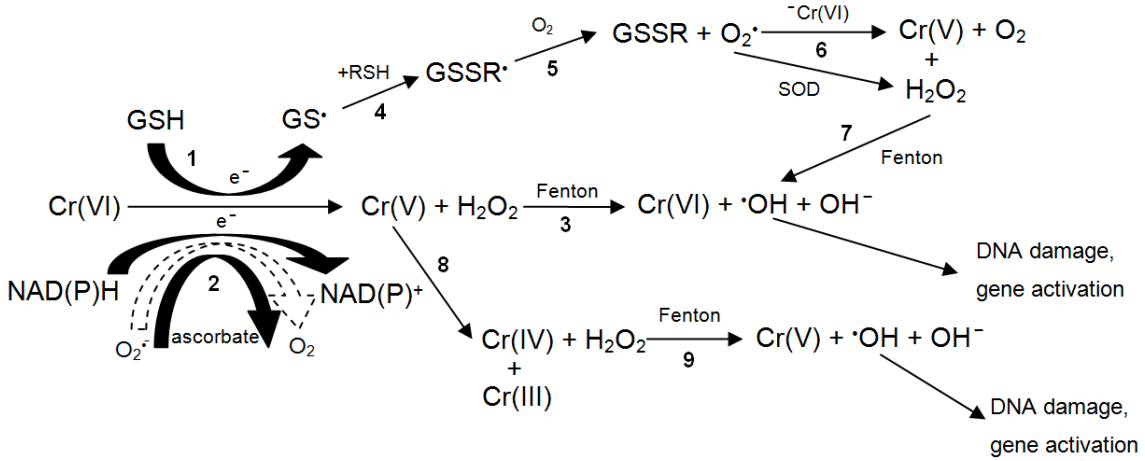

Figure 2.3: The reduction reactions of Cr(VI) SOD: superoxide dismutase (Valko, *et al*., 2006).

As mentioned above, DNA damage caused by •OH radicals can activate the p53 pathway. p53 is seen as a tumour suppressor as it is able to stop the cell cycle or initiate apoptosis if the cells are too severely injured and cannot be repaired (Leonard, *et al.,* 2004). This is not the only way in which Cr(VI) induces p53. Cr(VI) can also induce p53 by DNA binding to Cr(VI) reduction products, by activating the MAPKs before the p53s and by enhancing the activation of other carcinogens (Fig. 2.4) (Leonard, *et al.,* 2004). The MAPKs involved in Cr(VI) toxicity is the Jun N-terminal kinases (JNK) and p38 kinases, with the activation of these kinases Cr(VI) can induce apoptosis (Leonard, *et al.,* 2004). After activation, MAPKs act on the non-active NF-κB in the cells. The NF-κB is a redox-sensitive nuclear transcription factor that is bound to the inhibitor of NF-κB (I-κB) in the cytoplasm of the cell. When NF-κB is bound to I-κB it is in its inactive state. Once NF-κB is activated, I-κB is degraded and this allows the active NF-κB to move into the nucleus of the cell (Fig. 2.4) (Leonard, *et al.,* 2004). NF-κB binds to a specific DNA sequence and this allows the regulation of the transcription of the gene, mediating inflammation, carcinogenesis and anti-apoptotic reactions (Leonard, *et al.,* 2004). Although the net effect of the NF-κB is to inhibit apoptosis, NF-κB may also be

involved in apoptosis by interacting with cyclin D1 (Leonard, *et al.,* 2004). One of cyclin D1's functions includes initiation of apoptosis (Fu, *et al.,* 2004).

Cell cycle arrest is another way that apoptosis can be set in motion. As the cell undergoes cell proliferation it is put through a check-point in the cell cycle. This slows the cycle and if the cell is seen as too severely damaged or not properly developed, the cell can undergo apoptosis (Leonard, *et al.,* 2004). ROS and DNA damaging agents are able to cause these types of apoptosis. Little information is available on metal-reduced ROS cell cycle arrest, however Cr(VI) is known to cause cell cycle arrest, as earlier studies showed a direct link between DNA damage and S-phase cell cycle arrest (Leonard, *et al.,* 2004).

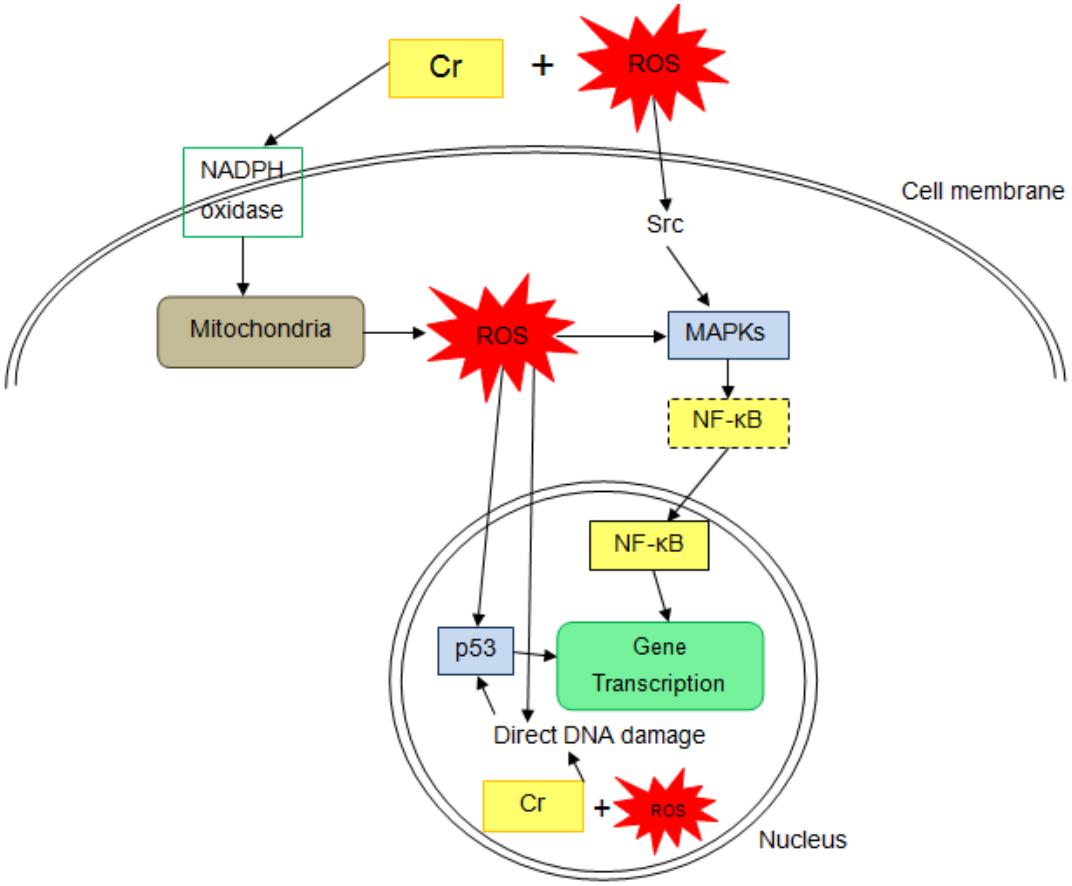

Figure 2.4: Pathway of Cr metal-induced proteins and ROS (modified from: Leonard, *et al.,* 2004; Valko, *et al.*, 2006).

Excretion

Following absorption, Cr(VI) is converted to Cr(III) in the body and thus Cr(III) will be the main compound that will be detected in the urine and faeces. It is only when the liver cells are compromised that Cr(VI) may be excreted in the bile. The excretion rate of chromium depends on the valence state of the chromium and thus excretion can occur after a few hours to a few days (Langård and Costa, 2007; Wilbur, *et al.,* 2012).

2.4. Metal combination

Although Cd and Cr affect the cells through different biochemical pathways, similar end results are seen. As described above, Cd will deplete protein-bound sulfhydryl groups and increase the production of ROS such as H_2O_2, O_2• and •OH (Bertin and Averbeck, 2006; Stohs, *et al*., 2000). In the case of Cr, it will enter the redox cycle and will also increase the production of ROS. The increase in ROS will cause certain alterations, which include lipid peroxidation, DNA and membrane damage, altered gene expression and apoptosis or necrosis (Stohs, *et al*., 2000). Limited information is available in the literature on the combined effects of these metals specifically on the brain, liver and kidneys.

2.5. Normal chick embryo development

There are no safe threshold levels of heavy metal exposure during pregnancy and it is generally accepted that environmental levels should be kept at a minimum (Taylor, *et al.,* 2014). Animal models in conjunction with sensitive techniques for the detection and quantification of cellular damage caused by heavy metals can be used to investigate the consequences of fetal exposure to these metals. One such model is the chick embryo model.

The development of the chick embryo is divided into stages that allow for comparison between chick and human embryo development (Table 2.1). This makes it possible to identify stages at which humans will be the most vulnerable to a certain teratogen.

Table 2.1: Comparison of Carnegie stages between human and chick embryo's (Butler H and Juurlink, 1987; Harkness and Baird, 1997)

HH Stages*		**7**	**10**	**12**	**15**	**17**	**18**	**20**	**22**	**25**	**27**	**29**	**31**	**31**	**35**	**36**
Stage		9	10	11	12	13	14	15	16	17	18	19	20	21	22	23
Human	Days	20	22	24	28	30	33	36	40	42	44	48	52	54	55	58
Chick	Days	1	1.5	2	2.25	2.5	3	3.25	3.75	4.75	5.5	6.25	7.25	7.75	8.5	10

* **Hamilton and Hamburger**

2.5.1. Brain

The brain is formed from the anterior end of the neural tube. By stage 9 the primary optic vesicles has started to form and by stage 10 the brain has already developed into its three primary regions, namely the prosencephalon (forebrain), the mesencephalon (midbrain) and

the rhombencephalon (hindbrain). By stage 11 the rhombencephalon has become subdivided into the metencephalon (cerebellum and pons) and the myelencephalon (medulla oblongata) (Bellairs and Osmond, 1998). The prosencephalon divides into the telencephalon (cerebral hemispheres) and the diencephalon (thalami, metathalami, pituitary gland, pineal gland) by stage 12-13. Anterior to the optic vesicles, paired swellings appear that communicate with the median telocoele (the central lumen of the brain at that region) by the foramen of Monro. Almost during the same period the cranial flexure starts to appear and bend at the anterior end of the mesencephalon (Bellairs and Osmond, 1998). The cephalic flexure only begins to develop at stage 18 (day 3). These two structures will reduce by stage 36 (day 10) and will allow the neck to become less convex and thus the head is no longer tucked against the thorax (Bellairs and Osmond, 1998).

At stage 13 (day 2), the walls of the telencephalic vesicles have thickened and form the cerebral hemispheres with their lumina that will form the lateral ventricles. The cerebral hemispheres will expand over the diencephalon by stage 37 (day 11) and will continue to overlap the mesencephalon by stage 44 (day 18). The wall of the optic recess (Fig. 2.5) that forms part of the diencephalon, decreases in thickness by stage 18 (day 5) and a thickened area directly posterior to the optic recess, marks the development of the optic chiasm (Bellairs and Osmond, 1998). Posterior to the chiasm the infundibulum develops and combines with Rathke's pouch to form the pituitary gland. During stage 19, the median part of the roof of the diencephalon gives rise to the pineal gland. At about stage 18, the mesencephalon has increased in size and is separated from the rhombencephalon by a narrower region, called the isthmus that is found in the mesometencephalic fold (Fig. 2.5). The mesencephalon grows over the metencephalon at stage 22 (day 5-5.5) and contains the optic fibres that play an important role in the excellent vision of birds (Bellairs and Osmond, 1998).

In the early stages of development the rhombencephalon has a thin-walled roof and by day 4 the walls get thicker as the metencephalon develops into the two halves of the cerebellum. The cerebellum will increase in size and fuse in the midline during the following five days and will further increase in size and complexity by day 16. By this stage it will almost border the cerebral hemispheres. The myelencephalon develops the characteristic shape of the medulla oblongata by day 9-10 (Bellairs and Osmond, 1998).

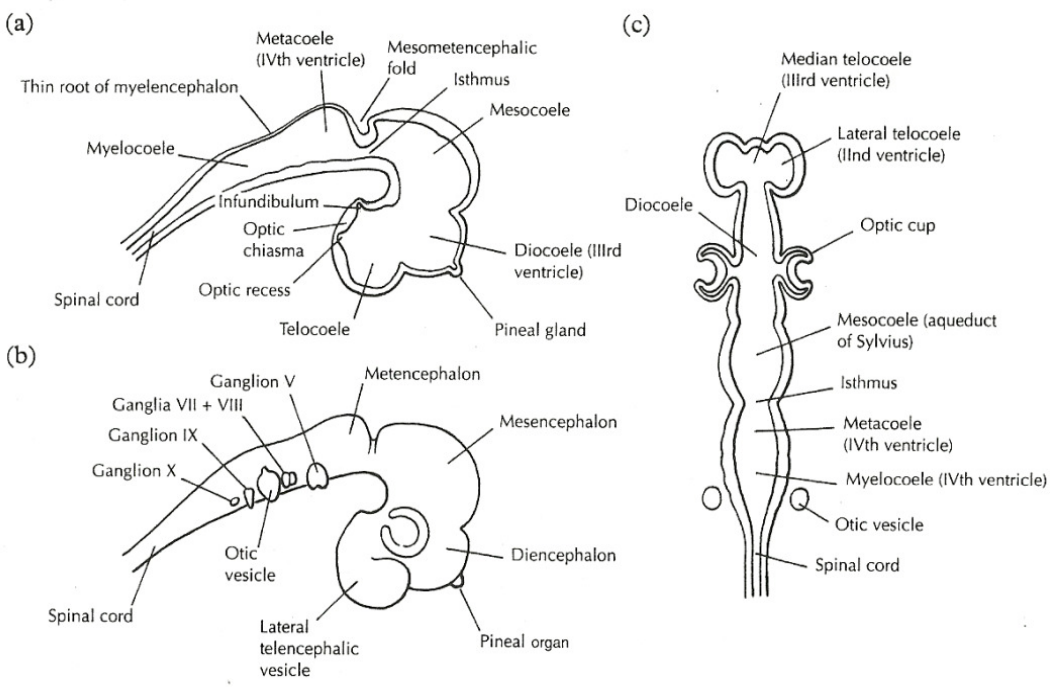

Figure 2.5: Diagrams of the developing brain at day 4. (a) Sagittal section. (b) View of the brain from the right side. (c) Schematic representation of the frontal section plan (Bellairs and Osmond, 1998).

2.5.2. Liver

The developing liver areas are closely located to that of the heart and are thus known as the cardio-hepatic regions. At stages 4-5 these organs lie on either side of the anterior end of the primitive streak, also known as Hensen's node. Here the liver is formed from both mesoderm and endoderm. At stage 12 the endoderm, derived from the diverticulum, is found in the floor of the anterior intestinal portal. During stage 14 the endoderm invades the mesoderm and forms the matrix of the liver (Bellairs and Osmond, 1998). The mesoderm forms part of the ventral mesoderm, which itself is derived from the splanchnic mesoderm and is present as a large patch extending to about the level of the fifteenth somite (Bellairs and Osmond, 1998). During stages 15-17, the anterior diverticulum has moved over the ductus venosus and lies in the left side of it and the posterior part lies on the right (Bellairs and Osmond, 1998). After stage 8, the ectoderm is induced by the mesoderm of the hepatic-cardiac region and forms the hepatic mesenchyme that leads to the formation of the hepatic cords (Bellairs and Osmond, 1998).

2.5.3. Kidneys

The kidneys develop from the intermediate mesoderm. The kidneys start to appear and develop with the somites, but do not extend into the region of the postcloacal tail. The intermediate mesoderm becomes a thick band that is known as the nephrogenous mesenchyme or nephrogenic cord that extends down the trunk (Bellairs and Osmond, 1998). The nephrogenous mesenchyme or nephrogenic cord is the precursor for the non-functional posteriorly situated pronephric kidneys, which are followed by the more posteriorly located mesonephric kidneys. These are mostly active throughout the embryos life. They develop into the final metanephric kidneys that are fully functional by day five (Bellairs and Osmond, 1998).

Both kidneys are supplied with an excretory duct that is known as the pronephric duct in the early stages when the pronephros are developing and in the later stages as the mesonephric duct when the mesonephros are developing. In some instances this duct is also referred to as the nephric duct for both early and late stages of development (Bellairs and Osmond, 1998). After the first thirty hours the nephric duct is visible and lengthens in the next thirty hours and will fuse with the cloaca. After the nephric duct has reached the cloaca the development of the metanephros can start. Before the metanephros develops the metanephric duct is formed and is later known as the ureter. The metanephric kidneys are formed from the metanephric ends, nephrogenous mesenchyme and partly from the metanephric duct. The mesenchyme part is responsible for the development of the renal corpuscles, the proximal and distal tubules and the loop of Henle and the capsule and stroma of the metanephric kidney. The metanephric duct is responsible for the formation of the collecting tubules and ureter (Bellairs and Osmond, 1998).

By day 11, the development of the metanephric kidneys is completed and will begin its excretion function. The glomeruli blood supply comes from the segmental branches of the dorsal aorta (Bellairs and Osmond, 1998). The metanephric kidneys in adult birds are different from the mammal kidneys as they have three lobes, are elongated and do not have the characteristic “kidney-shape”. The kidneys are also on the same antero-posterior level and the loop of Henle is not as well developed as in mammals (Bellairs and Osmond, 1998).

2.6. Normal human embryo development

2.6.1. Brain

Embryology

At the third week the central nervous system (CNS) appears as a slipper-shaped plate of thickened ectoderm, the neural plate, in the mid dorsal region in front of the primitive node (Sadler, 2010). The lateral edges of the neural plate elevates and forms the neural folds which will continue to elevate to finally meet in the midline and fuse to form the neural tube. The fusion of the neural folds starts in the cervical region and proceeds in the cephalic and caudal directions. The open ends of the neural tube form the cranial and caudal neuropores. The neuropores are the channels of communication with the over-lining amniotic cavity. The cranial neuropore will close at day 25 and will start to close cranially from the initial closure site in the cervical region. The caudal neuropore will close at about day 28 in the cranial direction till it reaches the cervical portion of the neural tube (Sadler, 2010). In the cephalic region of the neural tube, three swellings known as primary brain vesicles can be observed: the prosencephalon, mesencephalon and rhombencephalon (Fig. 2.6). Together with the vesicle formation, two flexures simultaneously form. They are termed the cervical flexure, which is situated at the junction of the rhombencephalon and the spinal cord, and the cephalic flexure that is found in the mesencephalon region (Sadler, 2010).

At five weeks the prosencephalon can be divided into two parts, the telencephalon, that forms the cerebral hemispheres and the lateral vesicles, and the diencephalon that will form the thalamus, hypothalamus and the third ventricle (Fig. 2.6) (Jacobs, *et al.*, 2006; Sadler, 2010). The rhombencephalic isthmus is a deep furrow that separates the mesencephalon and the rhombencephalon from each other (Fig. 2.6). The rhombencephalon also consists of two parts that are separated by the pontine flexure (Fig. 2.6). The two parts consists of the metencephalon that ultimately forms the pons, cerebellum and contains the fourth ventricle, and the myelencephalon that will form the medulla oblongata (Fig. 2.6) (Jacobs, *et al.*, 2006; Sadler, 2010).

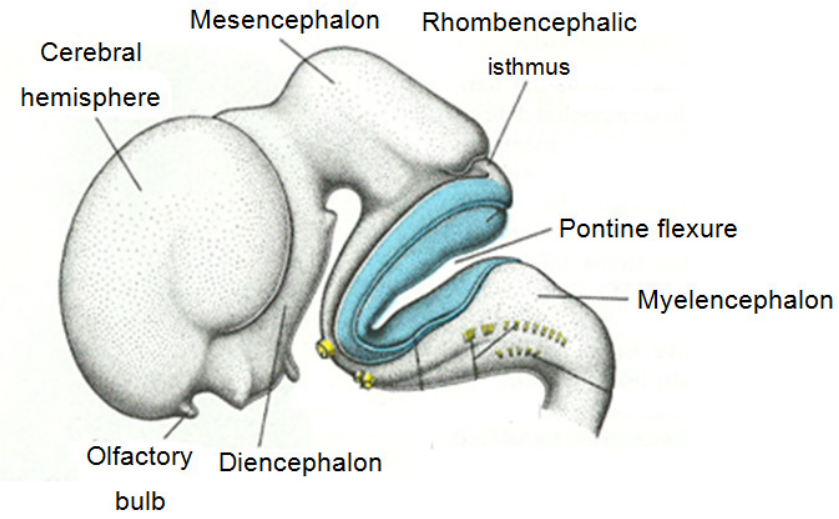

Figure 2.6: Lateral view of the brain vesicles and flexures (modified from Sadler, 2010).

Histology

The precursor nerve cell, the neuroblast, develops exclusively by division of the neuroepithelial cells. The neuroblast originally has a dendrite that extends into the lumen but when they migrate into the mental layer, the processes disappear and the neuroblast is temporarily round and apolar (Sadler, 2010). When the neuroblast differentiates further, two processes appear on either side of the cell body and create the bipolar neuroblast. One of these processes will elongate and form the primitive axon while the other process will develop a number of cytoplasmic arborizations and will form the primitive dendrites. The neuroblast is now known as a multipolar neuroblast and with further development it becomes the adult neuron (Sadler, 2010).

The other major cells that develop from the neuroepithelial cells are the majority of the primitive supporting cells, the gliablasts (Sadler, 2010). The production of the gliablasts only starts when the neuroblast production stops, thus neurogenesis occurs early in gestation and gliagenesis in late gestation (Ernst, *et al*., 2011; Sadler, 2010). After the gliablast is formed by the neuroepithelial layer, it migrates to the mantle and marginal layers. In the mantle layer the gliablasts differentiate into protoplasmic and fibrillar astrocytes (Sadler, 2010). These astrocytes are found between the blood vessels and neurons and provide support and have metabolic functions. Another type of supporting cell is the oligodendroglial cell that forms the myelin sheaths around the ascending and descending axons in the marginal layer. The third and final type of gliablast cell is the microglial cells. They are highly phagocytic cells and originate from the vascular mesenchyme when the blood vessels grow into the nervous system (Sadler, 2010).

2.6.2. Liver

Embryology

The fetal liver has important synthetic and haematopoietic functions and undergoes dramatic histological changes during the third trimester of gestation (Ernst, *et al*., 2011). In humans the liver starts to develop in the third and fourth week of development and commences from two primordia. The cranial portion of the hepatic diverticulum forms an outgrowth of the foregut endothelium, which invades the septum transversum that causes the mesodermal plate to separate the embryonic thoracic and abdominal cavities (Ernst, *et al*., 2011). These endothelial cells will differentiate into the hepatocytes (liver cells). The hepatocytes will ultimately make up 70% of the cells that are found in the liver (Ernst, *et al*., 2011). The caudal portion of the hepatic diverticulum will form the extrahepatic biliary tree and ventral pancreatic anlage and does not invade the septum transversum. The Kupffer cells, stellate cells and haematopoietic cells develop from the mesoderm of the septum transversum (Ernst, *et al*., 2011; Sadler, 2010).

The hepatoblasts (precursor of the hepatocyte) proliferate within the septum transversum. They organize in cords around the developing sinusoids derived from branches of the vitelline veins that penetrate the septum transversum (Ernst, *et al*., 2011). The liver development is regulated by an array of molecules. The foregut endoderm has the potential to express liver-specific genes and thus develop into liver tissue, but is blocked by inhibitors that are secreted by the neighbouring mesoderm, ectoderm and notochord. Hepatic development is stimulated by the secretion of fibroblast growth factor 2 (FGF2) by the cardiac mesoderm and bone morphogenetic proteins (BMPs) that are secreted by the septum transversum. The BMPs enhance the competence of prospective liver endoderm to respond to FGF2 (Sadler, 2010). Once the cells in the future hepatic region receive the “instruction” from the FGF2 and BMPs, the cells differentiate into both hepatocytes and biliary cell lineages (Sadler, 2010).

Histology

During prenatal development and for a few months postnatal, the early hepatocyte cords that develop around the sinusoids remain thick. At five months postnatal there is thinning to two-cell trabeculae and at five years of age the hepatocytes adopt the single-cell architecture of the adult liver. Ultrastructurally the rough endoplasmic reticulum (rER) and peroxisomes are easily seen by the seventh and eighth week respectively. During the third month, when bile formation starts, the Golgi apparatus moves from the perinuclear to the pericanalicular zone (Ernst, *et al*., 2011). The Kupffer cells are present in large numbers in the sinusoids after

thirty days of gestation. In the liver haematopoiesis starts during the sixth and seventh weeks of gestation and the haematopoietic activity increases dramatically through to twenty weeks of gestation (Ernst, *et al*., 2011). The haematopoietic activity of the liver decreases between 24-32 weeks of gestation, as the bone marrow becomes hematopoietic. After birth the haematopoiesis in the liver ends (Ernst, *et al*., 2011).

2.6.3. Kidney

Embryology

The urinary system develops from the intermediate mesoderm along the posterior abdominal wall of the embryo. In the human embryo, there are three overlapping urinary systems that develop, namely the pronephros, mesonephros and the metanephros (Jacobs, *et al*., 2006). The pronephros is non-functional and consists of 7-10 segmentally arranged cell clusters in the cervical region. The cranial cell groups are known as the nephrotomes, where the more caudally unsegmented masses are called the nephrogenic cords. The nephrotomes grow laterally and develop a lumen, where the lateral end of each nephric tubule grows caudally to join up with the next nephric tubule. The fusion of all the tubules develops a longitudinal duct on the lateral side. The medial end of the nephric tubules is invaginated by a small branch of the dorsal aorta (Jacobs, *et al*., 2006). By the end of the fourth week the pronephros system is no longer visible.

The mesonephros system develops from the intermediate mesoderm at the thoracic and upper lumbar regions during the regression of the pronephric system. During this time the nephric tubules lengthen and will form the S-shaped loops and tubules by the seventh week that will differentiate into the excretory units (Jacobs, *et al*., 2006). The metanephros will develop into the permanent kidney by the fifth week of gestation. The ureteric bud arises from the distal mensonephric duct close to its entrance into the cloaca. The ureters, renal pelvis, minor and major calyces and the collecting ducts will develop from the ureteric buds (Ernst, *et al*., 2011; Sadler, 2010). The blind end of the ureteric bud will dilate by the end of the fifth week, to form the primitive renal pelvis. It will then split into cranial and caudal parts, which will form the major calyces and will penetrate the metanephric tissue (Ernst, *et al*., 2011; Jacobs, *et al*., 2006). The major calyces will then subdivide until twelve or more generations of tubules are formed (Leonard, *et al*., 2004). The second order will enlarge to absorb the third and fourth generations and thus form the minor calyces. The fifth and successive generations of tubules will elongate and converge in the minor calyces and will form the renal pyramids (Jacobs, *et al*., 2006; Sadler, 2010).

At the distal end of the newly formed collecting ducts it is covered by a metanephric tissue cap. The metanephric tissue cap will form a small vesicle called the renal vesicles. The vesicles will give rise to the S-shaped tubules and will ultimately form the nephrons (Ernst, *et al*., 2011; Jacobs, *et al*., 2006; Sadler, 2010). In the eighth week, the first generation consisting of eighteen nephrons is complete. By the end of the eighth week, the characteristic histology of each part of the nephron is well developed, recognizable and some renin activity has begun (Ernst, *et al*., 2011).

Histology

The fetal kidney histology differs remarkably from the adult kidney. This is mostly due to the fact that the kidney continues to develop until the end of gestation, when nephrogenesis comes to an end (Ernst, *et al*., 2011). The kidneys also continue to mature during infancy and childhood. When not familiar with these differences it may lead to mistakenly considering normal findings as pathological ones, or to overlooking abnormalities of renal development (Ernst, *et al*., 2011).

The human kidney is divided into lobes, that consist of a medullary pyramid and is surrounded by a cortex. The nephrons are formed in the nephrogenic zone that is located on the most outer portion of the cortex. The glomeruli develop in layers with the oldest or first formed glomeruli situated on the inner cortex and with the last formed glomeruli in the outer cortex, just under the nephrogenic zone. It is presumed that developmental disturbances can be calculated by studying if the abnormalities involved the entire cortex (early event) or just the outer cortex (late event) (Ernst, *et al*., 2011). The stages (as described above) can be observed in the nephrogenic zone until 36 weeks of gestation. When the glomeruli are formed, they resemble the adult glomeruli, but are smaller. The podocytes also have a cuboidal appearance and will flatten out during the first year of life (Ernst, *et al*., 2011). The tubules of the nephrons can be easily recognized in early development. The proximal convoluted tubule (PCT) is situated directly under the S-shaped bodies and displays its characteristic deep eosinophilic cytoplasm. The juxtaglomerular apparatus develops very early in gestation, because the renin-angiotensin system plays a vital role in kidney development (Ernst, *et al*., 2011). This system's activity is high during development but declines during postnatal maturation. The juxtaglomerular apparatus is not easily identified on routine sections of fetal kidneys but with immunocytochemistry, renin expression can be demonstrated. The loops of Henle are relatively short in the fetus, but will lengthen after birth (Ernst, *et al*., 2011).

2.7. Teratogenic effects

Cadmium

In many animal species, Cd has no known physiological function and exposure to this metal threatens biological systems in various ways (Cullinane, *et al*., 2009). Cd toxicity is known to cause teratogenic effects in many animal species including rats, mice, hamsters, frogs and chickens, as Cd can be transported across the placental membrane at low levels (Nordberg, *et al*., 2007b). The effects of Cd differ between species according to the dose administered, the method in which the Cd was administered and the stage of embryogenesis (Thompson and Bannigan, 2008). Some alterations that occur when chick embryos are exposed to Cd include abnormal positioning of the limbs and alterations on the ventral body wall due to an abnormality in the direction of growth of the lateral plate mesoderm; neural tube and somites alterations caused by abnormal cell growth (Cullinane, *et al*., 2009; Thompson, *et al.,* 2005; Thompson and Bannigan, 2008; Yamamoto, *et al*., 2012).

Chromium

In previous animals studies it was recorded that Cr is able to move through the placenta and affects the embryo, but the mechanism by which it is transported through the placental membrane is still unknown (Langård and Costa, 2007). In an *in ovo* study researchers found that Cr caused a high incidence of malformations in the chick embryos. Some malformations that were observed included reduced body weight, microphthalmia, short and twisted limbs, ectopic heart, and everted viscera, with a lower occurrence in the controls than in the experimental animals (Langård and Costa, 2007). Cr(VI) can cause lung toxicity, bronchial asthma, nephro- and hepatotoxicity and is also able to affect the brain (Quinteros, *et al*., 2007). Although many animal studies have been done on the teratogenic effects of Cr, no teratogenic effects have been associated with human exposure to Cr (Dayan and Paine, 2001).

Although some studies have shown the teratogenic effects of these metals in chick embryos, very little information is available on the ultrastructural effects of these metals on different organ systems. Furthermore, little is known about the combinational effects of these heavy metals, where possible synergism can amplify/enhance toxicity.

2.8. Aims and objectives

The aim of this study was to investigate the cellular effects of the heavy metals Cd and Cr alone and in combination at different concentrations, on chick embryos by using light- and transmission electron microscopy (TEM) as well as to determine the glutathionine depletion and DNA damage in brain tissue by using the GSH assay and electrophoresis respectively.

Objectives:

1. Establishment of a chick embryo model exposed to the heavy metals Cd and Cr at different concentrations alone and in combination.
2. Histological and ultrastructural analysis of possible alterations in the brain by using light microscopy and TEM.
3. Histological and ultrastructural analysis of possible alterations in the liver by using light microscopy and TEM.
4. Histological and ultrastructural analysis of possible alterations in the kidneys by using light microscopy and TEM.
5. Determine the possible accumulation of heavy metals in above-mentioned organs by using energy dispersive spectroscopy (EDS) and electron energy-loss spectroscopy (EELS).
6. Test GSH depletion on brain tissue by using the GSH reductase assay, which indicates an increase in oxidative damage.
7. Evaluate the DNA damage in the brain tissue by performing DNA agarose gel electrophoresis and evaluate blood smears for the possible presence of micronuclei by using light microscopy.

Chapter 3

Establishment of the *in ovo* model

3.1 Introduction

The chicken (*Gallus gallus*) embryo or *in ovo* model is an extremely useful model in studying embryology and teratology (Drake, *et al*., 2006). The *in ovo* model is a model that utilizes fertilized chicken eggs for testing the effects of possible teratogens amongst others. It is such a great source of embryos that it attracted the attention of the Egyptians and even Aristotle (Stern, 2005). The *in ovo* model was used for the discovery of the functional differences between arteries and veins in 1628 by William Harvey (Harvey, 1628). Between 1672 and 1675 Marcello Malpigi discovered the existence of the neural tube, somites and that the embryonic heart starts to beat before the blood cells are formed, with the help of the *in ovo* model (Malpighi, 1672; Malpighi, 1675). At the end of the 19th century, Wilhelm Roux and his colleague realized that when development is disrupted it can provide more information about the developmental potential in an embryo (Roux, 1888). Although many discoveries have been made with the use of the chick embryo model, it's most momentous contributions have been made in the fields of virology, cancer and immunology with the isolation of the first cellular oncogene from chicken cells, the discovery of reverse transcriptase and the discovery of the T- and B-lymphocytes (Stern, 2005).

In more recent studies, the *in ovo* model has been extensively used to test many possible teratogens. Some of these include Valproic acid, Suramin and electromagnetic fields (Lahijani and Ghafoori, 2000; Männer, *et al.,* 2003; Whitsel, *et al*., 2002). Valproic acid is an anti-epileptic medication which has been studied since 1980 for its human teratogenic effects. The results of the study showed increased mortality, growth delay and anomalies similar to what was found in humans (Whitsel, *et al*., 2002). In the study with Suramin, a well-known chemotherapy drug, it was found that the Suramin is a potent teratogen. Some of its teratogenic effects include caudal dysgenesia, median facial clefts and malformations of the aortic arch arteries (Männer, *et al.,* 2003). In the study done by Lahijani and Ghafoori in 2000, the effects of electromagnetic fields were tested on chick embryos. The eggs were exposed to 24 different electromagnetic fields at 50 Hertz, 24 hours after the eggs were laid. The results showed that the electromagnetic fields caused irreversible developmental alterations to the chick embryos (Lahijani and Ghafoori, 2000).

The *in ovo* model has also been successfully used to study the teratogenic effects of heavy metals. Studies done on heavy metals, like cadmium (Cd), chromium (Cr), lead and

platinum, using the *in ovo* model have shown a wide range of teratogenic effects that include gross malformations, cellular and biochemical changes, that emphasise the importance of ensuring that these metals are not released into the environment (Asmatullah and Shakoori, 1998; Gagnon and Patel, 2007; Lee, *et al.,* 2002; Thompson and Bannigan, 2001). In South Africa these metals are unfortunately present in the water near mines (Binning and Baird, 2001; Cawthorn, 2010; Fatoki and Awofolu, 2003). People in the rural communities living near these mines are at risk for the toxic effects of these metals, with pregnant women and the developing fetuses being the most vulnerable. These communities are exposed to heavy metals by ingestion of contaminated water; be it by drinking the water, preparing food in it or irrigating crops with it (Awofolu, *et al*., 2005). In the South African context Cd and Cr were identified as two of the most common heavy metal contaminants that are present in the environment.

In this study the *in ovo* model was used to investigate the effects of two heavy metals Cd and Cr alone and in combination. In the current chapter the effect of these metals on embryo viability and weight changes in an established *in ovo* model are depicted.

3.2 Materials and methods

3.2.1 Obtaining fertilized eggs

Fertilized broiler hatching eggs were obtained from a local farmer in the Bronkhorstpruit district in Gauteng, South Africa. A total number of 225 eggs were obtained (15 eggs per group). Ethical clearance for the use of chick embryos for experimental purposes was obtained from the Animal Ethics Committee (AEC) of the University of Pretoria (ethical clearance number: h006-13). The eggs were incubated at 37ºC for two days before exposure.

3.2.2 Exposure

On the third embryonic day, the eggs were removed from the incubator and placed in an air-controlled, aseptic flow hood, where each egg was marked according to its exposure (Table 3.1). The blunt end (air chamber) of the eggs was then sterilized by wiping the eggshells with 70% ethanol, before a small hole was drilled with a sterile pair of scissors, without puncturing the underlying membrane. To increase the size of the hole, sterile needles and forceps were used to lift up pieces of the egg shell in order for the pipette tip to fit through (Fig. 3.1 A).

The embryos were exposed to the specific concentrations of the experimental groups by injection into the eggs, through the air sac onto the chorioallantoic membrane (CAM), by using a calibrated micropipette (Fig. 3.1 B). The experimental groups included three control groups and 12 groups exposed to different dosages of the two heavy metals used in this study as indicated in Table 3.1. The heavy metals were administered as $CdCl_2$ [Merck (Pty) Ltd, South Africa] and $K_2Cr_2O_7$ [Merck (Pty) Ltd, South Africa] dissolved in sterile water. The reason for including three different control groups was to ensure that the technique employed does not influence the results obtained. The first control group (Control 1) was uncompromised, in the second control group (Control 2) a hole was drilled with no injection and in the third control group (Control 3) sterile water was administered. The heavy metals were administered at physiological dose (PD), 10x, 100x and 1000x PD alone and in combination.

Table 3.1: Control and experimental group dosages

Group	Exposure (µM metal ion)
Control 1	-
Control 2	-
Control 3	ddH_2O
Cd PD	0.430µM
Cd x10 PD	4.30µM
Cd x100 PD	43.0µM
Cd x1000 PD	430µM
Cr PD	0.476µM
Cr x10 PD	4.76µM
Cr x100 PD	47.6µM
Cr x1000 PD	476µM
Cd + Cr PD	0.430µM and 0.476µM
Cd + Cr x10 PD	4.30µM and 4.76µM
Cd + Cr x100 PD	43.0µM and 47.6µM
Cd + Cr x1000 PD	430µM and 476µM

The Cd and Cr concentrations were calculated according to the human physiological dose [Cd: 30µg (Nordberg, *et al*., 2007b) and Cr: 284.28µg (Langård and Costa, 2007)] and were then downscaled to still be a physiologically appropriate concentration for the embryos. This was achieved by dividing the human PD of the respective heavy metals with the average weight of an adult human (70kg), where after it was multiplied by the average weight of a chick embryo (8.605g-obtained from the pilot study). The amount was then calculated to

g/50µℓ as this was the administered volume and then calculated for each of the concentrations.

After the heavy metal administration, the holes were sealed with paraffin wax (Fig. 3.1 C and D) and were then returned to the incubator for eleven days. The covering of the holes with the wax was localized to reduce the risk of the wax blocking the air pores and impeding gas exchange. The eggs were then placed apical side down in the incubator and tilted by lifting one side of the egg carton and then alternate between sides three times a day, until day fourteen.

3.2.3 Termination

On day fourteen, the eggs were removed from the incubator and the shells were cracked at the top with a spatula and peeled off to the edge of the air sac using forceps. The forceps were then used to peel off the CAM to expose the embryo. The embryo was lifted from the egg with a spatula and placed in a Petri dish containing Hank's balanced salt solution (HBSS) (Fig. 3.1 E).

The chick embryos were weighed and any morphological abnormalities were documented. Brain, liver and kidney samples were then harvested and processed for the glutathione (GSH) assay, DNA agarose gel electrophoresis, light microscopy and transmission electron microscopy (TEM) as will be described in the chapters to follow.

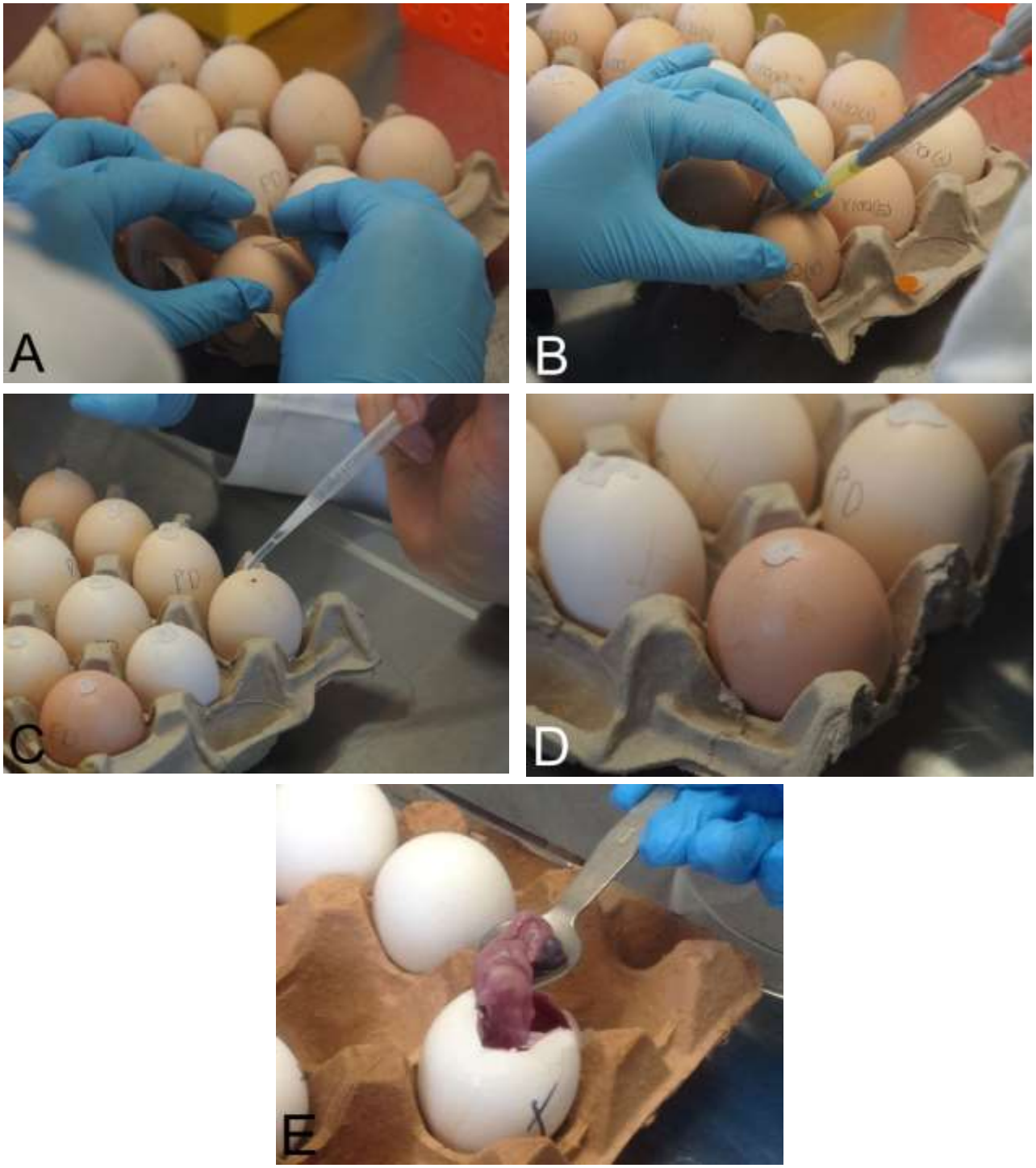

Figure 3.1: Exposure and termination of chick embryos. A: a needle is used to increase the size of the hole; B: Administration of water and/or heavy metal; C and D: sealing with paraffin wax; E: removing the embryo on the day of termination.

3.3 Results

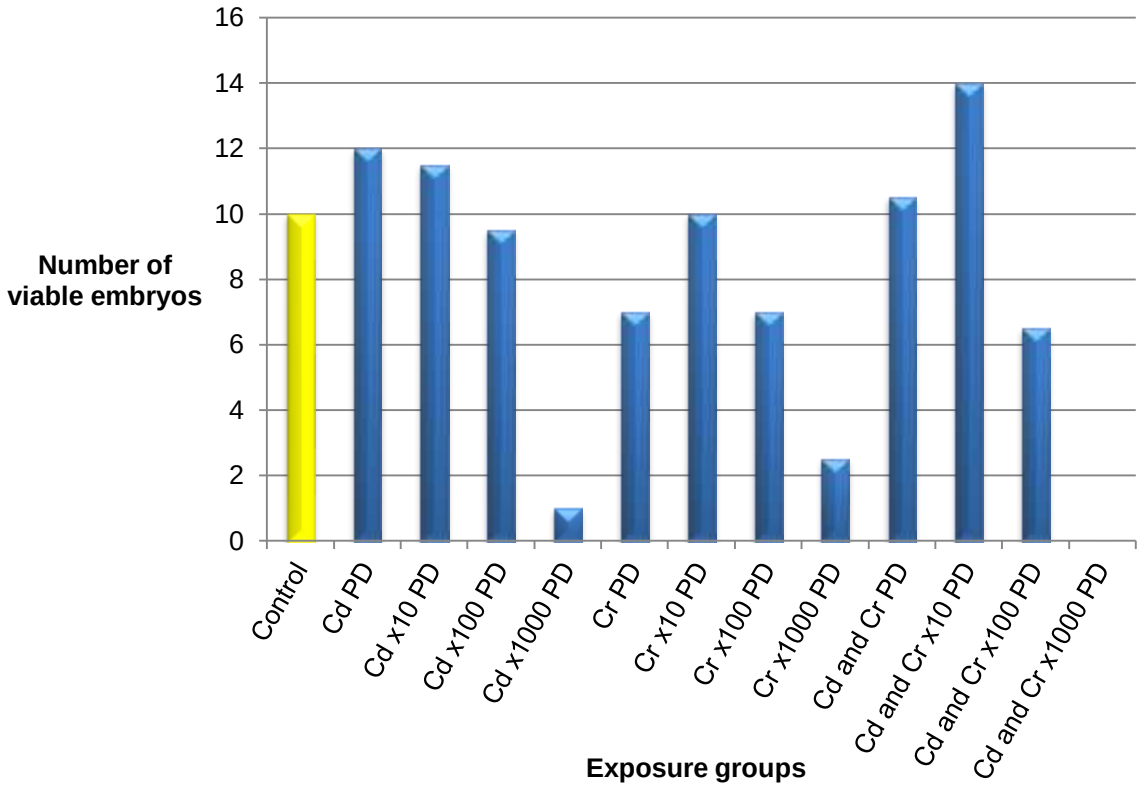

Figure 3.2: Survival rates of the chick embryos

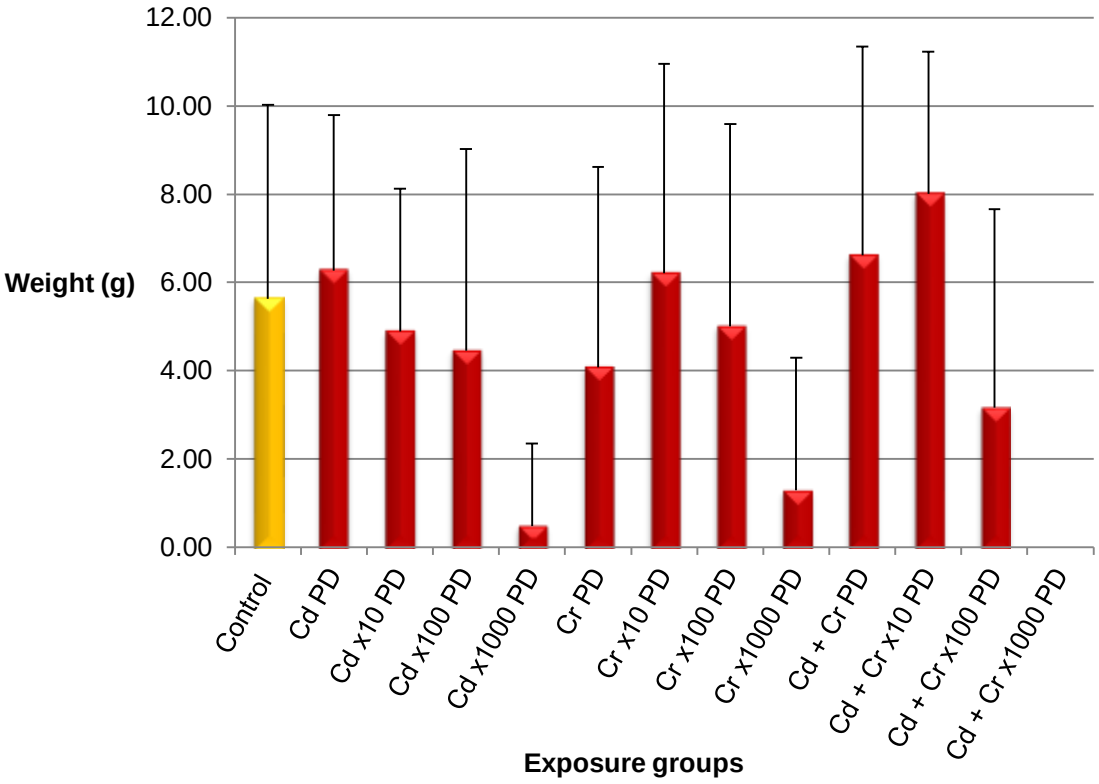

Figure 3.3: Weight averages of chick embryos (Erro bars: Standard deviation)

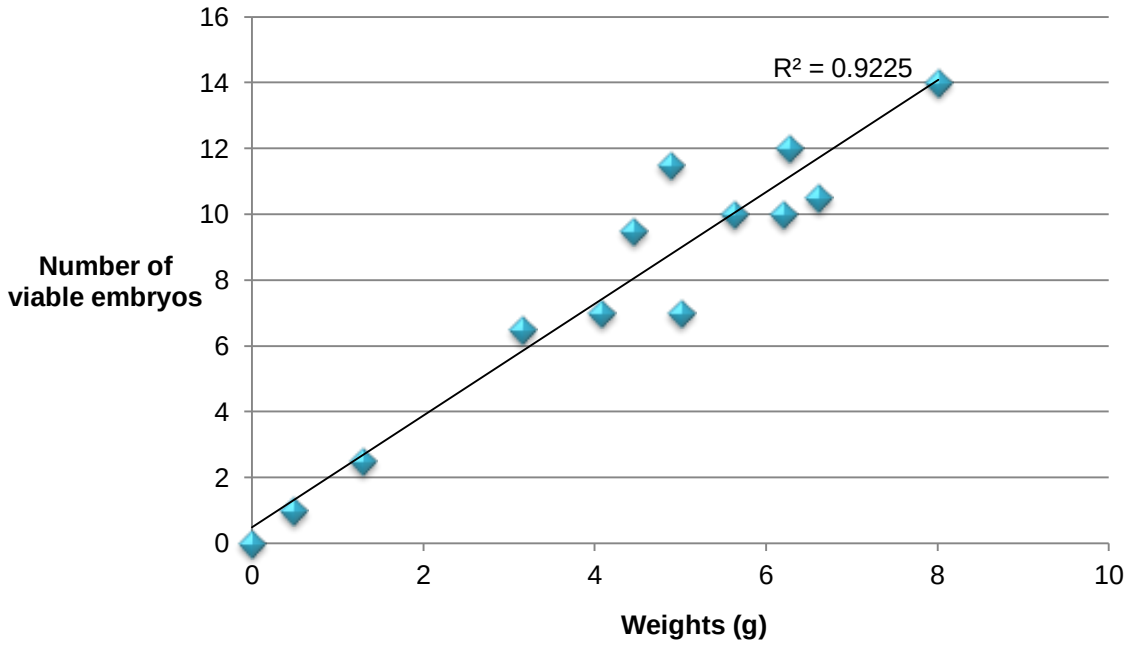

Figure 3.4: Correlation between chick embryo survival rates and weights

Figure 3.2 depicts the survival rates of the control and exposed embryos, with clear differences seen between the different experimental groups. The Cd experimental group revealed a decline in survival rate with increasing concentrations, with the Cd PD and Cd x10 PD group's survival rates being above the controls survival rates and the Cd x1000 PD group showing a sharp decrease in survival rate. The Cr experimental group's survival rates are either equal to or below the control survival rates, with the Cr PD showing the same survival rate as the Cr x100 PD and the Cr x10 PD showing an increase in the survival rate compared to the Cr PD and Cr x100 PD groups. The Cr x1000 PD group showed a definite decrease in the survival rate. The same trend is seen in the metal combination groups, as the Cd and Cr x10 PD group's survival rate is higher than those of the combined PD and x100 PD groups, with no x1000 PD metal combination group chick embryos surviving. In Figure 3.3 (weights with standard deviation) the same trend is seen in the weights of the embryos and Figure 3.4 supports the correlation between the two graphs with a R^2 value of 0.9225.

3.4 Discussion

The *in ovo* model was utilized in this study as it is an excellent model to obtain stable and uncontaminated samples. The exposure times of the chick embryo chosen in this study, correlates with crucial embryonic development not only in the chick, but also in human embryonic development. The Cd experimental groups showed an expected decrease in the

survival rates with an increase in Cd concentration, with a sharp decrease in survival rate seen at the highest Cd concentration. The Cr and metal combination groups showed a different pattern than the Cd survival rates, as there is an increase in the x10 PD groups before the expected decrease of the survival rates is observed. Also, a strong correlation was observed between the weights of the embryos and the survival rates. Similar results were obtained in studies done by Damelin, *et al*., Heinz, *et al.* and Stebbing where this phenomenon is described as hormesis, a term first used by Schulz in 1888 (Damelin, *et al*., 2000; Heinz, *et al*., 2012; Schulz, 1888; Stebbing, 1982). Hormesis is defined as the dose response to an environmental agent that is firstly stimulated by the environmental toxin at a low dose and then at a high dose an inhibitory effect is observed (Mattson, 2008). This explains the sudden and unexpected increase in the survival rates of the embryos at x10 PD, followed by the expected decrease in embryo survival rates.

3.5 Conclusion

The *in ovo* model was an excellent model to use in this study as it created a stable and controlled environment to conduct experiments. The *in ovo* model ensures precise targeted exposure that reduces the chance for environmental interference and allows for exposure at specific developmental stages that is crucial for evaluating the possible teratogenic effects of these metals on the chick embryos on the day of termination (Drake, *et al*., 2006). This model is relatively easy to perform and is a great initial model to use for evaluating the effects of a possible teratogen. With the survival rates and weights of the chick embryos, Cd revealed an expected decrease; with Cr and the metal combination groups first showing an increase at the x10 PD exposed groups, where after a decrease was also observed. The initial increase and then decrease in survival rates, termed hormesis, was also observed by other research groups (Damelin, *et al*., 2000; Heinz, *et al.*, 2012). They found that exposure of mallard eggs and mouse cell cultures to methylmercury, cadmium and cupric chloride, showed results where at a low concentration the toxic substance stimulates growth, activity or survival of the organisms before a decline is observed (Damelin, *et al*., 2000; Heinz, *et al.*, 2012).

The chick embryo model was successfully implemented in the current study and the results obtained will further support the effectiveness of this model.

Chapter 4

Investigating changes in the brain, liver and kidneys of chick embryos exposed to Cd and Cr alone and in combination by using light microscopy

4.1. Introduction

In this chapter we investigated the effects of cadmium (Cd) and chromium (Cr) alone and in combination on the brain, liver and kidney tissue of chick embryos using light microscopy. The organs used in this study were chosen based on the specific functions of these organs. The liver and kidneys were chosen based on the fact that they are respectively the main detoxification and filtering systems in the body and by protecting the body against toxic substances, they cause damage to their own cells (Coetzee, *et al.*, 2009). The brain was chosen based on its possible lack of defence mechanism, as the blood brain barrier (BBB) of embryos are not as well developed as in adults and this can allow unwanted particles to infiltrate the brain tissue (Nordberg, *et al.*, 2007b). Since this chapter involves light microscopic information, the normal histology of the brain, liver and kidney will be explained, in conjunction with the criteria used to evaluate the alterations caused by the metal toxicity.

The normal brain histology comprises of two types of cells, namely neurons and their supporting cells. Neurons consist of a cell body, where the nucleus and organelles can be found, with two types of processes that arise from the cell body, known as dendrites and axons. The neurons are classified into two types according to their shape, size and axon length, where type I neurons are large and have a long axon and type II have a smaller neuron with a short or absent axon (Coetzee, *et al.*, 2009). Four neuroglial cells namely the oligodendrocytes, astrocytes, microglial and ependymal cells are found and are mainly supporting cells of the central nervous system but also perform other functions (Coetzee, *et al.*, 2009). The brain tissue was evaluated for metal toxicity by screening for cytoplasmic vacuolization and necrotic neuronal cells. Cytoplasmic vacuolization occurs, according to Sherlock and Doely (Sherlock and Doely, 1993), because of an increase in intercellular water due to membrane damage and subsequent membrane permeability caused by reactive oxygen species (ROS) (Sherlock and Doely, 1993). Necrosis was evaluated not only in the brain, but also in the liver and kidney, as Cd and Cr induces ROS that influences the organs through specific biochemical pathways that ultimately cause necrosis (Leonard, *et al.,* 2004; Méndez-Armenta and Ríos, 2007). Necrosis is indicated by cell swelling, vacuolation, karyolysis and cell contents release (Jaeschke, *et al.,* 2004).

When observing normal liver histology, it mainly consists of hepatocytes that are arranged into thin plates and separated by fine vascular sinusoids the walls of which consist of fenestrated endothelium and Kupffer cells (Coetzee, *et al*., 2009; Young, *et al*., 2006). The sinusoids allow for absorption of nutrients from digestion as well as secretion of products into the blood (Young, *et al.,* 2006). Between the sinusoid and hepatocyte, the space of Disse is found. The liver criteria used for possible liver metal intoxication was an increase in the sinusoidal space and necrosis (Coetzee, *et al*., 2009). The sinusoidal widening observed might be the result of an increase in lipid peroxidation caused by the Cd and Cr intoxication, but another feasible explanation can be that the sinusoidal widening may be due to the activation of the Kupffer cells, as activation of these cells will lead to the release of a number of inflammatory mediators like cytokines, adhesion molecules, chemokines and cytotoxic molecules or radicals. This cascade of cellular and hormonal responses will cause inflammation and further damage to the liver (Koyu, *et al.,* 2006; Rikans and Yamano, 2000).

Normal kidney histology, important for this chapter, includes the renal capsule and the proximal- and distal convolutes tubules (DCT). The renal capsule consists mainly of the oval shaped double-walled Bowman's capsule that surrounds the capillaries of the glomerulus. Between the glomerulus and Bowman's capsule, Bowman's space can be found and is continuous with the proximal convoluted tubule (PCT) (Coetzee, *et al*., 2009). The glomerular capillaries are fenestrated and are surrounded by a thick basal lamina. The PCT and DCT consist of distinctive cuboidal cells. The nuclei of the cuboidal cells of the PCT are situated near the base of the cell with a well-developed brush border on the luminal surface. The DCT cuboidal cells are smaller, with larger lumens than the PCT cells. No brush border is present on the luminal surface of the DCT and due to the smaller size of the cells the nuclei are situated closer to each other (Coetzee, *et al*., 2009). The criteria for evaluating changes in kidney morphology of the Cd-exposed groups included dilation of the glomerulus, thus reducing Bowman's space, apoptosis or necrosis and hypertrophy of the renal tubular cells (Brzóska, *et al.,* 2003; Jihen, *et al*., 2008). Unlike the criteria for evaluation of the glomeruli in the Cd-exposed groups, the Cr-exposed groups were evaluated based on the contraction of the glomerulus and thus an increase in Bowman's space, where the rest of the criteria is the same as mention above (Mishra and Mohanty, 2008). Dilation of the glomeruli may be caused by the hypertrophy of the epithelial cells found in the glomerulus (Aughey, *et al*., 1984), whereas contraction of the glomerulus may be caused by glomerular atrophy (Kajikawa, *et al.,* 1981; Kirubagaran and Joy, 1988).

4.2. Materials and methods

4.2.1. Tissue for light microscopy

Samples were obtained as described in Chapter 3.

4.2.2. Paraffin wax embedding

The harvested brain tissue was cut into ±0.5mm^3 samples and fixed in 2.5% glutaraldehyde (GA)/formaldehyde (FA) (1mℓ of 25% GA, 1mℓ of 25% FA, 5mℓ phosphate (PO_4) buffer (0.15M), 3mℓ ddH_2O) for an hour, rinsed three times in 0.075M PO_4 buffer (pH=7.4) for 15 minutes each before the tissue samples were dehydrated in 30%, 50%, 70%, 90% and three changes of 100% ethanol. The tissue was left in the 100% ethanol overnight. The next day the tissue was placed in 50% xylene in ethanol for thirty minutes and then in 100% xylene for two hours. After the xylene the tissue was placed in the first wax solution, containing 30% wax in xylene for an hour at 60ºC followed by a 70% wax solution in xylene for an hour. The samples were then transferred to a 100% wax solution for two hours at 60ºC. In the final step the tissue were placed in a steel mould, filled with wax and a marked grid were placed on top. The moulds with the grids were then placed on a cooling plate to allow the wax to cool and harden. Sections of 3-5µm were made with a Leica RM 2255 wax microtome.

4.2.3. *tert*-Butyl alcohol wax embedding

The liver and kidney tissue were fixed in 2.5% GA/FA (1mℓ of 25% GA, 1mℓ of 25% FA, 5mℓ PO_4 buffer (0.15M), 3mℓ ddH_2O) for an hour, rinsed three times in 0.075M PO_4 buffer (pH=7.4) for 15 minutes each before the tissue samples were dehydrated in 30%, 50%, 70%, 90% and three changes of 100% ethanol.. The tissue samples were then left overnight in 100% ethanol. The next day the liver and kidney samples were placed in *tert*-Butyl alcohol (TBA) for 2 days, renewing the TBA three times a day. After the two days, wax pellets were added to create a 50:50 mixture. The samples were then placed in an oven at 60ºC for two days, renewing the TBA-wax mixture three times a day. The TBA-wax mixture was followed by a 100% wax solution for a day at 60ºC, where after the samples were placed in a steel mould, filled with wax and a marked grid was placed on top. The moulds with the marked grids were then placed on a cooling plate to allow the wax to cool and harden. Sections of 3-5µm were made with a Leica RM 2255 wax microtome. The TBA wax embedding was done since previous experiments in our laboratory revealed that the normal paraffin wax

embedding (explained in section 4.2.2) resulted in irregular sectioning of the liver and kidney samples due to impaired infiltration of the tissue.

4.2.4. Haematoxylin and Eosin staining

Haematoxylin and Eosin (H&E) staining was done to evaluate general tissue morphology. To achieve this, slides with the sections were cleared in xylene for five minutes to remove the paraffin wax. The slides were then placed in a series of descending ethanol concentrations to rehydrate the tissue. The series started with placing the slide twice in 100% ethanol for two minutes, then the slides were placed in 90% ethanol for a minute and then in 70% ethanol for another minute. Before the slides were placed in the haematoxylin for five minutes it was rinsed in ddH_2O for a minute. The haematoxylin is used to stain the cell nucleus, RNA-rich portions of the cytoplasm, like the ribosomes and rough endoplasmic reticulum (Jacobs, *et al.*, 2006) in the cells. After the haematoxylin staining, the slides were rinsed with tap water and then placed into the Scott's blue buffer solution for five minutes, this changes the reddish-purple colour of the haematoxylin into a purple-bluish colour (Ernst, *et al.*, 2011). The tissue was then dipped in acidic ethanol where after it was counterstained by leaving it in eosin for five minutes, which stains the cytoplasm and collagen, pink (Coetzee, *et al.*, 2009). After the eosin, the tissue was dipped in a series of ascending ethanol concentrations (70%, 90% and 100% ethanol) to dehydrate the tissue and ensure that excess dye is removed. Finally the slides are dipped in xylene before the coverslip is mounted using entellen. The slides were viewed with a Nikon Optiphod transmitted light microscope.

4.3. Results

4.3.1. Brain tissue

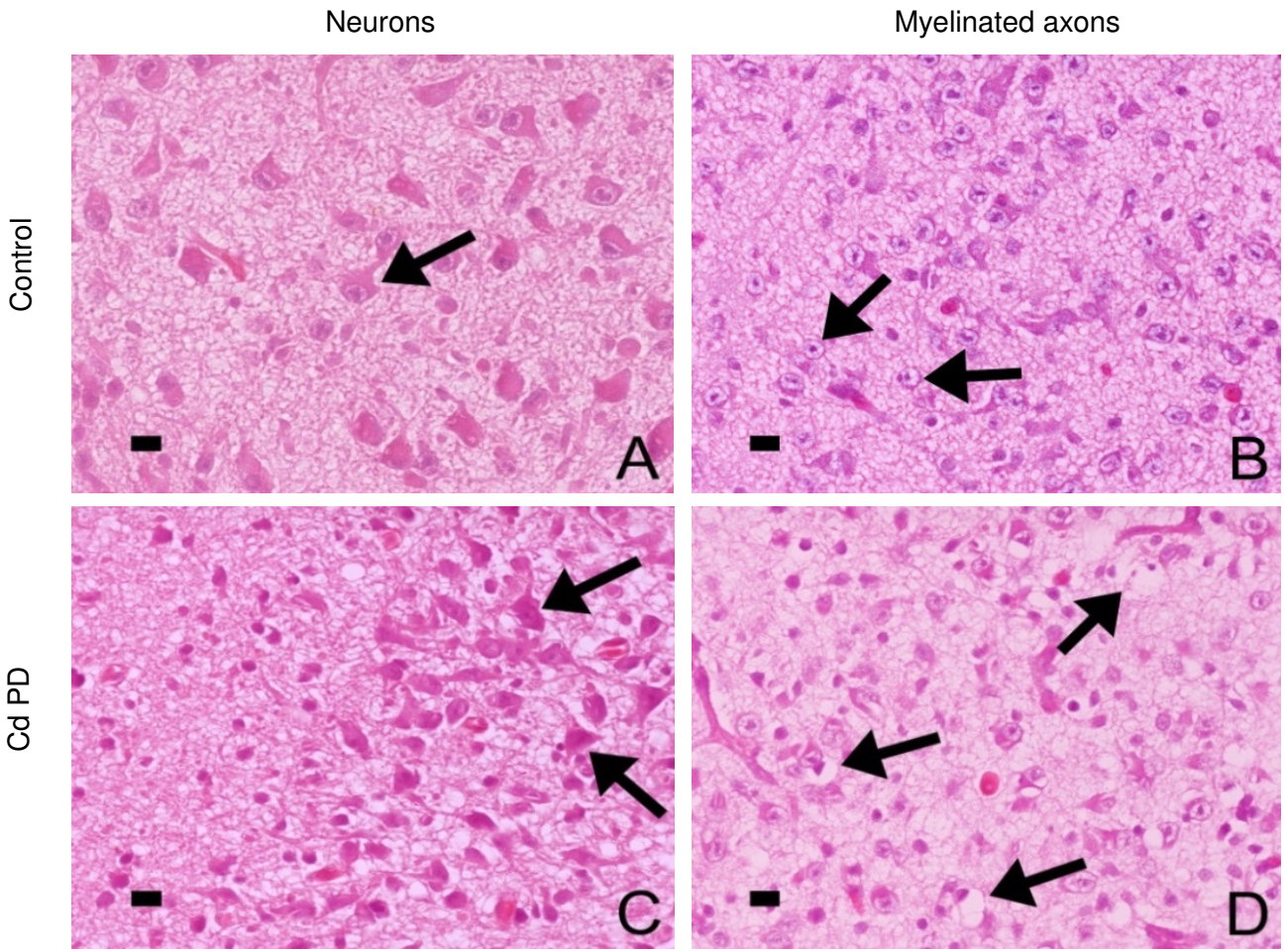

Figure 4.1: Light microscopy micrographs of the brain tissue from the control and Cd groups. Figure A and B (control) indicate normal neurons (arrows) and myelinated axons (arrows), respectively. Figure C and D indicates the Cd PD group, with Figure C showing unaltered neurons (arrows), with no chromatin condensation present. Figure D indicates the cytoplasmic vacuolization observed in the myelinated axons (arrows) (Scale bars: 10µm).

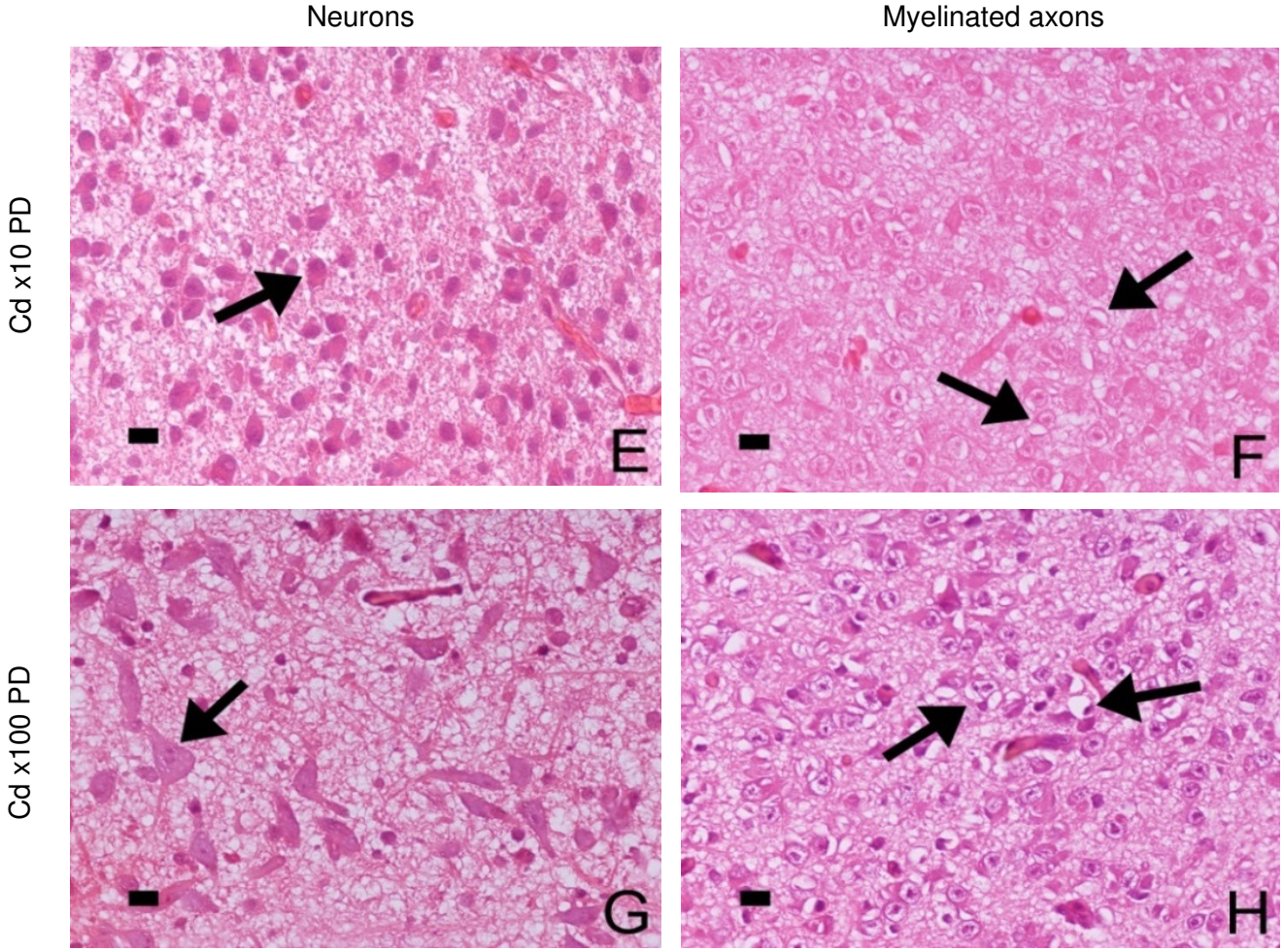

Figure 4.1 continued: Light microscopy micrographs of the brain tissue from the control and Cd groups. Arrows in Figures E (Cd x10 PD) and G (Cd x100 PD) indicate normal neurons, with slight nuclear damage observed in Figure G (arrow). Figures F (Cd x10 PD) and H (Cd x100 PD), indicate cytoplasmic vacuolization present in the myelinated axons (arrows) (Scale bars: 10µm).

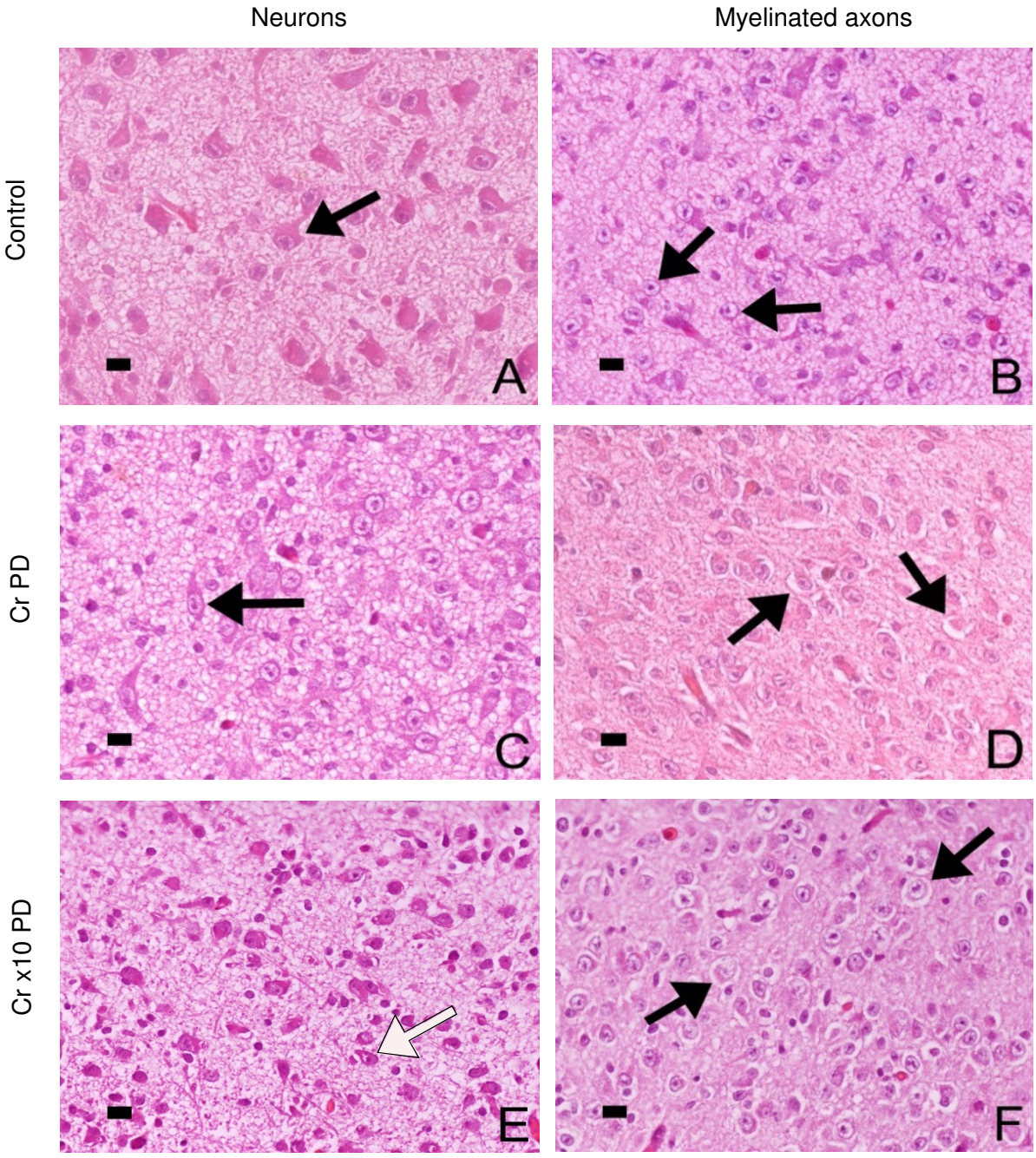

Figure 4.2: Light microscopy micrographs of the brain tissue from the control and Cr groups. Figures A (Control) and C (Cr PD) indicate the normal, unaltered neurons (black arrows) and E (Cr x10 PD) indicates the chromatin condensation found in the nuclei of the neurons (white arrow). Figures B (Control) show normal myelinated axons, with Figures D (Cr PD) and F (Cr x10 PD) indicating cytoplasmic vacuolization observed in the myelinated axons (arrows). (Scale bars: 10µm).

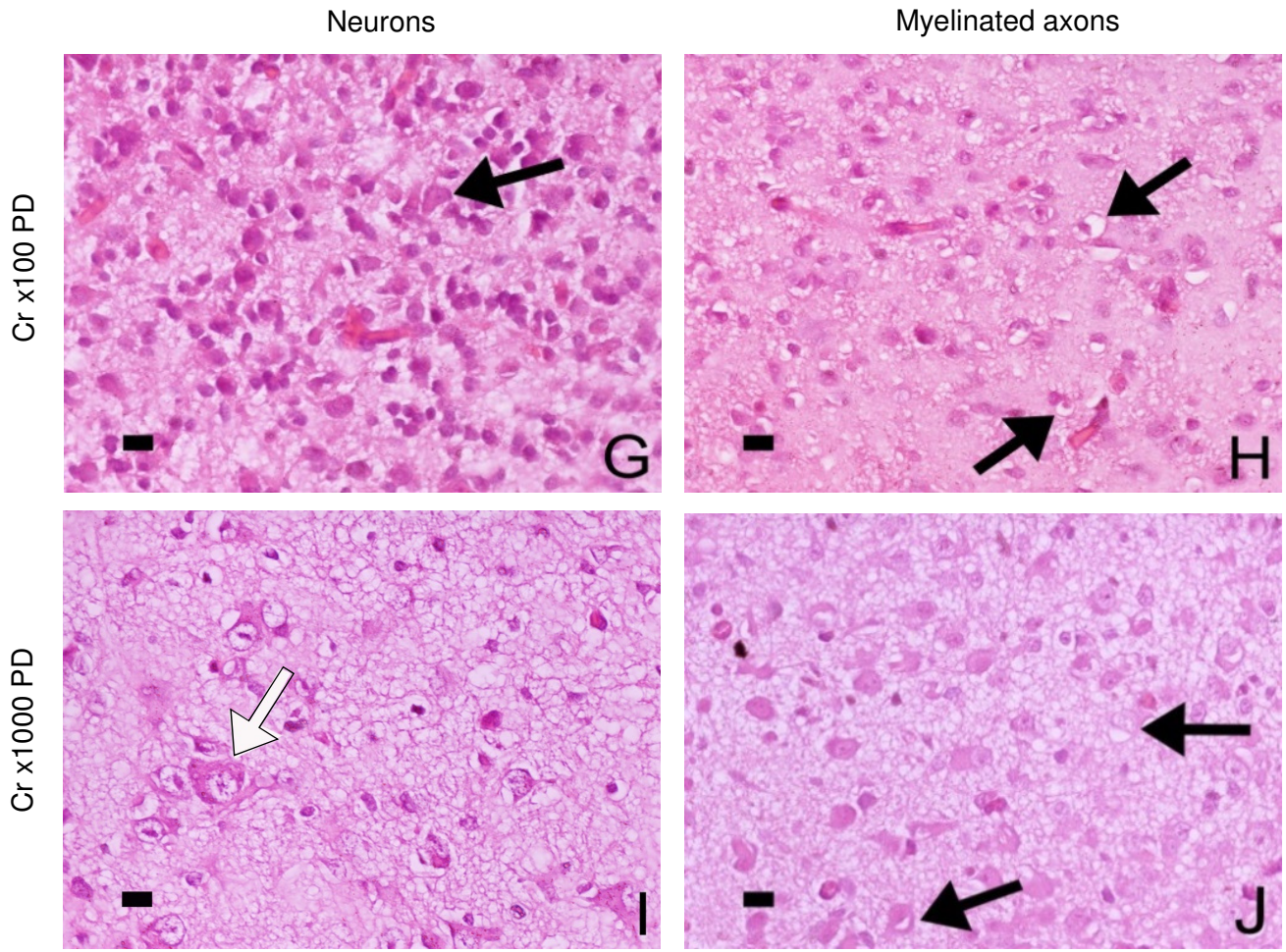

Figure 4.2 continued: Light microscopy micrographs of the brain tissue from the control and Cr groups. Figure G (Cr x100 PD) indicates the normal neurons (black arrow) and Figure I (Cr x1000 PD) indicates the chromatin condensation found in the nuclei of the neurons (white arrow). Figures H (Cr x100 PD) and J (Cr x 1000 PD) indicate the cytoplasmic vacuolization present in the myelinated axons (arrows) (Scale bars: 10µm).

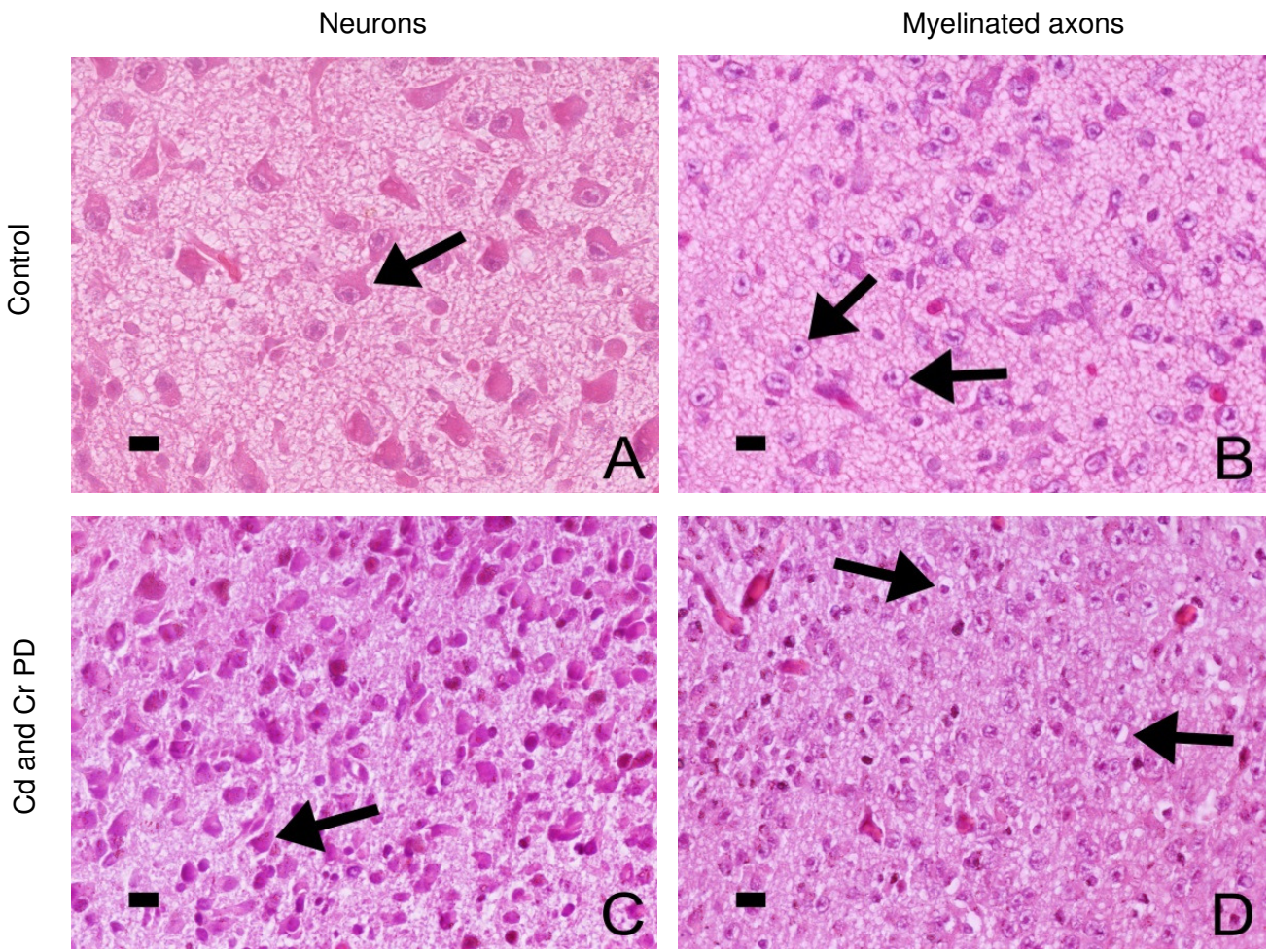

Figure 4.3: Light microscopy micrographs of the brain tissue from the control and Cd and Cr combination groups. Figures A (Control) and C (Cd and Cr PD) indicate the normal neurons (arrows). Figure B (Control) indicates unaltered myelinated axons (arrows), with Figure D (Cd and Cr PD) indicating cytoplasmic vacuolization observed in the myelinated axons (arrows) (Scale bars: 10µm).

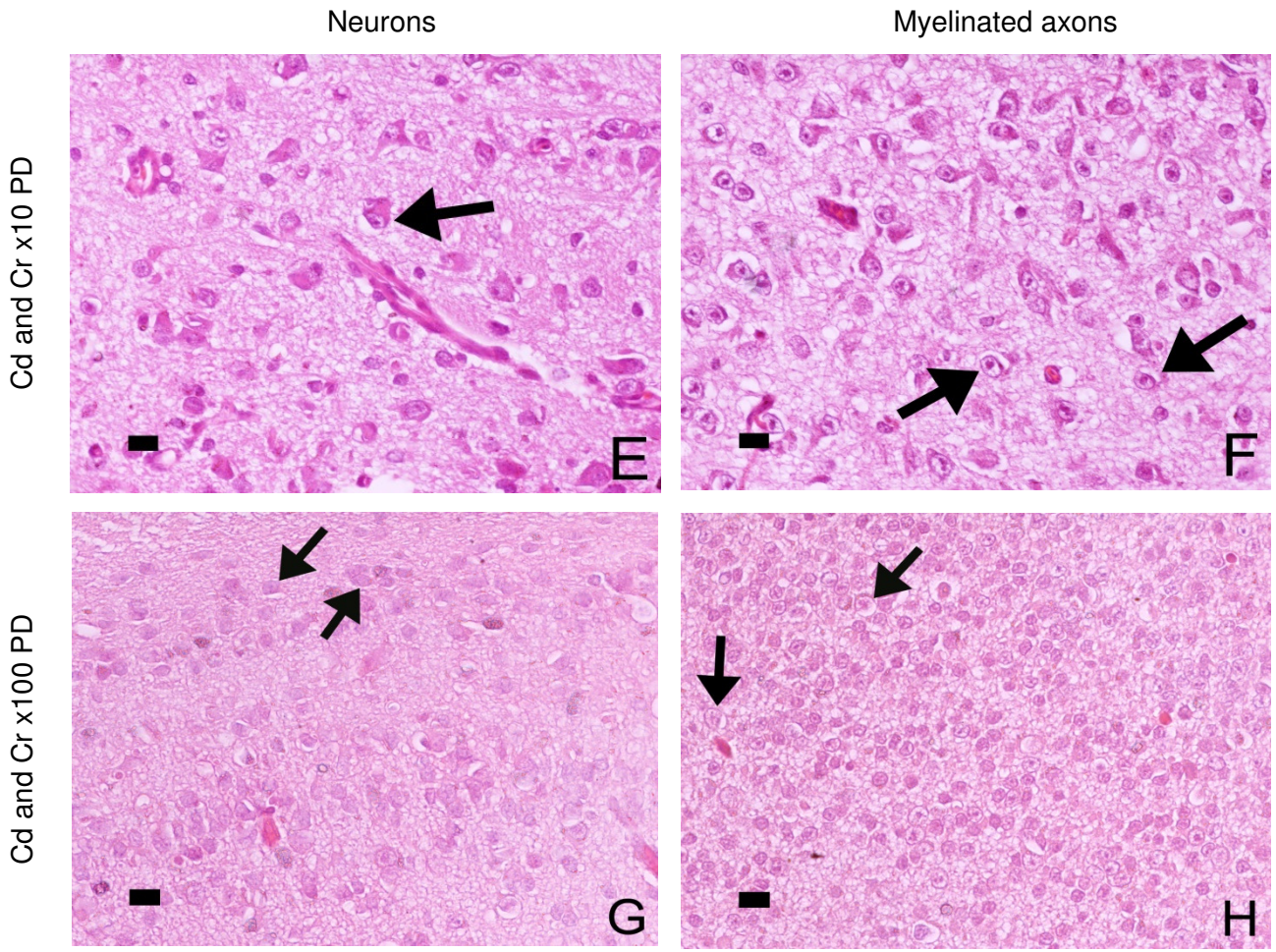

Figure 4.3 continued: Light microscopy micrographs of the brain tissue from the control and Cd and Cr combination groups. Figure E (Cd and Cr x10 PD) shows minimal amounts of chromatin condensation (arrow), with Figure G (Cd and Cr x100 PD) indicating unaltered neurons (arrows). Figures F (Cd and Cr x10 PD) and H (Cd and Cr x100 PD) indicate cytoplasmic vacuolization present in the myelinated axons (arrows) (Scale bars: 10µm).

The normal cellular arrangement of structures in the brain (Fig. 4.1-4.3 A and B), liver (Fig. 4.4-4.6 A and B) and kidney (Fig. 4.7-4.9 A and B) are shown in the control group. These structures were altered in all the experimental groups. The brain tissue was evaluated for necrosis, chromatin condensation and cytoplasmic vacuolization. In the brain tissue from the control animals, neurons [Fig. 4.1-4.3 A (arrow)] and myelinated axons [Fig. 4.1-4.3 B (arrows)] are shown with no alterations seen in these structures. The brain tissue exposed to increasing concentrations of Cd (Fig. 4.1 C-H) showed no chromatin condensation with only slight nuclear damage observed in the Cd x100 PD [Fig. 4.1 G (arrow)]. However, cytoplasmic vacuolization was observed in the Cd PD (Fig. 4.1 D), Cd x10 PD (Fig. 4.1 F) and Cd x100 PD (Fig. 4.1 H) groups. No Cd x1000 PD brain tissue was viable for microscopy use and thus no evaluation was possible. In the Cr exposed groups (Fig. 4.2 C-J) some chromatin condensation were observed in the brain tissue in the Cr x10 PD (Fig. 4.2 E) and Cr x1000 PD (Fig. 4.2 I) groups, with all the Cr experimental groups showing cytoplasmic vacuolization [Fig. 4.2 D, F, H, J (arrows)]. In the metal combination groups there were no noticeable differences observed in terms of chromatin condensation, with only minimal amounts present in the Cd and Cr x10 PD group (Fig. 4.3 E). Cytoplasmic vacuolization was observed in all the Cd and Cr groups [Fig. 4.3 D, F, H (arrows)]. Table 4.1 displays a summary of the histological findings in the brain tissue.

Table 4.1: Summary of histological findings in the brain tissue

Group	Necrosis	Chromatin condensation	Cytoplasmic vacuolization
Control	-	-	-
Cd PD	-	-	++
Cd x10 PD	-	-	+
Cd x100 PD	-	+	++
Cr PD	-	-	+
Cr x10 PD	-	+	++
Cr x100 PD	-	-	++
Cr x1000 PD	-	+	++
Cd and Cr PD	-	-	+
Cd and Cr x10 PD	-	+	++
Cd and Cr x100 PD	-	-	+

-, none; +, minimal; ++, mild; +++, severe

4.3.2. Liver tissue

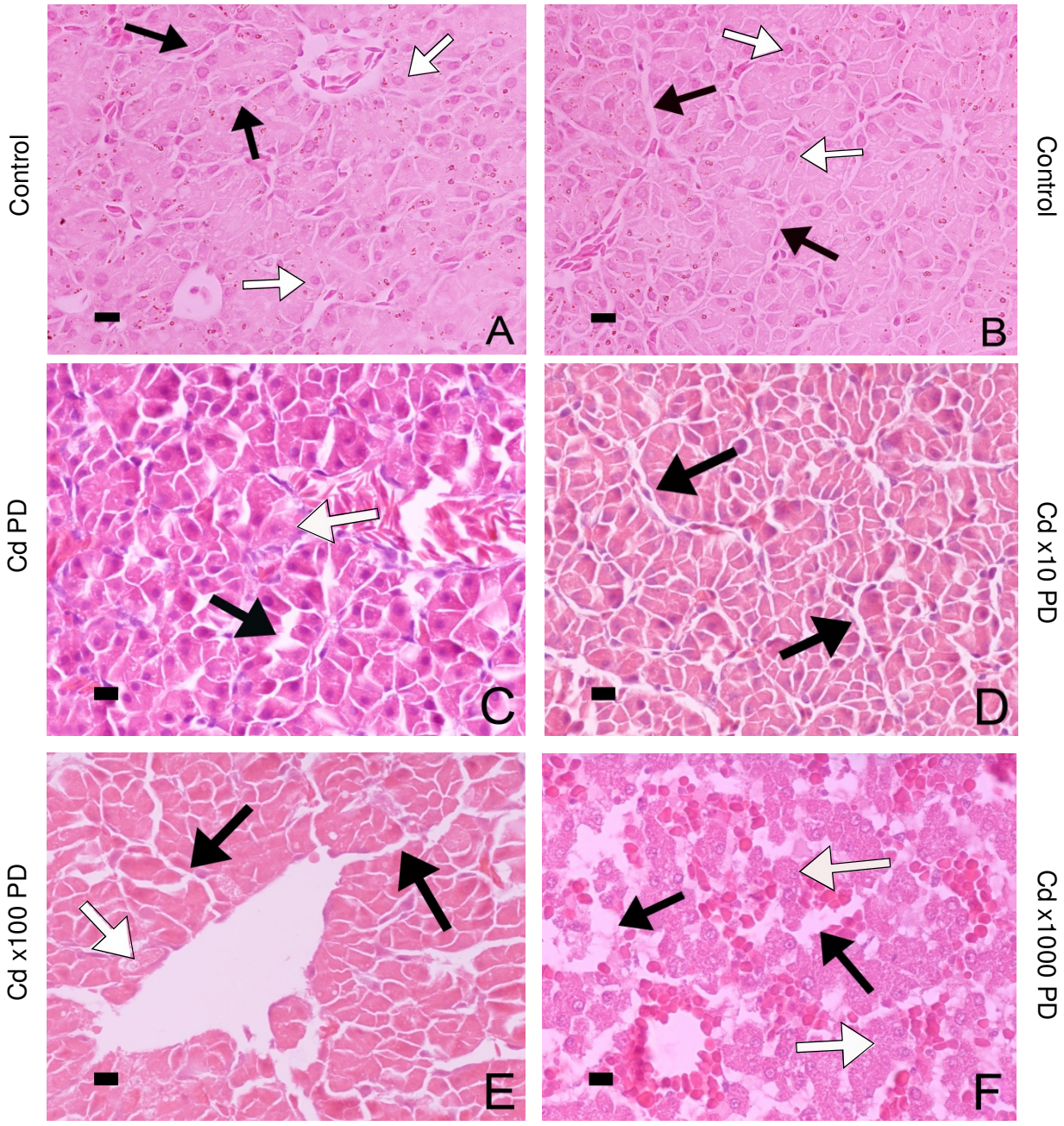

Figure 4.4: Light microscopy micrographs of liver tissue from the control and Cd groups. Figures A and B (Control) indicate normal cellular arrangement of the liver, with the black arrows showing the sinusoids and the hepatocytes are indicated with the white arrows. Figures C (Cd PD), D (Cd x10 PD), E (Cd x100 PD) and F (Cd x1000 PD) show minor sinusoidal dilation (black arrows) and some necrosis (white arrows) (Scale bars: 10µm).

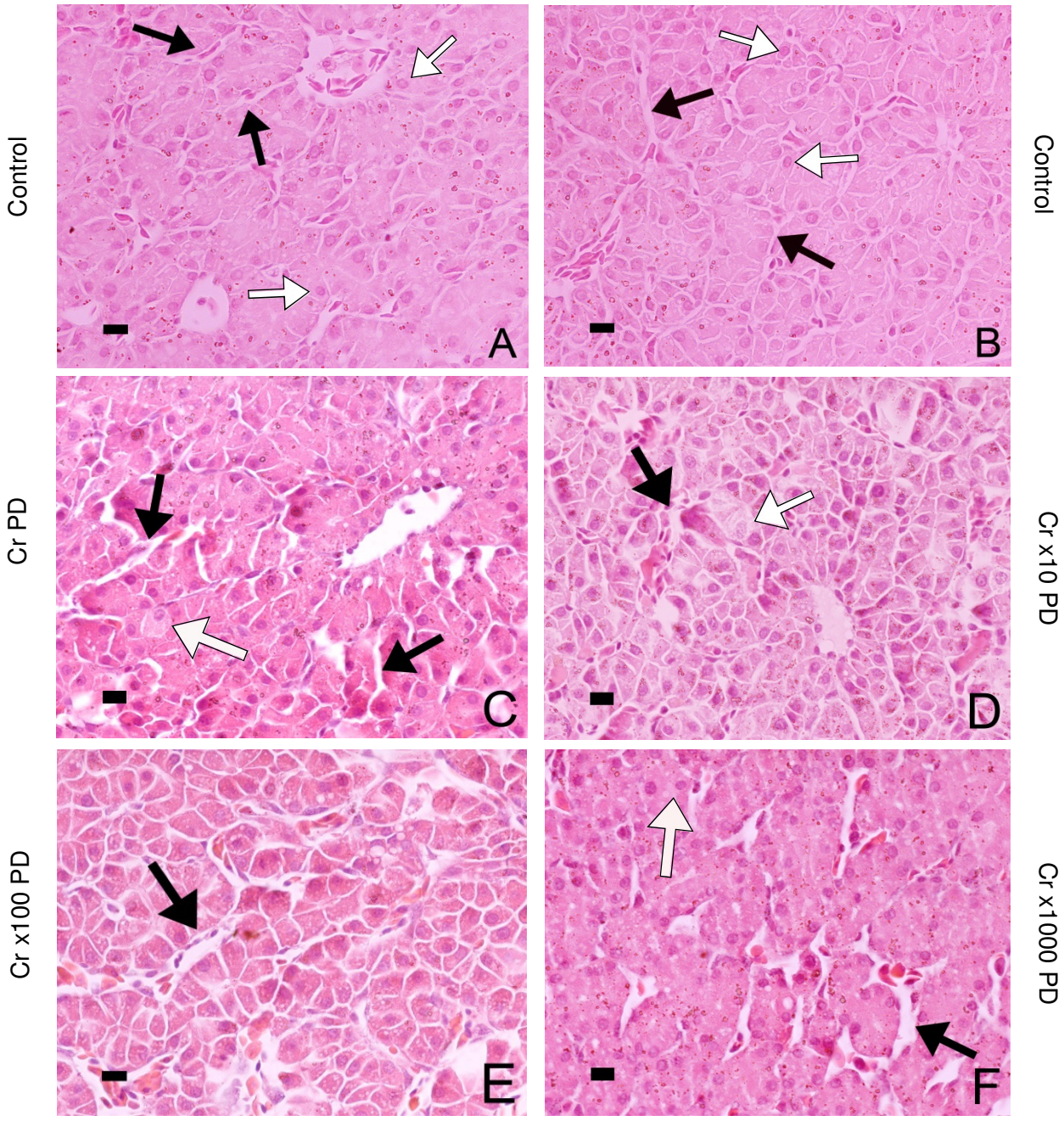

Figure 4.5: Light microscopy micrographs of liver tissue from the control and Cr groups. Figure A and B (Control) indicate normal cellular arrangement of the liver, with the sinusoid indicated by the black arrows and the white arrows showing the hepatocytes. Figures C (Cr PD), D (Cr x10 PD), E (Cr x100 PD) and F (Cr x1000 PD) show the sinusoidal dilation (black arrows) and necrosis (white arrows) observed (Scale bars: 10µm).

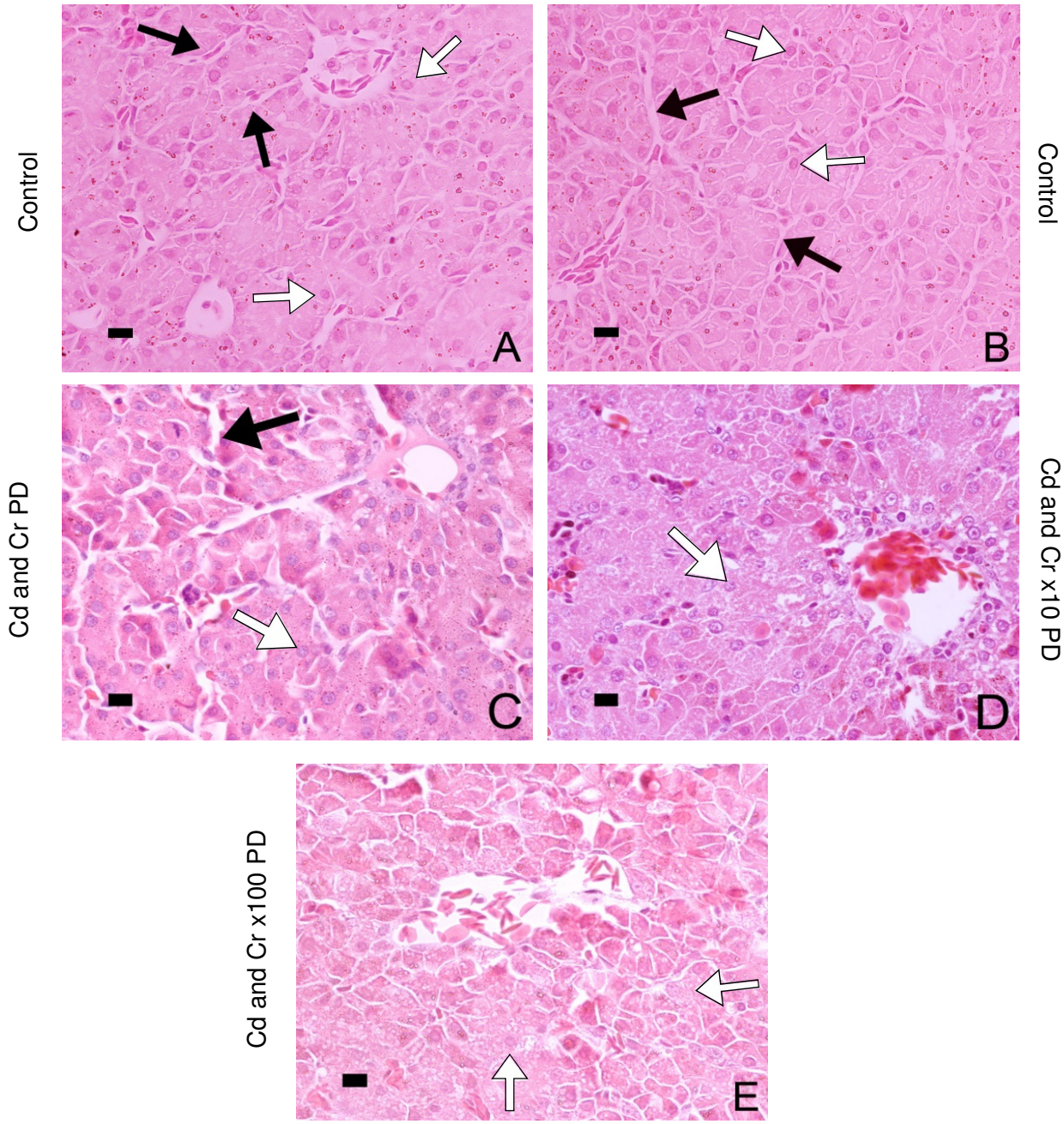

Figure 4.6: Light microscopy micrographs of liver tissue from the control and Cd and Cr groups. Figures A and B (Control) indicate normal cellular arrangement of the liver, with the sinusoid indicated by the black arrows and the white arrows showing the hepatocytes. Figure C (Cd and Cr PD) indicates sinusoidal dilation (black arrow), as well as necrosis (white arrow). Figures D (Cd and (Cr x10 PD) and E (Cd and Cr x100 PD) only indicate necrosis (white arrows) (Scale bars: 10µm).

Alterations in the histology of the liver tissue were found in all the experimental groups, but with nothing observed in the control group (Fig. 4.4 A and B). Figure 4.4 C (Cd PD), D (Cd x10 PD) and E (Cd x100 PD) showed minor sinusoidal dilation (black arrows), with some necrosis (white arrow) present in the Cd PD (Fig. 4.4 C) group. When comparing the Cd x1000 PD (Fig. 4.4 F) to the control and lower Cd concentrations, major differences, such as sinusoidal dilation and severe necrosis, were observed. When comparing the control to the Cr experimental groups, sinusoidal dilation (black arrows) and necrosis (white arrows) were seen in the Cr PD, Cr x10 PD, Cr x100 PD and Cr x1000 PD groups (Fig. 4.5 C-F respectively). This however was not present in the control group. In the metal combination groups, sinusoidal dilation is depicted in Cd and Cr PD [Figure 4.6 C (black arrow)], with necrosis (white arrows) indicated in Figure 4.6 C (Cd and Cr PD), D (Cd and Cr x10 PD) and E (Cd and Cr x100 PD). A summary of the histological findings in the liver tissue is shown in Table 4.2.

Table 4.2: Summary of histological findings in the liver tissue

Group	Necrosis	Sinusoidal dilation
Control	-	-
Cd PD	+	++
Cd x10 PD	-	+
Cd x100 PD	-	+
Cd x1000 PD	++	+++
Cr PD	+	+
Cr x10 PD	+	+
Cr x100 PD	+	+
Cr x1000 PD	+	++
Cd and Cr PD	+	+
Cd and Cr x10 PD	++	-
Cd and Cr x100 PD	++	-

-, none; +, minimal; ++, mild; +++, severe

4.3.3. Kidney tissue

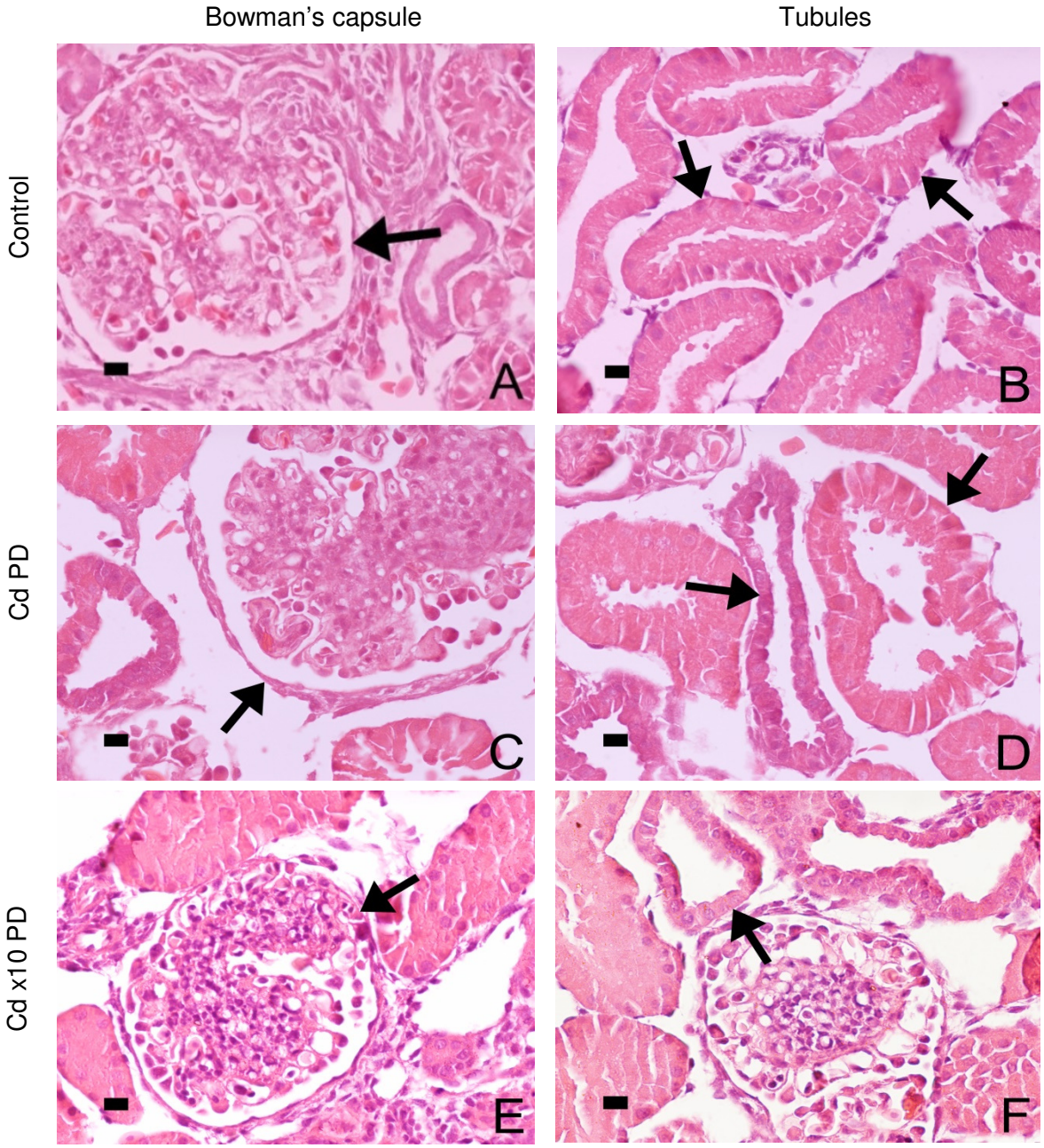

Figure 4.7: Light microscopy micrographs of kidney tissue from the control and Cd groups. Figures A and B (Control) indicate no cellular alterations in the glomeruli (arrow) and renal tubules (arrows), respectively. Figures C (Cd PD) and E (Cd x10 PD) show minimal dilation of the glomerulus in the Bowman's capsules (arrows). Figures D (Cd PD) and F (Cd x10 PD) indicate the kidney tubules (arrows) that show no observable changes (Scale bars: 10µm).

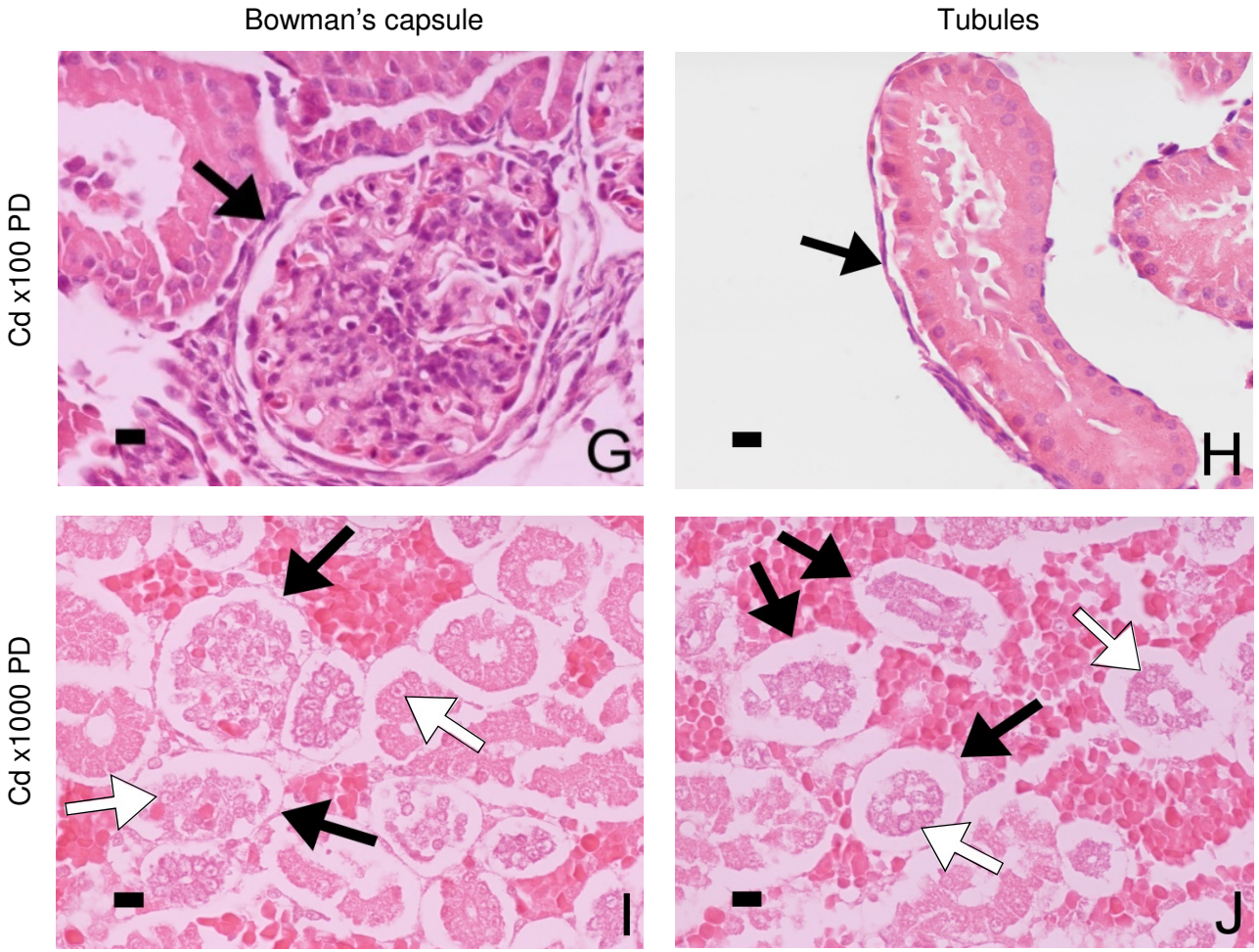

Figure 4.7 continued: Light microscopy micrographs of kidney tissue from the control and Cd groups. Figures G and H (Cd x100 PD) indicate minimal dilation of the glomerulus in the Bowman's capsule (arrow) and no changes in the renal tubules (arrow), respectively. Figure I (Cd x1000 PD) shows atrophy of the glomerulus in the Bowman's capsules (black arrows), with severe necrosis indicated by the white arrows. Figure J (Cd x1000 PD) indicates atrophy of the kidney tubules (black arrows) and severe necrosis (white arrows) (Scale bars: 10µm).

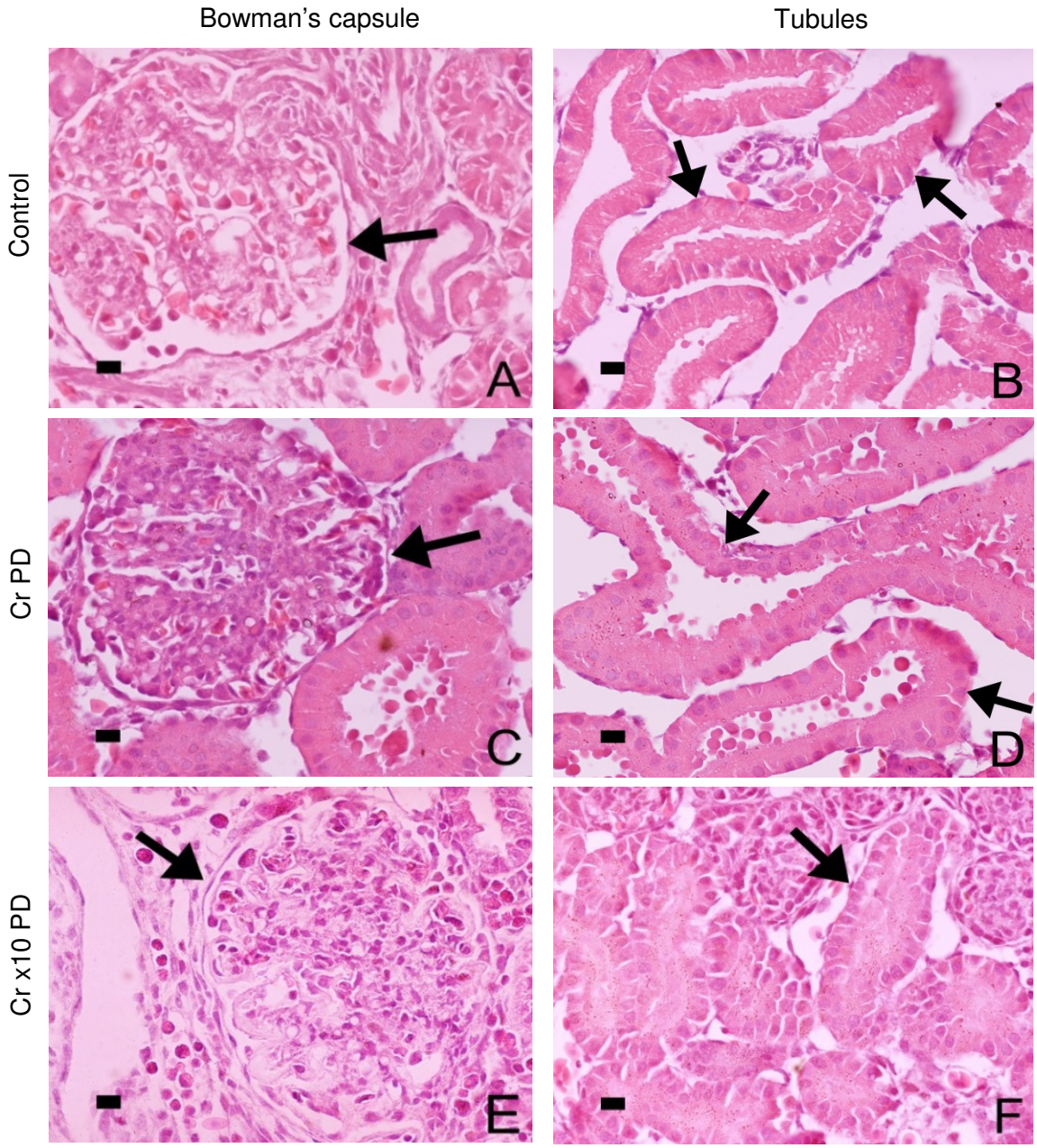

Figure 4.8: Light microscopy micrographs of kidney tissue from the control and Cr groups. Figures A (Control), C (Cr PD) and E (Cr x10 PD) indicate the Bowman's capsules (arrows), with dilation of the glomeruli visible in the Cr PD (Fig. C) and Cr x10 PD (Fig. E) groups. Figures B (Control), D (Cr PD) and F (Cr x10 PD) indicate no alterations in the kidney tubules (arrows) (Scale bars: 10µm).

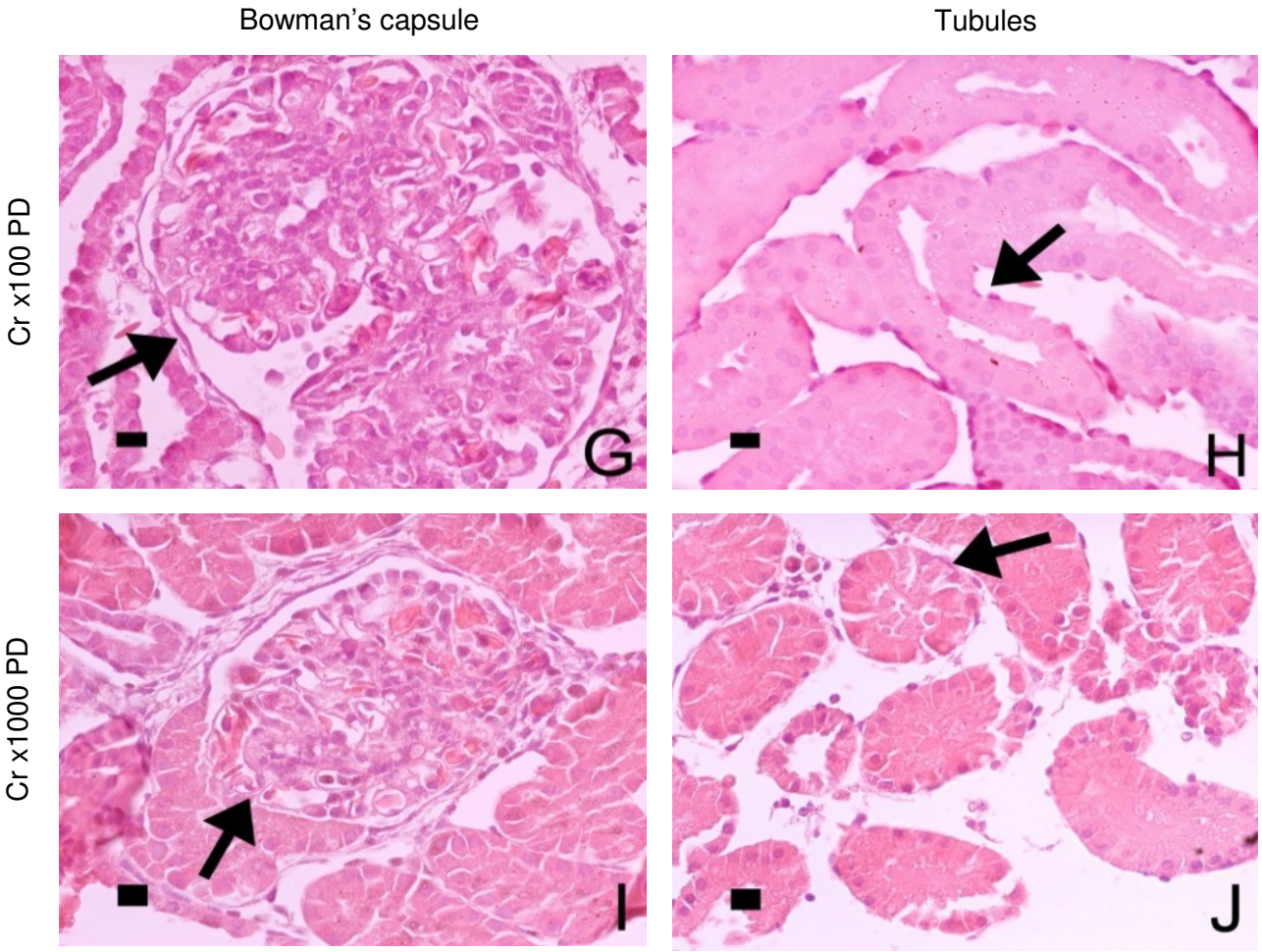

Figure 4.8 continued: Light microscopy micrographs of kidney tissue from the control and Cr groups. Figures G (Cr x100 PD) and I (Cr x1000 PD) indicate dilation of the glomeruli in the Bowman's capsules (arrows). Figures H (Cr x100 PD) and J (Cr x1000 PD) indicate no alterations in the kidney tubules (arrows) (Scale bars: 10µm).

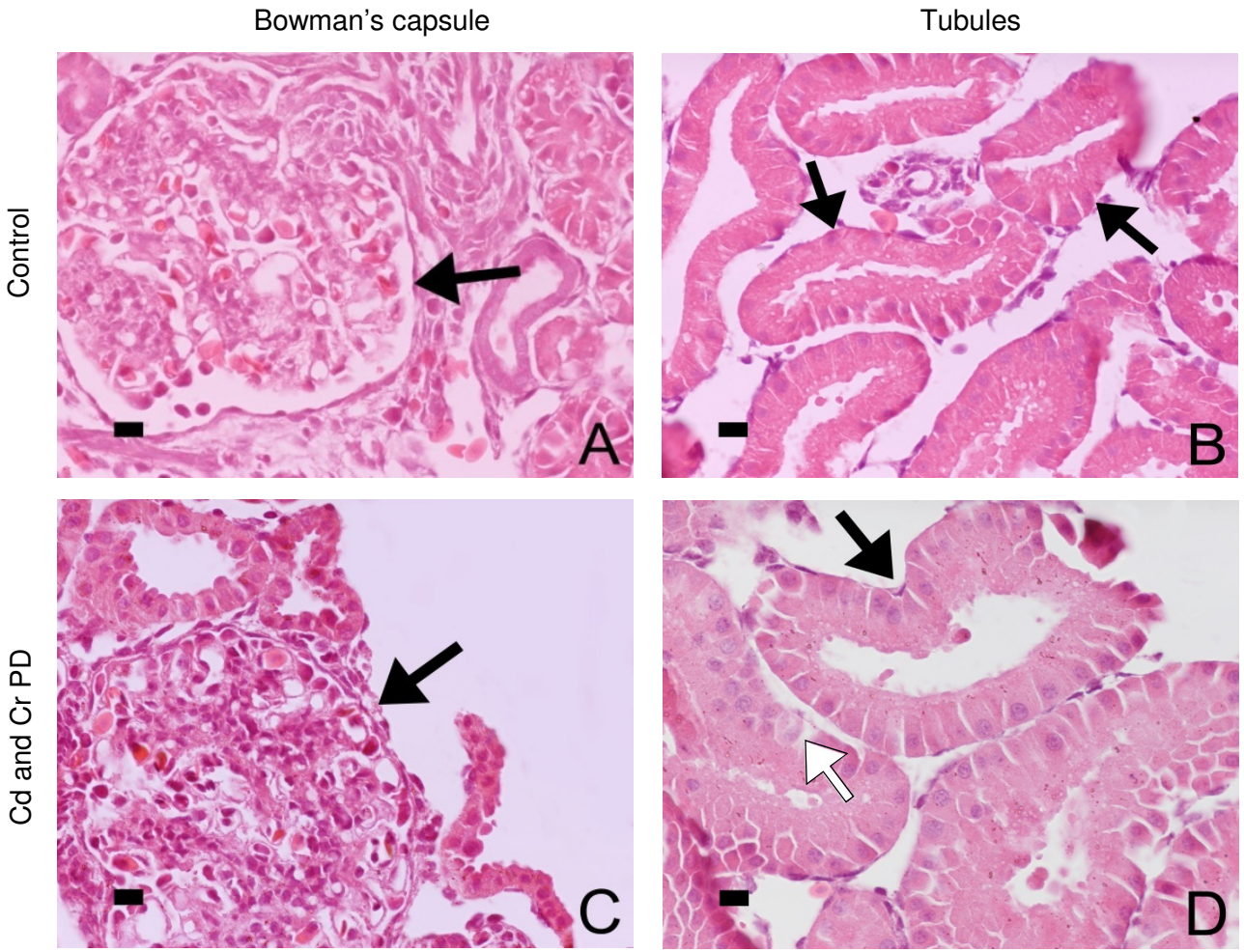

Figure 4.9: Light microscopy micrographs of kidney tissue from the control and Cd and Cr groups. Figure A and B (Control) shows normal Bowman's capsules (arrow) and renal tubules (arrows), respectively. Figure C (Cd and Cr PD) indicates dilation of the glomerulus in the Bowman's capsule (arrow) and Figure D (Cd and Cr PD) indicates hypertrophy of the cuboidal cells of the kidney tubule (black arrow), with necrosis indicated by the white arrow (Scale bars: 10µm).

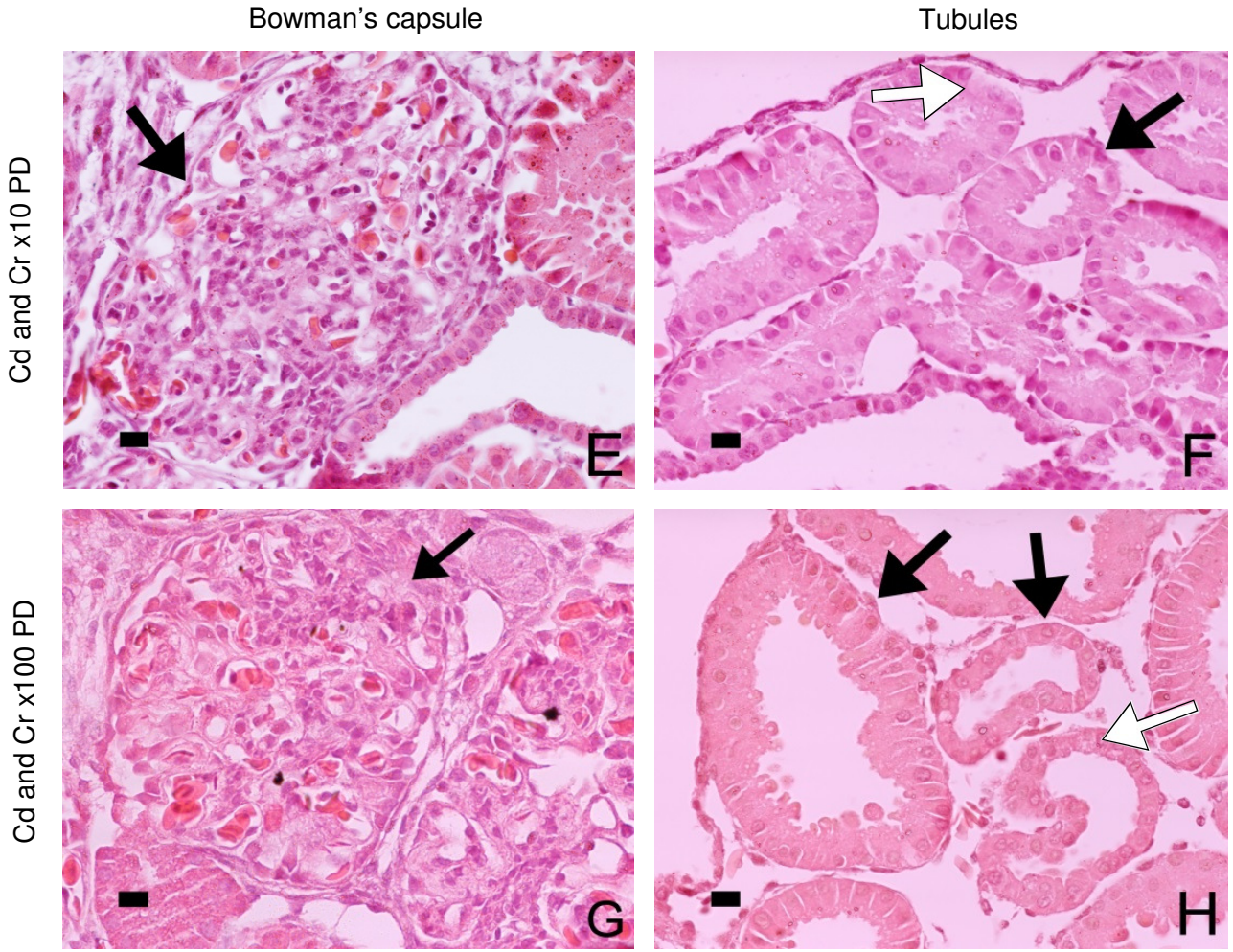

Figure 4.9 continued: Light microscopy micrographs of kidney tissue from the control and Cr groups. Figure E (Cr x10 PD) and G (Cr x100 PD) indicate dilation of the glomeruli in the Bowman's capsules (arrows). Figure F (Cr x10 PD) and H (Cr x100 PD) indicate hypertrophy of the cuboidal cells in the kidney tubules (black arrows), with necrosis indicated by the white arrows (Scale bars: 10µm).

Evaluation of the glomeruli (Fig. 4.7 A) and renal tubules (Fig. 4.7 B) in the control group revealed no cellular alterations. In the Cd PD (Fig. 4.7 C and D), Cd x10 PD (Fig 4.7 E and F) and Cd x100 PD (Fig. 4.7 G and H) only minor changes were seen, with minimal dilation of the glomerulus and little to no changes observed in the tubules. Atrophy of the glomerulus (black arrows) was observed in the Cd x1000 PD group (Fig. 4.7 I) and this was the only experimental group to display severe necrosis as well [Fig. 4.7 J (white arrows)]. Figure 4.8 C, E, G, and I depict the Cr PD, Cr x10 PD, Cr x100 PD and Cr x1000 PD respectively and with the increase in Cr concentrations, the dilation of the glomeruli also increased (black arrows). There were no differences observed in the renal tubules in any of the Cr groups [Fig. 4.8 D (Cr PD), F (Cr x10 PD), H (Cr x100 PD) and J (Cr x1000 PD) (black arrows)]. The Cd and Cr combination groups showed dilation of the glomeruli in all the concentration groups [Fig. 4.9 C (Cd and Cr PD), E (Cd and Cr x10 PD) and G (Cd and Cr x100 PD) (black arrows)]. Necrosis (white arrows), chromatin condensation and hypertrophy were also observed in all the Cd and Cr concentrations [Fig. 4.9 D (Cd and Cr PD), F (Cd and Cr x10 PD) and H (Cd and Cr x100 PD)]. A summary of all the histological changes observed in the kidney is presented in Table 4.3.

Table 4.3: Summary of histological findings of the kidney tissue

Group	Glomeruli dilation	Glomeruli contraction	Necrosis	Chromatin condensation	Renal tubule alterations
Control	-	-	-	-	-
Cd PD	+	-	-	+	+
Cd x10 PD	+	-	-	+	+
Cd x100 PD	+	-	-	+	+
Cd x1000 PD	-	+++	+++	+	+++
Cr PD	+	-	-	-	-
Cr x10 PD	+	-	-	-	-
Cr x100 PD	++	-	-	-	-
Cr x1000 PD	++	-	+	-	-
Cd and Cr PD	++	-	+	++	+
Cd and Cr x10 PD	+++	-	+	++	++
Cd and Cr x100 PD	+++	-	++	+++	++

-, none; +, minimal; ++, mild; +++, severe

4.4. Discussion

In this chapter the effects of Cd and Cr alone and in combination on brain, liver and kidney tissue were examined by using light microscopy. The neurons and myelinated axons in the brain were chosen as they are the main cells present in the brain and sensitive to the effects of the metals under investigation (Nordberg, *et al.*, 2007b). The hepatocytes and sinusoids of the liver and Bowman's capsule and tubules of the kidneys, were chosen as they are the areas involved in the detoxifying and filtering of undesired substances in the organs (Coetzee, *et al.*, 2009). This makes these areas more susceptible to toxic effects of the metals. Upon evaluation of the brain control sample, no cytoplasmic vacuolization and necrosis were found in either the neurons or the myelinated axons. Cytoplasmic vacuolization was found in the neurons and myelinated axons in all the experimental groups (Fig. 4.1 and 4.3 D, F, H and Fig. 4.2 D, F, H and J) with only a few observed necrotic cells. Similar findings with neuronal cells were shown by Soudnai, *et al.* (Soudani, *et al.*, 2012) and Unsal, *et al.* (Unsal, *et al.*, 2013), where in their respective studies they found cytoplasmic vacuolization and necrotic cells forming after exposure to Cr and Cd respectively (Soudani, *et al.*, 2012; Unsal, *et al.*, 2013). It should be noted that brain tissue from the Cd x1000 PD and Cd and Cr x1000 PD was not evaluated, as these samples were not viable for histological use.

Typical liver histology was seen in the control group, where in most of the experimental groups sinusoidal dilation and necrosis were seen. The only metal concentration that showed severe damage was the Cd x1000 PD (Fig. 4.4 F), with clear sinusoidal dilation and necrosis. These findings correlate with the results obtained in the study by Jihen, *et al.*, where the researchers also found sinusoidal dilation and necrosis in the liver tissue after Cd exposure (Jihen, *et al.*, 2008). In the kidney tissue, severe morphological alterations were also present in the Cd x1000 PD group (Fig. 4.7 I and J) and it was the only experimental group that revealed major alterations in the morphology of the kidney cells. The results obtained from evaluation of the kidney tissue in the Cd x1000 PD group revealed shrinkage of the glomeruli, which was contrary to what was found in literature, and both the renal tubules and the glomeruli displayed necrosis of the epithelial cells. In a study by Kajikawa, *et al.*, the authors did also found a reduction in the size of the glomeruli and the tubular cells were necrotic after exposure of the rats to Cd (Kajikawa, *et al.,* 1981). The lower concentrations of the Cd (Fig. 4.7 C-H) only revealed minor morphological differences when compared to the control.

In the kidney tissue from the Cr and metal combination groups, glomerular dilation was observed (Fig. 4.8 C, E, G, I; Fig. 4.9 C, E, G) with only the combination groups [Fig. 4.9 D (Cd and Cr PD), F (Cd and Cr x10 PD) and H (Cd and Cr x100 PD)] indicating modifications in the renal tubules which included necrosis, chromatin condensation and hypertrophy. Contrary to what was found by Mishra and Mohanty, as described in the introduction (Mishra and Mohanty, 2008), the evaluation of the kidney samples in the Cr-exposed groups showed dilation of the glomerulus with a reduction of the Bowman's capsule space. These results may be due to the nuclear factor kappa B cells (NF-kB) activation. NF-kB is a redox-sensitive transcription factor that mediates the expression of proinflammatory cytokines and chemokines, which may be a possible explanation for the inflammation seen in the glomerulus of the kidney (Ruiz, *et al.,* 2013). The glomerular dilation seen in the Cr-exposed groups may contribute to the initiation of diabetes mellitus, as Cr(III) is an essential nutrient that plays an important role in regulating the levels of glucose in the blood. With Cr toxicity this balance is altered (Quinteros, *et al*., 2007; Sharma, *et al.,* 2003; Valko, *et al*., 2006).

To our knowledge, no literature pertaining to the effects of simultaneous exposure to Cd and Cr is available and thus there were no comparison to previous literature in terms of the metal combination groups, but with individual evaluation of Cd and Cr, the combined metal results were similar to what was found in the individual evaluation. Again the results of the liver and kidney tissue of the 1000x combined metal groups were not evaluated due to the fact that these organs were not viable for histological use.

4.5. Conclusion

Cd and Cr alone and in combination cause neurotoxicity with all the tested metal concentrations. The BBB of chick embryos did not protect against the toxic effects of these metals and thus may compromise neurological development. Minor alterations were observed in the lower concentrations of the Cd groups, with only the highest concentration of Cd that caused severe cellular damage in the liver and kidney of the exposed embryos, where Cr had minor alterations at all concentrations. This may be due to the fact that Cr is naturally found in the body and is easily converted to a less toxic form. Cd on the other hand is not naturally found in the body and thus the body needs to produce metallothionein (MT) to restrict the toxicity of Cd and during production of MT, Cd can damage the tissue, which may lead to altered liver and kidney functions. The metal combination group showed minor damage to the liver and kidney tissue.

Chapter 5

Investigating changes in the brain, liver and kidneys of chick embryos exposed to Cd and Cr alone and in combination by using transmission electron microscopy

5.1. Introduction

Heavy metal contamination in South African mine water and air, especially cadmium (Cd) and chromium (Cr) (Fatoki and Awofolu, 2003; Molokwane, *et al*., 2008; Tempelhoff, 2013) and the effects they may have specifically on pregnant woman and their unborn children, has led to the evaluation of the possible adverse effects of these metals on chick embryos. With transmission electron microscopy, these possible alterations can be observed under higher resolution and thus allows a closer evaluation of the organelles and membranes of the different cells (Meek, 1976; Williams and Carter, 1996a). In the previous chapter showing the light microscopy results, it was indicated that Cd and Cr alone and in combination caused neurotoxicity that may cause altered neurological development in embryos. In the liver and kidney, the highest concentration of Cd caused major alterations whereas the lower concentrations of the Cd as well as all the Cr and metal combination groups only causing minimal damage.

Studies have shown that when cells are exposed to Cd or Cr the effects caused by these metals are similar and include chromatin condensation, swelling of the mitochondria and dilation and vesiculation of the rough endoplasmic reticulum (rER) (Fu, *et al*., 2008; Thophon, *et al*., 2004). These results were also seen in laboratory based evaluation done on different types of cells (Bagchi, *et al*., 2002; Hassoun and Stohs, 1996). Therefore, in this chapter a brief description of the normal ultrastructure and function of the organelles is given, as well as the criteria used to evaluate the alterations caused by the metal toxicity.

Continuing from the description of the brain, liver and kidney cells in chapter 4, these cells are different in function and location, but their cellular content are very similar, varying only in the amount of each organelle. The cell membrane surrounds all the organelles of the cell and consists of two double phospholipid layers that contain proteins which assist in the transport of molecules in and out of the cell. The cell membrane also acts as a protective barrier (Coetzee, *et al*., 2009). Within the cell membrane, the nucleus, thousands of mitochondria, rER's, Golgi complexes, lysosomes and many more organelles can be found (Young, *et al.,* 2006).

Nuclei are found in the centre of the cells and consist of a nuclear envelope, nucleolus and chromatin (Coetzee, *et al*., 2009). The nuclear envelope consists of a double membrane with nuclear pores that allows for metabolic exchange. The chromatin appears as small, dark granules when observed with transmission electron microscopy (TEM) and is composed of DNA and histone proteins, which plays a crucial role in cell division. The nucleolus consists of mainly RNA, some DNA and proteins associated with nucleic acids (Coetzee, *et al*., 2009). In this study, the nuclear membrane was investigated for membrane alterations based on the fact that heavy metals can cause lipid peroxidation and thus causes loss in membrane integrity (Bertin and Averbeck, 2006).

The mitochondria vary significantly in size and shape in all the different types of cells, but overall are elongated and always consist of four compartments, namely the outer and inner membranes, mitochondrial matrix and inner-membranous space. The outer membrane plays a role in the transport of small molecules and converts lipid substances into usable molecules for the mitochondria. The inner membrane folds into shelf-like folds called cristae, that project into the mitochondrial inner cavity (Coetzee, *et al*., 2009; Young, *et al.,* 2006). The mitochondrial matrix and inner-membranous space contains enzymes, calcium, magnesium and even DNA and RNA, which all plays a role in the energy production function of the mitochondria (Coetzee, *et al*., 2009; Young, *et al.,* 2006). The mitochondria were evaluated for possible loss in membrane integrity and inner matrix swelling in this study, which might indicate that lipid peroxidation and an increase in fluid in the mitochondria occurred (Bertin and Averbeck, 2006; Thophon, *et al*., 2004).

The Golgi complex consists of a stack of saucer-shaped membranous sacs known as cisternae (Coetzee, *et al*., 2009; Young, *et al.,* 2006). The Golgi complex comprises of two sides, the *cis* and *trans* Golgi networks. The *cis* Golgi network is the convex part of the Golgi complex that faces the rER and is the site of entrance of the incomplete proteins synthesized in the rER (Coetzee, *et al*., 2009; Young, *et al.,* 2006). In the Golgi complex, sugar residues are added to the proteins to finalize the glycosylation process started in the rER. The proteins move through the Golgi complex and when they arrive at the concave *trans* Golgi network, they are sorted into specific secretory vesicles to be transported to the extracellular space, plasma membrane or they remain in the cell to form part of the intracellular organelles such as the lysosome (Coetzee, *et al*., 2009; Young, *et al.,* 2006). In the current study the Golgi complex was investigated for unknown particles, which might indicate that some form of metal detoxification took place.

Therefore, in the current chapter the chick embryo model was used to investigate any possible ultrastructural changes that may occur in the brain, liver and kidney after exposure to the heavy metals alone and in combination and at different concentrations using TEM.

5.2. Materials and methods

5.2.1. Tissue for TEM

Samples were obtained as described in Chapter 3.

5.2.2. 2.5% Glutaraldehyde/Formaldehyde fixating

Tissue were cut into $1mm^3$ blocks and were fixed in 2.5% glutaraldehyde (GA)/ formaldehyde (FA) (1mℓ of 25% GA, 1mℓ of 25% FA, 5mℓ phosphate (PO_4) buffer (0.15M), 3mℓ ddH_2O) for 1 hour, rinsed three times in 0.075M PO_4 buffer (pH=7.4) for 15 minutes each before it is placed in secondary fixative, 1% osmium tetroxide solution, for 1 hour. Following secondary fixation, the tissues were rinsed again as described above. The tissues were then dehydrated in 30%, 50%, 70%, 90% and three changes of 100% ethanol. The samples were embedded in EMbed 812 resin and ultra-thin sections (70-100nm) were cut with a diamond knife using an ultramicrotome (Reichert-Jung Ultracut E). Samples were then contrasted with uranyl acetate for 5 minutes followed by 2 minutes of contrasting with lead citrate, after which samples were allowed to dry for a few minutes before being examined with the JEOL transmission electron microscope (JEM 2100F).

5.3. Results

5.3.1. Brain

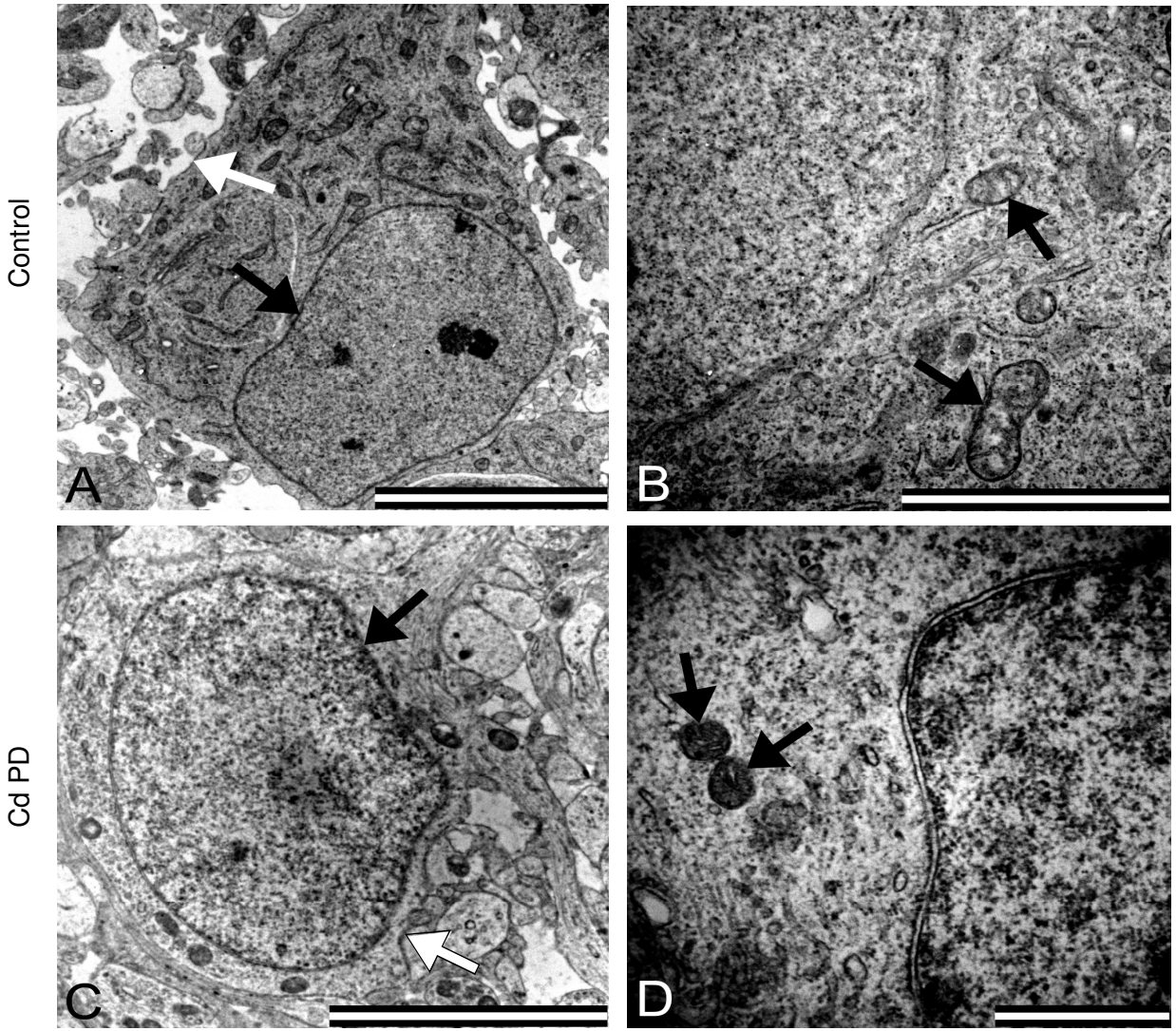

Figure 5.1: Transmission electron micrographs of brain tissue from the control and Cd-exposed groups. Figures A and B indicate the control, Figure A indicating the neuron (black arrow: nucleus and white arrow: cellular membrane) and Figure B the mitochondria (arrows). Figure C represents the neurons in the Cd PD group (black arrow: nucleus and white arrow: cellular membrane) and Figure D represents the mitochondria of the Cd PD group [Fig. D (arrows)] (Scale bars: A, C: 5µm; B: 2µm; D: 1µm).

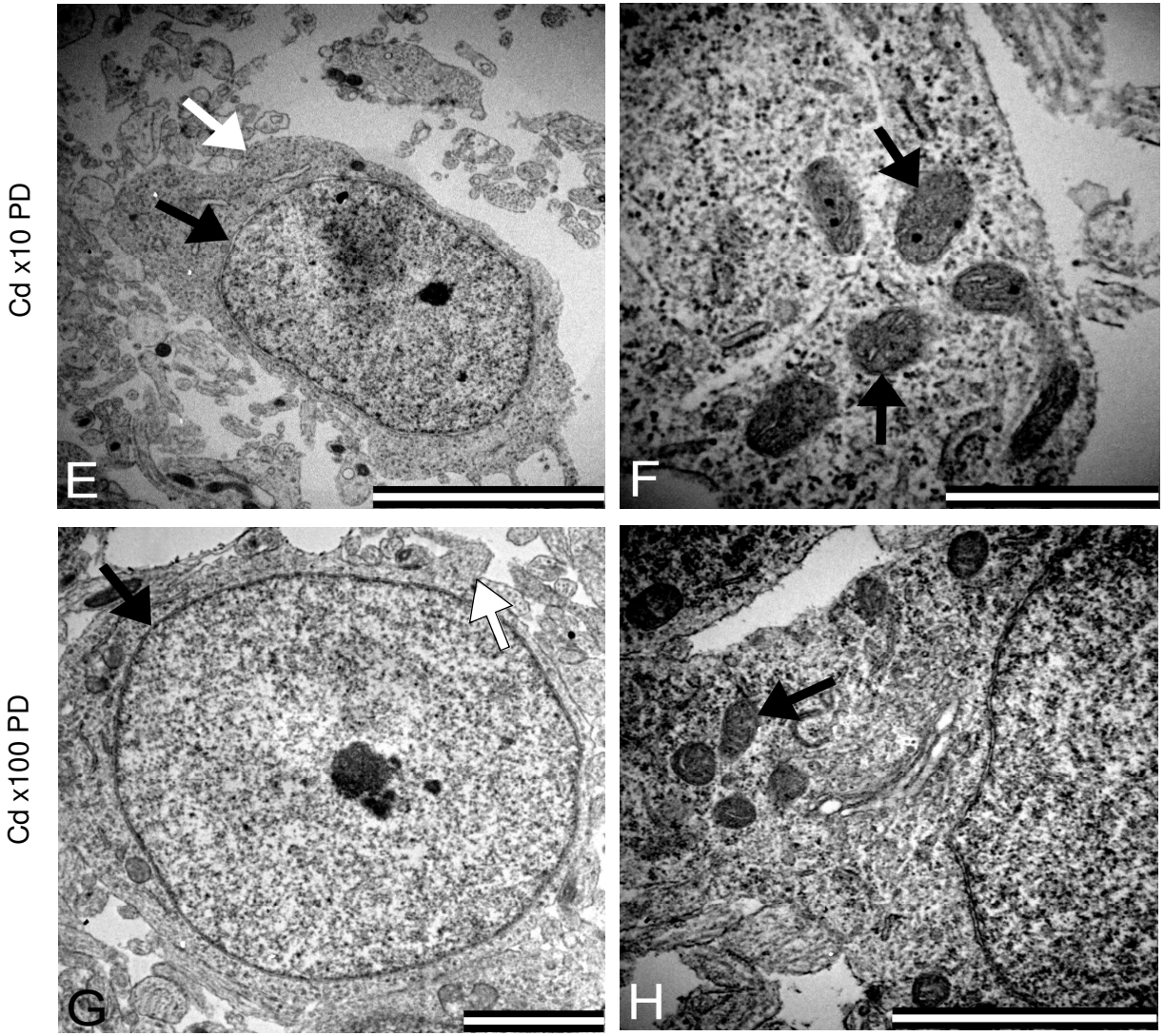

Figure 5.1 continued: Figures E and F are transmission electron micrographs of the Cd x10 PD group, with Figures G and H representing the Cd x100 PD group. Figures E and G illustrate the neurons (black arrows: nucleus and white arrows: cellular membrane) and Figures F and H show the mitochondria (arrows) (Scale bars: E: 5µm; G, H: 2µm; F: 1µm).

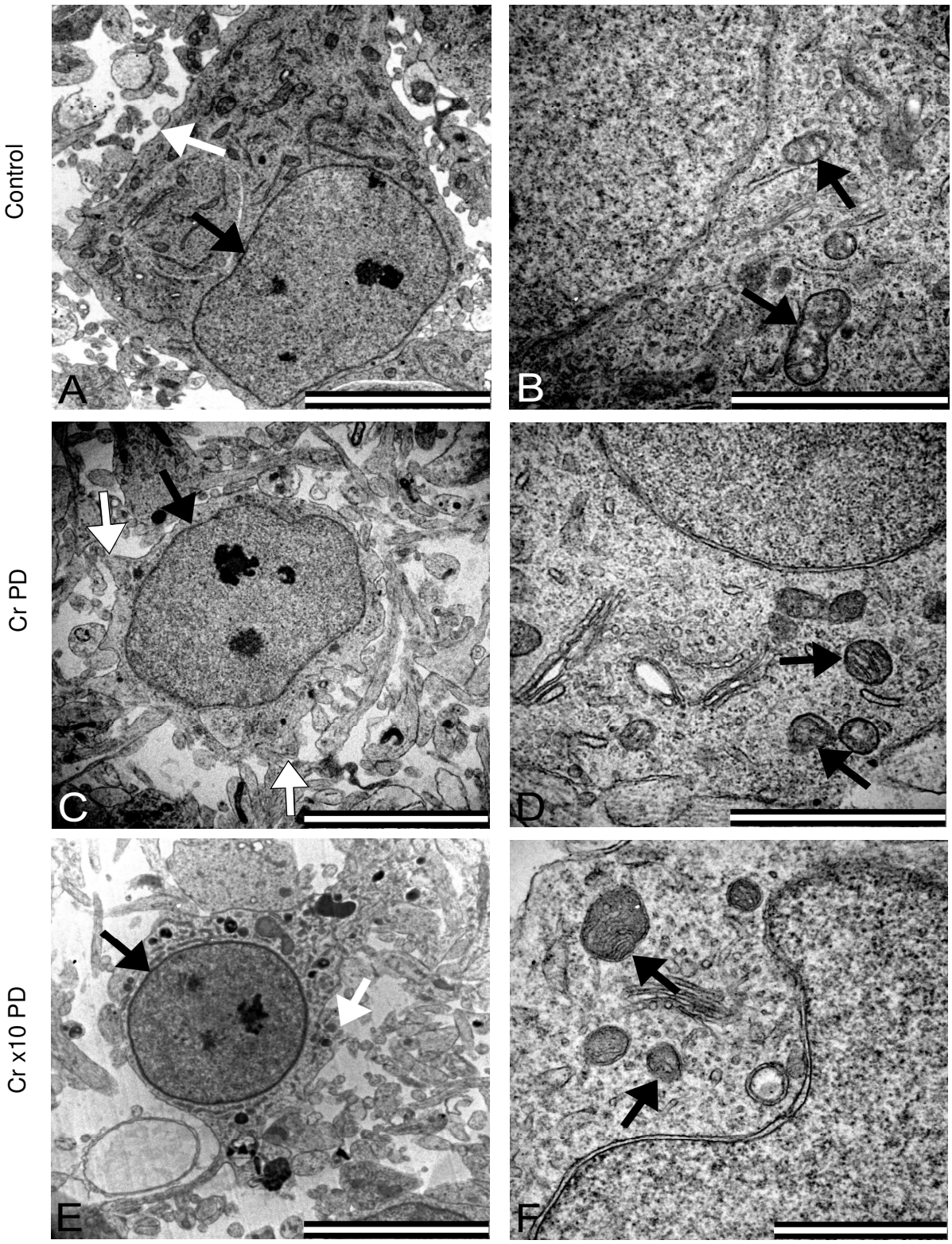

Figure 5.2: Transmission electron micrographs of brain tissue in the control and Cr experimental groups. Figures A-F represent the control (Fig. A and B), Cr PD (Fig C and D) and Cr x10 PD (Fig. E and F) groups. Figures A, C, E illustrate the neurons (black arrows: nucleus and white arrows: cellular membrane) found in the respective groups and Figures B, D and F show the mitochondria (arrows) (Scale bars: A, C, E: 5µm; B, D: 2µm; F: 1µm).

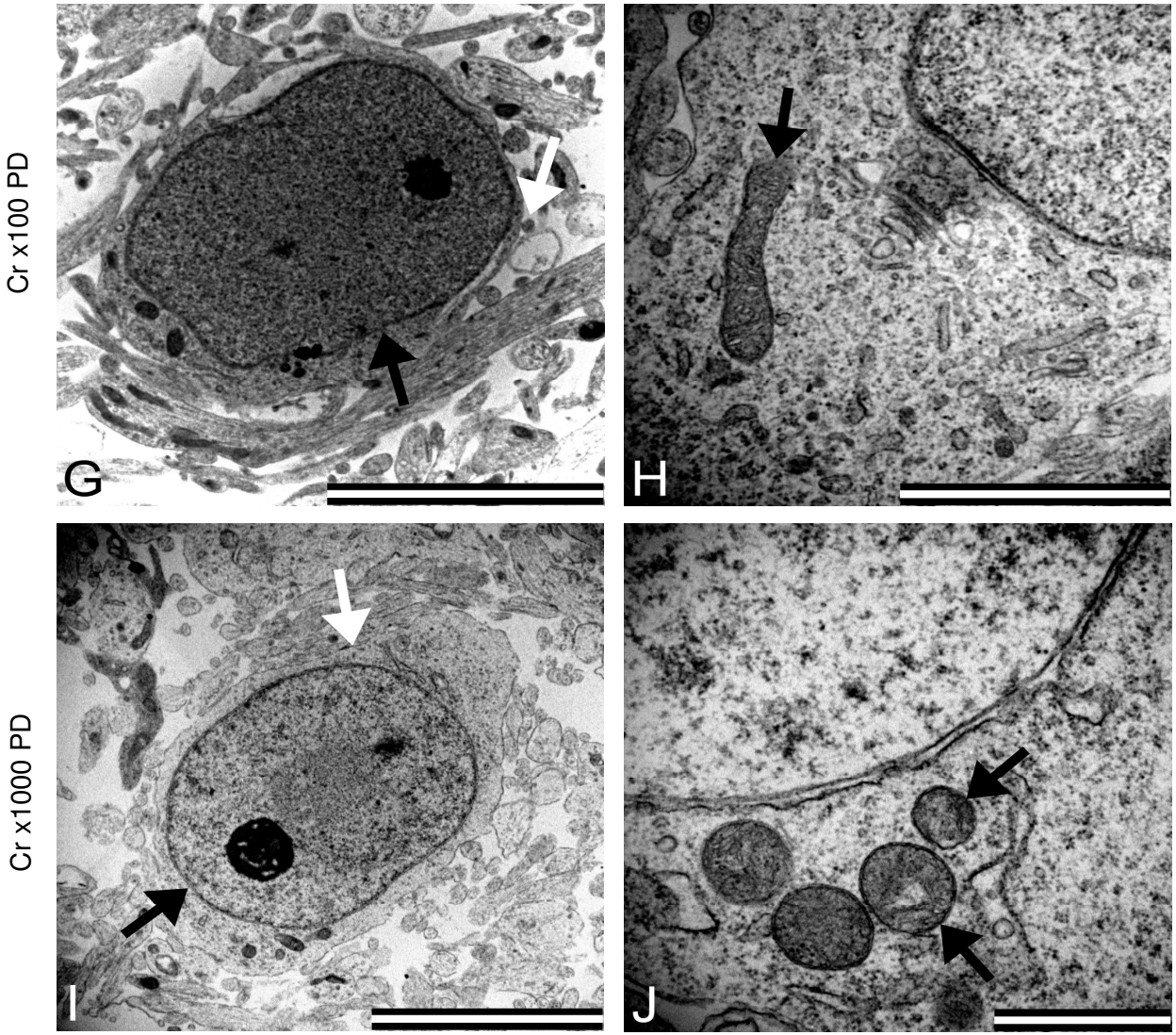

Figure 5.2 continued: Figures G and H are transmission electron micrographs of the Cr x100 PD group, with Figures I and J representing the Cr x1000 PD group. Figures G and I illustrate the neurons (black arrows: nucleus and white arrows: cellular membrane) and Figures H and J the mitochondria (arrows) (Scale bars: G, I: 5µm; H: 2µm; J: 1µm).

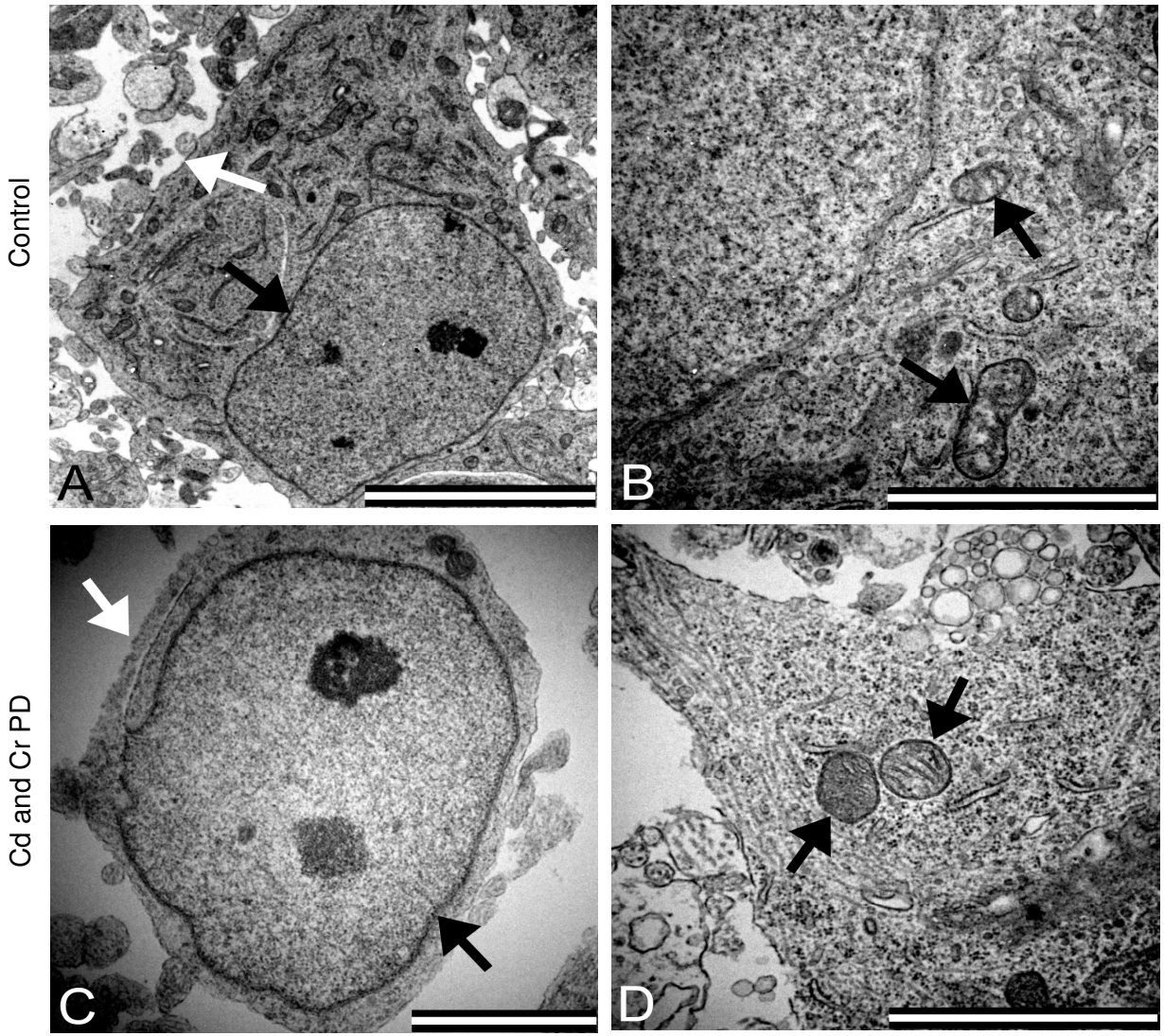

Figure 5.3: Transmission electron micrographs of brain tissue from the control and Cd and Cr experimental groups. Figures A and B indicate the control, Figure A indicates the neurons (black arrow: nucleus and white arrow: cellular membrane) and Figure B the mitochondria (arrows). Figure C represents a neuron from the Cd and Cr PD group (black arrow: nucleus and white arrow: cellular membrane) and Figure D represents the mitochondria (arrows) of the Cd and Cr PD group (Scale bars: A: 5µm; B, C, D: 2µm).

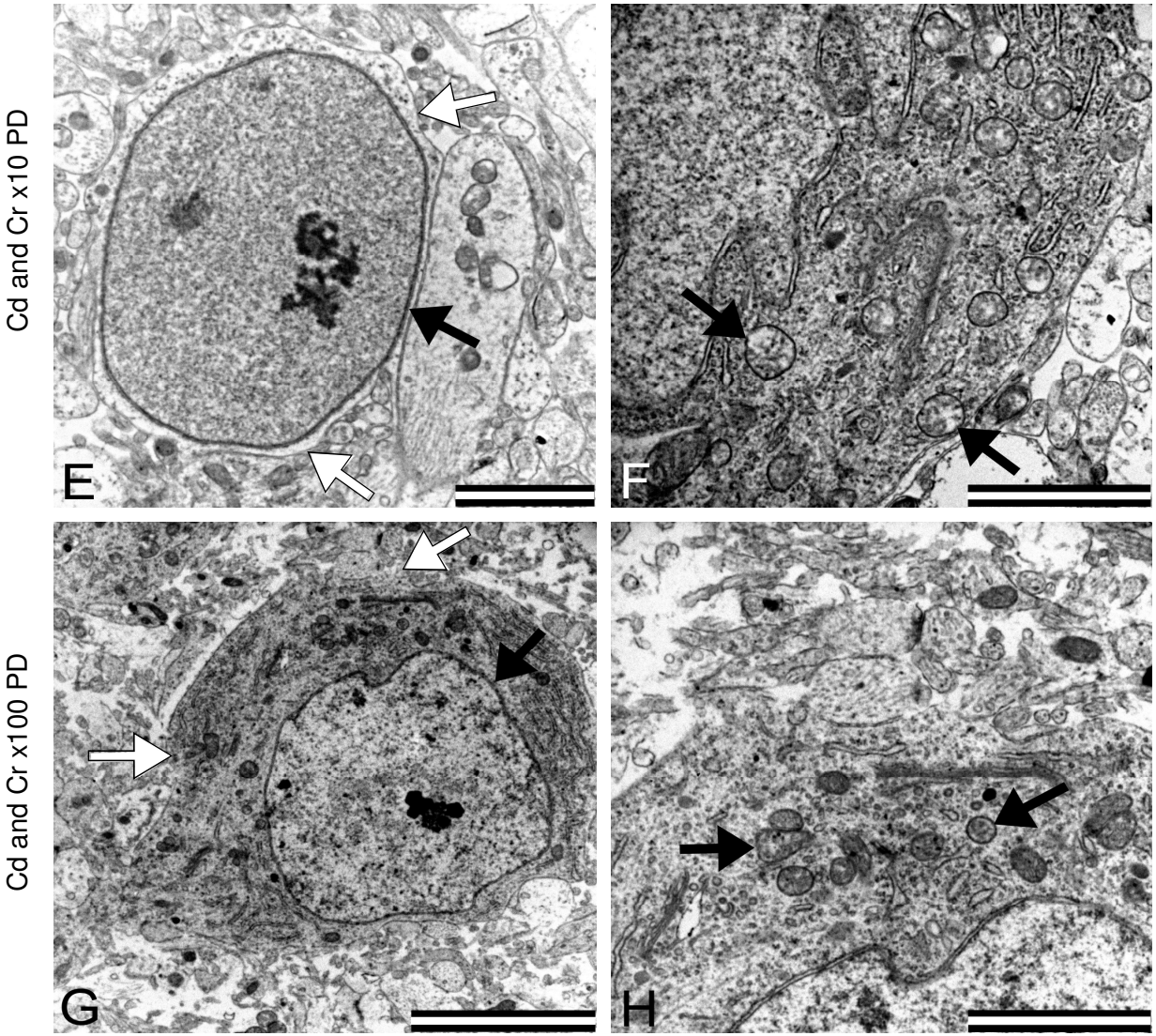

Figure 5.3 continued: Figures E and F are transmission electron micrographs of the Cd and Cr x10 PD groups, with Figures G and H representing the Cd and Cr x100 PD group. Figures E and G illustrate the neurons (black arrows: nucleus and white arrows: cellular membrane) and Figures F and H the mitochondria (arrows) (Scale bars: G: 5µm; E, F, H: 2µm).

In Figure 5.1 the ultrastructure of the brain tissue from the control (Fig. 5.1 A and B) and Cd experimental groups (Fig. 5.1 C-H) are seen. Neurons in the control group (Fig. 5.1 A) revealed normal nuclear morphology (black arrow) and no loss of membrane integrity of the nuclear and cellular membranes (white arrow). In Figure 5.1 B, some loss in mitochondrial membrane integrity and minimal inner matrix swelling (black arrows) are visible. Figures 5.1 C and D (Cd PD), E and F (Cd x10 PD) and G and H (Cd x100 PD) represent the neurons (Fig 5.1 C, E and G) and mitochondria (Fig. 5.1 D, F and H) of the Cd-exposed groups. The Cd experimental groups revealed nuclear morphology [Fig 5.1 C, E and G (black arrows)] similar to that of the control group, with intact nuclear and cellular membranes [Fig 5.1 C, E and G (white arrows)]. Some loss of mitochondrial membrane integrity and minimal inner matrix swelling [Fig. 5.1 D, F and H (arrows)] was also observed. The same trend is seen in the Cr experimental groups shown in Figure 5.2 C and D (Cr PD), E and F (Cr x10 PD), G and H (Cr x100 PD) and I and J (Cr x1000 PD).

In all the metal combination groups (Fig. 5.3 C, E and G), no changes were seen in the nuclear membranes (black arrow) and chromatin distribution in the neurons. In the Cd and Cr PD groups (Fig. 5.3 C), minimal cellular membrane disruption was visible, with ruptured cellular membranes present in the Cd and Cr x10 PD [Fig. 5.3 E (white arrows)] and Cd and Cr x100 PD groups [Fig. 5.3 G (white arrows)]. Regarding the mitochondria, some membrane disruption and inner matrix swelling were observed in the metal combination groups as shown in Fig. 5.3 D, F and H (arrows). Table 5.1 contains a summary of the ultrastructural changes present in the brain tissue.

Table 5.1: Summary of ultrastructural changes in the brain tissue

Group	Chromatin condensation	Nuclear membrane disruption	Mitochondrial membrane disruption	Mitochondrial swelling	Golgi particles	Cellular membrane disruption
Control	-	-	+	+	-	-
Cd PD	-	-	++	+	++	-
Cd x10 PD	+	-	++	+	++	+
Cd x100 PD	-	-	-	+	++	+
Cr PD	-	+	++	-	++	+
Cr x10 PD	-	-	++	-	++	+
Cr x100 PD	-	-	++	+	++	+
Cr x1000 PD	-	-	++	++	++	+
Cd and Cr PD	-	-	++	+	++	+
Cd and Cr x10 PD	-	+	++	++	++	+++
Cd and Cr x100 PD	-	+	+	++	++	+++

-, none; +, minimal; ++, mild; +++, severe

5.3.2. Liver

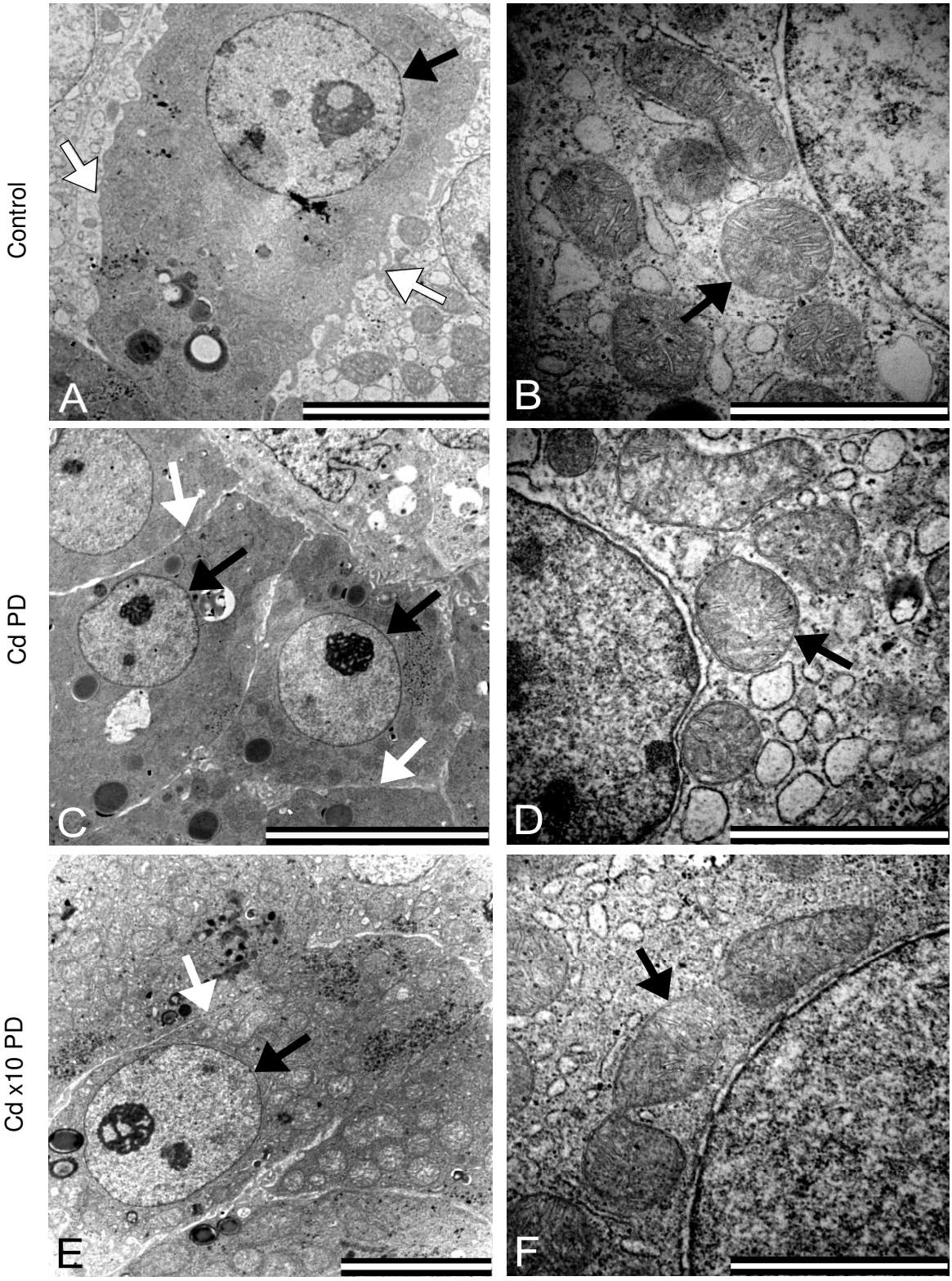

Figure 5.4: Transmission electron micrographs of liver samples from the control and Cd experimental groups. Figures A-F represent the control (Fig. A and B), Cd PD (Fig C and D) and Cd x10 PD (Fig. E and F) groups. Figures A, C, E illustrate the hepatocytes (black arrows: nucleus and white arrows: cellular membrane) found in the respective groups and Figures B, D and F represent the mitochondria (arrows) present in the liver tissue (Scale bars: A, C, E: 5µm; B, D, F: 2µm).

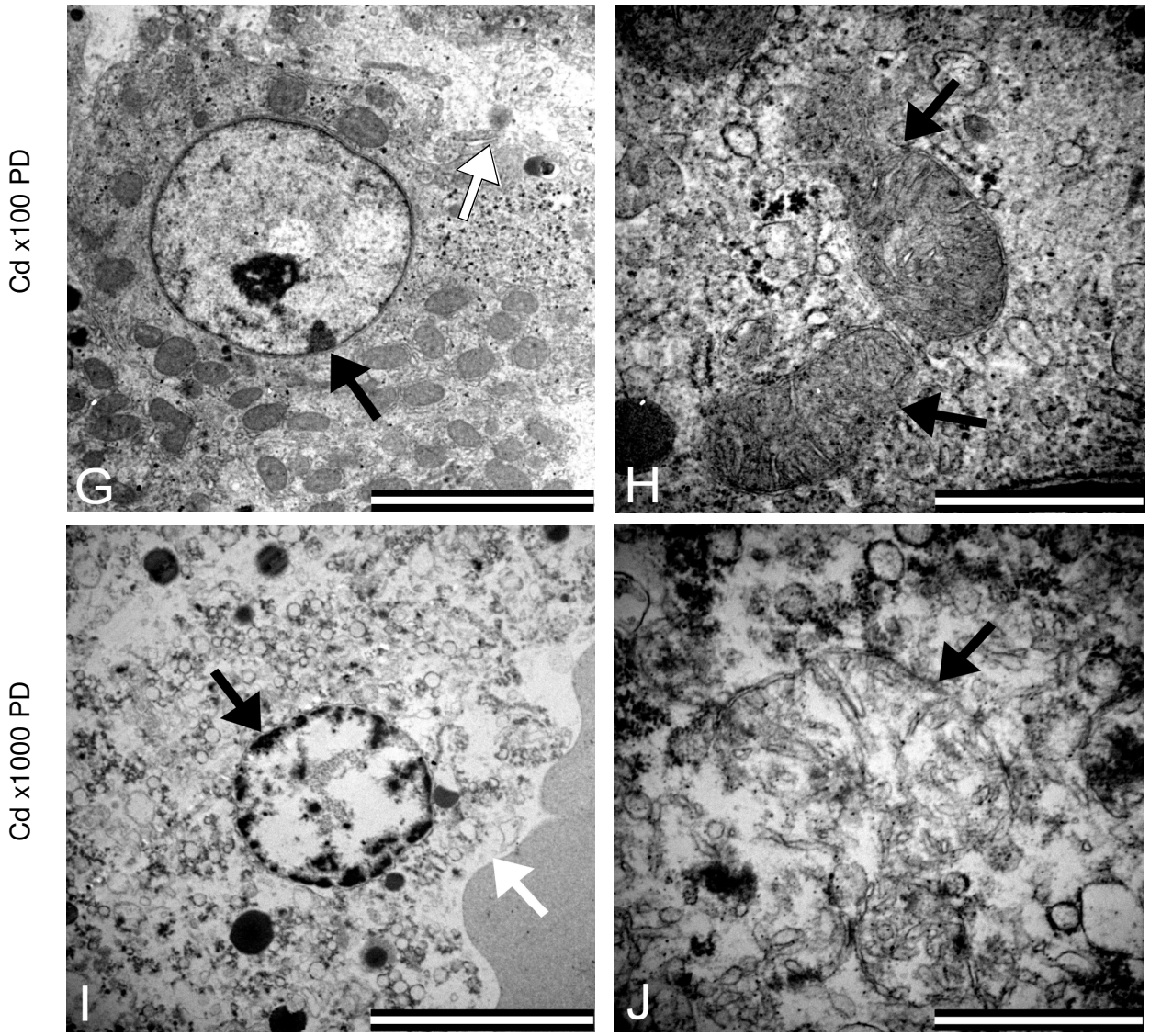

Figure 5.4 continued: Figures G and H are transmission electron micrographs of the Cd x100 PD group, with Figures I and J representing the Cd x1000 PD group. Figures G and I illustrate the hepatocytes (black arrows: nucleus and white arrows: cellular membrane) and Figures H and J the mitochondria (arrows) of the liver (Scale bars: G, I: 5µm; H, J: 1µm).

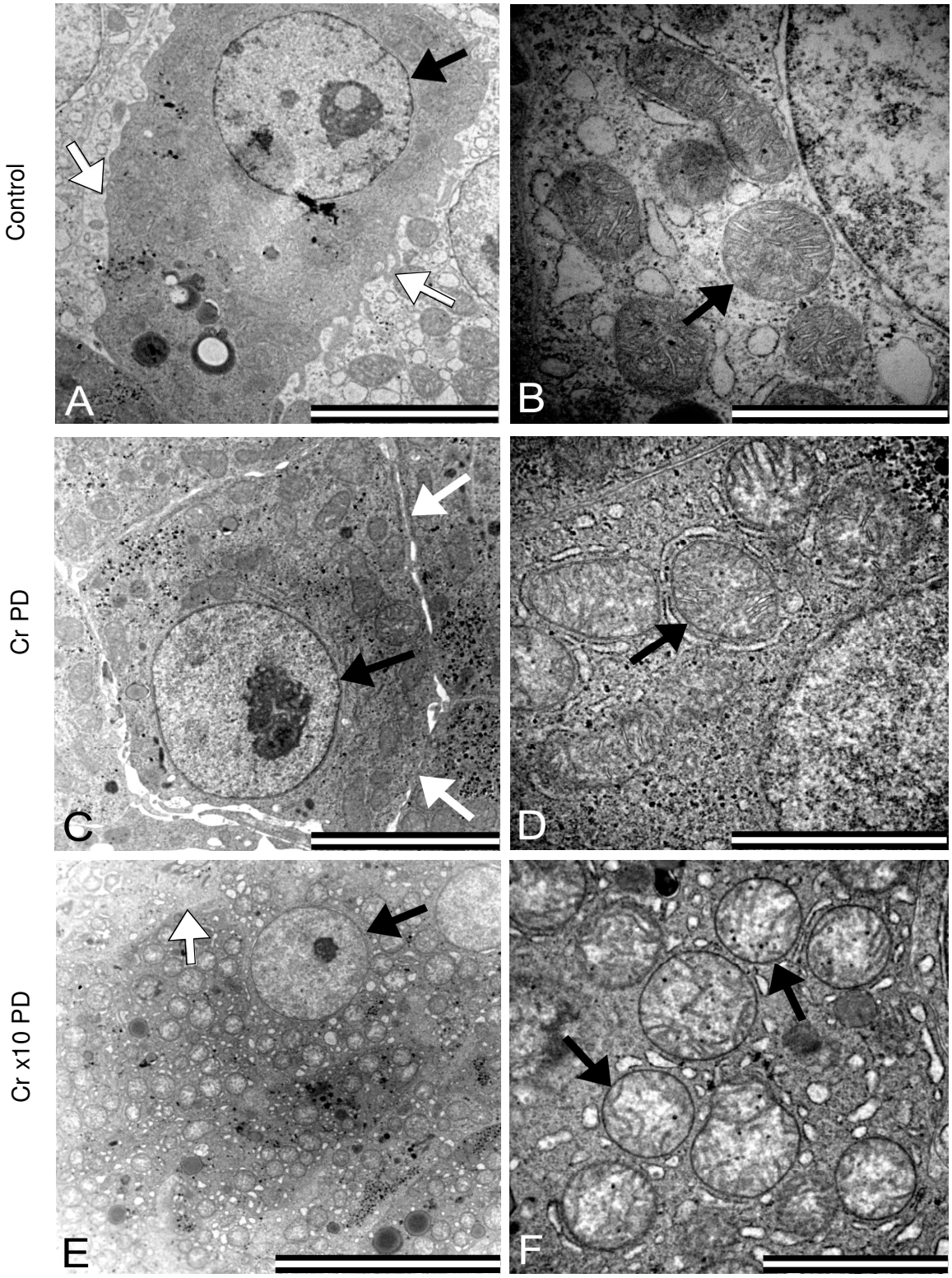

Figure 5.5: Transmission electron micrographs of liver samples from the control and Cr experimental groups. Figures A-F represent the control (Fig. A and B), Cr PD (Fig C and D) and Cr x10 PD (Fig. E and F) groups. Figures A, C, E show the hepatocytes (black arrows: nucleus and white arrows: cellular membrane) found in the respective groups and Figures B, D and F represent the mitochondria (arrows) present in the liver tissue (Scale bars: E: 10µm; A, C: 5µm; B, D, F: 2µm).

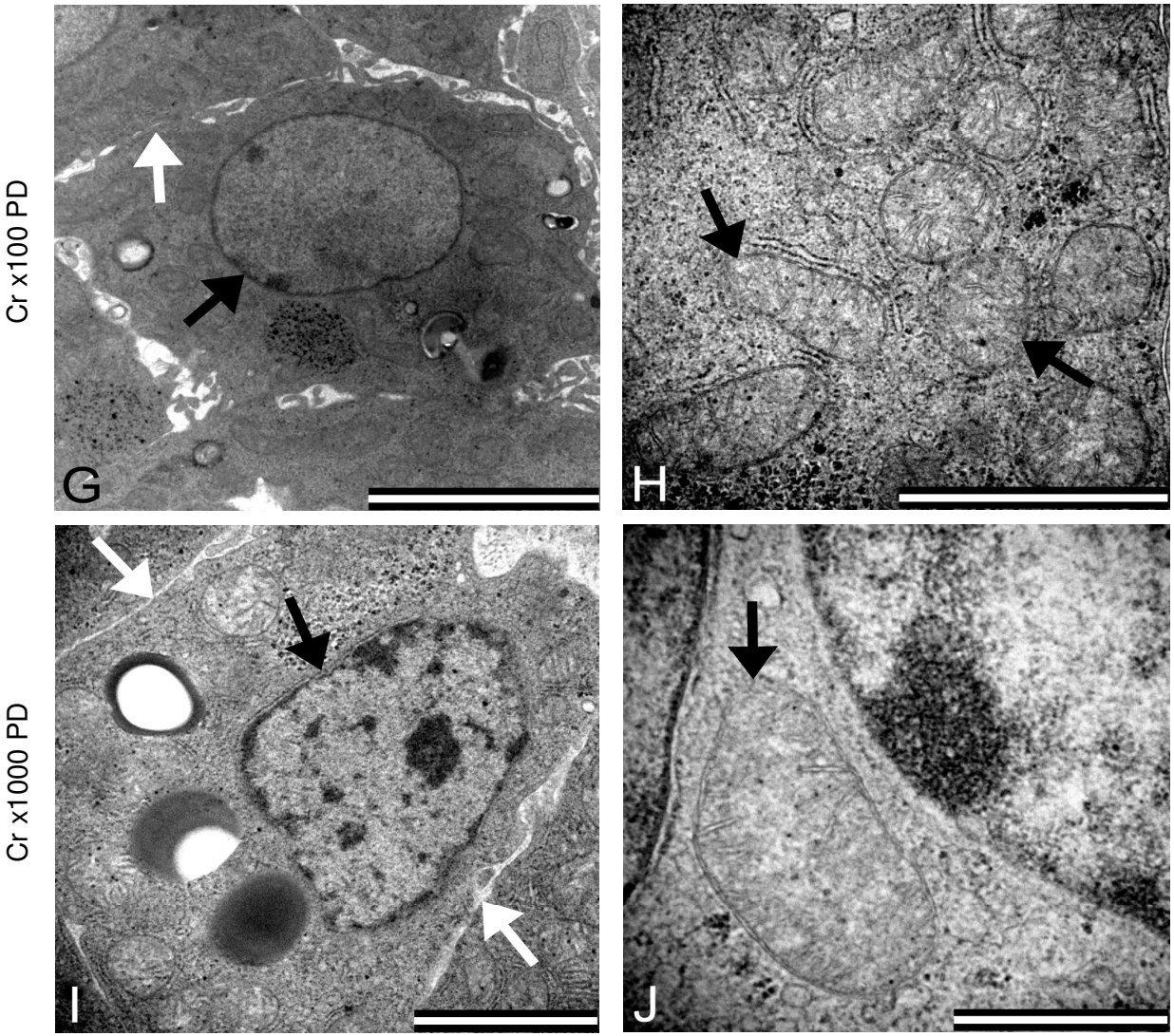

Figure 5.5 continued: Figures G and H are transmission electron micrographs of the Cr x100 PD group, with Figures I and J representing the Cr x1000 PD group. Figures G and I illustrate the hepatocytes (black arrows: nucleus and white arrows: cellular membrane) and Figures H and J the mitochondria (arrows) of the liver (Scale bars: G: 5µm; H, I: 2µm; J: 1µm).

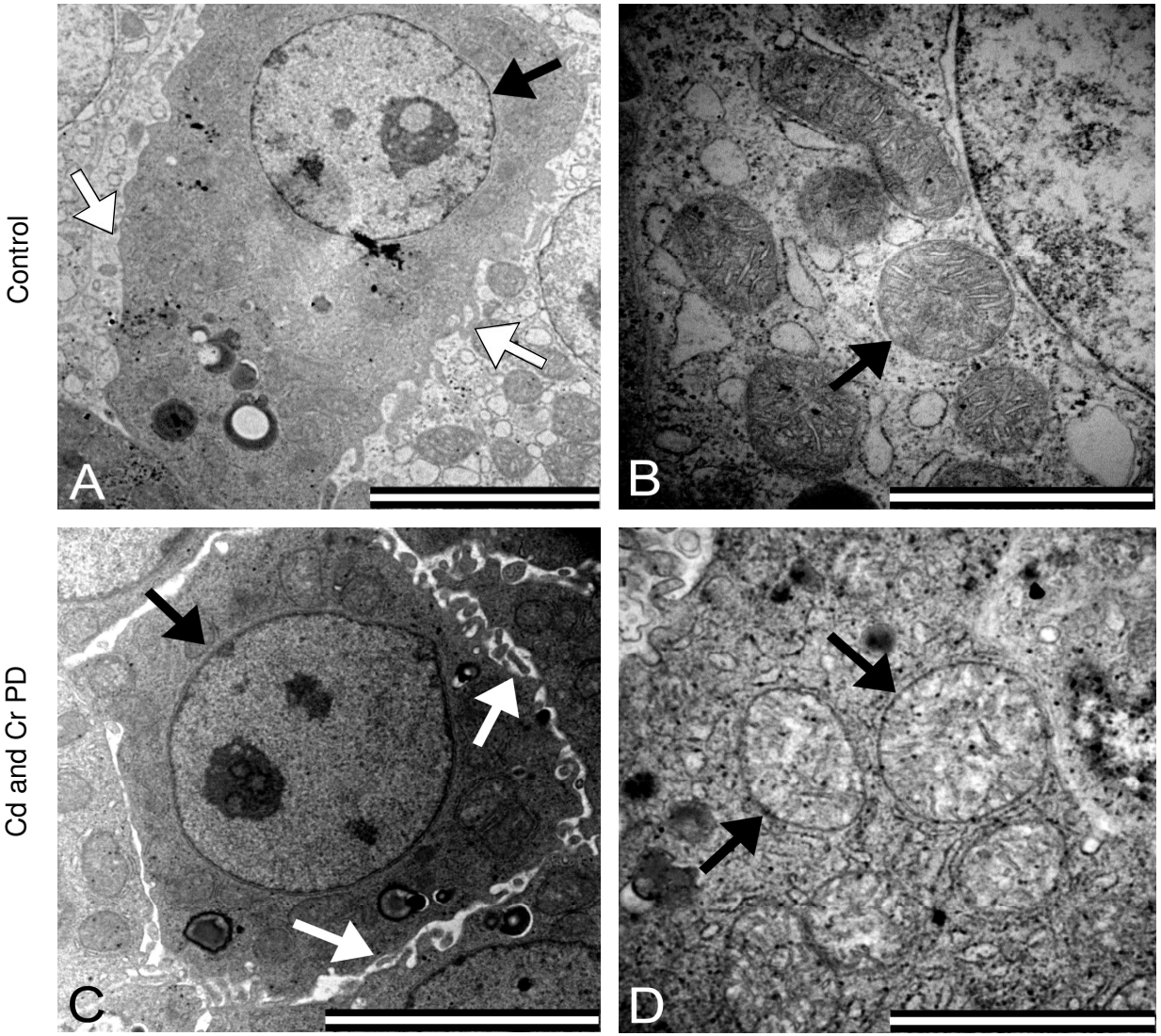

Figure 5.6: Transmission electron micrographs of liver tissue from the control and Cd and Cr experimental groups. Figures A and B indicate the control, Figure A shows a hepatocyte (black arrow: nucleus and white arrows: cellular membrane) and Figure B the mitochondria (arrow). Figures C and D represent the hepatocytes and mitochondria from the Cd and Cr PD group [Fig. C (black arrow: nucleus and white arrows: cellular membrane) and Fig. D (arrows)] (Scale bars: A, C: 5µm; B, D: 2µm).

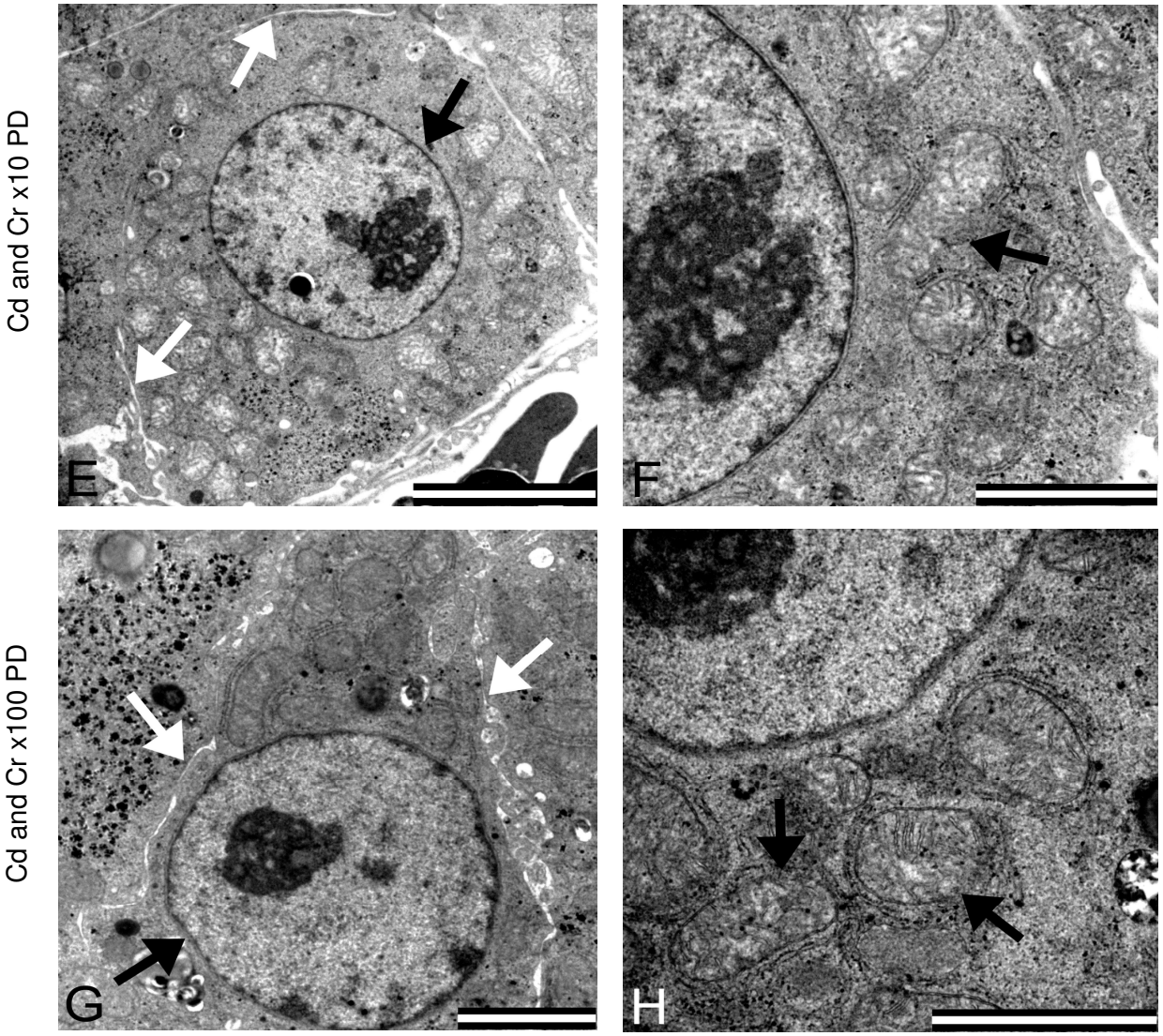

Figure 5.6 continued: Figures E and F are transmission electron micrographs of the Cd and Cr x10 PD groups, with Figures G and H representing the Cd and Cr x100 PD group. Figures E and G illustrate the hepatocytes (black arrows: nucleus and white arrows: cellular membrane) and Figures F and H the mitochondria (arrows) of the liver (Scale bars: E: 5µm; F-H: 2µm).

The liver transmission electron micrographs of the control and Cd experimental groups are represented in Figure 5.4. In the control group (Fig. 5.4 A and B) normal hepatocyte morphology is shown with intact nuclear (black arrow) and cellular membranes (white arrows) and evenly distributed chromatin. In Figure 5.4 B normal mitochondrial ultrastructure (arrow) is visible, as no inner matrix swelling or ruptured membranes are present. Figures 5.4 C-F represent the results obtained from the Cd PD and Cd x10 PD groups respectively, where evenly distributed chromatin (black arrows), intact nuclear and cellular membranes (white arrows), no sinusoidal dilation and no mitochondrial alterations (black arrows) were visible. Irregular chromatin condensation was observed in the Cd x100 PD group as shown in Fig. 5.4 G with intact nuclear membranes (black arrow). Ruptured cellular membranes (white arrow) and minimal sinusoidal dilation was also seen in this group. The mitochondria (Fig. 5.4 H) also presented with loss of membrane integrity and some inner matrix swelling (arrow). The Cd x1000 PD group (Fig. 5.4 I and J) showed severe alterations to both the hepatocytes and mitochondria. Irregular chromatin condensation (black arrow), ruptured cellular membranes (white arrow) and sinusoidal dilation were clearly visible as can be seen in Figure 5.4 I, with ruptured mitochondrial membranes and inner matrix swelling in Figure 5.4 J (arrow).

Figure 5.5 represents liver transmission electron micrographs of the control and Cr experimental groups. In the Cr PD (Fig. 5.5 C and D), Cr x10 PD (Fig. E and F), Cr x100 PD (Fig. G and H) and Cr x1000 PD (Fig. I and J), no nuclear [Fig. 5.5 C, E, G, I (black arrows)] or cellular [Fig. 5.5 C, E, G, I (white arrows)] membrane ruptures occurred, with evenly distributed chromatin in all the Cr experimental groups, except the Cr x1000 PD, where some irregular chromatin condensation is visible. No sinusoidal dilation could be seen in all the Cr experimental groups. The Cr experimental groups show minimal loss of mitochondrial membrane integrity and some inner matrix swelling is present [Fig. 5.5 D, F, H, J (arrows)]. In the metal combination groups shown in Fig. 5.6 C (Cd and Cr PD), E (Cd and Cr x10 PD), G (Cd and Cr x100 PD), both the nuclear (black arrows) and mitochondrial (white arrows) membranes are intact, with no sinusoidal dilation visible. Minimal uneven chromatin distribution could be seen in all the Cd and Cr experimental groups (Fig. 5.6 C, E and G). In all the metal combination groups [Fig. 5.6 D (Cd and Cr PD), F (Cd and Cr x10 PD) and H (Cd and Cr x100 PD)] the mitochondria show minimal membrane disruptions and some inner matrix swelling (arrows). A summary of the ultrastructural changes present in the liver can be seen in Table 5.2.

Table 5.2: Summary of ultrastructural changes in the liver tissue

Group	Chromatin condensation	Nuclear membrane disruption	Mitochondrial membrane disruption	Mitochondrial swelling	Golgi particles	Cellular membrane disruption	Sinusoidal dilation
Control	-	-	-	-	-	-	-
Cd PD	-	-	-	-	++	-	-
Cd x10 PD	-	-	-	-	++	-	-
Cd x100 PD	++	-	++	++	++	+++	+
Cd x1000 PD	+++	-	+++	+++	-	+++	+++
Cr PD	-	-	-	++	++	-	+
Cr x10 PD	-	-	+	++	++	-	-
Cr x100 PD	-	-	++	++	++	-	-
Cr x1000 PD	++	-	++	+	++	-	-
Cd and Cr PD	+	-	-	++	++	-	-
Cd and Cr x10 PD	+	-	+	++	++	-	-
Cd and Cr x100 PD	+	-	+	+	++	-	-

-, none; +, minimal; ++, mild; +++, severe

5.3.3. Kidney

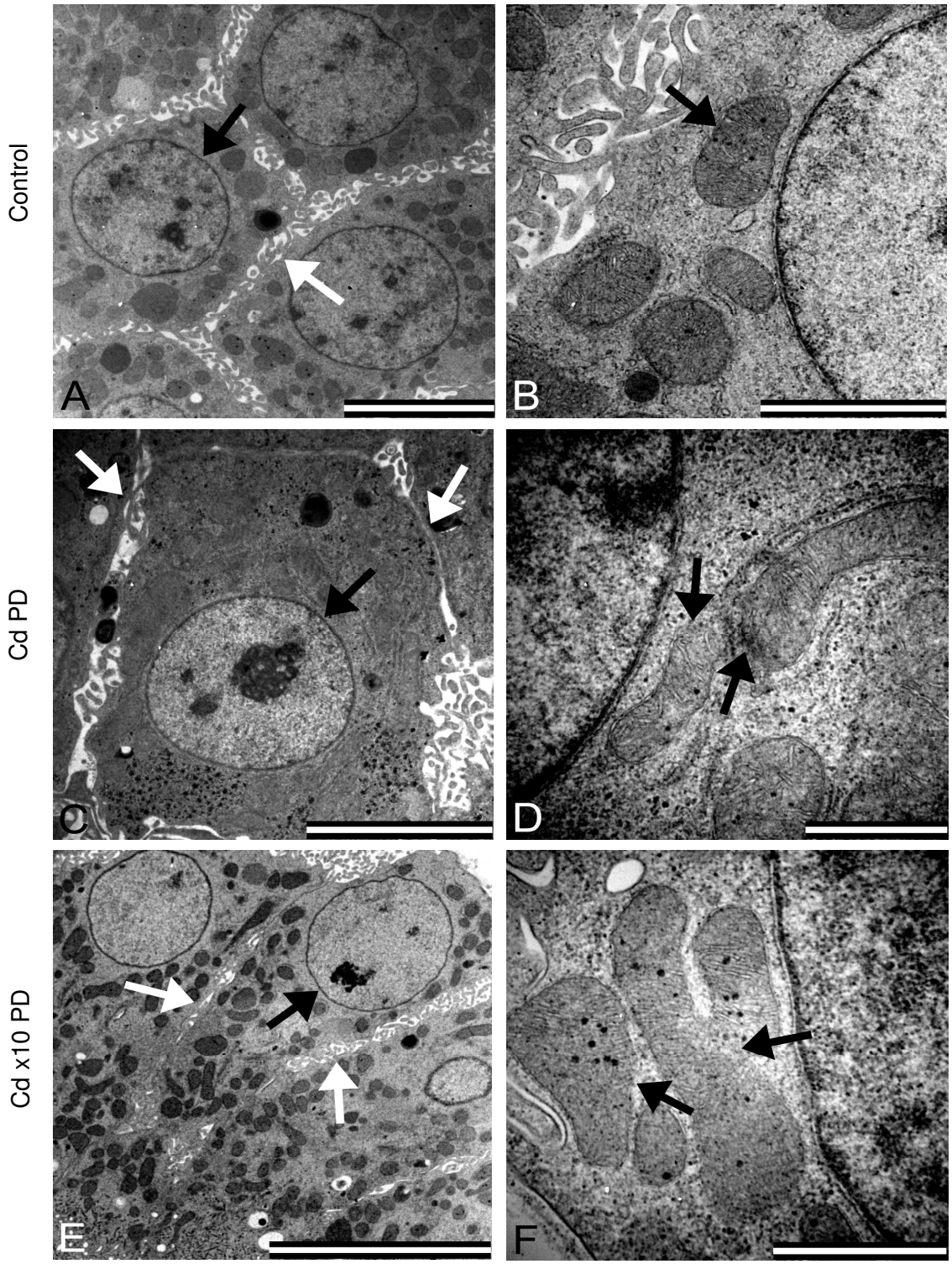

Figure 5.7: Transmission electron micrographs of kidney tissue from the control and Cd experimental groups. Figures A-F represent the control (Fig. A and B), Cd PD (Fig C and D) and Cd x10 PD (Fig. E and F). Figures A, C and E illustrate the cuboidal cells (black arrows: nucleus and white arrows: cellular membrane) found in the respective groups and Figures B, D and F represent the mitochondria (arrows) present in the kidney tissue (Scale bars: E: 10µm; A, C: 5µm; B: 2µm; D, F: 1µm).

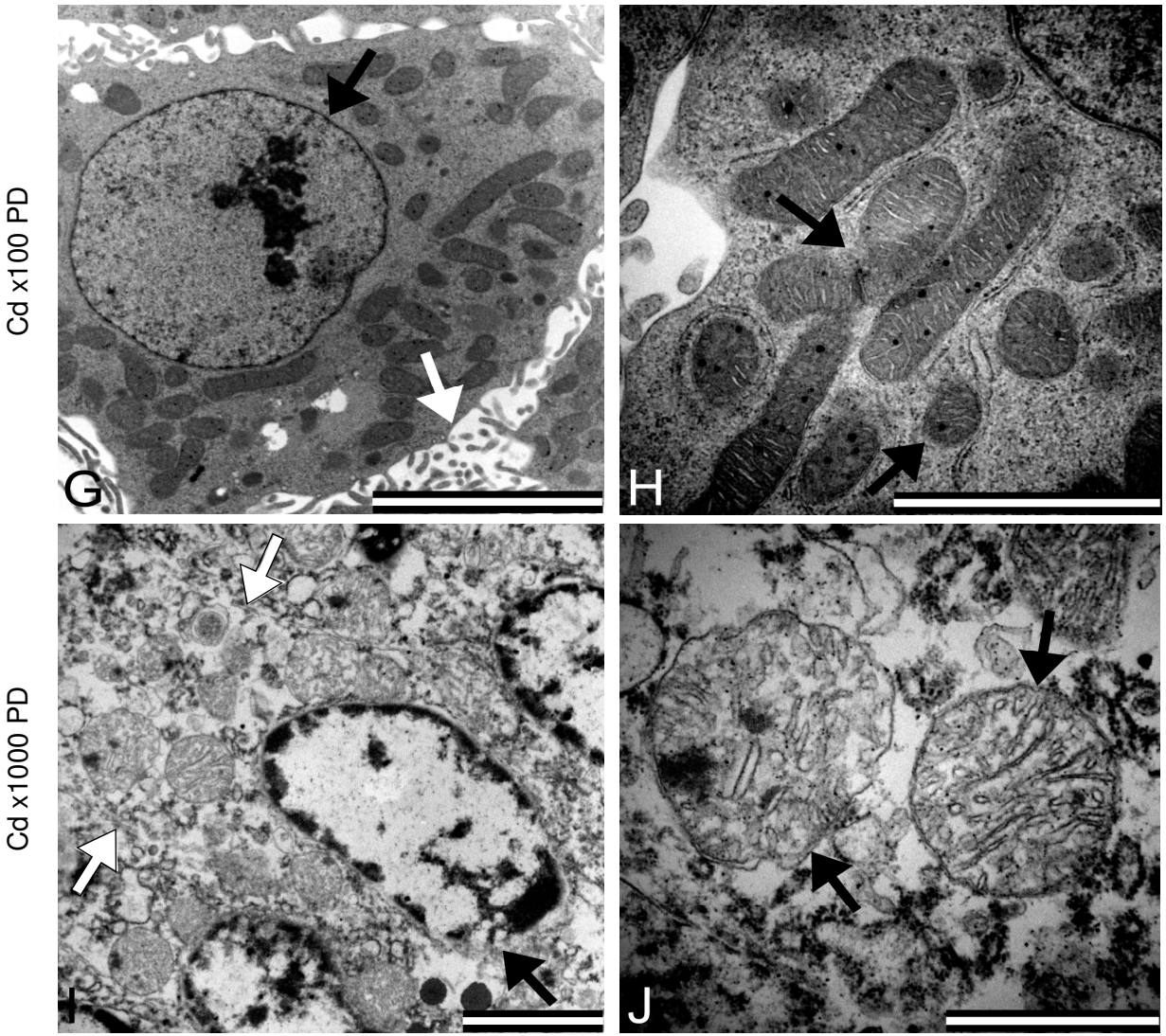

Figure 5.7 continued: Figures G and H are transmission electron micrographs of the Cd x100 PD group, with Figures I and J representing the Cd x1000 PD group. Figures G and I illustrate the cuboidal cells (black arrows: nucleus and white arrows: cellular membrane) and Figures H and J the mitochondria (arrows) (Scale bars: G: 5µm; H, I: 2µm; J: 1µm).

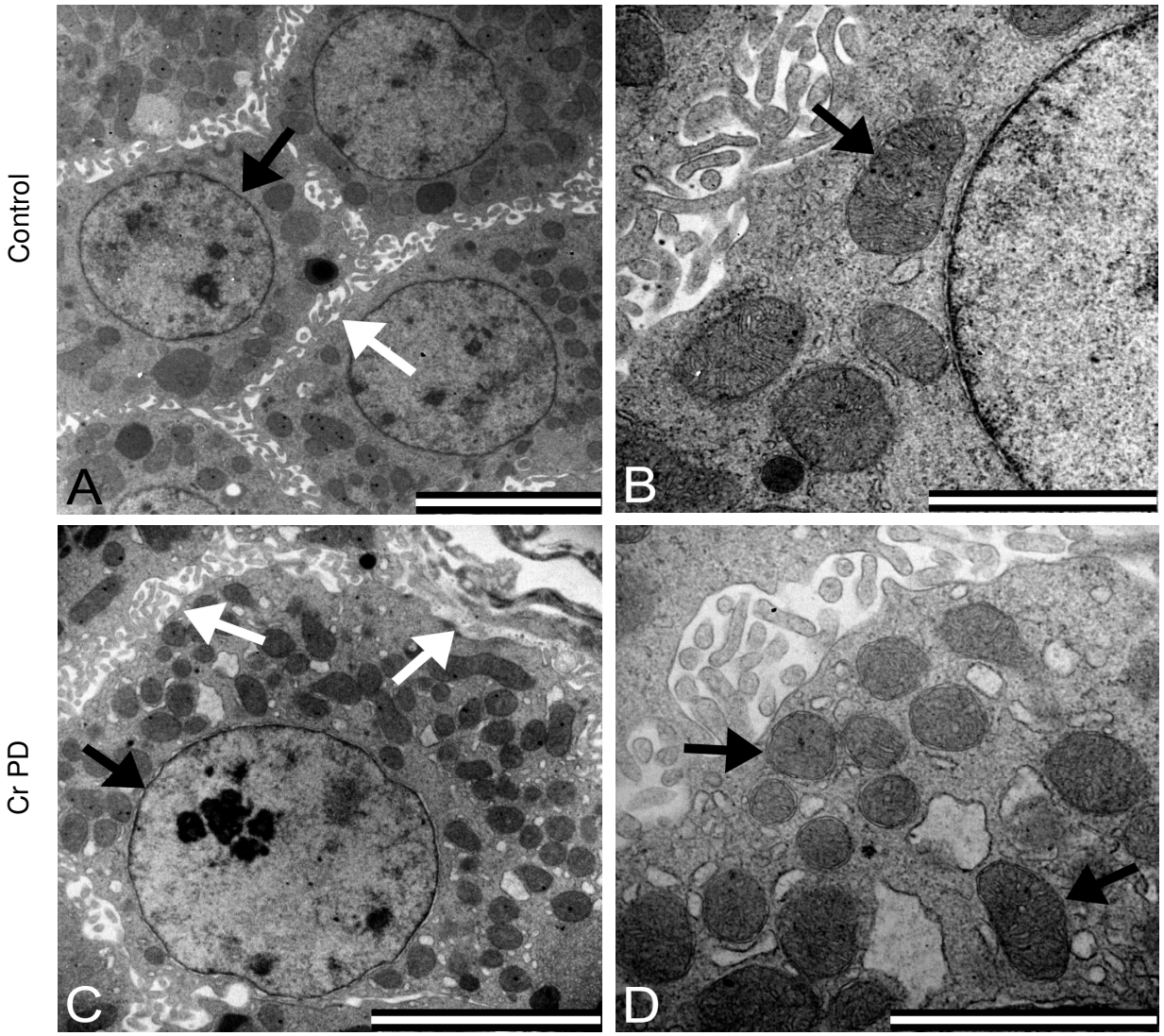

Figure 5.8: Transmission electron micrographs of kidney tissue from the control and Cr experimental groups. Figures A and B indicate the control, with Figure A indicating cuboidal cells (black arrow: nucleus and white arrow: cellular membrane) and Figure B the mitochondria (arrow). Figures C and D represent the cuboidal cells and mitochondria from the Cr PD group [Fig. C (black arrow: nucleus and white arrows: cellular membrane) and Fig. D (arrows)] (Scale bars: A, C: 5µm; B, D: 2µm).

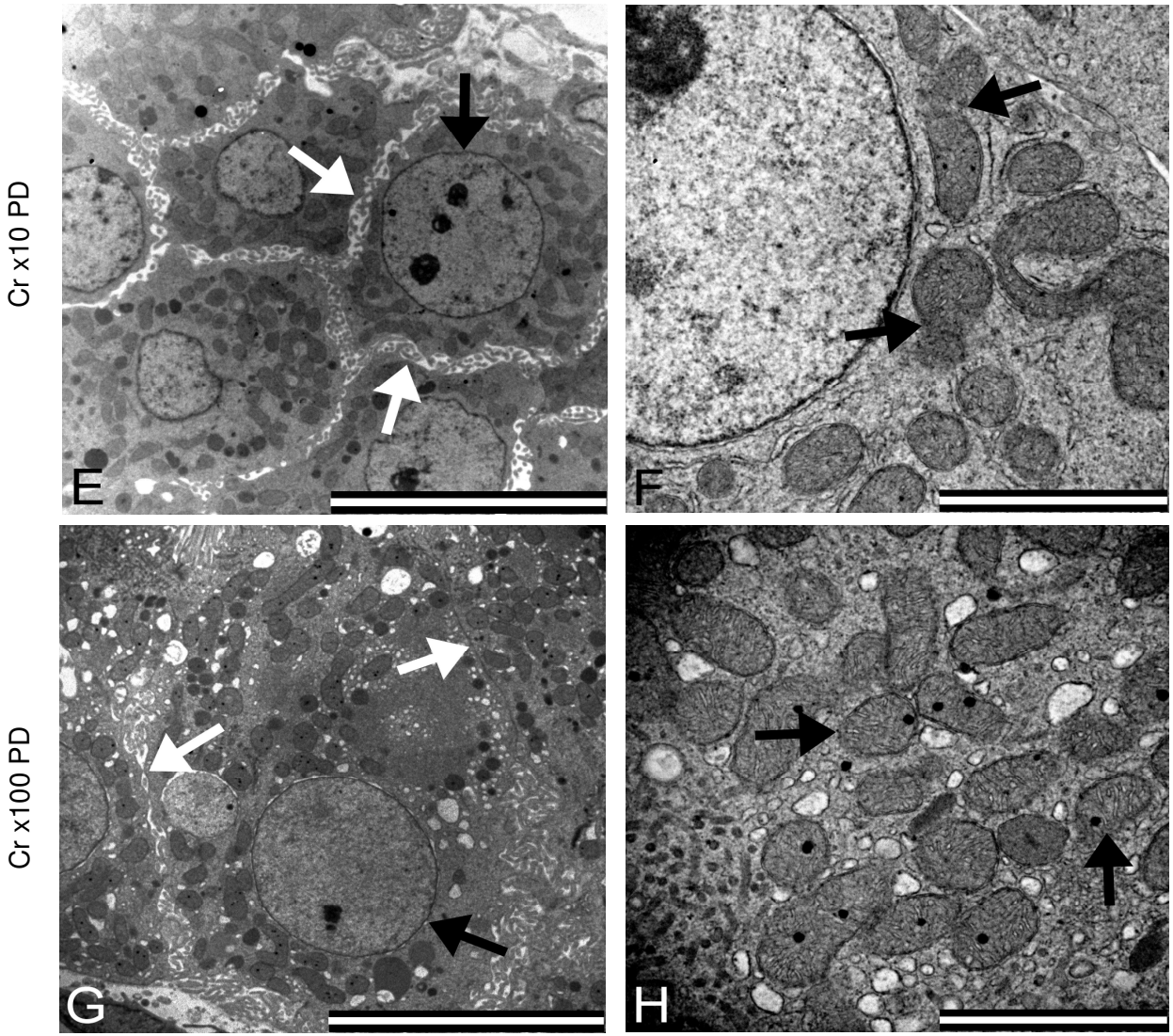

Figure 5.8 continued: Figures E and F are transmission electron micrographs of the Cr x10 PD group, with Figures G and H representing the Cr x100 PD group. Figures E and G illustrate the cuboidal cells (black arrows: nucleus and white arrows: cellular membrane) and Figures F and H the mitochondria (arrows) of the kidney (Scale bars: E, G: 10µm; F, H: 2µm).

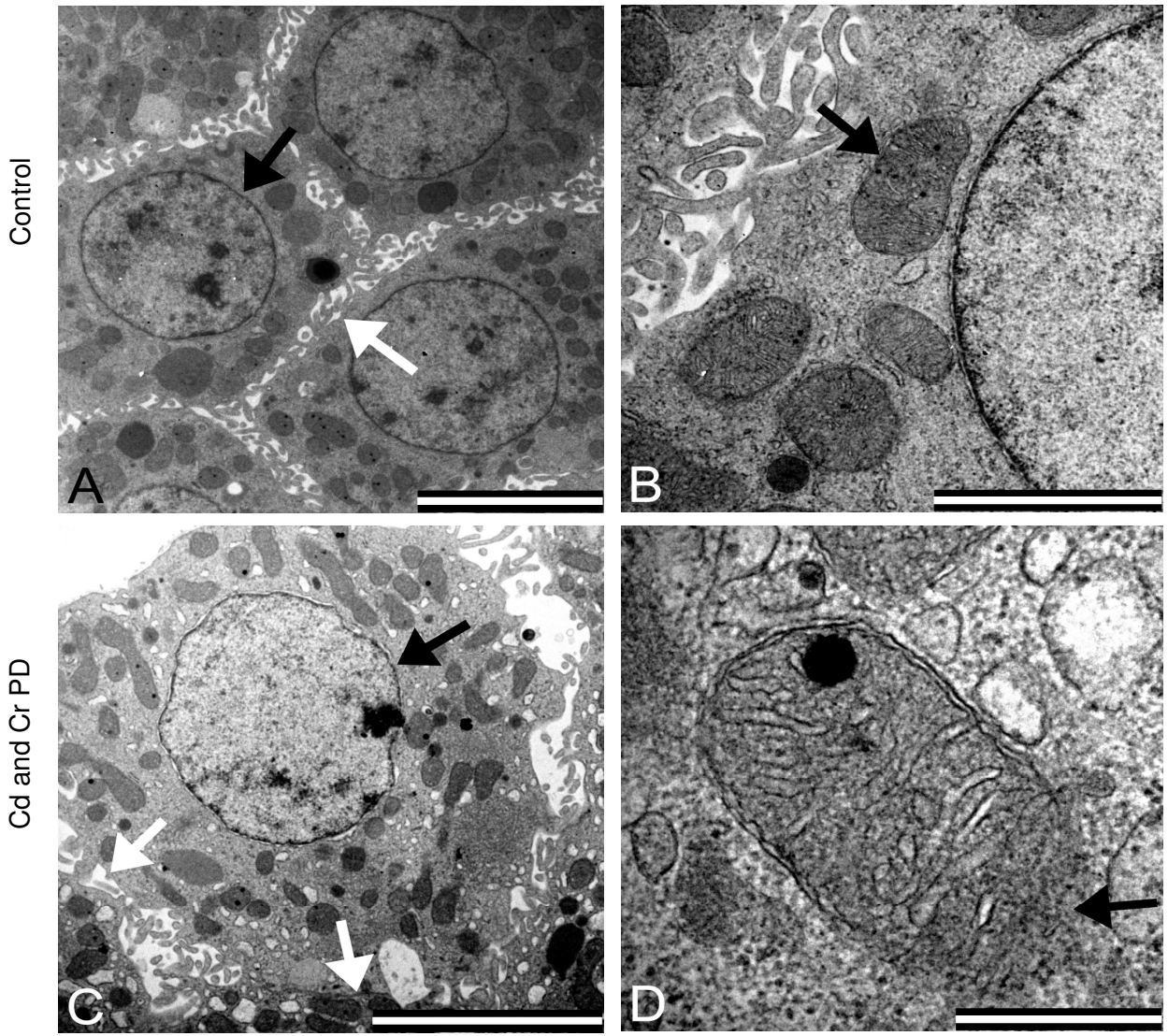

Figure 5.9: Transmission electron micrographs of kidney tissue from the control and Cd and Cr experimental groups. Figures A and B indicate the control, with Figure A showing a cuboidal cell (black arrow: nucleus and white arrow: cellular membrane) and Figure B the mitochondria (arrow). Figures C and D represent the cuboidal cells and mitochondria from the Cd and Cr PD group [Fig. C (black arrow: nucleus and white arrows: cellular membrane) and Fig. D (arrow)] (Scale bars: A, C: 5µm; B: 2µm).

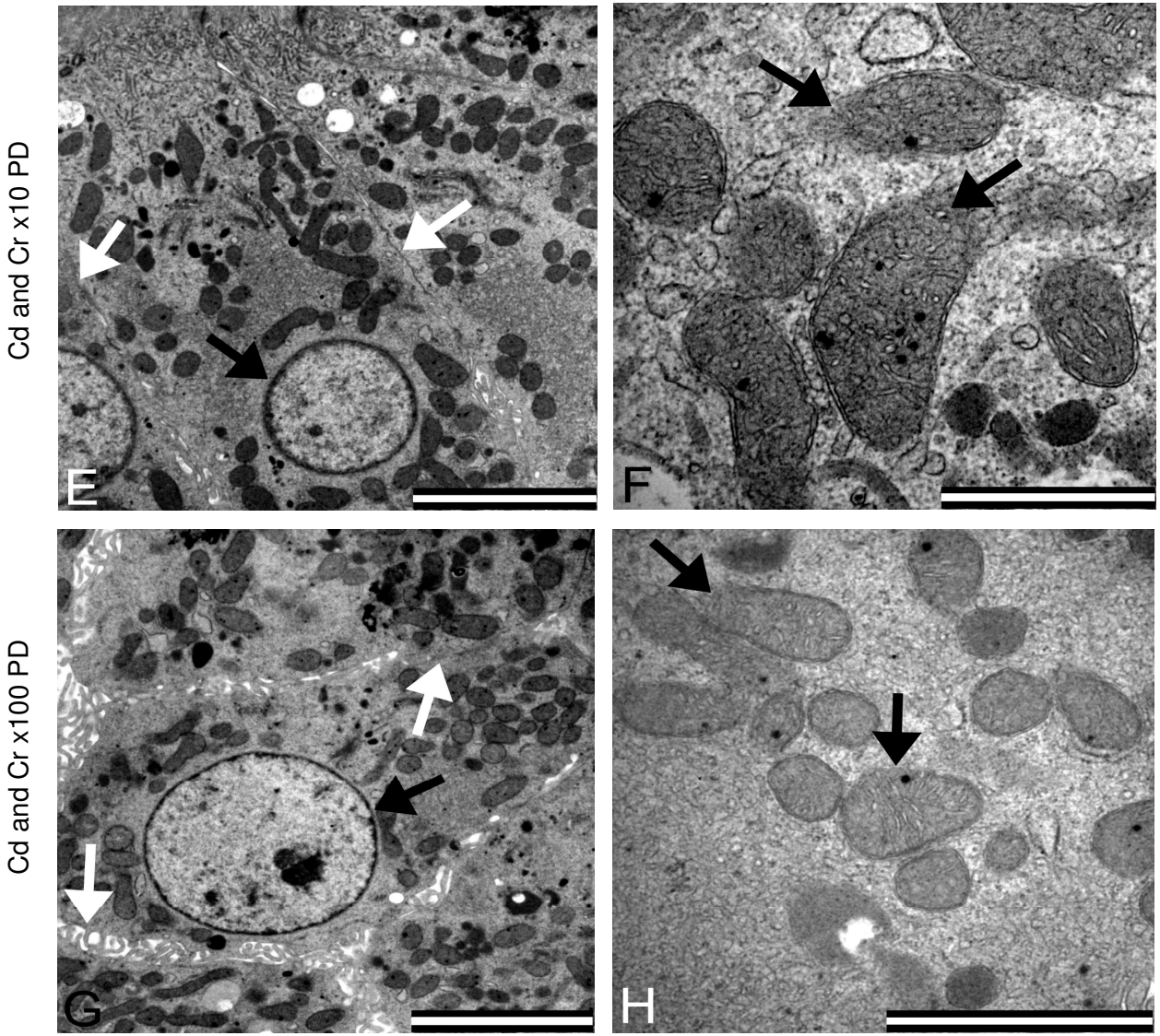

Figure 5.9 continued: Figures E and F are transmission electron micrographs of the Cd and Cr x10 PD groups, Figures G and H represent the Cd and Cr x100 PD groups respectively. Figures E and G illustrate the cuboidal cells (black arrows: nucleus and white arrows: cellular membrane) and Figures F and H the mitochondria (arrows) present in the kidney (Scale bars: A, C, E, G: 5µm; B, F, H: 2µm; F: 1µm).

Figure 5.7 represents kidney transmission electron micrographs of the control and Cd experimental groups. In the control (Fig. 5.7 A and B), the cuboidal cells of the renal tubules [Fig.5.7 A (white arrow)] and normal nuclear morphology [Fig.5.7 A (black arrow)] can be seen and in Figure 5.7 B the mitochondria (arrows) show minimal membrane disruption with no inner matrix swelling. In the Cd PD, Cd x10 PD and Cd x100 PD (Fig. 5.7 C-H respectively) no nuclear [Fig. 5.7 C, E, G (black arrow)] or cellular [Fig. 5.7 C, E, G (white arrows)] membrane disruptions could be seen with some irregular chromatin condensation and mitochondrial membrane disruption observed [Fig. 5.7 D, F, H (arrows)], with only the Cd x100 PD group [Fig. 5.7 H (arrow)] that showed some inner matrix swelling. The Cd x1000 PD group (Fig. 5.7 I and J) on the other hand showed severe rupture of the nuclear [Fig. 5.7 I (black arrow)] and cellular [Fig. 5.7 I (white arrows)] membranes, with unevenly distributed chromatin. In Figure 5.7 J (arrows) the mitochondria also showed ruptured membranes and inner matrix swelling.

No nuclear [Fig. 5.8 C, E, G (black arrows)] or cellular [Fig. 5.8 C, E, G (white arrows)] membrane disruptions were present in the Cr experimental groups (Fig 5.8 C-H), with minimal irregular chromatin condensation also present. Minimal amounts of vacuoles were also present in the cytoplasm that might be the rER lumen that increased in size. In the Cr PD and Cr x10 PD groups, no mitochondrial inner matrix swelling were visible, but in the Cr x100 PD some inner matrix swelling was visible, with minimal mitochondrial membrane [Fig. 5.8 D, F, H (black arrows)] disruption present in all the Cr experimental groups. In Figure 5.9 C-H the metal combination groups showed no nuclear or cellular membrane disruptions [Fig. 5.9 C, E and G (black and white arrows respectively)], but minimal chromatin condensation was visible in the Cr x10 PD and Cr x100 PD groups. Some ruptured mitochondrial membranes [Fig. 5.9 D, F and H (arrows)] and minimal inner matrix swelling were present in all the metal combination groups. The ultrastructural alterations seen in the kidney are summarized in Table 5.3.

Table 5.3: Summary of ultrastructural changes in the kidney tissue

Group	Chromatin condensation	Nuclear membrane disruption	Mitochondrial membrane disruption	Mitochondrial swelling	Golgi particles	Cellular membrane disruption
Control	-	-	-	-	-	-
Cd PD	++	-	++	-	++	-
Cd x10 PD	++	-	++	-	++	-
Cd x100 PD	++	-	++	+	+	-
Cd x1000 PD	+++	+++	+++	+++	++	+++
Cr PD	+	-	+	-	++	-
Cr x10 PD	+	-	+	-	++	-
Cr x100 PD	-	-	++	++	-	-
Cd and Cr PD	-	-	++	+	++	-
Cd and Cr x10 PD	+	-	++	++	++	-
Cd and Cr x100 PD	++	-	++	++	++	-

-, none; +, minimal; ++, mild; +++, severe

5.3.4. Golgi complex: Brain

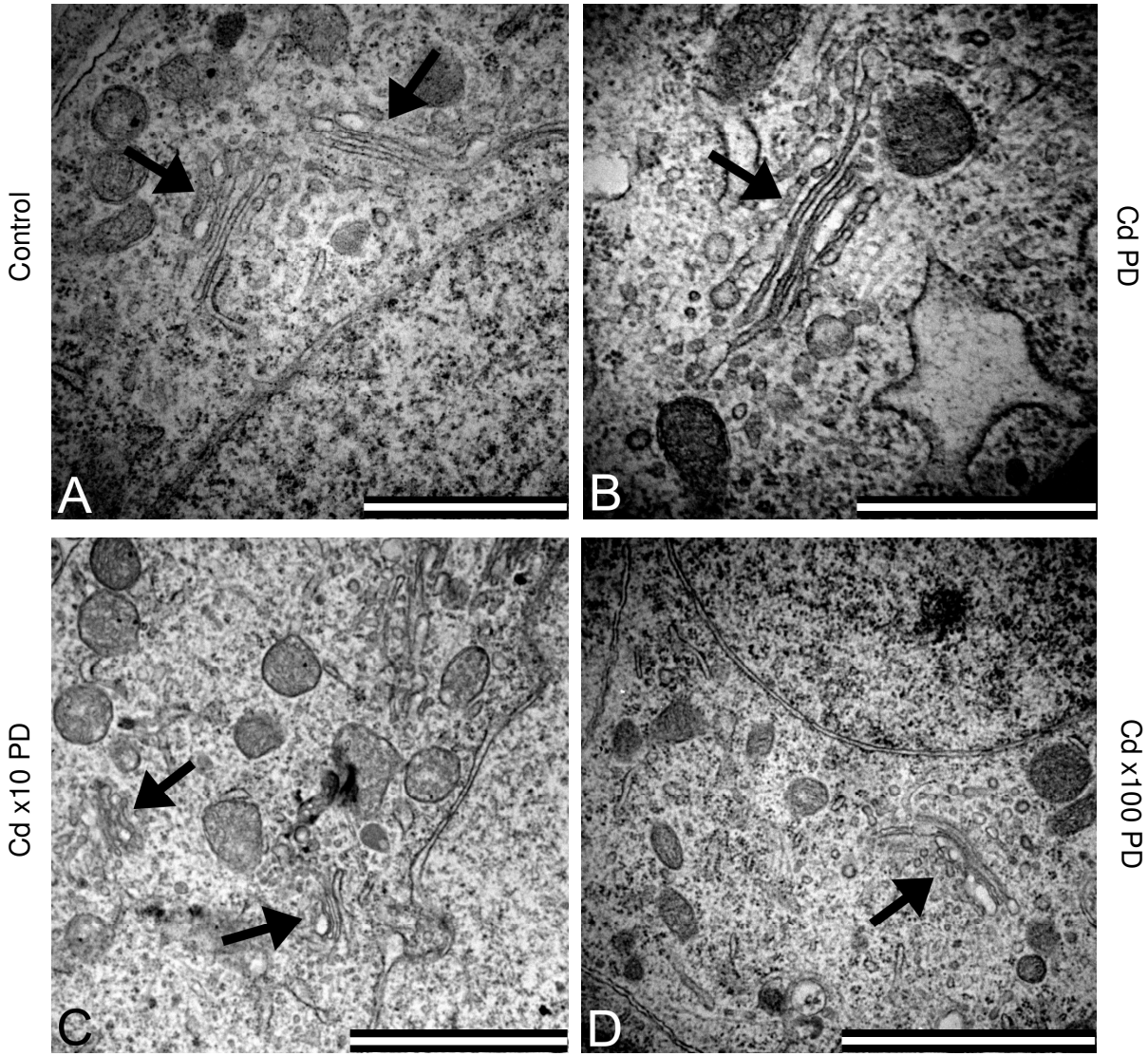

Figure 5.10: Transmission electron micrographs of the brain tissue, illustrating the Golgi complex (arrows) of the control (Fig. A), Cd PD (Fig. B), Cd x10 PD (Fig. C) and Cd x100 PD (Fig. D) groups, where no particles are visible (Scale bars: C, D: 2µm; A, B: 1µm).

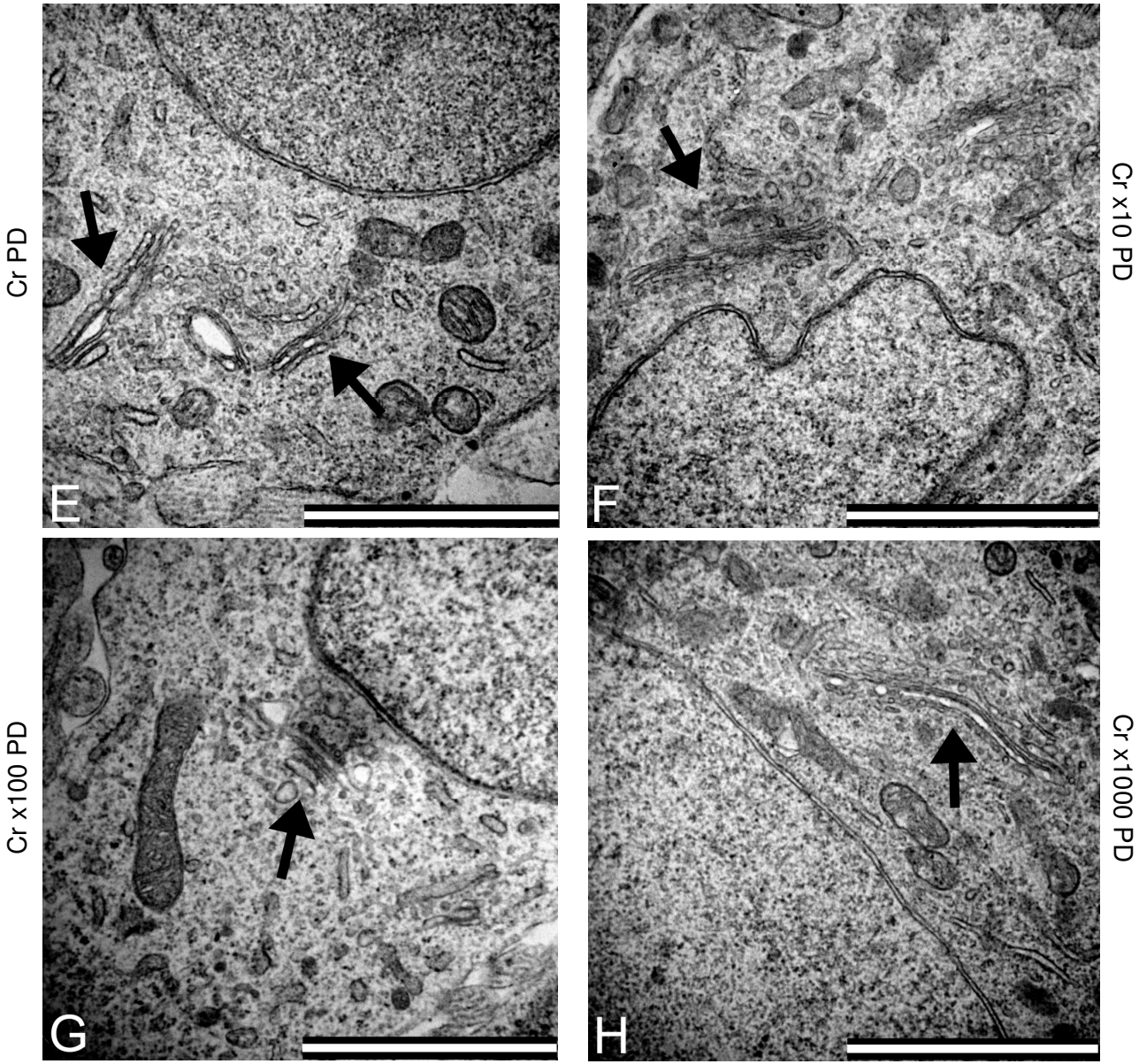

Figure 5.10 continued: Transmission electron micrographs of the brain tissue, illustrating Golgi complex (arrows) of the Cr PD (Fig. E), Cr x10 PD (Fig. F), Cr x100 PD (Fig. G) and Cr x1000 PD (Fig. H) groups, where no particles are visible (Scale bars: E-H: 2µm).

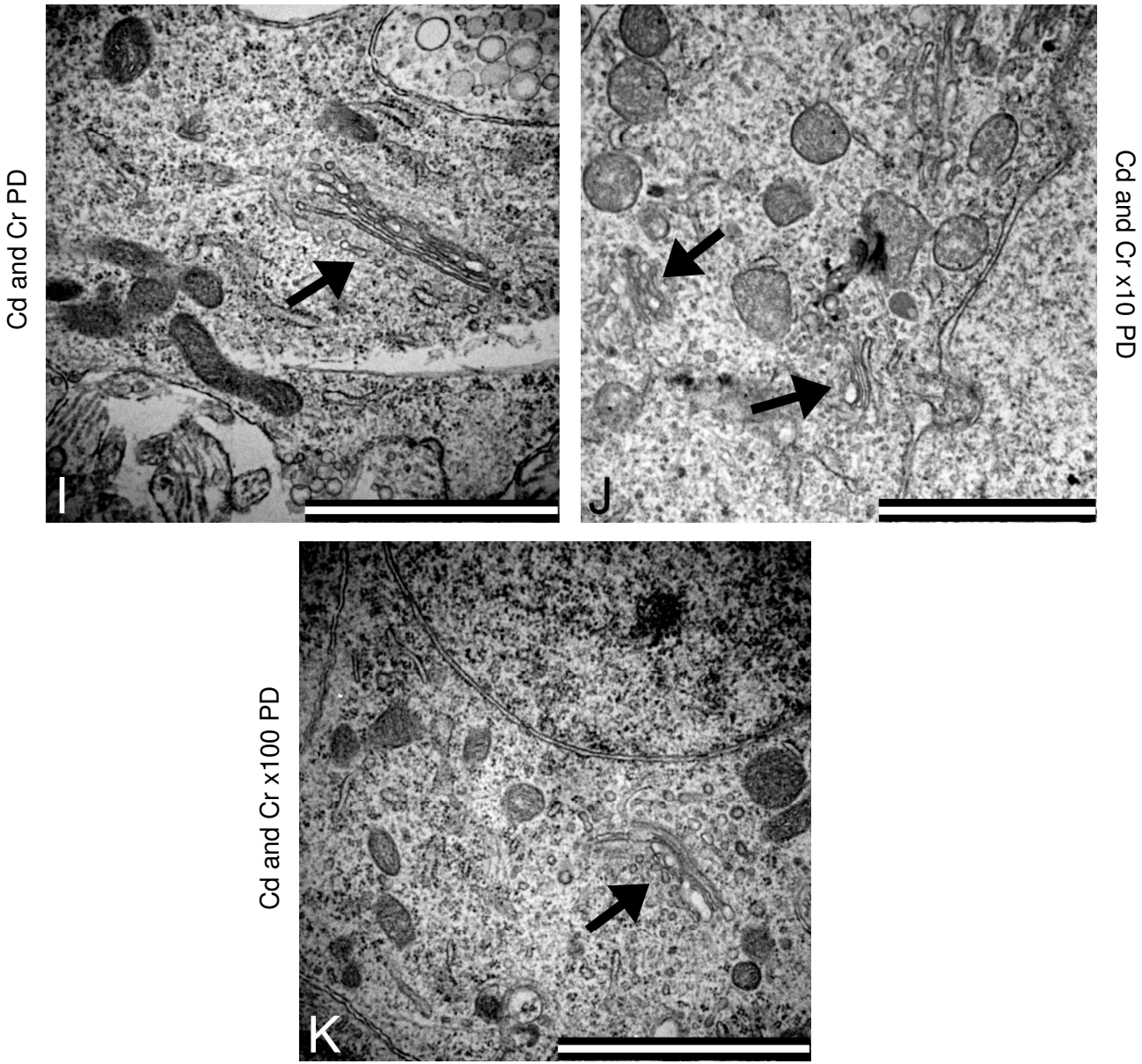

Figure 5.10 continued: Transmission electron micrographs of the brain tissue, illustrating the Golgi complex (arrows) of the Cd and Cr PD (Fig. I), Cd and Cr x10 PD (Fig. J) and Cd and Cr x100 PD (Fig. K) groups, where no particles are visible (Scale bars: I-K: 2µm).

5.3.5. Golgi complex: Liver

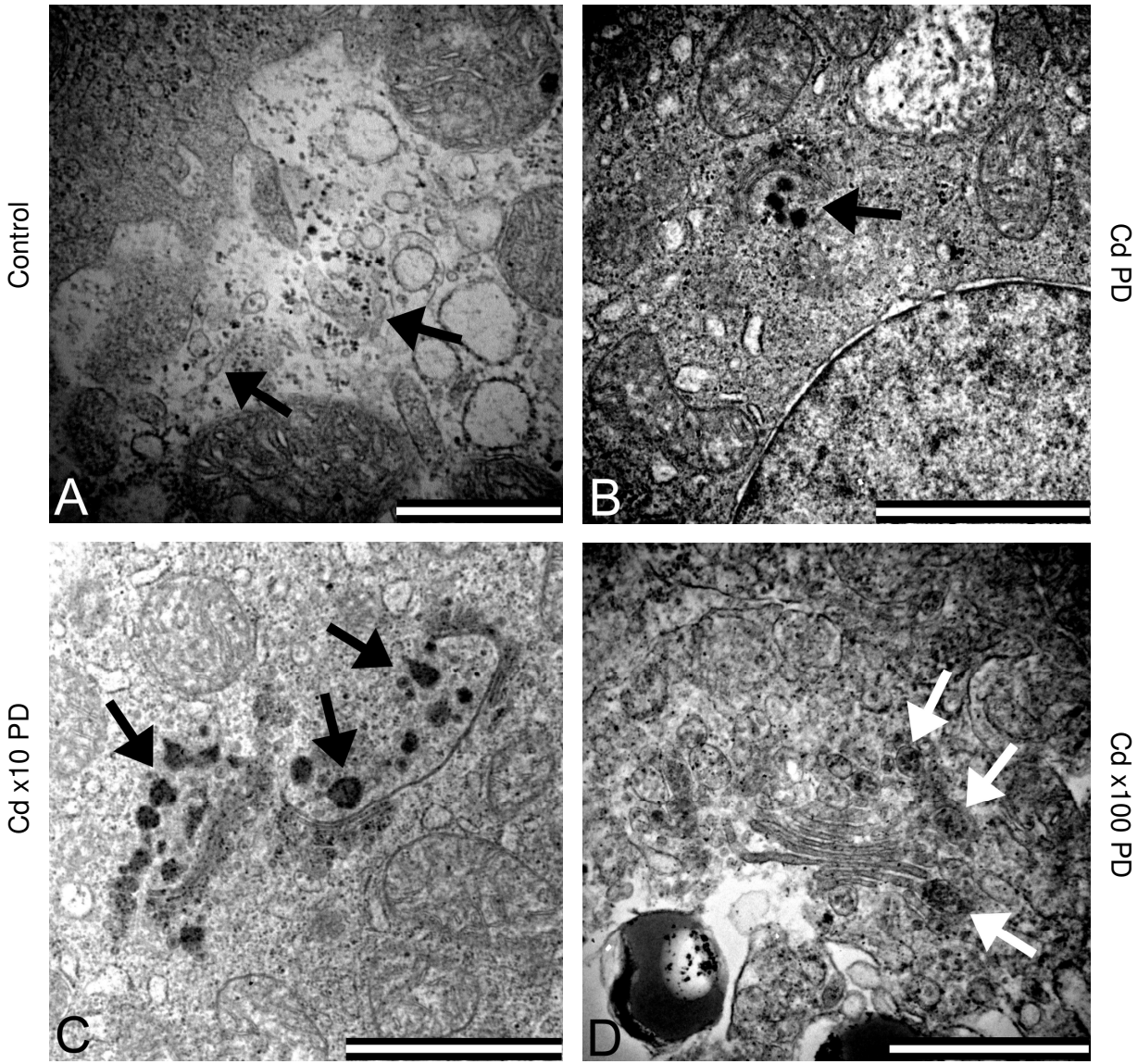

Figure 5.11: Transmission electron micrographs of the liver tissue, illustrating the Golgi complex of the control [Fig. A (arrows)], Cd PD (Fig. B), Cd x10 PD (Fig. C) and Cd x100 PD (Fig. D) groups, where particles (arrows) are visible in the Cd PD, Cd x10 PD and Cd x100 PD (Fig. B-D respectively) groups (Scale bars: B, C: 2µm; A, D: 1µm).

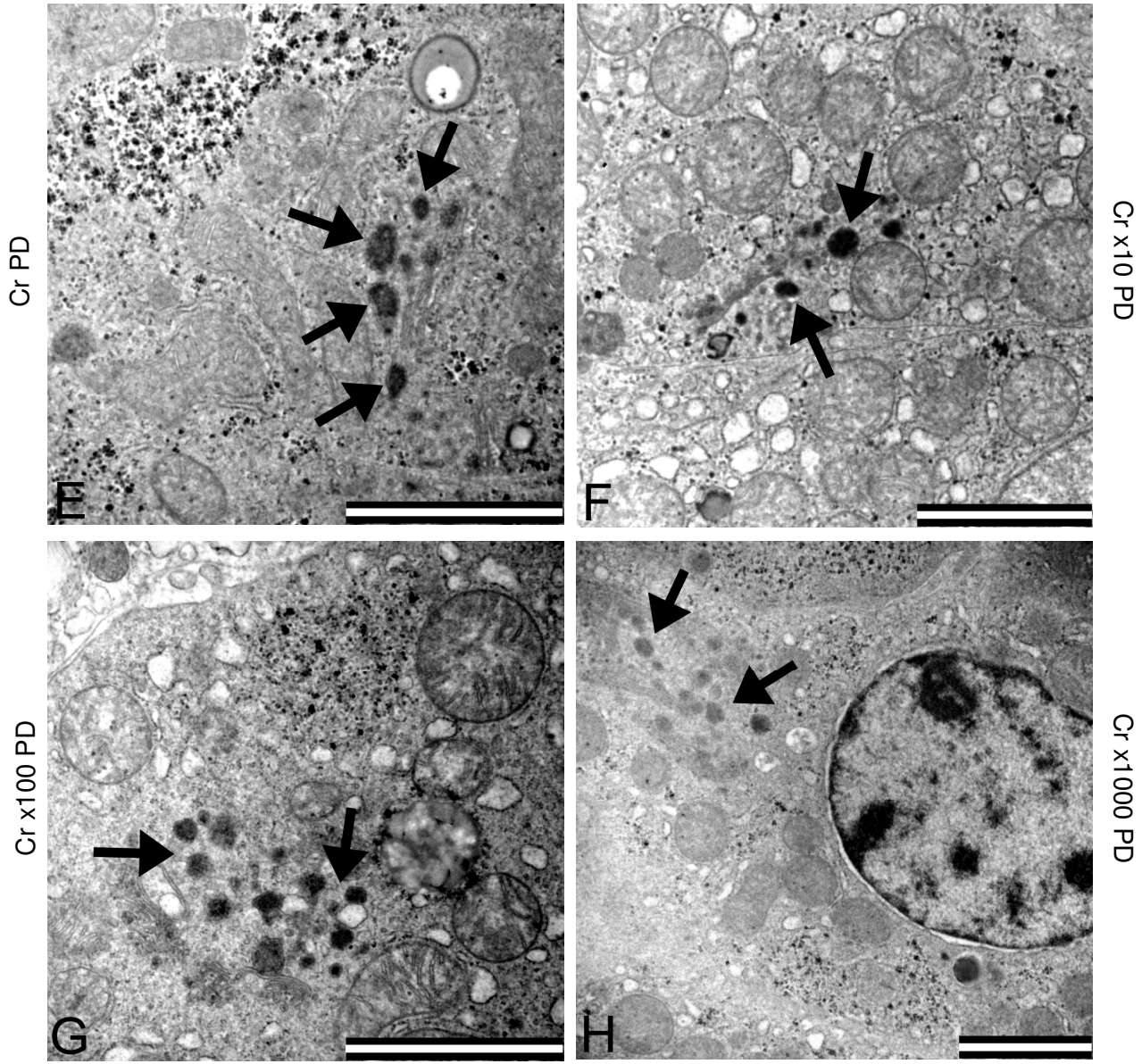

Figure 5.11 continued: Transmission electron micrographs of the liver tissue, illustrating the Golgi complex of the Cr PD (Fig. E), Cr x10 PD (Fig. F), Cr x100 PD (Fig. G) and Cr x1000 PD (Fig. H) groups, where particles (arrows) are visible at the ends of the Golgi cisternae, secretory vesicles and lysosomes (Scale bars: E-H: 2µm).

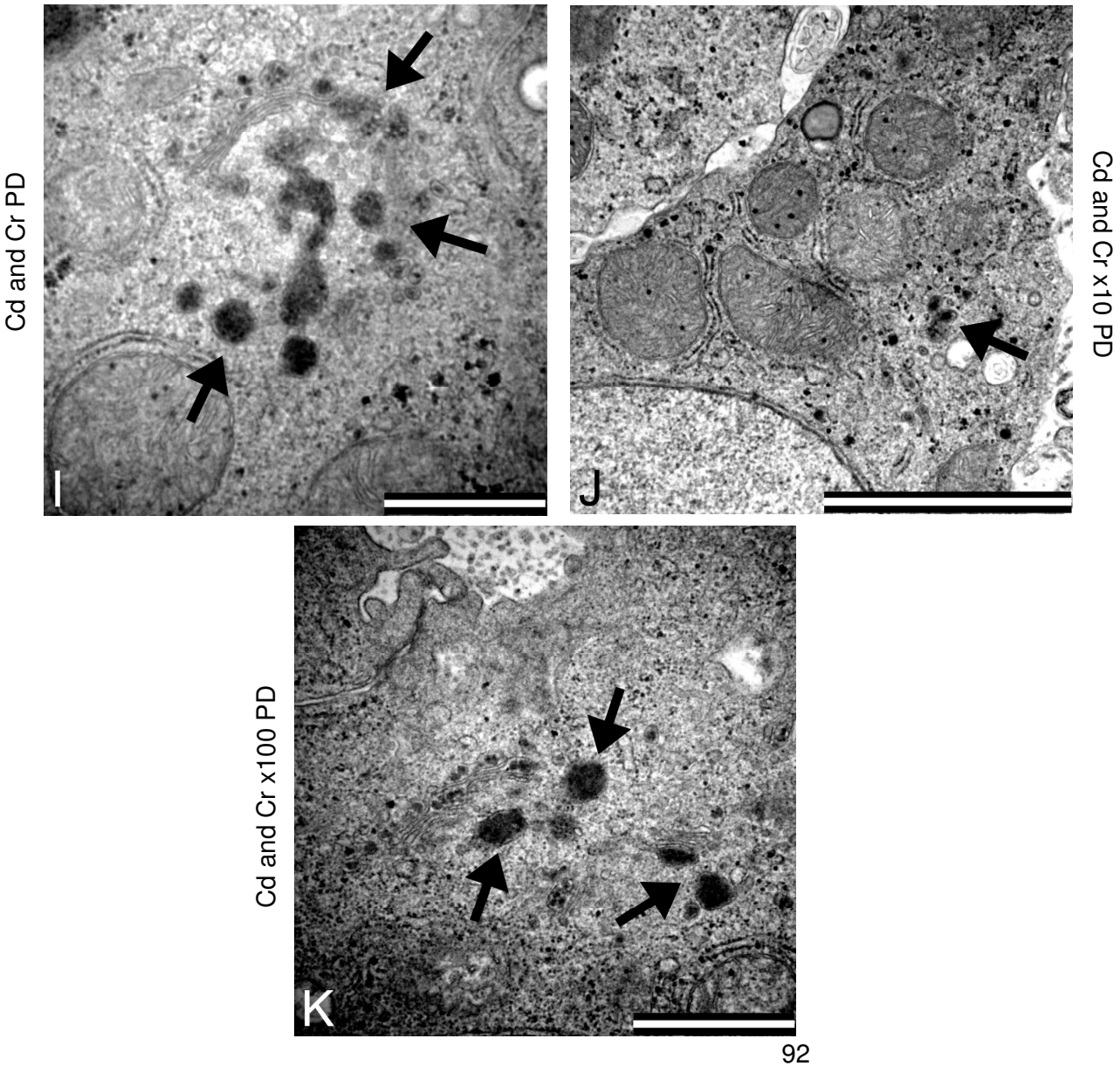

Figure 5.11 continued: Transmission electron micrographs of the liver tissue, illustrating the Golgi complex of the Cd and Cr PD (Fig. I), Cd and Cr x10 PD (Fig. J) and Cd and Cr x100 PD (Fig. K) groups, where particles (arrows) are visible at the ends of the Golgi cisternae, secretory vesicles and lysosomes (Scale bars: J: 2µm; I, K: 1µm).

5.3.6. Golgi complex: Kidney

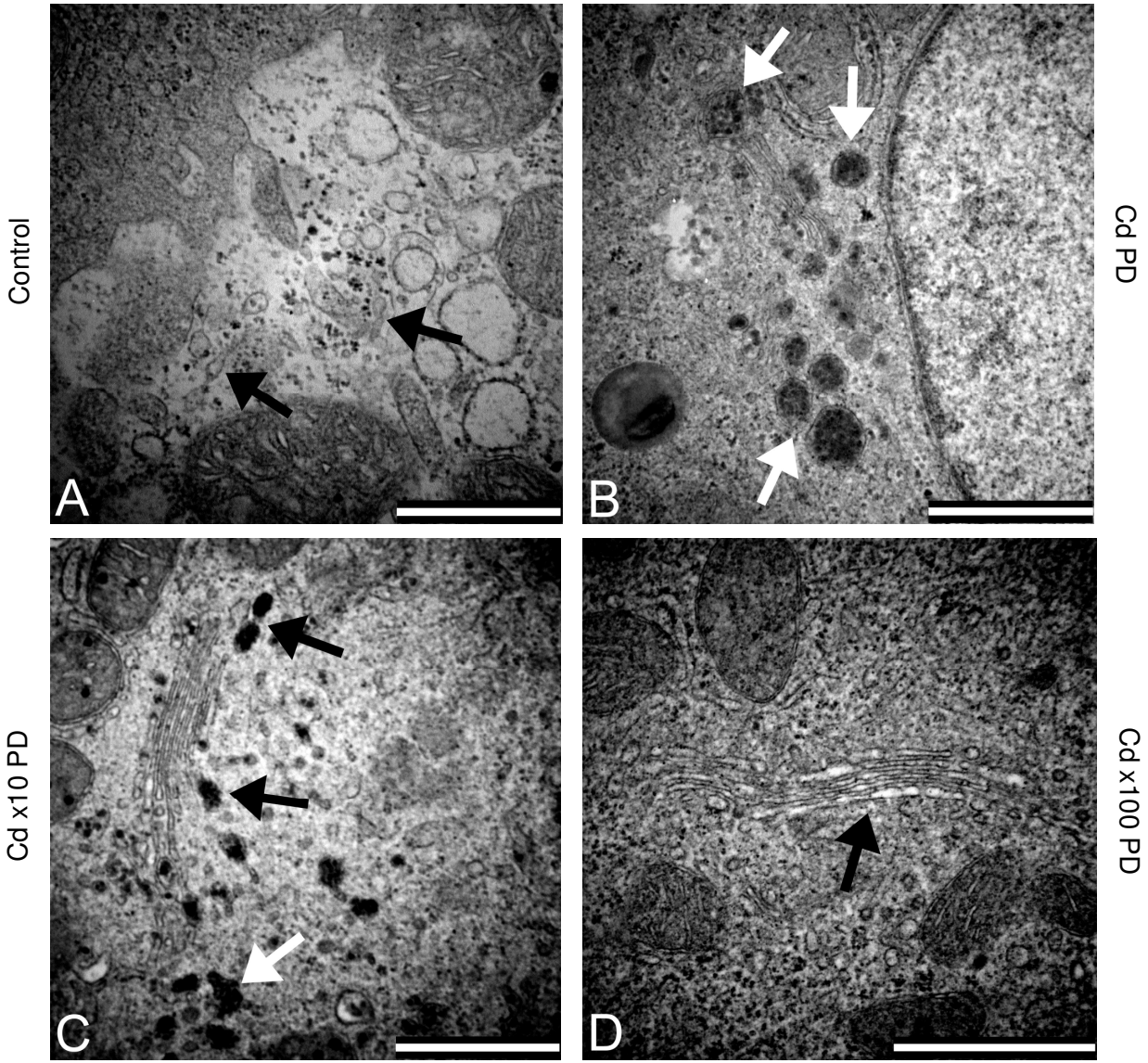

Figure 5.12: Transmission electron micrographs of the kidney tissue, illustrating the Golgi complex of the control [Fig. A (arrows)], Cd PD (Fig. B), Cd x10 PD (Fig. C) and Cd x100 PD [Fig. D (arrow)] groups, where particles (arrows) are visible in the Cd PD, Cd x10 PD and Cd x100 PD (Fig. B-D respectively) groups (Scale bars: A: 2µm; B-D: 1µm).

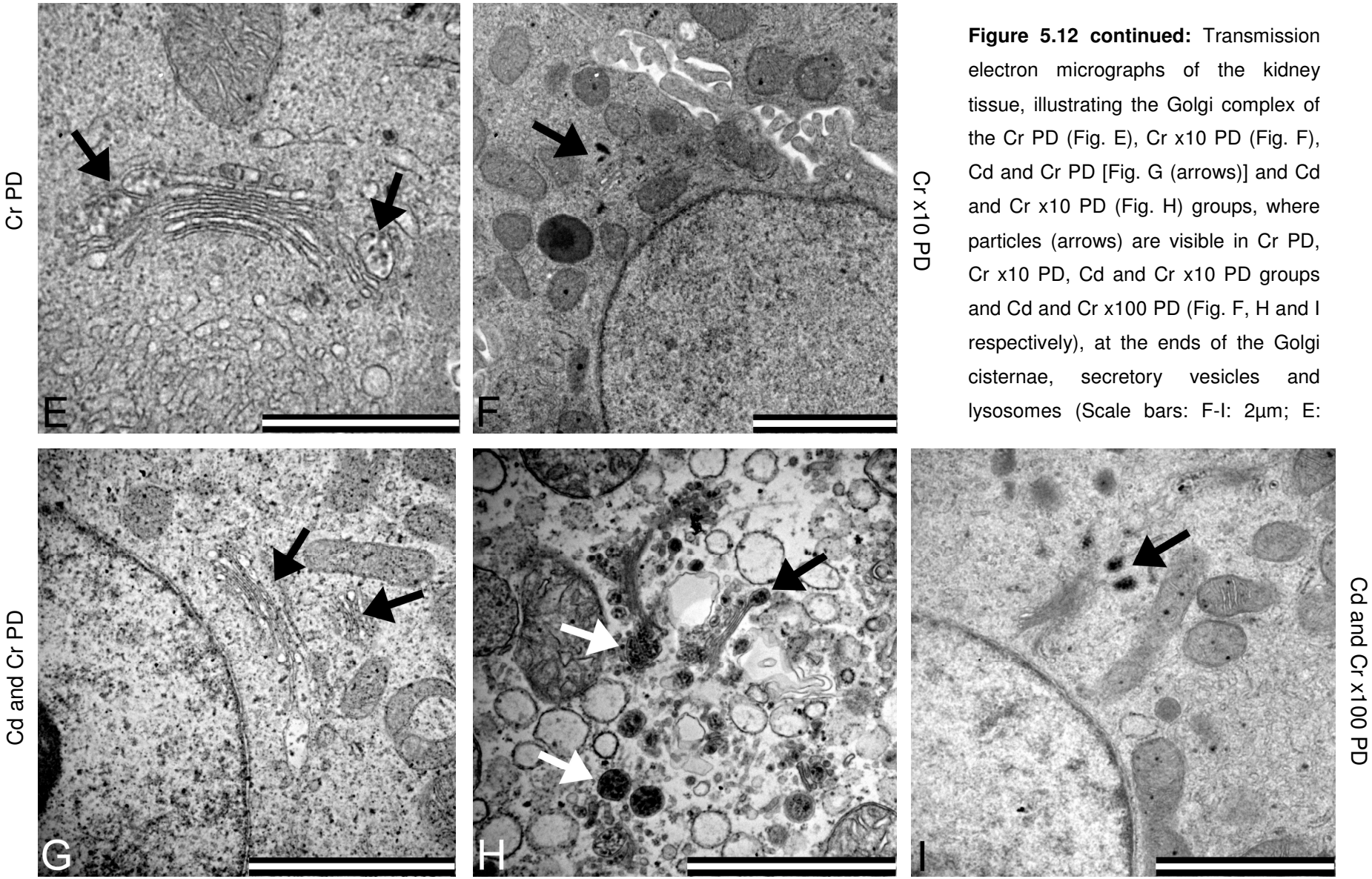

Figure 5.12 continued: Transmission electron micrographs of the kidney tissue, illustrating the Golgi complex of the Cr PD (Fig. E), Cr x10 PD (Fig. F), Cd and Cr PD [Fig. G (arrows)] and Cd and Cr x10 PD (Fig. H) groups, where particles (arrows) are visible in Cr PD, Cr x10 PD, Cd and Cr x10 PD groups and Cd and Cr x100 PD (Fig. F, H and I respectively), at the ends of the Golgi cisternae, secretory vesicles and lysosomes (Scale bars: F-I: 2µm; E:

Figures 5.10-5.12 show the Golgi complexes and particles found in the brain, liver and kidney tissue of the Cd and Cr alone and in combination groups. In the Golgi complexes in the brain [Fig. 5.10 (arrows)], no particles were found at the ends of the Golgi cisternae, secretory vesicles and lysosomes. On the other hand, most of the ends of the Golgi cisternae, secretory vesicles and lysosomes of the liver (Fig. 5.11) and kidney (Fig. 5.12) contained particles (arrows) that may suggest heavy metal detoxification. The presence or absence of particles found in the Golgi complex of the different organs is summarized in Tables 5.1-5.3.

5.4. Discussion

The presence of heavy metals such as Cd and Cr in the water supply and air, is a great cause of concern as these heavy metals may affect not only the environment, but also human health (Fatoki and Awofolu, 2003; Molokwane, *et al*., 2008; Tempelhoff, 2013). In this chapter the ultrastructural effects of Cd and Cr alone and in combination were evaluated on brain, liver and kidney tissue by using TEM. The criteria for the possible alterations that may be found in the cellular organelles and membranes included, nuclear and cellular membrane disruption, chromatin condensation, mitochondrial membrane disruption and mitochondrial inner matrix swelling. The chromatin condensation is an indication of DNA damage, with the membrane disruption of both the nucleus and mitochondria indicating lipid peroxidation (Bertin and Averbeck, 2006). Mitochondria act as osmometers in the cells and the mitochondrial swelling that was seen, reflects the entry of solutions and water into the mitochondrial matrix (Thophon, *et al*., 2004). In the Golgi complex, the presence or absence of dark particles in the ends of the Golgi cisternae, secretory vesicles and lysosomes were evaluated as this may be an indication of the removal of particles from the cell. In the cell, the function of the lysosomes is to digest worn-out organelles and the content of pinosomes or phagosomes and then transfer it out of the cells (Rink, *et al.,* 2005).

The transmission electron micrographs of the brain tissue from the control group revealed normal cellular ultrastructure, with only a slight loss of mitochondrial membrane integrity and inner matrix swelling. This may be due to the preparation technique used, as it is known that fixation with GA/FA, can cause changes in ultrastructure (Venter, *et al.,* 2013). In the individual Cd and Cr experimental groups (Fig. 5.1-5.2), no alterations were seen in the nuclear and cellular membranes, with some loss in mitochondrial membrane integrity and inner matrix swelling. Severe brain damage, which includes severe mitochondrial alteration, with almost all the cristae damaged and loss of cell membrane integrity was observed in

perinatal rat pups by Zhang and colleagues in 2009 after exposure to Cd (Zhang, *et al.*, 2009), however this could not be seen in the current study. The metal combination groups (Fig. 5.3) revealed no changes in the nuclear membrane or chromatin distribution however, with increasing concentrations, minimal disruptions in the cellular membrane could be seen, in conjunction with some alterations in the mitochondrial membrane and inner matrix.

In the liver tissue from the control group, normal ultrastructure of the hepatocytes was observed (Fig. 5.4; 5.5; 5.6 A and B). In the groups exposed to Cd, the Cd PD (Fig. 5.4 C and D) and Cd x10 PD (Fig. 5.4 E and F) revealed no ultrastructural changes compared to the control, whereas in the Cd x100 PD group (Fig. 5.4 G and H) some irregular chromatin condensation, cellular and mitochondrial membrane disruption and mitochondrial inner matrix swelling were observed, as well as minimal sinusoidal dilation. The Cd x1000 PD group (Fig. 5.4 I and J) displayed major ultrastructural alterations, with only the nuclear membrane that remained intact. Similar observations were seen in a study by Thophon, *et al.* in 2004 where the authors found chromatin clumping and swollen mitochondria after exposure of White Sea bass to Cd (Thophon, *et al.,* 2004). With the Cr (Fig. 5.5) and metal combination groups (Fig. 5.6), no nuclear and cellular membrane disruption and sinusoidal dilation were visible. All the metal combination groups illustrated minimal chromatin condensation. The Cr x1000 PD group revealed some irregular chromatin condensation (Fig. 5.5 I). Both the Cr and metal combination groups displayed minimal mitochondrial membrane disruptions and inner matrix swelling. Alterations similar to what was seen in the results obtained from the Cr-exposed groups were also reported by Wang, *et al*. in 2006, where the toxicity of Cr on mice liver tissue was evaluated (Wang, *et al.,* 2006).

Major ultrastructural changes were also observed in the kidney cells of the Cd x1000 PD group (Fig. 5.7 I and J), where nuclear, cellular and mitochondrial membrane disruptions, irregular chromatin condensation and mitochondrial inner matrix swelling was apparent. Chromatin condensation and swollen mitochondria were also found in the kidney cells of White Sea bass in the study done by Thophon, *et al*. in 2004. These authors concluded that the presence of Cd at specific sites in both the liver and kidney, can help with the understanding of the underlying toxicological processes (Thophon, *et al*., 2004). Some chromatin condensation and loss of mitochondrial membrane integrity were visible in all the lower Cd concentration groups (Fig. 5.7 C-H) with only the Cd x100 PD group (Fig. 5.7 H) showing minimal mitochondrial inner matrix swelling. This might indicate that after the mitochondrial membrane was damaged, the additional Cd could enter the mitochondria and influence the mitochondrial matrix.

The Cr (Fig 5.8) experimental groups had no nuclear or cellular membrane disruptions with minimal mitochondrial membrane ruptures present. Slight chromatin condensation was observed in all the Cr groups, with only the Cr x100 PD group revealing some inner matrix swelling (Fig. 5.8 H). Previous studies done by Kim and Na in 1991, indicated that nephrotoxicity occurs when rats are exposed to hexavalent chromium (Kim and Na, 1991) and thus some nuclear and mitochondrial alterations are expected due to the physiology of Cr (See Chapter 2, section 2.4). In the Cr PD (Fig 5.8 D) and Cr x100 PD (Fig. 5.8 H), a different variation was seen in the rER, as the cisternae were dilated compared to the normal parallel arranged cisternae (Coetzee, *et al*., 2009). Although this was not expected in this study, it was found previously by Doughtie and Rao in 1984 that swollen rER can also be one of the effects of Cr on kidney tissue, as the dilation of the rER can be caused by the increase of water in the cells due to intoxication with harmful substances like heavy metals (Doughtie and Rao, 1984; Ghadially, 1988).

In the metal combination groups (Fig. 5.9 C-H), no nuclear and cellular membrane disruptions were seen, with minimal chromatin condensation in the Cd and Cr PD (Fig. 5.9 C) and Cd and Cr x100 PD (Fig. 5.9 E) groups. Some mitochondrial membrane disruption and inner matrix swelling was seen in all the metal combination groups. Golgi complex particles were seen at the ends of the Golgi cisternae, secretory vesicles and lysosomes in all the experimental groups of the liver and kidney tissue (Fig 5.11-5.12). The particles seen at the ends of the Golgi cisternae, secretory vesicles and lysosomes consist of Cd and Cr as detected by the electron energy-loss spectroscopy (EELS), explained in Chapter 6. The presences of the metals in the lysosomes may indicate that the metals are already being processed to be removed from the cells. The reason for the presence of metals at the ends of the Golgi cisternae and secretory vesicles is unknown, as metals are not processed by the Golgi complex and requires further investigation.

5.5. Conclusion

From the ultrastructural findings of the current chapter it can be concluded that Cd and Cr alone and in combination had no major effect on the brain tissue. These results indicated that even though the blood brain barrier (BBB) of the chick embryo is still developing and is not as effective as that of an adult (Nordberg, *et al*., 2007b), it does protect against major neuronal alterations. In the results obtained from analysis of the liver and kidney tissue, the Cr and metal combination groups showed irregular chromatin condensation, loss of mitochondrial membrane integrity and swelling of the inner matrix. These findings may lead to minimal functional changes at all the concentrations of Cr and Cd and Cr combined,

except at the highest concentration metal combination group, as no embryos survived. Only the two highest concentrations of Cd caused ultrastructural changes in the liver with only the nuclear membrane remaining intact. Kidney analysis of the Cd experimental groups also revealed major ultrastructural changes in the Cd x1000 PD group. These ultrastructural changes, seen at these higher dosages, may lead to functional changes in the liver and kidney and ultimately lead to organ failure. Particles were observed in the Golgi complexes in the liver and kidney cells of all the metal groups.

Thus, due to the detoxification and filtering functions of the liver and kidney respectively (Coetzee, *et al.,* 2009), more ultrastructural changes were observed in these organs compared to the brain. More severe ultrastructural alterations were observed at the higher concentrations of Cd exposure in the liver and kidney tissue, but the Cr and metal combination groups illustrated consistent minor nuclear chromatin and mitochondrial alterations. This indicates that the Cr alone and the Cd and Cr in combination enters the cells without causing damage to the cellular or nuclear membranes, where Cd, at the higher concentrations, affects all the investigated components of the cell. Prolonged exposure to the lower concentrations of Cr and the metal combination might result in major cellular effects and changes in the function of these organs.

Chapter 6

Investigating the presence of Cd and Cr in brain, liver and kidney tissue by using EDS and EELS

6.1. Introduction

In this chapter, the ultrastructural damage observed in the previous chapter was further investigated by determining the presence of cadmium (Cd) and chromium (Cr) using energy dispersive spectroscopy (EDS) and electron energy-loss spectroscopy (EELS). In the previous chapter minimal ultrastructural alterations were seen in the brain with Cd and Cr alone and in combination. In the liver and kidney tissue exposed to the Cr and metal combination groups, irregular chromatin condensation, loss of mitochondrial membrane integrity and swelling of the inner matrix were observed. Only the highest concentrations of Cd caused major alterations in the liver and kidney. In order to analyse an unknown particle seen with the transmission electron microscope (TEM), EDS and EELS analytical techniques are used to allow a better understanding of the nature and localization of these particles. These types of electron microscopes are called analytical electron microscopes (AEM). Two types of AEM procedures exist namely EDS and EELS (Bozzola and Russell, 1999). Both these procedures were employed in this study and thus a brief explanation of each is given below.

When the electron beam strikes a thin specimen in the TEM, X-rays are generated. The EDS system detects these X-rays and identifies the elements present in the sample by using a computer program (Williams and Carter, 1996b). With EDS, two types of signals are produced, characteristic and continuum X-rays. Characteristic X-rays are produced when high-energy beam electrons penetrate the outer shell of a molecule and interact with the inner shell electron. An electron from the inner shell consequently gets ejected and leaves a space open for an electron of the outer shells to fill the space. When the outer shell electron moves to fill the space in the inner shell, it emits X-ray energy (Williams and Carter, 1996b) and because each element fills the vacancy of the shell in a unique way, each element will generate a unique series of peaks and this can be used to identify the element present in a specific sample (Bozzola and Russell, 1999). The characteristic X-rays are named according to the position from where the electron that replaces the empty space comes from. The shell closest to the nucleus is called the K-shell followed by the L and M-shells. Thus when the electron is ejected out of the K-shell and an electron from the L-shell fills the space, a K_α X-ray is formed and if it is filled from the M-shell, a K_β X-ray is generated. The same principle applies to the rest of the shells (Williams and Carter, 1996b).

Continuum X-rays are produced when the incoming beam electron passes close to the nucleus and is slowed by the coulomb field of the nucleus. The closer the electron gets to the nucleus, the more intense the X-ray energy is that is released (Bozzola and Russell, 1999). The energy distributions of these X-rays are variable and are thus known as the background X-rays. The continuum X-rays are always formed and may mask the discrete characteristic X-rays that are used for identifying elements. The continuum X-rays can be used to measure specimen mass thickness, when quantitative analysis is needed on the thin specimens (Bozzola and Russell, 1999). After EDS analysis on the unknown element in the tissue is performed, it produces a spectrum that plots the X-ray counts against the X-ray energy (Williams and Carter, 1996c). These spectra show the elements found in the tissue and from these spectra the computer software gives quantitative information that can be used to analyse the amount of the elements that are present and whether the amount analysed is statistically significant.

The other analytical procedure that can be performed is EELS. This technique measures the change in kinetic energy of electrons after it has interacted with a thin specimen (Bozzola and Russell, 1999; Egerton, 2009). The EELS detector can be positioned either below the viewing screen of the TEM or in the column of the TEM underneath the specimen (Bozzola and Russell, 1999; Egerton, 2009). The process starts when the electron beam has interacted with the specimen, where after the beam travels to the magnetic prism where it is bent in various degrees. The lower energy electrons are deflected further than the higher energy electrons, causing the various electron group focal points to be physically separated. The electron beam can be adjusted to only allow electrons of a certain energy range to pass into the detector. This is needed to identify a specific element in the tissue.

After analysis by the detector, a spectrum, given in electron volts (eV), is produced. With a typical spectrum 3 regions are identified. Firstly the zero-loss peak that occurs at 0eV to about 2eV and represents the electrons that did not undergo inelastic scattering (interaction with the electrons of the specimen). The next peak is at another low-loss peak that comes from inelastic scattering by conduction or valance electrons (Ahn, *et al.,* 1983; Egerton, 2009; Williams and Carter, 1996c). The next peak is situated at about 54eV, where inelastic scattering arises from the inner-shell electrons. This peak is characterized by a rapid rise and followed by a gradual fall that is termed the ionization edge. This edge, that is characteristic for each element, can then be used to identify if the element in question is located in the sample (Figure 6.1) (Ahn, *et al.,* 1983; Egerton, 2009; Williams and Carter, 1996c). With EELS the background energy can be extrapolated and subtracted to provide a quantitative estimation of the concentration of the element of interest (Figure 6.1) (Egerton,

2009). This makes EELS more sensitive than EDS, thus ideal for tissue with minimal amounts of the element of interest present in the sample (Egerton, 2011). With this more sensitive method, electron spectral imaging (ESI) analysis can be performed to produce elemental maps that provide a spatial distribution of the elements of interest (Egerton, 2009).

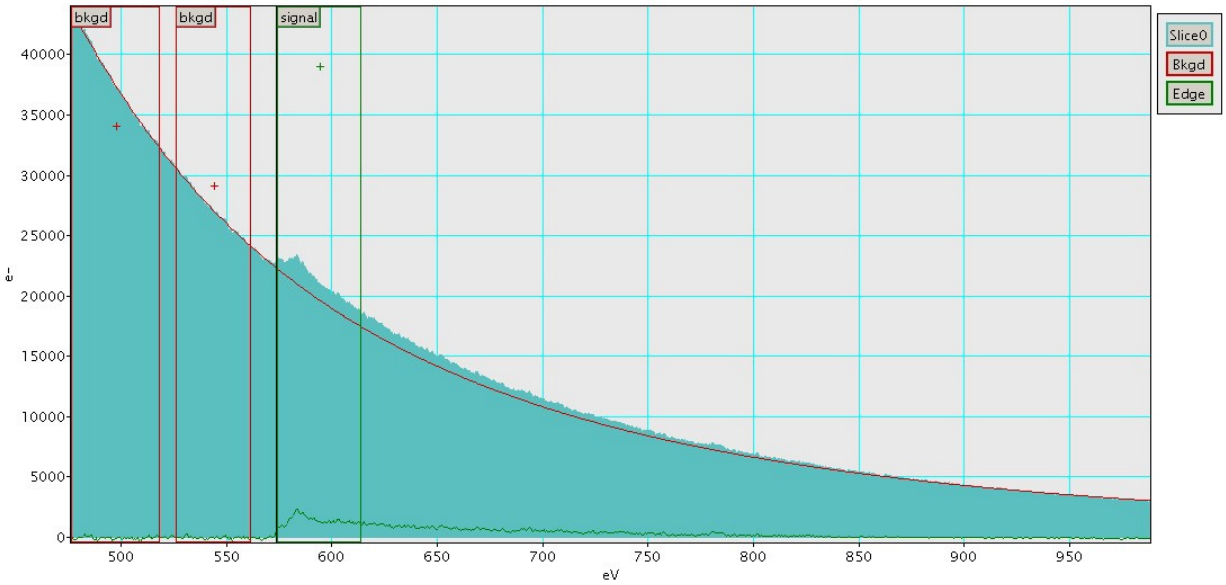

Figure 6.1: EELS spectrum that indicates the Cr edge at 574eV (Ahn, *et al.*, 1983) (green block), with the background noise (red blocks) subtracted.

Therefore, in this chapter the results obtained from EDS and EELS analyses are shown. The results include the chemically fixed and high pressure frozen analysis of the brain, liver and kidney tissue that were analysed for Cd and Cr, at their different dosages.

6.2. Materials and methods

Samples were obtained as described in Chapter 3.

6.2.1. 2.5% Glutaraldehyde/Formaldehyde fixing

The tissue samples were fixed in 2.5% glutaraldehyde (GA)/formaldehyde (FA) [1mℓ of 25% GA, 1mℓ of 25% FA, 5mℓ phosphate (PO_4) buffer (0.15M), 3mℓ ddH_2O] for 1 hour, rinsed three times in 0.075M PO_4 buffer (pH=7.4) for 15 minutes each before being placed in a secondary fixative, 1% osmium tetroxide solution, for 1 hour. Following fixation, the samples were rinsed again as described above before being dehydrated in 30%, 50%, 70%, 90% and three changes of 100% ethanol for 15 minutes each. The samples were then embedded in EMbed 812 resin and ultra-thin sections (70-100nm) were cut with a diamond knife using an

ultramicrotome (Reichert-Jung Ultracut E). Samples were then contrasted with uranyl acetate for 5 minutes followed by 2 minutes of contrasting with lead citrate, after which samples were allowed to dry for a few minutes before being examined with the JEOL TEM (JEM 2100F).

6.2.2. High Pressure Freezing

In addition the brain samples were subjected to high pressure freezing (HPF) with freeze substitution, because this procedure does not require chemical fixation and keeps the tissue close to its native state. Due to the fact the HFP with freeze substitution does not require chemical fixation, it makes it ideal method for EDS and EELS analysis. Brain samples were cut into a thickness of 200µm and then trimmed to 1mm in diameter. The samples were transferred to a flat membrane carrier and were loaded into the HPF and fast frozen. High pressure freezing is such a time consuming and expensive method and only a few samples can be processed at a time. Therefore the brain samples were processed by HPF and the rest of the organs were chemically fixed with 2.5% GA/FA.

6.2.3. Freeze substitution

After HPF, the samples were transferred to the freeze substitution (FS) machine by use of the flow-through rings. The samples were then covered with a 0.5% osmium and 99% acetone solution. The samples were slowly warmed up from -90ºC to 0ºC over a 48 hour period. After slowly warming, the samples were washed three times with 100% acetone for 5 minutes each. After the samples were washed, they were embedded in EMbed 812 resin and ultra-thin sections (90-150nm) were cut with a diamond knife using an ultramicrotome (Reichert-Jung Ultracut E) and were then contrasted with uranyl acetate for 5 minutes followed by 2 minutes of contrasting with lead citrate, after which samples were allowed to dry for a few minutes before examination with the JEOL TEM (JEM 2100F).

6.2.4 EDS measurements

EDS analysis was done with the aid of INCA Oxford software system on 90-150nm thick sections. When an unknown particle or cluster of particles was observed in the tissue with TEM, the focus was increased in that specific area and the TEMQuant software system was then used to determine the presence of the heavy metals under investigation. Different analysing tools were used with the TEMQuant software, namely individual point analysis and

mapping of an entire area of unknown particles. The results are displayed as an EDS spectrum together with a table that indicates the amount of each metal present in the sample. EDS analysis was performed on the brain (chemically fixed and HPF with FS samples), liver and kidney (only chemically fixed samples).

6.2.5. EELS measurements

Tecnai F20 high resolution TEM equipped with the GIF 2001 energy filter for EELS and electron spectral imaging (ESI) analyses were used to evaluate ±60nm thick liver sections. When an unknown particle or cluster of particles was observed in the tissue with TEM, EELS was used to determine the presence of the heavy metals under investigation. The results were displayed in an EELS spectrum [Cd: 403.7eV and Cr: 574eV (Ahn, *et al.,* 1983)], confirming the presence of the heavy metals in the sample. Together with the ESI colour map of the specific area analysed, the exact position of the metals in the sample was visually expressed. Due to limited time available on the microscope, only the liver tissue could be analysed with EELS. This was done at the Electron Microscope Unit of the University of the Western Cape, South Africa.

6.3. Results

6.3.1. EDS analysis results

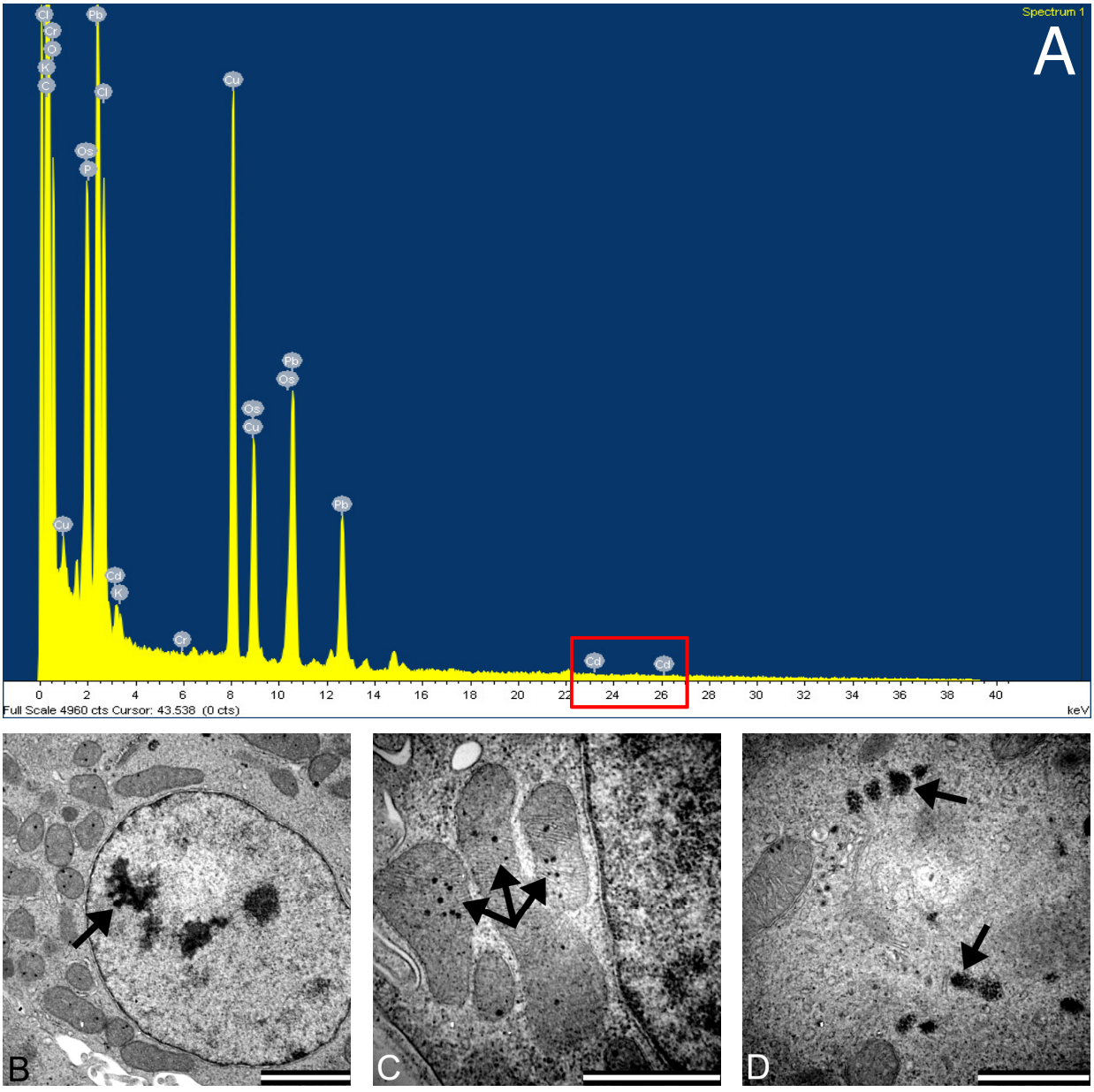

Figure 6.2: Representation of a Cd EDS spectrum [Fig. A (Cd detection in the red square)] and transmission electron micrographs that demonstrate typical particles (arrows) analysed in the nucleus (Fig. B), mitochondria (Fig. C) and Golgi complex (Fig. D) (Scale bars: B: 2µm; C, D: 1µm).

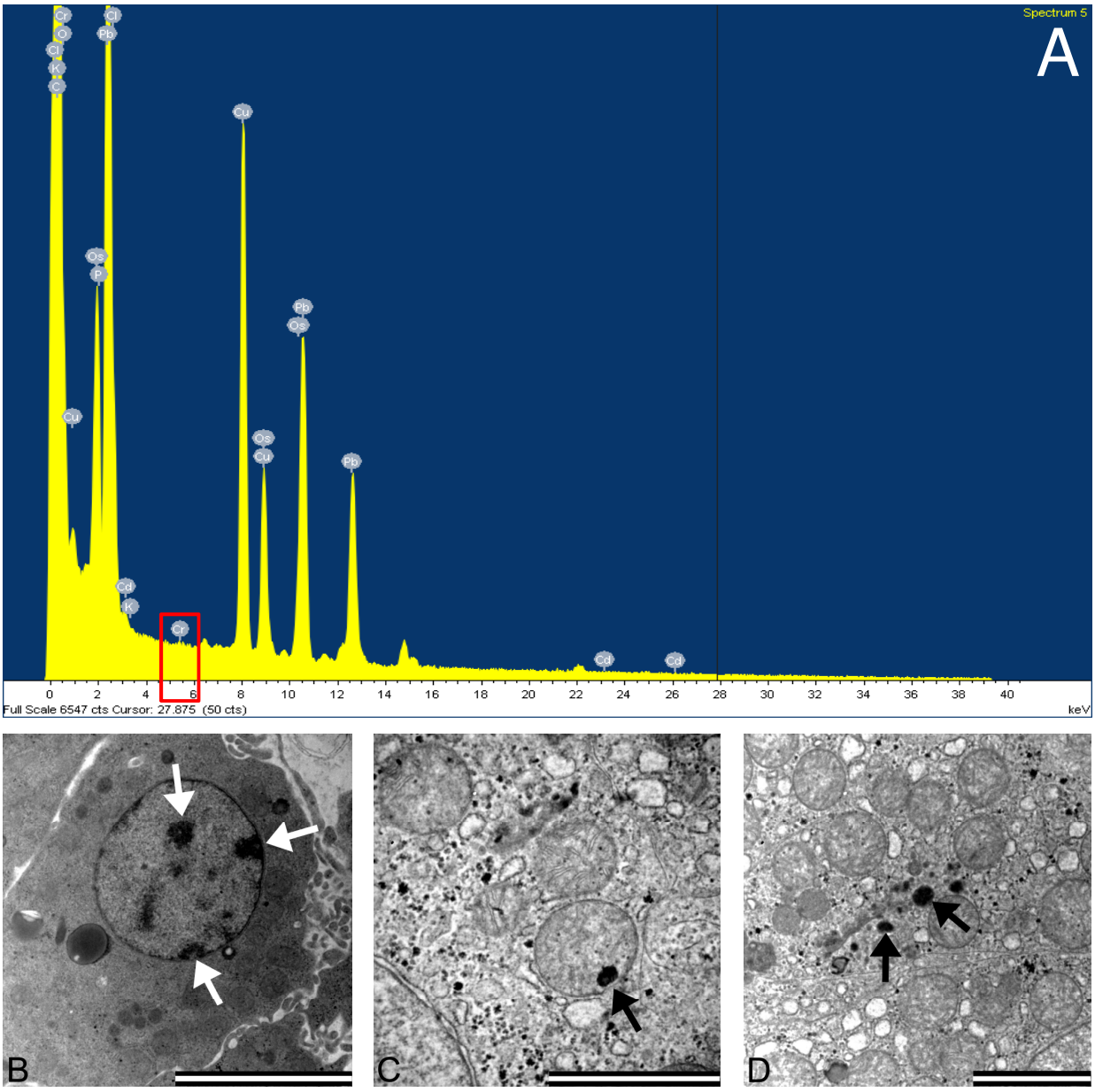

Figure 6.3: Representation of a Cr EDS spectrum [Fig. A (Cr detection in the red square)] and transmission electron micrographs that demonstrate typical particles (arrows) analysed in the nucleus (Fig. B), mitochondria (Fig. C) and Golgi complex (Fig. D) (Scale bars: B: 5µm; C, D: 2µm).

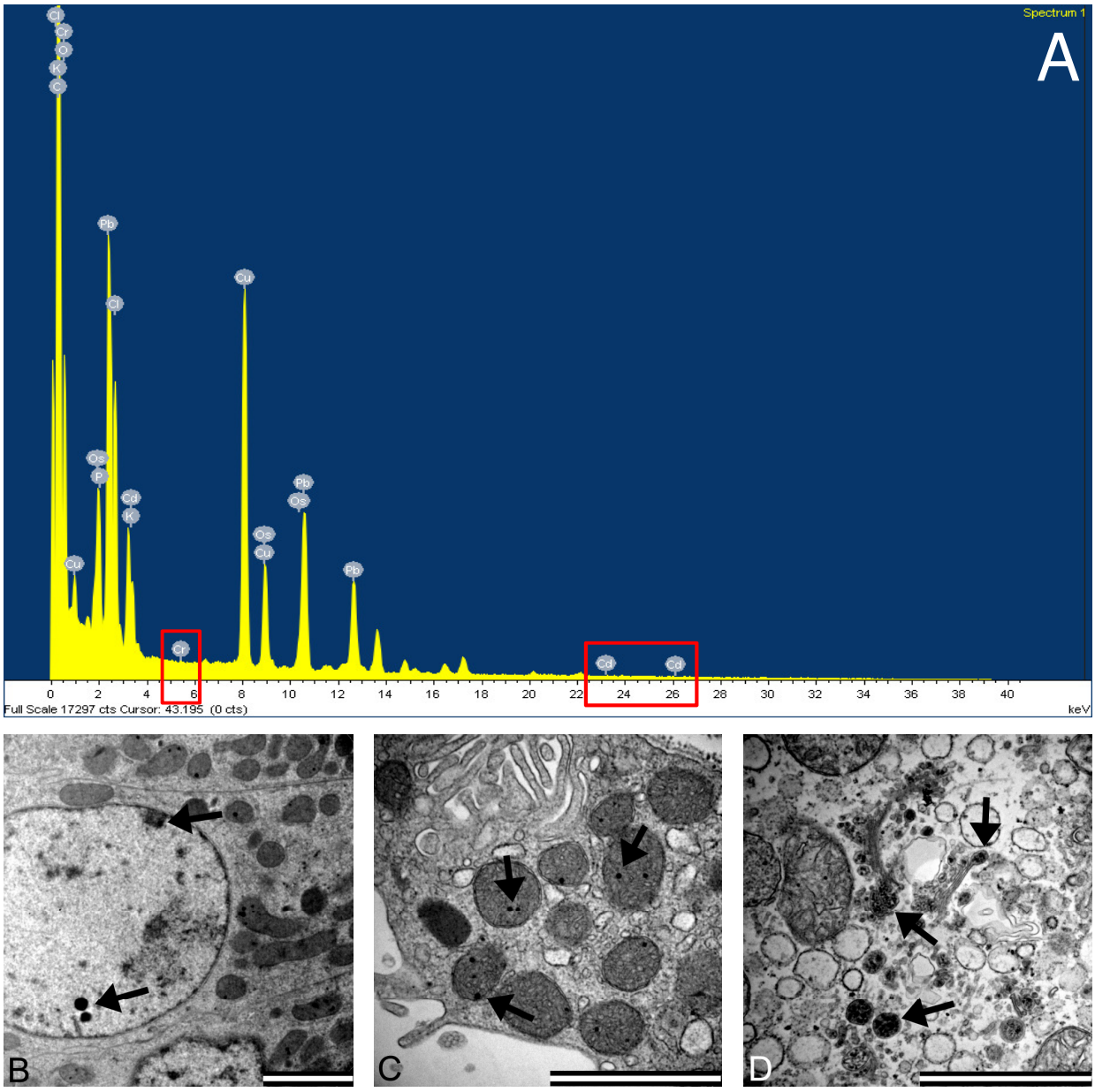

Figure 6.4: Representation of a Cd and Cr EDS spectrum [Fig. A (Cd and Cr detection in the red squares)] and transmission electron micrographs that demonstrate typical particles (arrows) analysed in the nucleus (Fig. B), mitochondria (Fig. C) and Golgi complex (Fig. D) (Scale bars: B-D: 2µm).

Figures 6.2-6.4 indicate the EDS spectra and transmission electron micrographs of the Cd and Cr alone and in combination. In the EDS spectra (Fig. 6.2-6.4 A) the Cd and Cr K-peaks are highlighted in the red squares. The K-peaks are the peaks at which the presence or absence of the metals were first analysed and then the rest of the peaks, i.e. L and M peaks, were taken into account. In these spectra both the Cd and Cr peaks (Fig. 6.2-6.4 A) were either not visible or minimal. A similar trend in lack of metal detection was found in the brain samples prepared by HPF with FS. The controls of both the chemically fixed and HPF with FS samples gave the same inconclusive results (results not shown). Thus it was difficult to

compare the experimental groups to the control groups. In Figure 6.2-6.4 B-D, the transmission electron micrographs are representative of the typical particles (arrows) that were analysed in the nucleus, mitochondria and Golgi complexes (Fig. 6.2-6.4 B-D respectively).

6.3.2. EELS analysis results

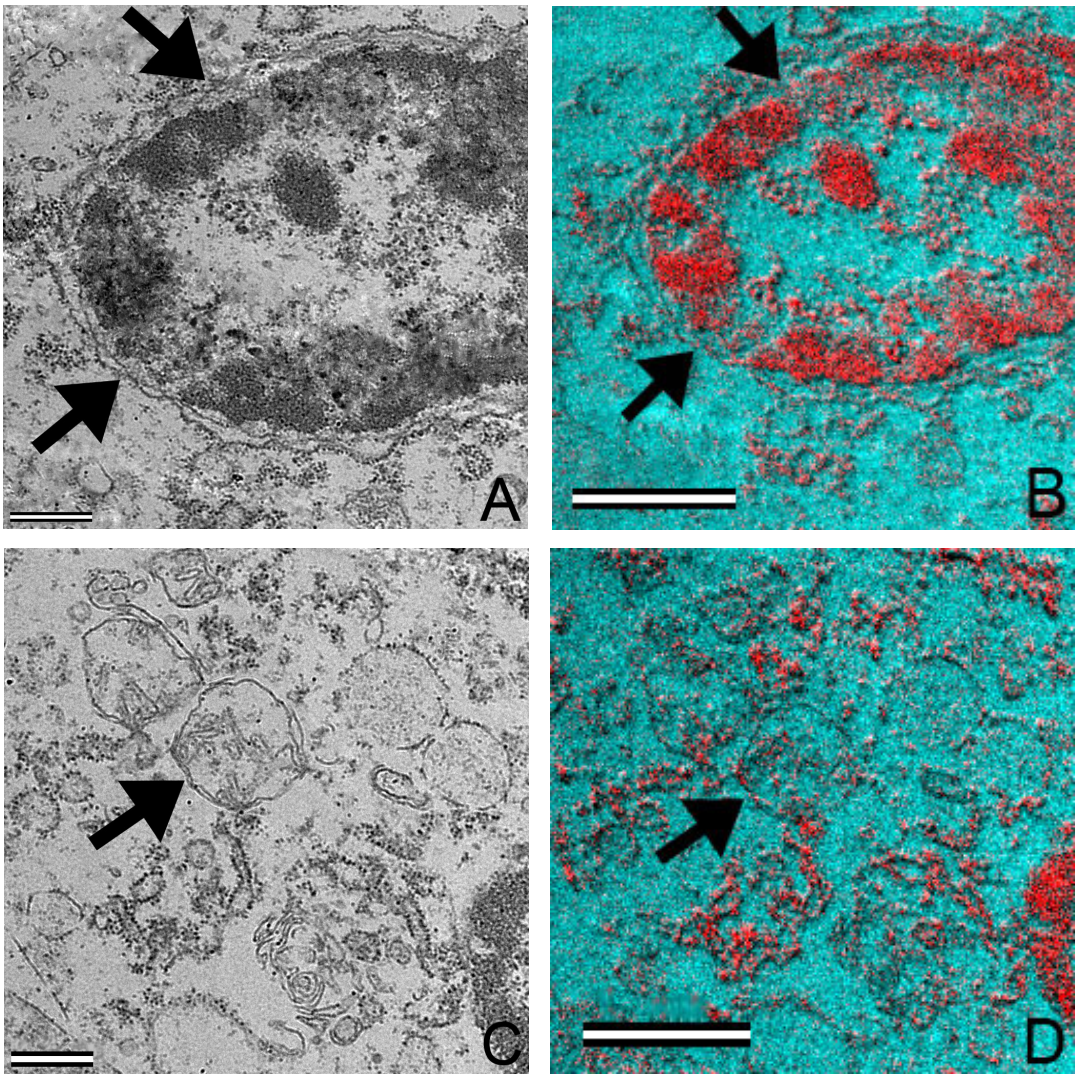

Figure 6.5: Transmission electron- and ESI micrographs of liver samples from the Cd x1000 PD group. Figure A and C indicate the transmission electron micrograph of the nucleus [Fig. A (arrows)] and mitochondria [Fig. C (arrow)] of the hepatocyte, respectively. Figure B and D shows the ESI micrographs of the nucleus [Fig. B (arrows)] and mitochondria [Fig. D (arrow)] of the hepatocyte, with Cd (red) deposited in the nucleus (arrows) and mitochondria (arrow) (Scale bars: A, C: 0.5µm; B, D: 1µm).

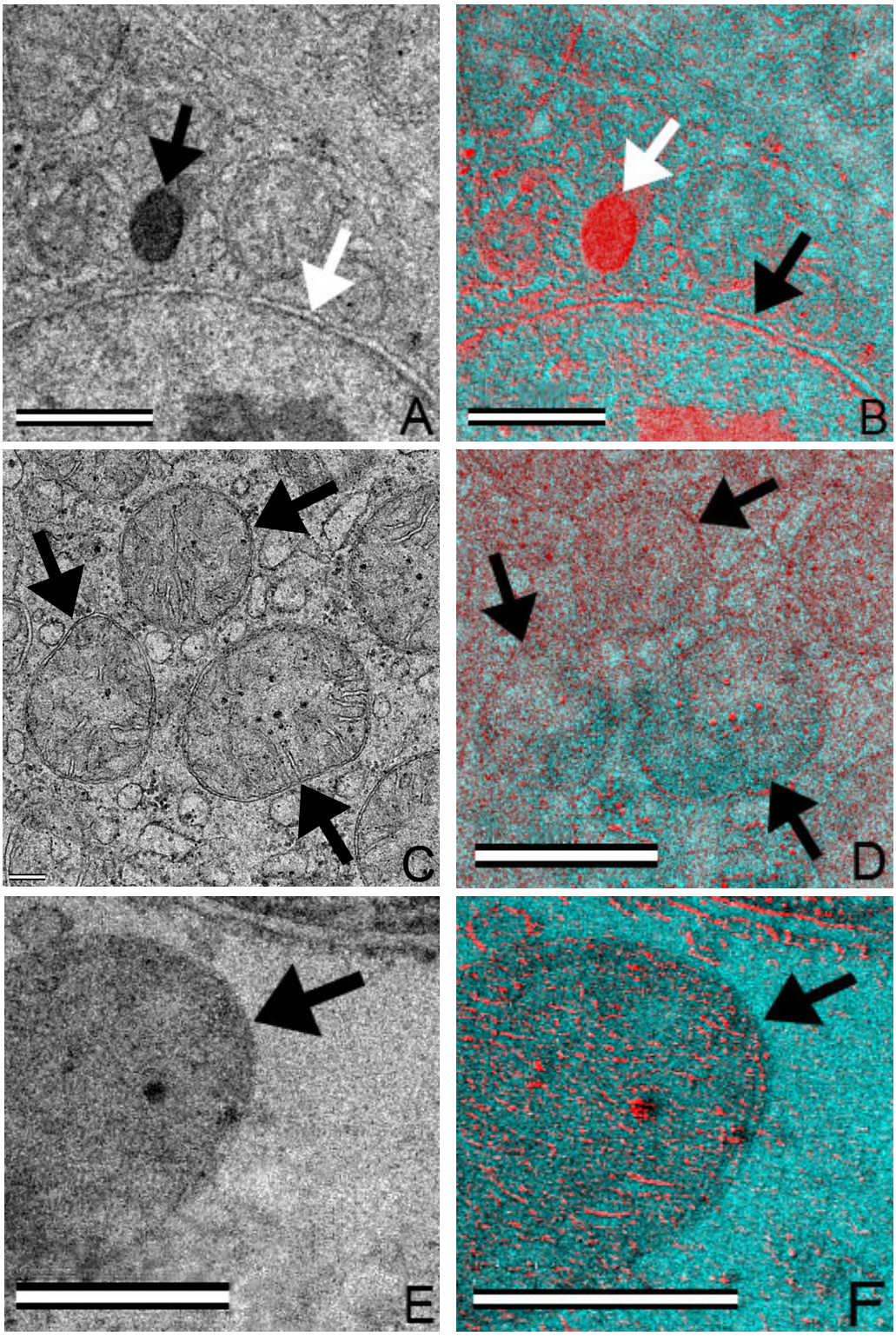

Figure 6.6: Transmission electron- and ESI micrographs of liver tissue from the Cr x100 PD (Fig. A-D) and Cr x1000 PD (Fig. E and F) exposed groups. Figure A, C and E represent transmission electron micrographs of the nucleus [Fig. A (white arrow), black arrow indicates a metal particle] and mitochondria [Fig. C and D (arrows)] analysed with EELS. Figures B, D and F reveal the Cr x100 PD and Cr x1000 PD groups ESI micrographs, with Cr (red) deposited in the nucleus [Fig. B (arrows)] and mitochondria [Fig. D and F (arrows)] (Scale bars: A, B and D: 1µm; C: 0.2µm; E and F: 0.5µm).

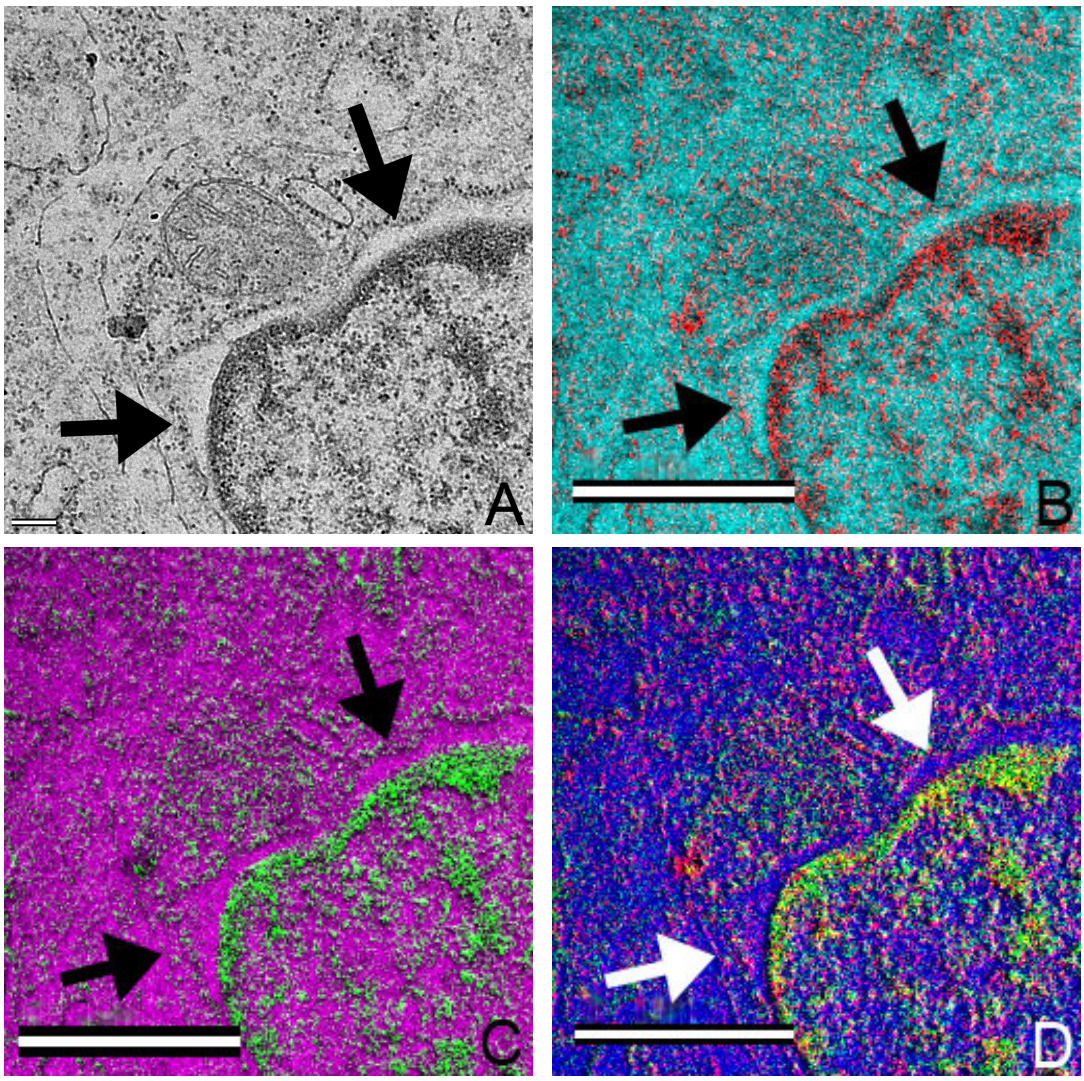

Figure 6.7: Transmission electron- and ESI micrographs of liver tissue from the Cd and Cr x100 PD combination groups. Figure A depicts the transmission electron micrograph of the nucleus (arrows) of the hepatocyte. Figures B-D are ESI micrographs of the nucleus (arrows). In Figure B the Cr (red) deposit is visible, where in Figure C the Cd (green) is shown. In Figure D the combined metal deposits are visible, with Cr (red), Cd (green) and the yellow indicating an overlapping of the two metals (Scale bars: A: 0.2 µm; B-D: 1µm).

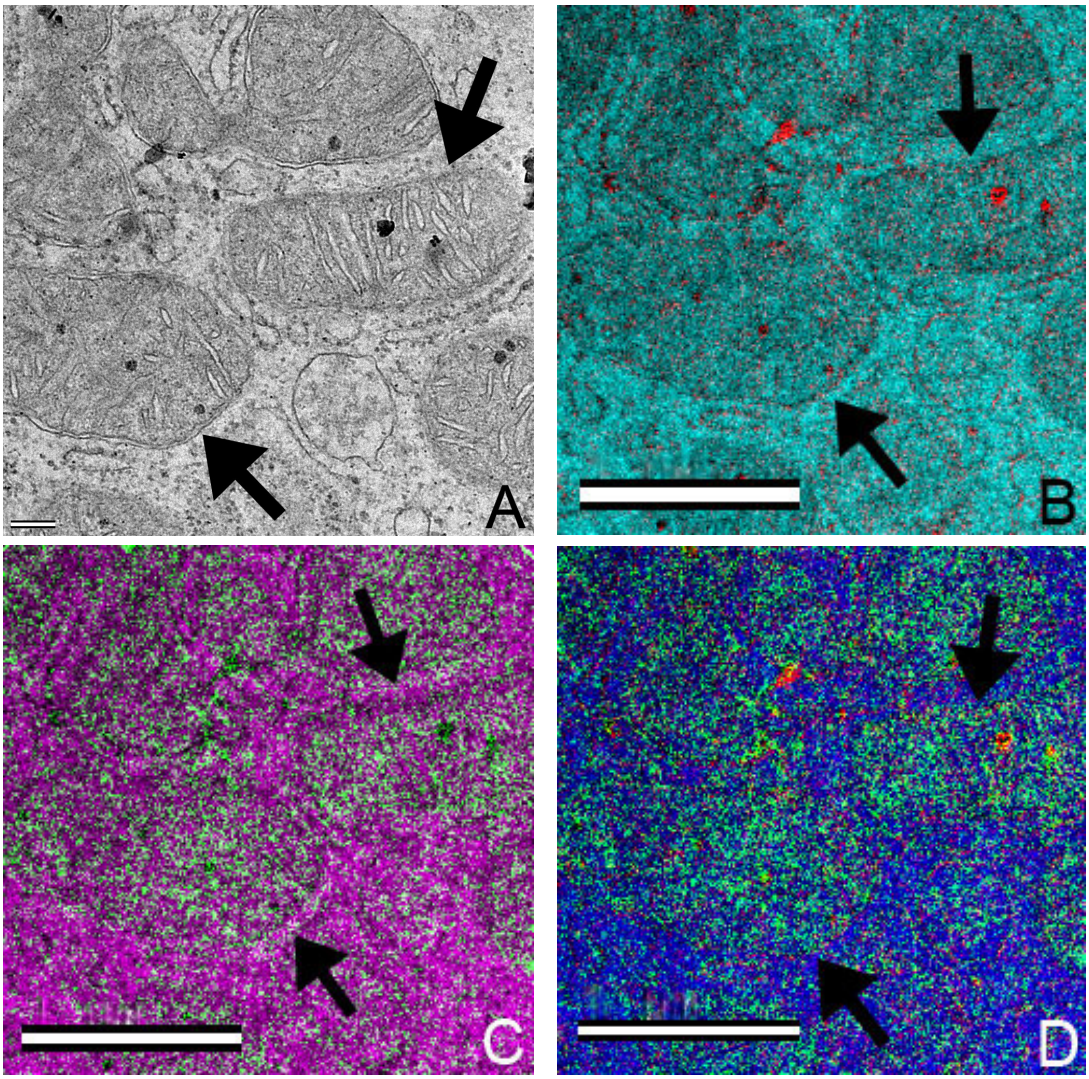

Figure 6.8: Transmission electron- and ESI micrographs of liver tissue from the Cd and Cr x100 PD combination group. Figure A depicts the transmission electron micrograph of the mitochondria (arrows) of the hepatocyte. Figures B-D are ESI micrographs of the mitochondria (arrows). In Figure B the Cr (red) deposit is visible, where in Figure C the Cd (green) is shown. In Figure D the combined metal deposits are visible, with Cr (red), Cd (green) and the yellow indicating an overlapping of the two metals (Scale bars: A: 0.2 µm; B-D: 1µm).

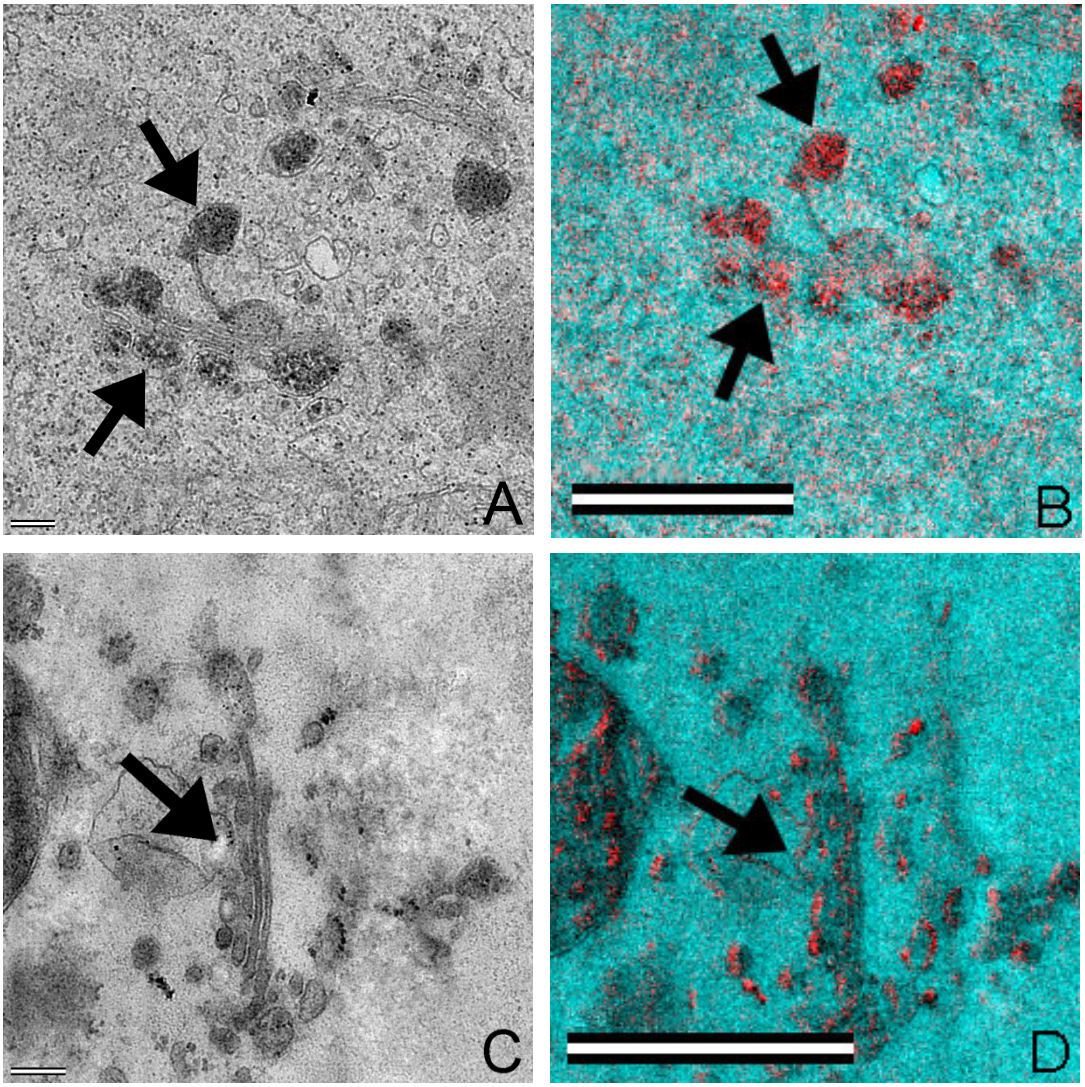

Figure 6.9: Transmission electron- and ESI micrographs representative of the Golgi complex of the hepatocyte in the Cr x100 PD and Cr x1000 PD groups. Figures A and B display the Golgi complex (arrows) present in the Cr x100 PD group, with A depicting the transmission electron micrograph and Figure B the ESI micrograph. Figure C, the transmission electron micrograph, shows the Golgi complex (arrow) present in the Cr x1000 PD group. Figure D shows the ESI micrograph of the Golgi complex (arrow) analysed with EELS (Scale bars: A and C: 0.2µm; B and D: 1µm).

Figure 6.5 shows the transmission electron- and ESI micrographs of the nucleus [Fig. 6.5 and B (arrows)] and mitochondria [Fig. C and D (arrows)] in the Cd x1000 PD, where the Cd located in the organelles is indicated by the red colour in the ESI micrographs. It is important to note that the Cd particles that were highlighted are located in the chromatin and membranes of the nucleus [Fig. 6.5 B (arrows)] and in the cristae and membranes of the mitochondria [Fig. 6.5 D (arrow)]. Figure 6.6 A, C and E indicate the transmission electron micrographs of the areas analysed with the EELS to produce the ESI micrographs (Fig. 6.6

B, D and F), where Cr is indicated by the red colour. Figure B shows the Cr that was found in the nucleus (chromatin and membrane) and in surrounding particles (arrows). In Figure D and F the Cr present in the mitochondria (arrows) is shown, with the Cr clearly visible in the cristae and membranes of the mitochondria. Also visible in Figure 6.6 D and F is the Cr in the small darker particles in the mitochondria. A control liver sample was tested and no Cd and Cr were found in the sample (results not shown, as no ESI micrograph could be produced due to the fact that no metals were detected).

The Cd and Cr x100 PD results are shown in Figure 6.7 and 6.8, with Figure 6.7 indicating the ESI micrographs of the nucleus (arrows) and Figure 6.8 the ESI micrographs of the mitochondria (arrows). Figures 6.7 and 6.8 B and C show the individual positioning of the Cd [Fig. B (red)] and Cr [Fig. C (green)], with Figure D indicating the combination of the metals (yellow) in the nucleus (Fig. 6.7 D) and mitochondria (Fig. 6.8 D). In Figure 6.7 D and Figure 6.8 D, some red (Cd) and green (Cr) colour is also visible where the metals do not overlap. The Cr found in the Golgi complexes of the Cr x100 PD [(Fig. 6.9 B (arrows)] and Cr x1000 PD [(Fig. 6.9 D (arrows)] liver samples are highlighted in red, with Figure A and C representing the transmission electron micrographs of the ESI areas. We also noted the presence of the Cr (red) at the ends of the Golgi cisternae, the secretory vesicles and lysosomes. To our knowledge no previous studies have analysed the presence of Cd or Cr with either EDS or EELS in the Golgi complex.

6.4. Discussion

The analyses of heavy metals with EDS and EELS have been used for many years in various types of studies, for example to determine the distribution of elements in cells to connect element compartmentation with biological function (Zierold, 2002). EELS is usually used for subcellular analysis as it has a higher spacial resolution than EDS (Michel, *et al.*, 2003). In the current chapter the presence of Cd and Cr were evaluated with both EDS and EELS to confirm that the *in ovo* method implemented was successful and that the ultrastructural changes observed with both the light microscope and TEM are most probably due to heavy metal toxicity. EDS analysis provided inconclusive results, as the concentration or precipitation of the metals in the tissue was too low and thus below the detection limit of the system. The same conclusion was reached by Zierold in 1997, where the author examined the accumulation of Cd and zinc in hepatocytes using EDS analysis (Zierold, 1997). The preparation techniques used in this study may also have negatively influenced the ability of the EDS system to detect the metals in tissue sections.

The lack of convincing results obtained with EDS analysis, lead to the analysis of liver tissue exposed to Cd and Cr alone and in combination with EELS. With the EELS analysis, both Cd and Cr were detected in the nucleus and mitochondria of the hepatocytes. In two studies done by Lui and Kottke in 2003, the authors found Cd and Cr present in the nuclei and cell membranes of root cells (Lui and Kottke, 2003a; Lui and Kottke, 2003b). It is important to take note of the position of the metals in the nuclei and mitochondria in the present study. In the nuclei of the hepatocytes, Cd and Cr can clearly be seen in the chromatin. This is consistent with previous reports that have found a correlation between DNA damage and Cd and Cr exposure (Bertin and Averbeck, 2006; Leonard, *et al.,* 2004; Valko, *et al*., 2006). In the mitochondria the presence of the metals can be seen in the cristae, that also correlates with literature as the mitochondria are involved with the detoxification of heavy metals in the cells (Bertin and Averbeck, 2006; Leonard, *et al.,* 2004; Valko, *et al*., 2006). Heavy metals are known to cause membrane damage by inducing lipid peroxidation (Bertin and Averbeck, 2006; Leonard, *et al.,* 2004; Valko, *et al*., 2006) and thus the presence of the metals in both the nuclei and mitochondrial membranes indicates an interaction with the membranes, possibly causing lipid peroxidation.

The presence of Cr at the ends of the Golgi cisternae and in the secretory vesicles may suggest an interaction of this metal with glucose, as Cr is involved in maintaining the glucose levels in the blood (Anderson, 1997; Wang, *et al*., 2005). The presence of Cr in the lysosomes may be due to the digestive function of the lysosome and that the Cr is possibly already being removed from the cells.

6.5. Conclusion

In this chapter the presence of Cd and Cr alone and in combination were evaluated by the use of EDS and EELS analysis on brain, liver and kidney tissue. The EDS analysis of all the organs led to no convincing results and thus neither the presence nor the absence of Cd and Cr could be confirmed. This can possibly be attributed to the metal concentrations being below the detection limit of the system and/or the lack of precipitation of the metals in the cells due to the preparation techniques used. With the inconclusive results obtained in the EDS analysis, EELS analyses was performed on the liver tissue. The EELS analysis provided irrefutable results of the presence of the metals in the hepatocytes. Thus it can be concluded that EELS analysis is a more efficient method to use as it is a more sensitive method for the detection of metals in biological tissue. The presence of these metals in the hepatocytes detected by EELS analysis might be the reason for the ultrastructural changes

observed in the previous chapter. A limitation from this chapter was that EELS analysis could not be done on other tissues as well.

Chapter 7

Analysis of the genotoxicity of Cd and Cr alone and in combination

7.1. Introduction

DNA and membranes are two major components in the human body important for cell viability and growth. The cell possesses an antioxidant defence system and DNA repair mechanisms that ensure protection against oxidative damage. However, the cell is unfortunately not always equipped to handle excessive oxidative damage caused by heavy metal exposure through agriculture, transport, mining and related operations (Al-Attar, 2011; Kalpana, *et al.,* 2008). DNA is affected by free radicals like hydroxyl radicals (•OH) that cause DNA strand breaks, which can then lead to DNA instability, mutations and ultimately carcinogenesis. Membrane integrity is reduced by lipid peroxidation due to the fact that the membrane contains lipids that are easily oxidised by free radicals and thus causes structural and functional changes in the membranes (Kalpana, *et al.,* 2008).

Many heavy metals, such as cobalt and lead, have been investigated to determine their effects on DNA by using DNA agarose gel electrophoresis (Hengstler, *et al*., 2003). Most studies also test substances, like antioxidant enzymes to determine if these enzymes can reduce heavy metal induced oxidative damage (Vitória, *et al.*, 2001). Avian blood, as in mammalian blood, contains erythrocytes, leukocytes and thrombocytes, but is different from mammalian blood, as each of these lines of cells retains their nuclei throughout the life span of these cells. The red blood cells (RBC's) are oval in shape and contain a centrally located oval nucleus with an eosinophilic cytoplasm (Clark, *et al*., 2009). Although the mature erythrocytes are the predominant type of erythrocyte found in avian blood, small amounts of the penultimate stage erythrocytes, known as the polychromatophilic erythrocytes, may be encountered (Clark, *et al*., 2009; Williams, 1972). The avian leukocytes consist of five types of cells, namely: heterophils, eosinophils, basophils, lymphocytes and monocytes. Heterophils are the most common type of leukocyte found in avian blood and thus atypical heterophils may be encountered in the blood (Clark, *et al*., 2009). Genotoxic compounds may cause micronuclei formation in the developing embryo's blood. Micronuclei are acentric chromatin or chromosome fragments or whole chromosomes that lag behind due to spindle malfunction and are used as an indication of chromosomal damage (Malladi, *et al*., 2007).

In this chapter, in a cell free system, the effect of Cd and Cr alone and in combination was used to determine if these metals can cause single or double strand breaks or DNA fragmentation by using DNA agarose gel electrophoresis. In addition, the morphology of

chick embryonic erythrocytes was evaluated to determine if these metals can cause micronuclei formation.

7.2. Materials and Methods

Samples were obtained as described in Chapter 3.

7.2.1. Effect on plasmid DNA structure

During DNA damage, conversion from supercoiled to circular and linear forms occurs. A different form of DNA damage can also occur and this is seen as fragmentation, due to different mechanisms of action of different compounds. These conversions are due to single-stranded (ssb) and double-stranded breaks (dsb). These various forms of DNA damage present differently on an agarose gel and can be used as a marker for DNA damage (Aronovitch, *et al.,* 2007; Serem, 2011). The methods used for this assay was modified from the methods of Wei *et al.* (Wei, *et al.,* 2006).

Four different groups were analysed with the agarose gel; a negative control that would indicate 0% damage and three experimental groups. The three experimental groups consisted of 2.5µℓ of pBR322 plasmid DNA (Promega, USA) and 2.5µℓ of either of Cd PD, Cr PD or Cd and Cr PD brain tissue. Before combining the two solutions, the metal-exposed brain tissue was diluted to 50% its original concentration (10µℓ metal exposed brain tissue and 10µℓ ddH_2O), as the PD of the metals in the brain were already too toxic for the plasmid and thus no results could be seen (results not shown). The experimental plasmid solution was incubated for 1 hour and then 5µℓ of the experimental plasmid solution was mixed with 5µℓ of gel loading buffer (0.13% bromophenol blue and 40% sucrose). The mixtures were then immediately loaded into a 1% agarose gel in 40 mM Tris, 20 mM glacial acetic acid and 0.5M Ethylenediaminetetraacetic acid (EDTA) pH 8.0 (TAE) and contained 50µg/mℓ ethidium bromide (EtBr). Electrophoresis was undertaken by using a horizontal slab gel apparatus in TAE buffer for 2 hours at 60V. The stained gels were placed in a ultra-violet (UV) trans-illuminator (Vilber Lourmat E-Box-1000-26M) at 254nm and were photographed (Vidamax VM-09) to tagged image format (TIFF).

7.2.2. Blood smear preparations

Blood smears were prepared on glass slides on the day of termination, stained with Giemsa-Wright for five minutes; rinsed with ddH_2O and viewed with a Nikon Optiphod transmitted light microscope for the presence of possible micronuclei. The criteria used for the genotoxicity tests, to evaluate if a structure in a red blood cell (RBC) is a micronucleus, was that it should have a three-dimensional shape and must have a similar staining reaction and texture as the nucleus. The size of the possible micronucleus should not exceed two-thirds of the size of the nucleus, contain a distinct border and have an oval shape (Wolf and Luepke, 1997).

7.3. Results

7.3.1. Effect on plasmid DNA structure

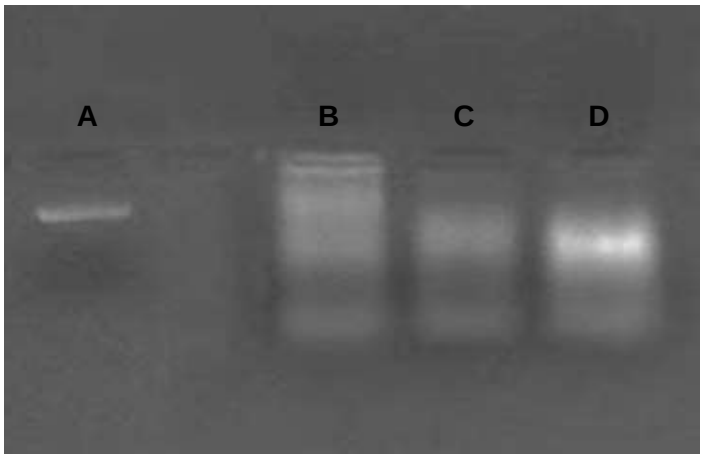

Figure 7.1: Agarose gel electrophoretic pattern of pBR322 DNA alone (A), exposed to Cd PD (B), exposed to Cr PD (C) and exposed to Cd and Cr PD (D).

From the DNA agarose gel electrophoresis results shown in Figure 7.1 it is clear that DNA fragmentation took place in all the experimental groups (Fig. 7.1 lanes B-D), with the control (Fig. 7.1 A) showing intact DNA. When evaluating the Cd and Cr lanes, Cd shows DNA fragmentation with some intact DNA still present at the same level as the control. Cr shows more damage than Cd, as less intact DNA can be observed in lane C compared to lane B, indicating that Cr may completely damage DNA compared to Cd. However, the fragmentation pattern of both Cd and Cr are similar past the point of intact/unfragmented DNA (using control as a point of reference).The bright band observed in lane D shows a

combined effect of the fragmented bands of lanes B and C at that same level and thus shows more DNA damage occurred by combining the two metals.

7.3.2. Blood smear results

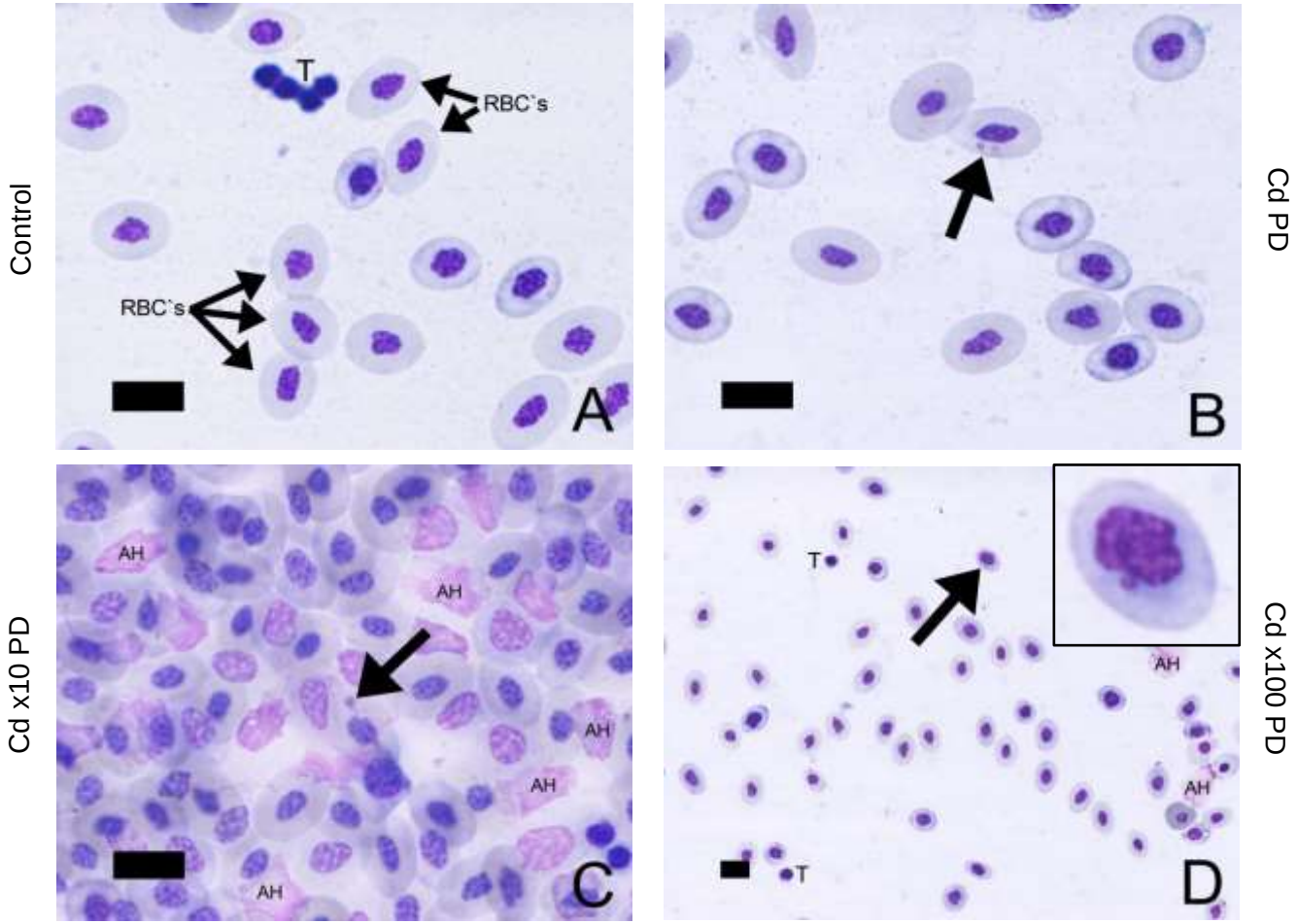

Figure 7.2: Light microscopy micrographs of the blood smears of the control and Cd groups. Figure A shows the normal morphology of the RBC's in the control group. Figure B (Cd PD), C (Cd x10 PD) and D (Cd x100 PD) show the presence of micronuclei (arrows) [AH: atypical heterophil; RBC's: Red blood cells; T: Thrombocyte(s)] (Scale bars: 10µm).

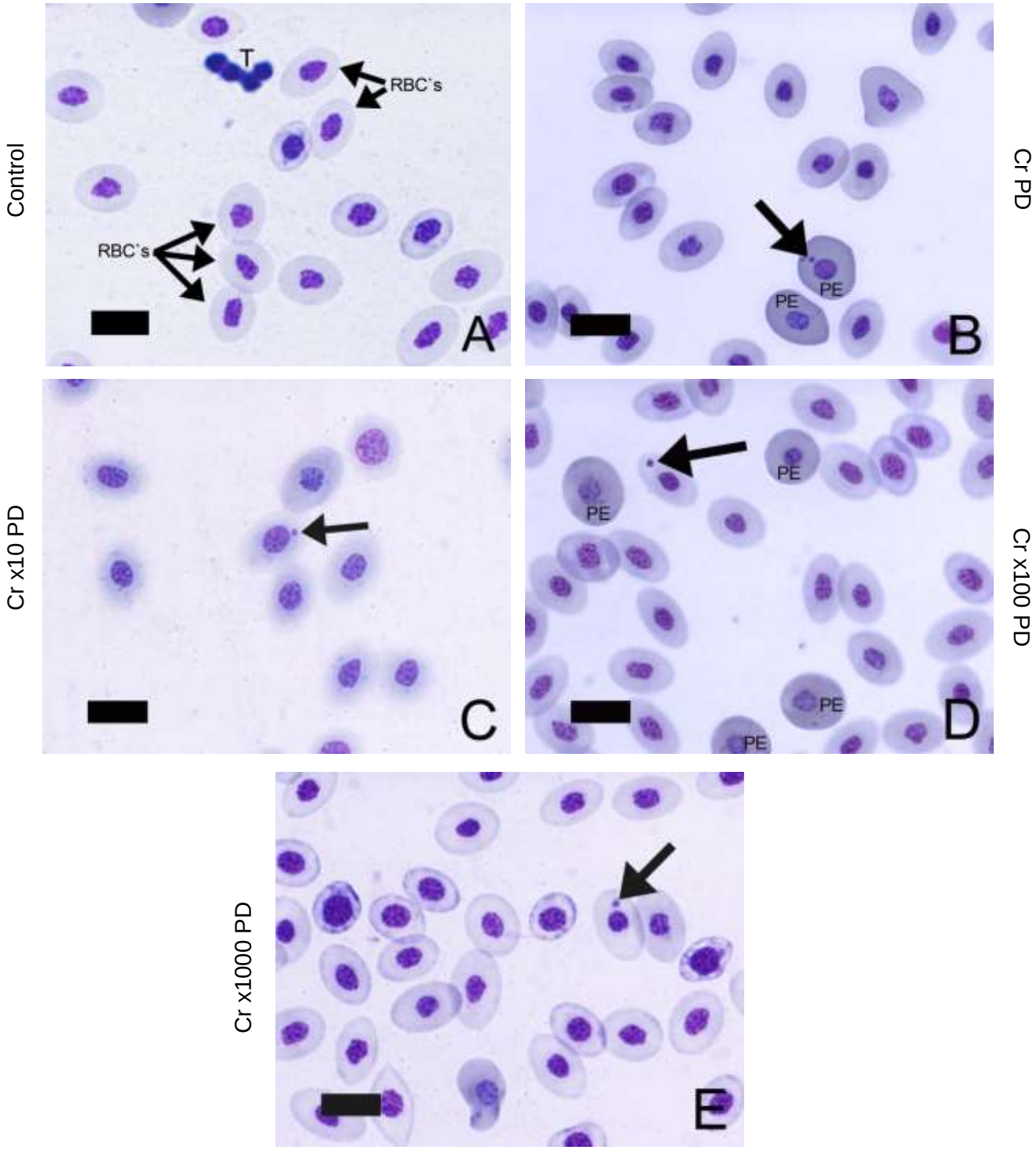

Figure 7.3: Light microscopy micrographs of the blood smears of the control and Cr groups. Figure A shows the normal morphology of the RBC's of the control group. Figure B (Cr PD), C (Cr x10 PD), D (Cr x100 PD) and E (Cr x1000 PD) show the presence of micronuclei (arrows) [PE: polychromatophilic erythrocytes; RBC's: Red blood cells; T: Thrombocyte(s)] (Scale bars: 10µm).

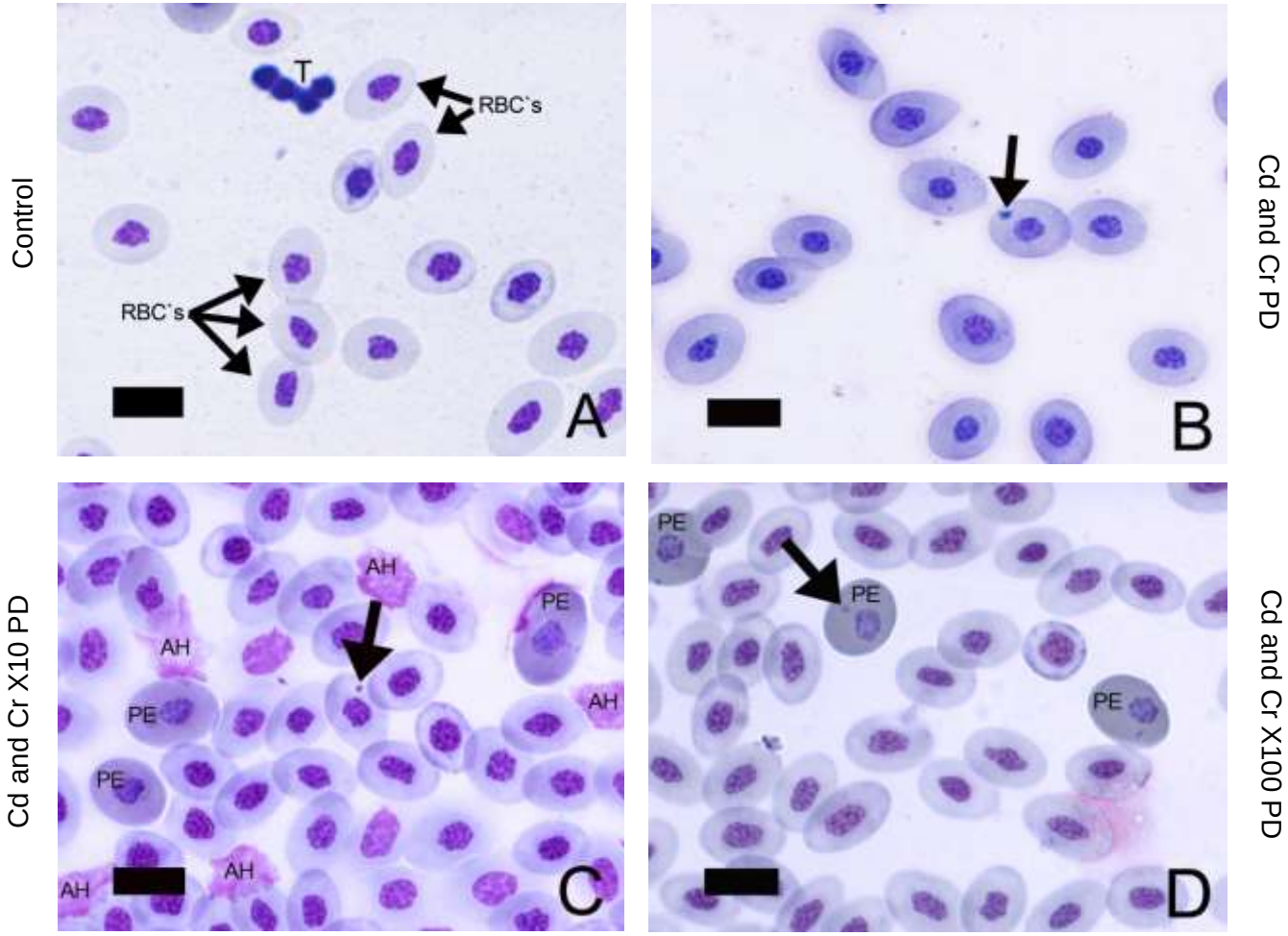

Figure 7.4: Light microscopy micrographs of the blood smears of the control and Cd and Cr combination groups. Figure A shows the normal morphology of the RBC's of the control group. Figure B (Cd and Cr PD), C (Cd and Cr x10 PD) and D (Cd and Cr x100 PD) show all the RBC's with micronuclei (arrows) [AH: atypical heterophil; PE: polychromatophilic erythrocytes; RBC's: Red blood cells; T: Thrombocyte(s)] (Scale bars: 10µm).

Figure 7.2 shows the light microscopy micrographs of the control and Cd experimental groups. In Figure 7.2 A the normal morphology of the erythrocytes in the control group can be seen. Figure 7.2 B indicates a possible micronucleus (arrow), as it was not clearly visible in this micrograph. The micronuclei in Figure 7.2 C and D were clearly visible (arrows) (Figure 7.2 D's RBC with the micronucleus enlarged in the right hand corner). Figure 7.3 illustrates the micrographs of the control and Cr experimental groups. Figures B (Cr PD), C (Cr x10 PD), D (Cr x100 PD) and E (Cr x1000 PD) illustrate micronuclei (arrows) in the RBC smears, with the same control as in Figure 7.2 A. Figure 7.4 illustrates the light microscopy micrographs of the control (same as in Figure 7.2) and Cd and Cr combination experimental groups, with micronuclei (arrows) present in all the Figures [B (Cd and Cr PD), C (Cd and Cr x10 PD) and D (Cd and Cr x100 PD)].

7.4. Discussion

Cd and Cr are heavy metals that produce free radicals in cells using different biochemical pathways; one of the end results of oxidative damage is DNA damage (Kalpana, *et al.,* 2008). In a study done by Wätjen and colleagues in 2002, the effects of Cd on C6 glioma cells were tested by the use of electrophoresis and it was found that Cd produced a typical DNA ladder that is an indication of apoptosis (Wätjen, *et al*., 2002). In a study done by Ram, *et al.,* Cr was used as an immunosuppressive agent, to test the anti-oxidant and immunomodulatory properties of fruit extracts of *Emblica officinalis* (Amla). The authors found that the splenocytes obtained from Sprague-Dawley rats, exposed to Cr showed enhanced apoptosis and DNA fragmentation (Ram, *et al*., 2002). Indications are that heavy metals cause oxidative damage which results in apoptosis and subsequent DNA laddering. In the previous chapter it was shown that Cd and Cr alone and in combination are present in the nucleus of the hepatocytes. It is unknown whether these metals have a direct effect on DNA. In a cell free system, the direct effect of the metals on DNA structure was determined using plasmid DNA. It was found that Cd and Cr alone and in combination had a direct effect on the integrity of the plasmid DNA and caused DNA fragmentation (Fig. 7.1).

Another method used to evaluate the effect of Cd and Cr alone and in combination was to investigate the possible presence of micronuclei in the RBC's of the chick embryos. Micronuclei were found in all the experimental groups (Fig. 7.2 B-D; Fig. 7.3 B-D; Fig. 7.4 B-E), but it should be noted that the micronuclei shown in Figures 7.2 B-D; 7.3 B-D and 7.4 B-E were the only ones found in the RBC smears of the experimental samples. These results were also observed in a study done by Lewińska *et al*., in 2007, where the genotoxic interactions between Cd and two other environmental pollutants namely arsenic and

benzo(a)pyrene were investigated in mice. No significant difference in the amount of micronuclei present in the Cd exposed mice was found as compared to the control mice (Lewińska, *et al*., 2007). In 1996, Mirsalis, *et al*. came to the same conclusion when the effects of Cr(VI) on mice were tested (Mirsalis, *et al.,* 1996).

7.5. Conclusion

From the results obtained in this chapter it can be concluded that Cd and Cr alone and in combination, at physiological doses in a cell free system, can induce DNA damage. The genotoxicity testing on the RBC's of the chick embryos revealed no substantial differences, as only a few micronuclei were found in the RBC's and thus Cd and Cr alone and in combination causes no substantial RBC DNA damage. Therefore, the cellular effects observed *in vivo* may be the result of oxidative damage rather than a direct interaction between the metals and DNA.

Chapter 8

Investigating the changes in glutathione levels in the brain tissue of chick embryos after exposure to Cd and Cr alone and in combination

8.1. Introduction

One of many mechanisms of cellular damage induced by heavy metals is the reduction of glutathione (GSH) to GSH disulfide (GSSG) due to oxidative damage (Olivieri, *et al.*, 2001; Valko, *et al.*, 2006). GSH is a tri-peptide that has many functions including being a xenobiotic detoxifier, endogenous antioxidant and metabolic regulator. In the body, GSH is the most abundant antioxidant present in aerobic cells. GSH protects the cells against oxidative stress by acting as a free radical scavenger and by inhibiting lipid peroxidation (Campbell and Farrell, 2008; Owen and Butterfield, 2010). The GSH molecule consists of l-glutamate, l-cysteine and l-glycine that are synthesized by two adenosine triphosphate (ATP) requiring steps that are catalysed by the enzymes ɣ-glutamylcystein ligase and glutathione systhetase (Fig. 8.1). The cysteine thiol moiety of the GSH molecule is responsible for its antioxidant properties (Owen and Butterfield, 2010). GSH is oxidized by reactive oxygen species (ROS) to form oxidized GSSG. GSSG can be reduced back to GSH by nicotinamide adenine dinucleotide phosphate (NADPH) that is catalysed by glutathione reductase (Fig. 8.1). In a normal healthy individual, reduced GSH is the most prevalent form of GSH, but with aging and exposure to substances that induce oxidative stress such as heavy metals, the GSH/GSSG ratio decreases (Owen and Butterfield, 2010).

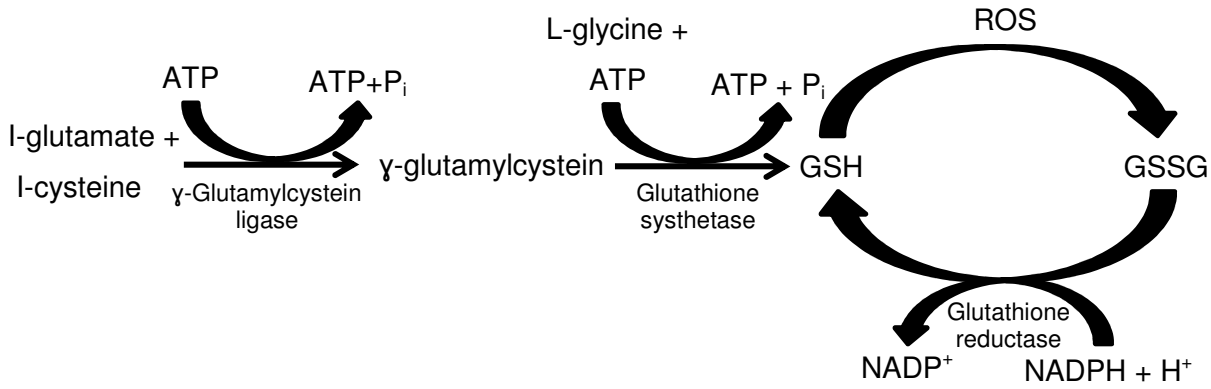

Figure 8.1: Synthesis, degradation and regeneration of glutathione. ATP + P_i: adenosine triphosphate and phosphate ion; ROS: reactive oxygen species; $NADP^+$: Nicotinamide adenine dinucleotide phosphate (oxidized form); NADPH + H^+: Nicotinamide adenine dinucleotide phosphate and hydrogen ion (modified from Owen and Butterfield, 2010).

Many different heavy metals, such as lead, mercury and cobalt have been investigated to observe the effect these metals may have on the GSH levels and most studies concluded that these metals reduce the GSH levels in the brain (Kaur, *et al*., 2006; Olivieri, *et al*., 2001; Sandhir, *et al.,* 1993). Both cadmium (Cd) and chromium (Cr) produce free radicals that result in the formation of GSSG molecules and thus is one of the many pathways that will ultimately cause DNA damage and apoptosis (Bertin and Averbeck, 2006; Leonard, *et al.,* 2004). Brain tissue was used to observe if the embryonic blood-brain barrier (BBB) can ensure sufficient protection against the heavy metal toxicity and thus observe if any brain alterations may occur due to the metal toxicity. The BBB is the protective mechanism of the brain, which in adults is more developed than in embryos (Chen, *et al*., 2008; Méndez-Armenta and Ríos, 2007; Nordberg, *et al*., 2007b). A decrease in GSH has also been associated with Parkinson's and Alzheimer's disease (Bharath, *et al.,* 2002; Lovell, *et al.,* 1998; Sian, *et al*., 1994).

In this chapter the results obtained from the GSH assays performed on the brain tissue of chick embryos exposed to Cd and Cr alone and in combination are depicted. Only the physiological dose (PD) and x10 PD groups were used, as these dosages are physiologically relevant.

8.2. Materials and methods

Samples were obtained as described in Chapter 3.

8.2.1. GSH assay

The brain tissue (n=135) was removed, weighed and frozen at -20ºC until further processing. The tissue was then thawed by sonicating the tissue for 5 minutes, after which phosphate buffer saline (PBS) (pH 7.4) was added according to the weight of the tissue. The tissue was vortexed and then sonicated again for 5 minutes. The tissue samples were centrifuged for 10 minutes at 4000 rpm. The supernatant was removed and 20µℓ of the supernatant was added to 180µℓ PBS (pH 8). For the assay, 50µℓ of the supernatant mixture was added to 50µℓ of DTNB [5'5-dithiobis (2-nitrobenzoic acid)] (Sigma, USA). This was performed in triplicate. The absorbency was read at 405nm against a GSH standard that contains triplicate forms of 50µℓ of the following GSH (Sigma, USA) concentrations: 0mM, 0.1mM, 0.2mM, 0.4mM, 0.6mM, 0.8mM, 1mM and 50µℓ of DTNB (Debnath, *et al.,* 2010).

8.2.2. Statistical analysis

Statistical analysis was performed using the Kruskal-Wallis analysis of variance (ANOVA) and P-values less than 0.05 were considered to be significant.

8.3. Results

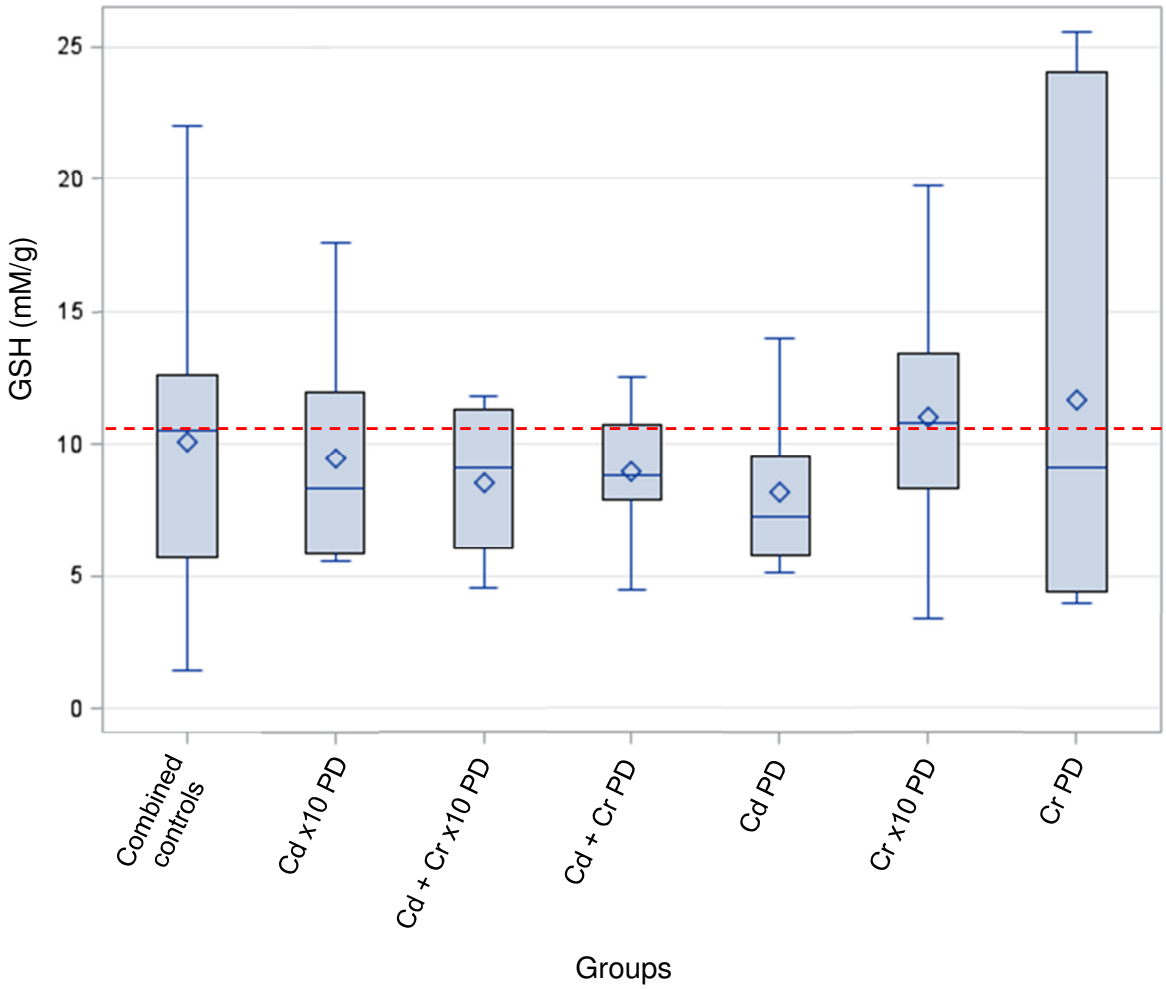

Figure 8.2: Distribution of GSH between the combined controls and the experimental groups (Red dashed line indicates level of median value of combined controls to compare with experimental groups median values).

In this chapter three different controls were used to ensure that the *in ovo* method employed did not influence the results obtained. Before the three control GSH results were tested against the experimental groups, the control groups were first compared to each other to analyse if there was any statistical difference. It was found that the controls (P-value= 0.7923) did not show significant differences from each other and thus could be pooled together and be used as one control. When comparing the combined controls with the

different experimental groups, no statistically significant differences were found (P-value= 0.8211), even with the decrease in the GSH median value that can be seen in all the experimental groups, except Cr x10 PD, when compared to the control (Fig. 8.2). The bigger variation seen in the GSH values in the Cr PD, contributes to the principle of GSH conversion to GSSG when a toxic agent is present, as the Cr PD GSH values indicate that there was still an adequate amount of GSH present in the cells and thus Cr at PD is the least toxic of all the experimental groups.

8.4. Discussion

GSH protects the cells from heavy metals, like Cd and Cr, by acting as a free radical scavenger (Campbell and Farrell, 2008; Owen and Butterfield, 2010). The conversion of GSH to GSSG by ROS is the indicator used to observe the amount of oxidative stress produced by the toxic effect of Cd and Cr alone and in combination on the brain tissue. In the results obtained in this chapter the GSH levels of the Cd and Cr alone and in combination did not produce statistically significant differences compared to the control. Thus the different concentrations of Cd and Cr did not produce significant levels of oxidative stress in the brain cells. A previous study done on the effects of Cr on goldfish brain tissue, also revealed no significant difference in the GSH levels when compared to the controls (Kubrak, *et al*., 2010). On the other hand, Almazan, *et al*., found that Cd depleted the GSH levels in brain primary cultures obtained from new-born Sprague-Dawley rats and these results are contradictory to what was found in the current study (Almazan*, et al*., 2000). The reason for contradictory results from previous studies can be contributed to the fact that not only were the previous studies performed on different animals but also at different developmental stages.

The statistically insignificant results obtained in this chapter can be attributed to the fact that although the BBB of the developing chick embryo is still vulnerable (Méndez-Armenta and Ríos, 2007; Nordberg, *et al*., 2007b), it provided adequate protection related to GSH levels against the effects of the heavy metals Cd and Cr alone and in combination. However these metals may have an effect on other antioxidant enzymes such as glutathione reductase, glutathione peroxidase, superoxide dismutase and catalase (Kim, *et al*., 2011).

8.5. Conclusion

From the results obtained in the current chapter it can be concluded that Cd and Cr alone and in combination did not cause a significant decrease in the GSH levels.

Chapter 9

Concluding discussion

South Africa is a country rich in mineral resources and therefore has a thriving mining industry. However, due to the incorrect method of disposal of the waste from these mines, substances, including heavy metals, get into the water and air supply. The people living in the surrounding areas are the most affected by the contaminated water and air supply. They are exposed through inhaling the contaminated air and eating and/or drinking the contaminated food and water. Based on the reports and articles found on contaminated water and air in the mining areas of South Africa, the two heavy metals cadmium (Cd) and chromium (Cr) were chosen based on the possibility of being exposed to them in South Africa (Fatoki and Awofolu, 2003; Molokwane, *et al*., 2008; Tempelhoff, 2013).

In this study, the *in ovo* model was used to investigate the effects of these heavy metals on specific organs of the chick embryo. The *in ovo* or chick embryo model is widely used to study embryology and teratology, by exposing the embryos to different compounds (Drake, *et al*., 2006). Therefore, in this study the *in ovo* model was used to investigate the cellular effects of Cd and Cr alone and in combination, at different concentrations, on the brain, liver and kidney tissue, by using light- and transmission electron microscopy (TEM), along with the analysis of glutathionine depletion and DNA damage in the brain tissue and blood smears by utilizing the GSH assay, DNA agarose gel electrophoresis and light microscopy respectively. In conjunction with TEM analysis, energy dispersive spectroscopy (EDS) and electron energy-loss spectroscopy (EELS) were used to investigate the presence and location of these metals in the tissue. The *in ovo* model was successfully implemented in the current study over a 14-day period during which the eggs were incubated, exposed and terminated. As indicated in chapter 3, the survival rates and weights of the embryos in the highest concentration of Cd and Cr alone and in combination were the lowest compared to all the lower metal concentrations and the control. Thus the metals at these higher concentrations had a more severe effect on the embryos.

Histological and ultrastructural changes in the brain, liver and kidney tissue of the embryos exposed to Cd and Cr alone and in combination were investigated and compared to that of the control embryos. With the histological and ultrastructural evaluation, certain criteria for each organ were used to determine if the metals had any cellular effects on the organs. The histological criteria for alterations in the brain included cytoplasmic vacuolization and necrosis (Leonard, *et al.,* 2004; Méndez-Armenta and Ríos, 2007; Sherlock and Doely, 1993), with an increase in sinusoidal space and necrosis used as the criteria for the liver

samples (Jihen, *et al.,* 2008; Mishra and Mohanty, 2008). In the kidney, dilation and/or contraction of the glomeruli as well as necrosis and hypertrophy of the renal tubular cells were evaluated (Brzóska, *et al.,* 2003b; Jihen, *et al*., 2008; Mishra and Mohanty, 2008). The results obtained indicated that Cd had major effects at higher concentrations; where the changes observed with Cr were present at all the concentrations in all the organs investigated. The metal combination group also showed minor alterations in the brain and liver when using the above mentioned criteria, whereas in the kidney, glomerular dilation, necrosis, chromatin condensation and renal tubule alterations were more severe at all the concentrations, compared to the effects seen in Cd and Cr alone.

Nuclear and cellular membrane disruption, chromatin condensation, cytoplasmic alterations, mitochondrial membrane disruption as well as mitochondrial inner matrix swelling were the criteria used for the ultrastructural evaluation of the organs. Any accumulation of unknown particles in the Golgi complex was also evaluated. The evaluation of the brain tissue showed no severe changes, as listed above, for any of the metal concentrations. In the liver and kidney tissue, the highest Cd concentrations resulted in severe alterations, ranging from ruptured cellular membranes to irregular chromatin condensation. Both the Cr and metal combination groups illustrated minor changes, when using the above mentioned criteria, throughout the different concentrations. Thus Cd may be more toxic at higher concentrations, but Cr alone and Cd and Cr together can alter cellular structures at much lower concentrations. Particles were observed at the ends of the Golgi cisternae and in the secretory vesicles and lysosomes of all the organs. The presence of the particles in the lysosome indicates that the cells might be in the process of removing the metals from the cells. The unknown particles, not only found in the Golgi complexes but also seen in other organelles, were analysed with EDS and EELS to confirm the presence or absence of the investigated metals. The presence of Cd and Cr would indicate whether the histological and ultrastructural alterations seen in chapter 4 and 5 were caused by the presence of these metals and not because of the preparation methods used.

EDS analysis of the brain, liver and kidney tissue, provided inconclusive results, after multiple analyses of all the metal concentrations in all the organs of both the chemically fixed and high pressure frozen with freeze substitution samples. No definite conclusion could be made to whether or not the metals were present in the organs. This can be attributed to a variety of reasons. Firstly, the lack of detection can be a result of the fact that the detection limit was reached, this might be because the count rate, i.e. the process time, spectrum range (KeV), etc., was not optimized for each reading. An increase in the count rate will increase the possibility of detecting the metals present. Another possible explanation might

be the preparation methods used, which may have caused the metals to be washed out of the tissue. The biochemical pathways involved in the process of how the metals enter the tissue may also cause low concentrations of the metals in the tissue. Due to the inconclusive results obtained by EDS, EELS analyses was undertaken on the liver tissue.

EELS analysis is known to be a more sensitive method than EDS and thus is ideal for detecting minimal amounts of a metal in tissue (Egerton, 2011). EELS analysis revealed remarkable results, as Cd and Cr alone and in combination were detected in the liver tissue. Not only did it confirm the presence of the metals, but also confirmed the position of the metals in the organelles of the liver. This might be the reason for the ultrastructural alterations seen in chapter 5. This is also a confirmation that the *in ovo* model was successful in terms of the presence of the metals in the cells and therefore the changes observed in the ultrastructure of the cells might be due to metal toxicity and not the preparation methods used.

In this study, the brain tissue was also evaluated using DNA agarose gel electrophoresis and the GSH assays. The presence of micronuclei in the blood smears of the chick embryos was also evaluated and did not reveal any substantial differences in the presence of micronuclei between the exposed and control groups. With the DNA agarose gel electrophoresis, the brain tissue was analysed for DNA damage caused by the metals. The results of this chapter revealed DNA damage to the plasmid DNA, which resulted in DNA fragmentation caused by all the groups. The results from the GSH assay revealed that Cd and Cr alone and in combination does not cause statistically significant oxidative damage to the brain tissue and thus no specific metal could be selected as the more toxic metal using this specific method.

Therefore, it can be concluded that Cd is more toxic at higher concentrations, but Cr and the metal combination groups, revealed that at all the concentrations these metals will have an effect on the brain, liver and kidney. Thus when exposed to the last mentioned metal groups for an extended period, these slight changes might produce minor functional and morphological changes from the beginning of exposure and might escalate as the exposure continues. In this thesis the effects of Cd and Cr were tested on chick embryos that were directly exposed to the metals. The fact that cellular effects were seen in the chick embryos organs shows that not only did the metals have the ability to penetrate the chorioallantoic membrane (CAM), but also have the ability to cause cellular alterations. This shows that when human embryos are exposed to the same concentrations, similar effects might be observed, but the effects the mother's detoxification system might have on reducing these

metal concentrations before reaching the developing embryo, must be taken into account and require further investigation.

The research reported in this thesis, may contribute to the pool of knowledge regarding the adverse effects of heavy metals on organ structure and function. However, since the main focus of this thesis was morphology and ultrastructure, more extensive research needs to be conducted on the effects caused by these metals, possibly by implementing an *in vivo* model. Chronic exposure to these and other heavy metals might be important for future research. Also, EELS analysis should be used as the primary method for metal detection as the results obtained in this thesis indicated this method to be more sensitive for the detection of particles in biological samples.

Chapter 10

Reference list

Ahn CC, Krivanek OL, Burgner RP, Disko MM and Swann PR. 1983. EELS atlas. USA: Gatan, Inc. and ASU HREM. 1-93 p.

Al-Attar AM. 2011. Antioxidant effect of vitamin E treatment on some heavy metals-induced renal and testicular injuries in male mice. Biol Sci 18: 63–72.

Almazan G, Liu H-N, Khorchid A, Sundararajan S, Martinez-Bermusez AK and Chemtob S. 2000. Exposure of developing oligodendrocytes to cadmium causes HSP72 induction, free radical generation, reduction in glutathione levels, and cell death. Free Radical Bio Med 29: 858–869.

Anderson, RA. 1997. Nutritional factors influencing the glucose/insulin system: chromium. Amer Coll Nutr 16: 404-410.

Aronovitch Y, Godinger D, Israeli A, Krishna MC, Samuni A, Goldstein S. 2007. Dual activity of nitroxides as pro- and antioxidants: Catalysis of copper-mediated DNA breakage and H_2O_2 dismutation. Free Radical Bio Med 42: 1317–1325.

Asmatullah, SNQ and Shakoori AR. 1998. Hexavalent chromium-induced congenital abnormalities in chick embryos. Appl Toxicol 18: 167–171.

Aughey E, Fell GS, Scott R and Black M. 1984. Histopathology of early effects of oral cadmium in the rat kidney. Environ Health Persp 54: 153-161.

Awofolu OR, Mbolekwa Z, Mtshemla V and Fatoki OS. 2005. Levels of trace metals in water and sediment from Tyume River and its effects on an irrigated farmland. Water SA 31: 87-94.

Bagchi D, Stohs SJ, Downs BW, Bagchi MB, Preuss HG. 2002. Cytotoxicity and oxidative mechanisms of different forms of chromium. Toxicology 180: 5-22.

Begun SKR, Padmavathi K, Bhanu SKH, *et al*. 2008. Micronuclei analysis: Stress of acrylamide and cadmium chloride on chick embryo. Adv Lif Sci 2: 15-22.

Bellairs R and Osmond M. 1998. The atlas of chick development. San Diego: Academic Press. 59-89 p.

Bertin G and Averbeck D. 2006. Cadmium: cellular effects, modifications of biomolecules, modulation of DNA repair and genotoxic consequences (a review). Biochimie 88: 1549–1559.

Bharath S, Hsu M, Kaur D, Rajagopalan S, Andersen JK. 2002. Glutathione, iron and Parkinson's disease. Biochem Pharmacol 64: 1037–1048.

Binning K and Baird D. 2001. Survey of heavy metals in the sediments of the Swartkops River Estuary, Port Elizabeth South Africa. Water SA 27: 461-466.

Bozzola JJ and Russell LD. 1999. Electron microscopy. Sudbury: Jones and Bartlette. 369-385 p.

Brzóska MM, Moniuszko-Jakoniuk J, Pilat-Marcinkiewicz B and Sawicki B. 2003. Liver and kidney function and histology in rats exposed to cadmium and ethanol. Alcohol Alcoholism 38: 2–10.

Butler H and Juurlink BHL. 1987. An atlas for staging mammalian and chick embryos. Baco Raton: CRC Press Inc.

Campbell MK and Farrell SO. 2008. Biochemistry. USA: Brooks/Cole. 80-82 p.

Cawthorn RG. 2010. The Platinum Group Element Deposits of the Bushveld Complex in South Africa. Platinum Metals Rev 54: 205–215.

Chen L, Liu L and Huang S. 2008. Cadmium activates the mitogen-activated protein kinase (MAPK) pathway via induction of reactive oxygen species and inhibition of rotein phosphatases 2A and 5. Free Radical Bio Med 45: 1035–1044.

Chowdhury AR. 2009. Recent Advances in Heavy Metals Induced Effect on Male Reproductive Function-A Retrospective. Med Sci 2: 37-42.

Clark P, Boardman W and Raidal S. 2009. Atlas of clinical avian hematology. UK: Wiley-Blackwell. 33-124 p.

Coetzee HL, Loots GP, Meiring JH. 2009. Human Histology. South Africa: Van Schaik Publishers. 151-347 p.

Damelin LH, Vokes S, Whitcutt JM, Damelin SB and Alexander JJ. 2000. Hormesis: a stress response in cells exposed to low levels of heavy metals. Human and Experimental Toxicology 19: 420-430.

Dayan AD and Paine AJ. 2001. Mechanisms of chromium toxicity, carcinogenicity and allergenicity: Review of the literature from 1985 to 2000. Hum Exp Toxicol 20: 439-451.

Debnath S, Kannadasan M, Acharjee A, Bhattacharjee C, Kumar SC and Kumar G. 2010. Antioxidant activity of the hydro-alcoholic extract of Erythrina fusca Lour. Bark against the animal models of epilepsy. Chem Pharm Res 2: 379-383.

Doughtie D and Rao R. 1984. Histopathological and ultrastructural changes in the adtennal gland midgut, hepatopancreas and gill of Grass Shrimp following exposure to hexavalent chromium. Invertebr Pathol 43: 89-108.

Drake VJ, Koprowski SL, Lough JW and Smith SM. 2006. Gastrulating chick embryo as a model for evaluating teratogenicity: A comparison of three approaches. Birth Defects Res 76: 66–71.

Egerton RF. 2009. Electron energy-loss spectroscopy in the TEM. Rep Prog Phys 72: 1-25.

Egerton RF. 2011. Electron energy-loss spectroscopy in the electron microscope. New York: Springer. 22-26 p.

Ernst LM, Ruchelli ED and Huff DS. 2011. Color atlas of fetal and neonatal histology. USA: Springer. 67-320 p.

Fatoki OS and Awofolu R. 2003. Levels of Cd, Hg and Zn in some surface waters from the Eastern Cape Province, South Africa. Water SA 29: 375-380.

Fu J, Liang X, Chen Y, Tang L, Zhang Q-H and Don Q. 2008. Oxidative stress as a component of chromium-induced cytotoxicity in rat calvarial osteoblasts. Cell Biol Toxicol 24: 201–212.

Fu M, Wang C, Li Z, Sakamaki T, and Pestell RG. 2004. Minireview: Cyclin D1: Normal and Abnormal Functions. Endocrinology 145: 5439 –5447.

Gagnon ZE and Patel A. 2007. Induction of metallothionein in chick embryos as a mechanism of tolerance to platinum group metal exposure. Environ Sci Health A Tox Hazard Subst Environ Eng 42: 381-387.

Ghadially FN. 1988. Ultrastructural pathology of the cell and matrix. England: Butterworths. 428-434 p.

Harkness LM and Baird DT. 1997. Morohological and molecular charateristics of living human foetuses between Carnegie stages 7 and 23: immunolocalization of inhibin alpha and bata subunits. Hum Reprod Update 3: 35-57.

Harvey W. 1628. Exercitatio anatomica de motu cordis et sanguinis in animalibus. Germany.

Hassoun EA and Stohs SJ. 1996. Cadmium-induced production of superoxide anion and nitric oxide, DNA single strand breaks and lactate dehydrogenase leakage in J774A. 1 cell cultures. Toxicology 112: 219-226.

Heinz GH, Hoffman DJ, Klimstra JD, Stebbins KR, Kondrad SL, Erwin CA. 2012. Hormesis Associated with a Low Dose of Methylmercury Injected into Mallard Eggs. Arch Environ Contam Toxicol 62: 141–144.

Hengstler JG, Bolm-Audorff U, Faldum A, *et al*. 2003. Occupational exposure to heavy metals: DNA damage induction and DNA repair inhibition prove co-exposures to cadmium, cobalt and lead as more dangerous than hitherto expected. Carcinogenesis 24: 63-73.

Jacobs CJ, Greyling LM and Meiring JH. 2006. Embryology for the Health Science Student. South Africa: University of Pretoria. 74-136 p.

Jaeschke H, Gujral JS and Bajt ML. 2004. Apoptosis and necrosis in liver disease. Liver Int 24: 85–89.

Järup L. 2003. Hazarda of heavy metal contamination. Brit Med Bull 68: 167-182.

Jihen EH, Imed M, Fatima H and Abdelhamid K. 2008. Protective effects of selenium (Se) and zinc (Zn) on cadmium (Cd) toxicity in the liver and kidney of rats: Histology and Cd accumulation. Food Chem Toxicol 46: 3522-3527.

Kajikawa K, Nakanishi I and Kuroda K. 1981. Morphological changes of the kidney and bone of rats in chronic cadmium poisoning. Expl Mol Pathol 34: 9-24.

Kakkar P and Jaffery FN. 2005. Biological markers for metal toxicity. Environ Toxicol Phar 19: 335–349.

Kalpana KB, Srinivasan M and Menon VP. 2008. Antioxidant potential of aminothiazole derivative and its protective effect on H_2O_2-induced oxidative damage on pBR322 DNA and RBC cellular membrane. Mol Cell Biochem 314: 95-103.

Kaur P, Aschner M, Syversen T. 2006. Glutathione modulation influences methyl mercury induced neurotoxicity in primary cell cultures of neurons and astrocytes. Neurotoxicology 27: 492–500.

Kearney L. 2012. Mining and minerals in South Africa. Available from: www.southafrica.info [Accessed: May 2013].

Kim E and Na KJ. 1991. Nephrotoxicity of sodium dichromate depending on the route of administration. Arch Toxicol 65: 537-541.

Kim SH, Jung MJ and Lee YM. 2011. Effects of heavy metals on the antioxidant enzymes in the marine ciliate Euplotes Crassus. Toxicol Environ Health Sci 3: 213-219.

Kirubagaran R and Joy KP. 1988. Toxic effects of three mercurial compounds on survival, and histology of the kidney of the catfish Clarias batrachus (L.). Ecotox Enviton Safe 15: 171–179.

Koyu A, Gokcimen A, Ozguner F, Bayram DS and Kocak A. 2006. Evaluation of the effects of cadmium on rat liver. Mol Cell Biochem 284: 81-85.

Kubrak OI, Lushchak OV, Lushchak JV, *et al*. 2010. Chromium effects on free radical processes in goldfish tissues: Comparison of Cr(III) and Cr(VI) exposures on oxidative stress markers, glutathione status and antioxidant enzymes. Comp Biochem Phys C 152: 360–370.

Lahijani MS and Ghafoori M. 2000. Teratogenic effects of sinusoidal extremely low frequency electromagnetic fields on morphology of 24 hr chick embryos Exp Biol 38: 692-699.

Langård S and Costa M. 2007. Chromium. In: Handbook on the Toxicology of Metals. Nordberg GF, Fowler BA, Nordberg M and Friberg LT, editors. Academic Press Inc., Amsterdam and Boston, pp 487-510.

Leal BR, Rieger DK, Peres TV, Lopes MW and Gonçalves CAS. 2012. Cadmium neurotoxicity and its role in brain disorders. In: Metal Ion in Stroke. Li YV and Zhang JH, editors. Springer Science and Business Media, New York, pp 751-766.

Lee J-E, Naqi SA, Kao E and Dietert RR. 2002. Embryonic exposure to lead: comparison of immune and cellular responses in unchallenged and virally stressed chickens. Arch Toxicol 75: 717–724.

Leonard SS, Harris GK and Shi X. 2004. Metal-induced oxidative stress and signal transduction. Free Radical Bio & Med 37: 1921–1942.

Lewińska D, Arkusz J, Stańczyk M, Palus J, Dziubałtowska E and Stępnik M. 2007. Comparison of the effects of arsenic and cadmium on benzo(a)pyrene-induced micronuclei in mouse bone-marrow. Mutat Res 632: 37–43.

Lovell MA, Xie C and Markesbery WR. 1998. Decreased glutathione transferase activity in brain and ventricular fluid in Alzheimer's disease. Neurology 51: 1562-1566.

Lui D and Kottke I. 2003a. Subcellular localization of Cd in the root cells of Allium sativum by electron energy loss spectroscopy. Biosci 28: 471–478.

Lui D and Kottke I. 2003b. Subcellular localization of chromium and nickel in root cells of *Allium cepa* by EELS and ESI. Cell Biol Toxicol 19: 299-311.

Malladi SM, Bhilwade HN, Khan MZ and Chaubey RC. 2007. Gamma ray induces genetic changes in different organs of chick embryo using peripheral blood micronucleus test and comet assay. Mutat res 630: 20-27.

Malpighi M. 1672. De formatione pulli in ovo. In: Marcello Malpighi and the evolution of embryology. Adelmann HB, editor. Cornell University Press, Ithaca.

Malpighi, M. 1675. Repetitas auctasque de ovo incubato observationes continens. London: Johannis Martyn.

Männer J, Seidl W, Hesse FHH. 2003. Teratogenic effects of suramin on the chick embryo. Anat Embryol 206: 229–237.

Matésa JM, Pérez-Gómeza C, De Castroa IN. 1999. Antioxidant enzymes and human diseases. Clin Biochem 32: 595–603.

Mattson MP. 2008. Hormesis defined. Ageing Res Rev 7: 1–7.

Meek GA. 1976. Practical electron microscopy for biologist. Chichester: John Wiley and son. 1-4 p.

Méndez-Armenta M and Ríos C. 2007. Cadmium neurotoxicity. Environ Toxicol Phar 23: 350–358.

Michel J, Sauerwein W, Wittig A, Balossier G, and Zierold K. 2003. Subcellular localization of boron in cultured melanoma cells by electron energy-loss spectroscopy of freeze-dried cryosections. Microscopy 210: 25–34.

Mirsalis JC, Hamilton CM, O'Loughlin KG, Paustenbach DJ, Kerger BD and Patierno S. 1996. Chromium (VI) at plausible drinking water concentrations is not genotoxic in the *in vivo* bone marrow micronucleus or liver unscheduled DNA synthesis assays. Environ Mol Mutagen 28:60-63.

Mishra A and Mohanty B. 2008. Acute toxicity impacts of hexavalent chromium on behaviour and histolpathology of gill, kidney and liver of the freshwater fish, *Channa punctatus* (Bloch). Environ Toxicol Phar 26: 136-141.

Molokwane PE, Meli KC and Nkhalambayausi-Chirwa EM. 2008. Chromium (VI) reduction in activated sludge bacteria exposed to high chromium loading: Brits culture (South Africa). Water Research 42: 4538-4548.

Naicker K, Cukrowskaa E, McCarthy TS. 2003. Acid mine drainage arising from gold mining activity in Johannesburg, South Africa and environs. Environ Pollut 122: 29–40.

Nordberg GF, Fowler BA, Nordberg M and Friberg LT. 2007a. Introduction—General Considerations and International Perspectives. In: Handbook of Toxicology of Metals. Nordberg GF, Nogawa K, Nordberg M, and Friberg LT, editors. Academic Press Inc., Amsterdam and Boston, pp 4-9.

Nordberg GF, Nogawa K, Nordberg M, and Friberg LT. 2007b. Cadmium. In: Handbook of Toxicology of Metals. Nordberg GF, Nogawa K, Nordberg M, and Friberg LT, editors. Academic Press Inc., Amsterdam and Boston, pp 445-486.

Olivieri G, Hess C, Savaskan E, *et al*. 2001. Melatonin protects SHSY5Y neuroblastoma cells from cobalt-induced oxidative stress, neurotoxicity and increased β-amyloid secretion. Pineal Res 31: 320–325.

Owen JB and Butterfield DA. 2010. Measurement of oxidized/reduced glutathione ratio. Method Cell Biol 648: 269-277.

Patlolla AK, Barnes C, Yedjou C, Velma VR and Tchounwou PB. 2009. Oxidative stress, DNA damage, and antioxidant enzyme activity induced by hexavalent chromium in Sprague-Dawley rats. Environ Toxicol 24: 66–73.

Prozialeck WC, Edwards JR and Woods JM. 2006. The vascular endothelium as a target of cadmium toxicity. Life Sci 79: 1493–1506.

Quinteros FA, Poliandri AHB, Machiavelli LI, Cabilla JP, Duvilanski BH. 2007. *In vivo* and in vitro effects of chromium VI on anterior pituitary hormone release and cell viability. Toxicol Appl Pharm 218:79–87.

Raghunathan VK, Ellis EM, Grant MH. 2009. Response to chronic exposure to hexavalent chromium in human monocytes. Toxicol in Vitro 23: 647–652.

Ram MS, Neetu D, Yogesh B, *et al.* 2002. Cyto-protective and immunomodulating properties of Amla (Emblica officinalis) on lymphocytes: an in-vitro study. Ethnopharmacol 81: 5-10.

Rikans LE and Yamano T. 2000. Mechanisms of cadmium-mediated acute hepatotoxicity. Biochem Toxicol 14: 110–117.

Rink J, Ghigo E, Kalaidzidis Y and Zerial M. 2005. Rab conversion as a mechanism of progression from early to late endosome. Cell 122: 735-749.

Roux W. 1888. Contributions to the developmental mechanics of the embryo. On the artificial production of half-embryos by destruction of one of the first two blastomeres and the later development (postgeneration) of the missing half of the body. Foundations of experimental embryology 2-37.

Ruiz S, Pergola PE, Zager RA and Vaziri ND. 2013. Targeting the transcription factor Nrf2 to ameliorate oxidative stress and inflammation in chronic kidney disease. Kidney Int 83: 1029-1041.

Sadler TW. 2010. Langman's Medical Embryology. Philadelphia: Lippincott Williams & Wilkins. 219-293 p.

Sandhir R, Julka D and Gill KD. 1993. Lipoperoxidative Damage on lead exposure in rat brain and its implications on membrane bound enzymes. Pharmacol Toxicol 14: 6-71.

Schulz H. 1888. Ueber hefegifte. Pfügers Arch. Ges. Physiol 42: 517.

Serem JC. 2011. An exploratory investigation into the physicochemical, antioxidant and cellular effects of a selection of honey samples from the Southern African region, masters thesis, University of Pretoria, Pretoria.

Sharma K, McCue P and Dunn SR. 2003. Diabetic kidney disease in the db/db mouse. Am J Physiol Renal Physiol 284: 1138–1144.

Sherlock S and Doely J. 1993. Diseases of the liver and biliary system. Cambridge: Blackwell Scientific publication. 335-364 p.

Shi X. 2010. Reduction of chromium (VI) and its relationship to carcinogenesis. Toxicol Environ Health 2: 87-104.

Sian J, Dexter DT, Lees AJ, *et al*. 1994. Alterations in glutathione levels in Parkinson's disease and other neurodegenerative disorders affecting basal ganglia. Ann Neurol 36: 348–355.

Soudani N, Troudi A, Amara IB, Bouaziz H, Boudawara T and Zeghal N. 2012. Ameliorating effect of selenium on chromium (VI)-induced oxidative damage in the brain of adult rats. Physiol Biochem 68: 397-409.

Stebbing ARD. 1982. Hormesis- The stimulation of growth by low levels of inhibitors. Sci Total Environ 22: 213-234.

Stern CD. 2005. The chick: A great model system commentary becomes even greater. Dev Cell 8: 9–17.

Stohs SJ, Bagchi D, Hassoun E, Bagchi M. 2000. Oxidative mechanisms in the toxicity of chromium and cadmium ions. Environ Pathol Toxicol Oncol 19: 201-213.

Taylor CM, Golding J and Emond AM. 2014. Lead, cadmium and mercury levels in pregnancy: the need for international consensus on levels of concern. Dev Orig Health Dis 5: 16–30.

Tempelhoff E. 2013. Lug bo dié stad vuilste in wêreld. Available from: www.beeld.com [Accessed: April 2013].

Thévenod F. 2009. Cadmium and cellular signalling cascades: To be or not to be? Toxicol Appl Pharm 238: 221–239.

Thompson J and Bannigan J. 2001. Effects of cadmium on formation of the ventral body wall in chick embryos and their prevention by zinc pretreatment. Teratology 64: 87–97.

Thompson J and Bannigan J. 2008. Cadmium: Toxic effects on the reproductive system and the embryo. Reprod Toxicol 25: 304–315.

Thompson J, Hipwell E, Loo HV and Bannigan J. 2005. Effects of cadmium on cell death and cell proliferation in chick embryos. Reprod Toxicol 20: 539–548.

Thophon S, Pokethitiyook P, Chalermwat K, Upatham EU and Sahaphong S. 2004. Ultrastructural alterations in the liver and kidney of White Sea Bass, *Lates calcarifer*, in acute and subchronic cadmium exposure. Environ Toxicol 19: 11–19.

Unsal C, Kanter K, Aktas A and Erboga M. 2013. Role of quercetin in cadmium-induced oxidative stress, neuronal damage, and apoptosis in rats. Toxicol Ind Health 0748233713486960.

Valko M, Rhodes CJ, Moncola J, Izakovic M, Mazura M. 2006. Free radicals, metals and antioxidants in oxidative stress-induced cancer. Chem-Biol Interact 160: 1–40.

Venter C, Van der Merwe CF, Oberholzer HM, Bester MJ and Taute H. 2013. Feasibility of high pressure freezing with freeze substitution after long-term storage in chemical fixatives. Microsc Res Techniq 76: 942–946.

Vitória AP, Lea PJ and Azevedo RA. 2001. Antioxidant enzymes responses to cadmium in radish tissues. Phytochemistry 57: 701-710.

Waisberg M, Joseph P, Hale B, Beyersmann D. 2003. Molecular and cellular mechanisms of cadmium carcinogenesis. Toxicology 192: 95–117.

Wang H, Kruszewski A and Brautigan DL. 2005. Cellular chromium enhances activation of insulin receptor kinase. Biochemistry 44: 8167-8175.

Wang X-F, Xing M-L, Shen Y, Zhu X and Xu L-H. 2006. Oral administration of Cr(VI) induced oxidative stress, DNA damage and apoptosis cell death in mice. Toxicology 228: 16-23.

Wätjen W, Cox M, Biagioli M and Beyersmann D. 2002. Cadmium-induced apoptosis in C6 glioma cells: Mediation by caspase 9-activation. BioMetals 15: 15–25.

Wei Q-Y, Zhou B, Cai Y-J, Yang L, Liu Z-L. 2006. Synergistic effect of green tea polyphenols with trolox on free radical-induced oxidative DNA damage. Food Chem 96: 90–95.

Wilbur S, Abadin H, Fay M, *et al*. 2011. Toxicological profile for chromium. Available from: http://www.atsdr.cdc.gov [Accessed: April 2013].

Whitsel AI, Johnson CB and Forehand CJ. 2002. An *in ovo* chicken model to study the systemic and localized teratogenic effects of valproic Acid. Teratology 66: 153-163.

Williams AF. 1972. DNA synthesis in purifies populations of avian erythroid. Cell Sci 10: 27-46.

Williams DB and Carter CB. 1996a. The transmission electron microscope. In: Transmission electron microscopy: Basics. Williams DB and Carter CB, editors. Plenum Press, New York, pp 5-17.

Williams DB and Carter CB. 1996b. Inelastic scattering and beam damage. In: Transmission electron microscopy: Basic. Williams DB and Carter CB, editors. Plenum Press, New York, pp 52-57.

Williams DB and Carter CB. 1996c. X-ray spectrometry. In: Transmission electron microscopy: Spectrometry. Williams DB and Carter CB, editors. Plenum Press, New York, pp 553-666.

Wolf T and Luepke N-P. 1997. Formation of micronuclei in incubated hen's eggs as a measure of genotoxicity. Mutat Res 394: 163–175.

Yamamoto FY, Netoa FF, Freitas PF, Ribeiroa CAO, Ortolani-Machadoa CF. 2012. Cadmium effects on early development of chick embryos. Environ Toxicol Phar 34: 548-555.

Yoon S, Han SS and Rana SVS. 2008. Molecular markers of heavy metal toxicity – A new paradigm for health risk assessment. Environ Toxicol 29: 1-14.

Young B, Lowe JS, Stevens A and Heath JW. 2006. Wheater's Functional Histology: A text and colour atlas. Philadelphia: Churchill Livingstone Elsevier. 2-325 p.

Zierold K. 1997. Effects of cadmium on electrolyte ions in cultured rat hepatocytes studied by X-ray microanalysis of cryosections. Toxicol Appl Pharm 144: 70–76.

Zierold K. 2002. Limitations and prospects of biological electron probe X-ray microanalysis. Trace Microprobe Techniques 20: 181–196.

Zhang Y-M, Liu X-Z, Lu H, Mei L and Liu Z-P. 2009. Lipid peroxidation and ultrastructural modifications in brain after perinatal exposure to lead and/or cadmium in rat pups. Biomedical and environmental sciences 22: 423-429.

Appendix A

MICROSCOPY RESEARCH AND TECHNIQUE 76:942–946 (2013)

Feasibility of High Pressure Freezing With Freeze Substitution After Long-Term Storage in Chemical Fixatives

CHANTELLE VENTER,[1] CHRISTIAAN FREDERICK VAN DER MERWE,[2] HESTER MAGDALENA OBERHOLZER,[1]* MEGAN JEAN BESTER,[1] AND HELENA TAUTE[1]
[1]*Department of Anatomy, Faculty of Health Sciences, University of Pretoria, South Africa*
[2]*Laboratory for Microscopy and Microanalysis, Faculty of Natural and Agricultural Sciences, University of Pretoria, South Africa*

KEY WORDS high pressure freezing; transmission electron microscopy; hepatocytes; sample storage

ABSTRACT Fixation of biological samples is an important process especially related to histological and ultrastructural studies. Chemical fixation was the primary method of fixing tissue for transmission electron microscopy for many years, as it provides adequate preservation of the morphology of cells and organelles. High pressure freezing (HPF) and freeze substitution (FS) is a newer alternative method that rapidly freezes non-cryoprotected samples that are then slowly heated in the FS medium, allowing penetration of the tissue to insure adequate fixation. This study addresses several issues related to tissue preservation for electron microscopy. Using mice liver tissue as model the difference between samples fixed chemically or with HPF immediately after excision, or stored before chemical or HPF fixation were tested with specific focus on the nuclear membrane. Findings are that immediate HPF is the method of choice compared to chemical fixation. Of the chemical fixatives, immediate fixation with 2.5% glutaraldehyde (GA)/formaldehyde (FA) is the best in preserving membrane morphology, 2.5% GA can be used as alternative for stored and then chemically processed samples, with 10% formalin being suitable as a storage medium only if followed by HPF fixation. Overall, storage leads to lower ultrastructural preservation, but HPF with FS can minimize these artifacts relative to other processing protocols. *Microsc. Res. Tech. 76:942-946, 2013.*

INTRODUCTION

With the advances in microscopy, the preservation of tissue has become important in understanding the tissue structure and function. The purpose of chemical tissue fixation is to preserve tissue with minimal alterations to the native state (DiStefano, 2008). When it came to achieving the goal of minimal alterations to the native state, two types of preservation methods came to existence namely chemical fixation protocols and the rapid freezing of samples. The reason for the universal use of chemical fixation can be attributed to the adequate preservation of many cell components and the clarity of structural detail viewed with Transmission Electron Microscopy (Hayat, 1989). With chemical fixation, the commonly used fixatives in most laboratories are glutaraldehyde (GA) and paraformaldehyde. The reason for the use of aldehydes is due to the formation of protein, carbohydrate, and nucleic acid crosslinks. These crosslinks form a mesh-work that secures the tissue molecules in place, in a near native state (DiStefano, 2008). Paraformaldehyde is a white powder that is the polymer of formalin and was the main fixative to use until Karnovsky proposed that GA and paraformaldehyde should be used together to increase the preservation of the specimens (Ellis, 2009). Paraformaldehyde's reaction with proteins and peptides is efficient, as it produces protein-bridges between the neighbouring protein chains (Coetzee and Loots, 1993). GA is seen as one of the best chemical fixatives for preservation of detailed structure. However high concentrations of GA can denature the proteins in the sample and especially in immunohistochemistry analysis this tissue cannot be used. The penetration rate of the fixative is also significant, as inadequate penetration in a given time will render the tissue unusable. Thus formaldehyde (FA) will penetrate the sample faster than GA, as FA is a mono-aldehyde and thus a smaller molecule whereas GA is a di-aldehyde, bigger and less penetrating. The greater crosslinking ability creates a greater barrier to penetration into the tissue. GA/FA is a compromise between these.

The second method developed for specimen preservation is high pressure freezing (HPF). The idea for HPF already existed in 1968 with Moore and Riehle who first proposed the idea, but unfortunately since then the impact on biomedical research has been comparatively small (Studer et al., 2001). According to Studer et al. (2001) only about 100 papers have been published that dealt with HPF as a method for studying biological structures since it was first described. The reason for the low use of HPF may be due to the high cost of purchasing and operating a high pressure

*Correspondence to: H. M. Oberholzer, Department of Anatomy, Faculty of Health Sciences, University of Pretoria, Private Bag x323, ARCADIA 0007, South Africa. E-mail: nanette.oberholzer@up.ac.za

Received 15 April 2013; accepted in revised form 12 June 2013
DOI 10.1002/jemt.22252
Published online 1 July 2013 in Wiley Online Library (wileyonlinelibrary.com).

freezer, together with the additional equipment needed for processing the samples at low temperatures (Kan, 2010). HPF is a method that can vitrify non-cryoprotected samples thicker than 50 μm, without visible ice crystal damage when viewed with an electron microscope. What makes HPF so unique is the fact that the samples are physically immobilized in milliseconds (Studer et al., 2001). Freeze substitution (FS) entails that an organic solvent such as acetone, ethanol, or methanol substitutes the vitrified water in the cells, at a temperature of −90°C. Substitution of water at these low temperatures minimizes the collapse and shrinkage of cells that normally occurs at room temperature (McDonald, 1999). Osmium and GA are added to the FS medium as fixation agents, and the former for contrast enhancement of lipids in the membranes. When you combine the FS medium and fixative, the fixative penetrates the cells while the cells are immobilized. When the temperature is increased, the fixative has already penetrated the cell, where chemical crosslinking takes place and fixation of the cells occurs (McDonald, 1999).

Another tissue preservation method used in the medical sciences is embalming fluid. Embalming fluid is typically used to preserve cadavers for the purpose of dissection. The embalming fluid consists of a group of chemicals which serves to ensure preservation of the body and prevent deterioration and structural disturbances as well as contamination with microbes. Often the need exists for the use of cadaver tissue for histological and ultrastructural studies and therefore embalming fluid was included in this study to determine the possibility of using cadaver tissue in morphological studies by investigating the organelles and structures within the hepatocyte.

Therefore, in this article the effect of storage of mice liver tissue in chemical fixatives before further processing (chemical or HPF) was tested to address the question of whether HPF at a later stage can still yield high quality tissue preservation for morphological and ultrastructural studies, in cases where the tissue cannot be processed immediately. The nuclear membrane is the structure selected to demonstrate the effect of the different sample preparation methods. Although only the nuclear membranes are depicted in this article, the membranes of the hepatocytes, mitochondria, and rough endoplasmic reticulum (rER) were also investigated in order to determine the best processing method. The nuclear envelope consists of a double lipid bilayer which encloses the nucleus (Coetzee et al., 2003; Hetzer and Wente, 2009). In between these two layers an intramembranous space that is proximately 20–30 nm wide is found. The outer membrane, that is adjacent to the cytosol of the cell, is in some areas continuous with the rER (Coetzee et al., 2003). On the outer membrane surface ribosomes are also present. The inner membrane is located adjacent to the chromatin of the nucleus (Coetzee et al., 2003; Hetzer and Wente, 2009). In some places in the nuclear envelope, nuclear pores can be found. The nuclear pores are octagonal with a diameter of between 30 and 100 nm (Coetzee et al., 2003).

MATERIALS AND METHODS

Liver tissue from ten control BALB/c mice was obtained from the University of Pretoria Biomedical Research Centre (UPBRC) [Ethical clearance number H18/09 NECSA]. Liver tissue was cut into 1 mm^3 samples and fixed separately. The samples were fixed in either 2.5% GA/FA; 2.5% GA; 10% formalin or embalming fluid. The remaining liver sections were processed with HPF and FS. The stored samples were left in the fixatives for three weeks and then either further chemically processed or high pressure frozen. An ultramicrotome and JEOL 2100F transmission electron microscope were respectively used to section and view the samples.

Fixatives Used

2.5% Glutaraldehyde/Formaldehyde. Tissue samples were fixed in 2.5% GA/FA (1 mL of 25% GA, 1 mL of 25% FA (freshly prepared from paraformaldehyde), 5 mL PO_4 buffer (0.15M), 3 mL ddH_2O) for 1 h, rinsed three times in 0.075M sodium phosphate buffer (pH = 7.4) for 15 min each before they were placed in secondary fixative, 1% osmium tetroxide solution, for 1 h. Following fixation, the tissues were rinsed again as described above. The samples were dehydrated in a graded EtOH-H_20 series consisting of 30%, 50%, 70%, 90%, and three changes of 100% ethanol. The samples were embedded in epoxy resin and ultra-thin sections (70–100 nm) were cut with a diamond knife using an ultramicrotome (Reichert Ultracut E). Samples were then contrasted with 2% aqueous uranyl acetate for 5 min followed by 2 min of contrasting with lead citrate, after which samples were allowed to dry for a few minutes before examination with the JEOL Transmission Electron microscope (JEM 2100F).

2.5% Glutaraldehyde. Tissue samples were fixed in 2.5% GA (1 mL 25% GA, 5 mL PO_4 buffer, 4 mL ddH_2O) for 1 h after which the same sample preparation methods were followed as described above.

10% Formalin. Tissue samples were fixed in 10% formalin (1 mL commercial 40% formalin, 1 mL ddH_2O, 2 mL PO_4 buffer) for 1 h after which the same sample preparation methods were followed as described above.

Embalming Fluid. Embalming Fluid with the following formula was obtained from the Anatomy Department at the University of Pretoria: Industrial methylated spirits (45 L), phenol 85% diluted in water (10 L), mono-ethylene glycol (40 L), formalin (5 L), thymol (50 g) and is made up to 100 L. Tissue samples were fixed in embalming fluid for 1 h after which the same sample preparation methods were followed as described above.

High Pressure Freezing. Mice liver tissue samples were cut using a scalpel to a thickness of 200 μm and trimmed with specimen punch to 1 mm in diameter. The samples were placed into a flat membrane carrier, loaded into the HPF (Leica EM Pact 2) and fast frozen (Sosinsky et al., 2008).

Freeze Substitution. After HPF, the liver samples were transferred to the FS (Leica EM AFS 2) machine. FS was done with 0.5% osmium tetroxide in 99% acetone solution (Walther and Ziegler, 2002). The FS schedule used was: 8 h at −90°C, warming from −90°C to −70°C for 6 h, left at −70°C for 10 h, warming from −70°C to −60°C over a 4 h period and finally warming from −60°C to 0°C over a 20 h period. The samples were rinsed once with pure acetone while at

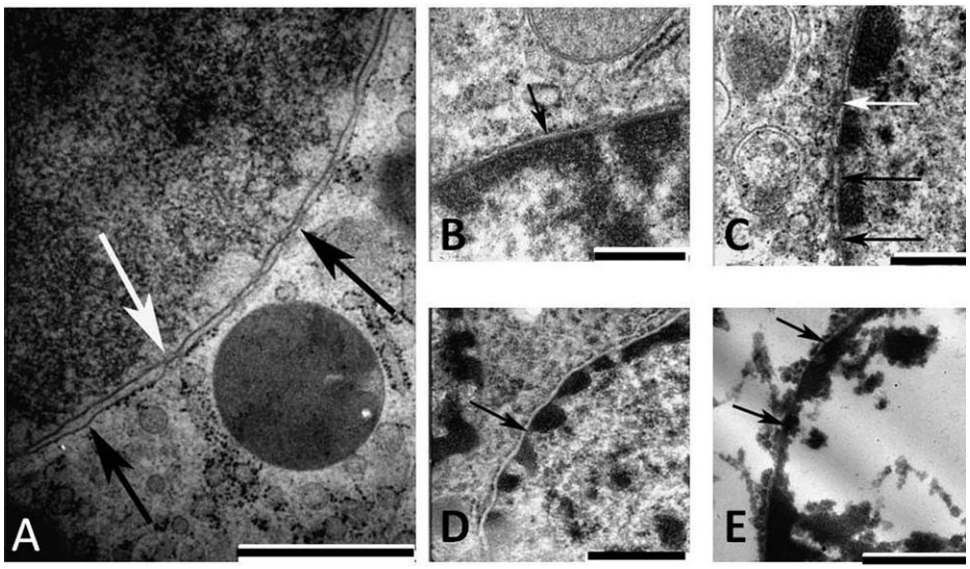

Fig. 1. TEM micrographs of immediately processed liver tissue. Nuclear membrane of hepatocyte of HPF samples (**A**); 2.5% GA/FA (**B**); 2.5% GA (**C**); 10% formalin (**D**), and embalming fluid (**E**). The nuclear membrane is indicated by the black arrows and white arrows indicate nuclear pores. (Scale bars A = 11 m; B = 500 nm; C = 500 nm; D = 11 m; E = 11 m).

−15°C. The samples were rinsed three times with 100% acetone, with 5 min intervals (Sosinsky et al., 2008) and embedded in epoxy resin. Ultra-thin sections (70–100 nm) were made with an ultramicrotome using a diamond knife, contrasted with uranyl acetate for 5 min followed by 2 min of lead citrate and viewed with the JEOL Transmission Electron microscope.

Storage Time. Tissue samples were also placed in the different chemical fixatives mentioned above and left for a period of three weeks, where after these were either fast frozen by HPF or further chemically processed as described above.

Evaluation of Samples. Micrographs of the membranes of the nuclei, mitochondria, and rER of hepatocytes were evaluated for any structural differences. The immediately processed HPF samples were used as reference to compare the other processing protocols with.

RESULTS

In Figure 1 the TEM micrographs of immediately processed liver tissue are shown. Figure 1A is representative of the liver tissue processed immediately with HPF after dissection. When comparing the samples in Figure 1, the HPF sample (Fig. 1A) has a clearly visible inner and outer nuclear membrane and the intramembranous space is clearly visible. Nuclear pores can be seen (white arrow) and ribosomes (black particles) are also visible on the nuclear envelope. In the 2.5% GA/FA sample (Fig. 1B), the intramembranous space is clearly visible, with somewhat unclear inner and outer membranes. In the samples processed with 2.5% GA (Fig. 1C), the membrane is unclear and undulated as is the case for the samples fixed in 10% formalin (Fig. 1D) as well. The liver tissue fixed in embalming fluid can be seen and in Figure 1E the inner membrane is still visible but the outer membrane is completely destroyed.

In Figure 2, TEM micrographs of liver tissue processed after a 3 week storage period in the same chemical fixatives as described above, and subsequently processed with HPF or chemical fixation are shown. Figure 2A is representative of the liver tissue stored in 2.5% GA/FA and then processed with HPF where the double membrane of the nucleus is still visible but unclear (black arrows) compared to Figure 1A where the tissue was processed immediately. In Figure 2B the outer membrane (black arrows) is destroyed, but the intramembranous space can still be identified. When comparing Figure 2C and D which represents the samples stored in 2.5% GA and then processed with HPF (Fig. 2C) or chemically processed (Fig. 2D), it can be seen that the membranes are not clearly visible in Figure 2C and in Figure 2D the outer membrane is undulated and appears uneven around the nucleus as indicated by the black arrows. In the samples stored in 10% formalin and then processed with HPF (Fig. 2E), the nuclear membrane is unclear but the intramembranous space can still be recognized, (black arrows) whereas the samples stored in 10% formalin and then chemically processed (Fig. 2F) revealed an undulated nuclear membrane that is unclear. Figures 2G and 2H are representative of the liver tissue samples stored in embalming fluid before being processed with HPF (Fig. 2G) or chemically processed (Fig. 2H). In Figure 2G the outer membrane is destroyed (black arrows), but with the intramembranous space still visible. In Figure 2H the outer membrane is completely destroyed, where the inner membrane is recognizable but fairly disrupted (black arrows).

DISCUSSION

Sample preparation of biological tissue plays a vital role in obtaining high quality ultrastructural preservation; therefore it is important to compare different sample preparation techniques to determine the

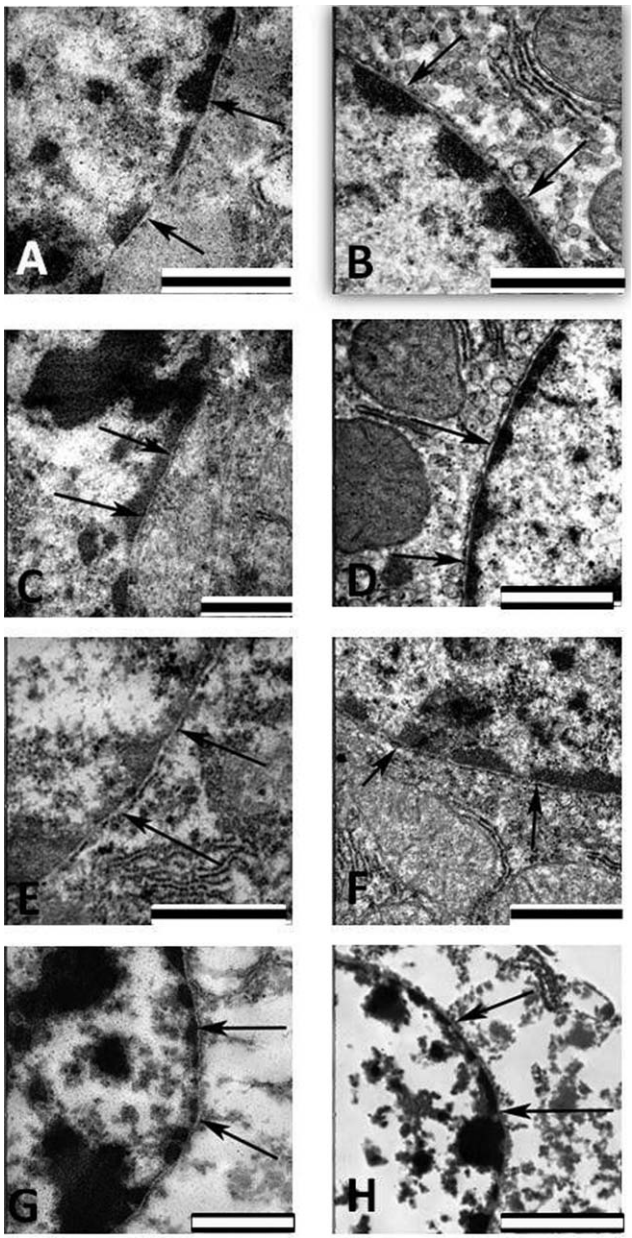

Fig. 2. TEM micrographs of liver tissue processed after a 3-week storage period. Nuclear membrane of hepatocyte of samples stored in 2.5% GA/FA and then HPF (**A**) and chemically processed (**B**); stored in 2.5% GA and then HPF (**C**) and chemically processed (**D**); stored in 10% formalin and then HPF (**E**) and chemically processed (**F**); stored in embalming fluid and then HPF (**G**) and chemically processed (**H**) (Black arrows indicate nuclear membranes) (Scale bars: A–G = 13 m; H = 23 m).

optimal technique for a specific application. In the current study, we investigated the possibility of storing mice liver tissue in chemical fixatives before further processing, whether via chemical or HPF fixation to determine whether HPF at a later stage can still yield high quality tissue preservation for morphological and ultrastructural studies, especially in cases where immediate tissue processing is not possible.

In 1996, Royer and Kinnamon compared HPF and FS with chemical fixation of catfish barbel taste buds (Royer and Kinnamon, 1996). These authors found an increase in smoothness of the plasma membrane of organelles; a more evenly distributed cytoplasmic matrix as well as a distinct perinuclear space when using HPF. This was also seen in the current study where the nuclear membranes of the HPF samples were clearer, with the individual components of the membrane more distinguishable. With the analysis of the other structures used in this study, that included the hepatocytes, mitochondria, and rER membranes, the same results were obtained as seen in that of the nuclear membrane. The membranes of the high pressure frozen samples were more distinct than the results obtained from the chemically fixed, stored, and chemically processed and stored and high pressure frozen samples. These results further confirmed the results obtained from analysis of the nuclear membranes.

The results obtained in this study clearly indicate that the storage of samples in 10% formalin before further processing with HPF for ultrastructural studies is feasible. For storage in chemical fixatives for a period of time before continuation with the chemical preparation process, 2.5% GA showed promising results. Overall the stored and then HPF samples yielded better results compared to the stored and then chemically processed samples. HPF of samples stored in fixatives prevents structural damage associated with chemical preparation after a storage period. In the case where HPF-FS is not available and immediate chemical fixation is the method of choice, it was found that 2.5% GA/FA yields the best results compared to the other chemical fixatives used in this study.

CONCLUSION

Tissue preservation is a vital step in preparing samples for TEM to obtain high quality micrographs for morphological and ultrastructural studies. HPF is currently the optimum method to use, as it promises enhanced morphological results. Often, immediate processing of samples by HPF may not always be possible and chemical fixation is the only alternative. Immediate HPF is the method of choice compared to immediate chemical fixation. Of the chemical fixatives, immediate fixation in 2.5% GA/FA best preserves the membrane morphology, 2.5% GA can be used as alternative for stored and then chemically processed samples, with 10% formalin that can be used as the storage fixative when samples are prepared with HPF after a storage period. Storage in fixatives compromises sample quality and images obtained for morphological and ultrastructural studies. Therefore it can be concluded that HPF and FS result in optimum quality micrographs for ultrastructural studies even after prolonged storage in fixatives.

REFERENCES

Coetzee HL, Loots GP. 1993. Histologiese ligen elektronmikroskopie. South Africa: Department of Anatomy, University of Pretoria. pp. 4–6.

Coetzee HL, Loots GP, Meiring JH. 2003. Human histology, 1st ed. Pretoria, South Africa: Van Schaik Publishers. pp. 29–30.

DiStefano AK. 2008. Cryofixation and chemical fixation comparison based on extracellular matrix preservation. ProQuest. Basingstoke, Hampshire. 4–5.

Ellis EA. 2009. A fast, simple, and safe way to prepare paraformaldehyde solutions. Micros Today 17:48–49.

Hayat MA. 1989. Principles and techniques of electron microscopy: Biological applications, 3rd ed. Macmillan press scientific and medical, Macmillan Press. Basingstoke, Hampshire. p 4.

Hetzer MW, Wente SR. 2009. Border control at the nucleus: Biogenesis and organization of the nuclear membrane and pore complexes. Dev Cell 17:606–616.

Kan B-H. 2010. Chapter 12—Electron microscopy and high pressure freezing of Arabidopsis. Methods Cell Biol 96:259–283.

McDonald K. 1999. High pressure freezing for preservation of high resolution structures and antigenicity of immunolabeling, methods in molecular biology. In: Hajibagheri MAN, editor. Electron microscopy methods and protocols. London: Springer. pp. 77–97.

Royer SM, Kinnamon JC.1996. Comparison of high pressure freezing/freeze substitution and chemical fixation of catfish barbel taste buds. Microsc Res Tech 35:385–412.

Sosinsky GE, Crum J, Jones YZ, Lanman J, Smarr B, Terada M, Martone ME, Deerinck TJ, Johnson JE, Ellisman MH. 2008. The combination of chemical fixation procedures with high pressure freezing and freeze substitution preserves highly labile tissue ultrastructure for electron tomography applications. J Struct Biol 161:359–371.

Studer D, Graber W, Al-amound A, Eggli P. 2001. A new approach for cryofixation by high pressure freezing. J Microsc 203:285–294.

Walther P, Ziegler A. 2002. Freeze substitution of high-pressure frozen samples: The visibility of biological membranes is improved when the substitution medium contains water. J Microsc 208:3–10.